UNIVERSITAT DE BARCELONA

Connectivity of the deep-sea red shrimp *Aristeus antennatus* in the northwestern Mediterranean Sea by modeling the Lagrangian transport of larvae

Morane Clavel-Henry

Connectivity of the deep-sea red shrimp *Aristeus antennatus* in the northwestern Mediterranean Sea by modeling the Lagrangian transport of larvae

Morane Clavel-Henry

Thesis presented to obtain the Ph. D. Degree at the University of Barcelona
(Ph.D. program in Marine Sciences)

Ph. D. co-advisors:

Dr. Nixon Bahamon Rivera
ICM-CSIC

Dr. Jordi Solé Ollé
ICM-CSIC

Tutor:
Prof. Antonio Miguel Calafat Frau
Facultat de Geologia,
Universitat de Barcelona (UB)

2019

”To drift, or not to drift, that is the question”

adapted from Hamlet, W. Shakespeare

Funding

The present thesis was carried out in the Institut de Ciències del Mar (ICM-CSIC) within the framework of the **CONECTA** project (**CONEC**Tividad poblacional en la gamba rosada. ***A**risteus antennatus* en el Mediterráneo noroccidental entre el Golfo de León y el Golfo de Valencia modelo de deriva LARvaria; CTM2014-54648-C2-1-R) led by J.B. Company Claret. The thesis and the short-stay research grant were funded by the predoctoral fellowship from the Spanish Ministry of Economy and Competitiveness (BES-2015-074126).

Front and back covers: Morane Clavel-Henry, Watercolor 2019.

For clarity purpose, scales were not respected.

INDEX

Acknowledgements

For me, each contribution from everyone is important and that include all the people that gave me scientific support and friend support during the thesis period. Please, don't take it to heart if you are in the middle or last lines, it has no meanings: first persons to be acknowledged have as much importance as the last of the list. It may be possible that I forgot to include some names or some groups, do not take it to heart, it is a memory twist.

Many thanks to Joan B. Company. Unfortunately, the administrative system could not allow to have three thesis directors, but Joan B. Company, as the principal researcher of CONECTA project and as the main reason for which I was able to work on this thesis, is without hesitation the most essential person for this thesis origin and direction.

Thanks to Nixon Bahamon, and Jordi Solé, who, together with Joan Baptista Company, taught me, guided me, and cheered me in the many mazes of sciences. Without the three of them, this thesis would not have been achieved in its present form and substance. It was hard to comply with all their way to work, but it was also a good lesson for my carrier at the interface among numerous fields and for adapting the speech and vocabulary. *"Always taking the positive from the hardships, stay positive, stay motivated",* which is a mantra I own them to go through the troubles. I sought their expertise, and their approbation; no doubt, it will serve my work line conduct.

Thanks to Marine, Cécile, Amandine, that were from the beginning to the end, the most supportive persons about my settlement in Barcelona. Besides this fact, I thank them for being happy for me, for being the listeners of my worst moments, and the cheering friends when I dealt with hardship. I am so thankful to have met such wonderful crazy persons in my whole life.

Thanks to my thesis sister Marta Carretón, who shared a lot with me, good and bad times but lend me her time when I had to stress out. Numerous elements from her inspired and fire my spirits for doing good investigations. But my most precious moments are when

she disclosed her musical talent, either on some gatherings or during the scientific surveys.

Thanks to Elizabeth N. and Trond K, who on many points have taught me and guided me so well during my stay in the USA and Norway. I am glad I could have had an opportunity to learn from you, and I cannot imagine a better formation and experience while visiting you. I took it by heart when you invited me few moments within your family and I hope that a day, I can truly return what you offered to me. I am also very grateful to Trine B. and Anne G. who were both amazing women I met and had a lovely time. I do wish to meet them again and seek for this opportunity.

Thanks to my other family, those people who made me an expressive artist from Carol D., who initialized everything in various fields, to Maria C., who trusted me and dug all the emotions I never thought I could have. Here, have to be the ones that I saw almost every day, virtually or physically, and the ones that threw aside all my work concerns the moment I am with them. So then: Alenka, Isa, Daniela, Luciana, Ruben, Araceli, Ana, Luisa, Keysa, Karem, Eugenia, Mao, Alba, Ainhoa, Sara A, Miriam, Nadia, Carla. The moments we made art together are moments engraved in my nicest memories.

Thanks to to Villy C, Chiara P, and Isabel P, because without them, I would neither have discovered the joy of numerical modeling and simulation coding. To Guiomar, Marta Coll, the researchers from Norway, Jordi I, the researchers and technicians from ICM teaching me and guiding me with their experiences (Balbina, Emilio, Laura R, Amalia, etc…), to fishermen listening to my Spanish presentations or welcoming me on their boat. Speaking of boat, to the tribulación de García del Cid que han compartidos no solo momentos hermosos en mar pero también comidas, historias, y apoyos.

Thanks to the young crew of the ICM department, my old and new desk-mates from Xavier C, Mark F, Elena, and John R who dealt with my oddities such as my air conditioning intolerance and my bad desk posture. Thanks for their direct help and support when some issues appeared. Obviously, Marta A, Fafa, Alejandro, Joan M, Mariona, Federico, Vanessa, Anabel, Claudio, Ainhoa, Marta C., Carol, Marc B., Suzana, Guilia, Nuria, David, Dafni, who were there for works, parties, talks, calçotada,

congresses, holidays, fun and fun again. They made together, the department of Renewable Marine Resources, a lively place to work in. Besides, I have thankful thoughts for the students, post-docs and workers at HPL with who I regularly enjoyed international dinners, Wednesday's pizzas and Cambridge's life and who shared and helped me to explore the Eastern coast.

Thanks to Arthur, Jéremy, Charlie, my big boys that went through hardships like me, and are always a source of spiritual renewal. You made it, you will make it, soon it will be your turn. Thanks to Moshe and Gaetane, for all the hikes and my aside time, a group for hiking and outdoor activity that went beyond my expectations. True moments of freedom on the Pedraforca Mountain, along a GR or in rivers and sea. As persons, you inspire and motivate for more nature expeditions.

Thanks to my family, their education and morals which gave the will to be alone in a foreigner country. I believe it has a lot to do with my own background, but that were them who taught me how to be independent, autonomous and free. Then, to my mother, that is happy for me, but pouting at my wish not to come back to France, to my brothers and uncles, who came or not visiting me in Barcelona. To one of my grandmother, who never considered my working hours and had to deal with "I can't, I work". To my father, who surely is proud of me. To my grandparents that will count another Doctor in the family, not in medical fields, though.

Thanks.

Abstract

The connectivity of the deep-sea blue and red shrimp *Aristeus antennatus*, the most targeted species by trawl fisheries in the western and central Mediterranean Sea, is an information of interest for the management policies and contribute to shape the fishery-regulated areas, their sizes, and locations. In the northwestern Mediterranean Sea, genetic studies demonstrated high connectivity among the exploited shrimp populations living on the continental slope. Nonetheless, the process leading to the gene mixing has not been defined yet, which caused an issue for the fishery management. In fact, regulation can be addressed differently if the mixing is done by displacement of adults or by transport of larvae.

In this thesis, even though we lacked a strong knowledge about the shrimp egg and larval stages, we explored the larval transport that was assumed like the origin explaining high connectivity rates. To do so, several individual-based models (IBMs) were built by coupling hydrodynamic and Lagrangian transport models. They simulated the transport of the pelagic young stages by including hypothesis on the larval characteristics. With this method, we aimed to identify the larval traits that significantly modify the connectivity of the shrimp populations and to estimate the main paths of larval transport within variable hydrodynamics in time and space.

The IBM methods rely on the well-representation of the regional circulation that we checked by comparing the transport simulations between two differently-parameterized hydrodynamic models. The IBM methods rely as well on the model initialization driven by the spawners conditions such as the release time and location. For this last point, a species distribution model set on the spawner biomass allowed to adjust the locations of release.

With Individual-Based Models, we estimated high larval dispersal rates when a behavior simulated the rise of eggs toward the surface layers. Without behaviors, the eggs and larvae drifted close to the near-bottom and the length of the transport averagely measured 27 km. In that context, submarine canyons, which indent the northwestern Mediterranean margin, did not support significant vertical displacements. The needed behavior to implement an ontogenetic rise of the individuals was the buoyancy of the eggs, and possibly the nauplius as well. It was the only compatible behavior to provide a rise around 600 m (average depth of the spawning grounds) within the water column in a

few days. Consequently, because larvae accessed the warm and dynamic upper water layers, dispersal rates were amplified even though the temperature-dependent drift duration (also pelagic larval duration) was shortened. Because the water column is very well-stratified at summer, the connectivity path between sites depended on the depth position where the larvae drifted up to the moment they turned into early juveniles. Moreover, the surface Mediterranean Sea has many mesoscale circulations (e.g., eddies) that could retain the larvae nearby the spawning sites or prevent the larvae to cross a bottleneck channel. Besides, interannual drift simulations indicated that the time and location of a surface density front influenced the retention of larvae. This surface density front was located in the region of the submarine canyons and concentrated the individuals that were released at higher latitudes than the front position and underneath. In that same area, an IBM run backward in time showed that larvae collected at the surface during a meroplankton survey potentially came from different fishing grounds.

Overall, the results indicated that three regions within the NW Mediterranean Sea would drive three types of connectivity path because of the hydrodynamic and hydrography of the superficial waters. With additional analyses combining the fishery effort, the fishery management can consider to split the Spanish northwestern Mediterranean margin in two units: one around the submarine canyons, the other in the southern semi-enclosed basin bordered by the Gulf of Valencia and the Balearic Archipelago.

Resumen (Castellano)

Comprender los mecanismos que regulan la conectividad poblacional de la gamba roja de aguas profundas *Aristeus antennatus*, como especie objetivo de las pesquerías en el mar Mediterráneo occidental, es de gran interés para las políticas de gestión y puede contribuir a establecer tamaños y ubicaciones de áreas marinas protegidas. En el mar Mediterráneo noroccidental, estudios de genética poblacional de la gamba han mostrado que existe alta conectividad entre las diferentes poblaciones a lo largo del talud continental. Sin embargo, los factores que influyen en dicha conectividad aún se desconocen, lo cual dificulta la implantación de planes integrales de manejo. Las medidas de gestión podrían variar en función del mecanismo de conectividad ligado al desplazamiento de adultos o al transporte de huevos y larvas.

En esta tesis, a pesar de que se carecía de un conocimiento claro de los procesos de transporte de los huevos y larvas de la gamba roja, se exploró la dinámica del transporte larvario mediante simulaciones numéricas, para explicar las altas tasas de conectividad genética de las poblaciones. Para esto, se construyeron diversos modelos basados en el individuo (Individual-Based Models, IBM), combinando modelos de transporte hidrodinámico y de dispersión lagrangiana. Se simuló el transporte de larvas en sus primeras etapas de desarrollo, asumiendo diversas características larvarias, para identificar rasgos que pudieran estar influyendo de manera significativa en la conectividad entre poblaciones. Se identificaron diversas rutas de transporte larvario teniendo en cuenta las condiciones hidrodinámicas y sus cambios en el tiempo.

La construcción de los IBMs se realizó en varias etapas. Primero, se selectionó las salidas de modelos hidrodinámicos que se utilizaron en los IBMs. Segundo, se estimó la distribución espacial de los reproductores (adultos) y el tiempo de puesto mediante observaciones o el ajusto de modelos estadísticos que sirvieron para inicializar los IBMs. Tercero, las simulaciones realizadas para explicar la presencia en superficie de huevos de gamba y estadios tempranos de larvas y vincularla con las zonas en donde se encontraban los reproductores alrededor de 600 m de profundidad, requirieron de la aplicación de un factor de flotabilidad. De hecho, a los huevos a los que no se les aplicó flotabilidad, permanecieron cerca del fondo recorriendo distancias relativamente cortas de alrededor de 27 km, mientras que los individuos que alcanzaron la superficie mostraron una tasa de dispersión relativamente alta. Se determinó que la conectividad de las poblaciones entre

diversos lugares fue dependiente de la profundidad a la cual se encontraban los reproductores, ya que, a mayor profundidad, los huevos tardan más en llegar a la superficie y derivan a mayor distancia, al tiempo que eclosionan y se transformen en larvas.

En general, los resultados indican que, debido a la hidrodinámica e hidrografía de las aguas superficiales, existen tres regiones dentro del noroeste del Mar Mediterráneo que generan tres vías de conectividad de larvas: sin retención de larvas, con retención del 100% de las larvas producidas in-situ y con conectividad de diversos caladeros. En superficie, la presencia de eventos de mesoscala tales como remolinos, favorece la retención de larvas cerca de los sitios de desove y también puede evitar que las larvas cruzen el canal de Ibiza. Además, a partir de las simulaciones interanuales de la deriva larvaria, se encontró que el tiempo y la ubicación de frentes de densidad superficial modulan su dispersión. Un frente de densidad cercano a los cañones submarinos concentró a los individuos que fueron liberados en latitudes más altas. En esa misma área, las simulaciones con retroceso (backtracking), indicaron que las larvas recolectadas en la superficie mediante campañas de meroplancton, pueden provenir de diversos caladeros. Se sugiere la posibilidad de implementar dos unidades de manejo de la pesquería de la gamba en el Mediterráneo noroccidental español, que abarquen por separado el área alrededor de los cañones submarinos y por otra, la cuenca semicerrada más al sur bordeada por el Golfo de Valencia y las Islas Baleares.

Resum (Català)

La connectivitat de la gamba vermella d'aigües profundes, *Aristeus antennatus*, és de gran interès per a una adequada gestió pesquera. Aquesta espècie concentra el major esforç pesquer i reporta els majors beneficis econòmics de l'art d'arrossegament a l'oest i centre de la mar Mediterrània. El coneixement sobre la connectivitat d'una població contribueix a establir-ne els límits, dimensions i localització geogràfica i, per tant, ajuda a delimitar les àrees regulades de pesca. Els estudis de genètica poblacional duts a terme al nord-oest de la mar Mediterrània, demostren la existència d'una alta connectivitat entre les poblacions explotades de la gamba vermella present al talús continental. No obstant això, encara avui en dia hi ha una gran manca que coneixement sobre el procés que condueix a la barreja de gens, això impedeix una gestió pesquera acurada d'aquest important recurs. La barreja de gens depèn directament de si es dóna durant la fase larvària o post-larvària, és a dir, de si la barreja genètica es realitza per desplaçament d'adults o per transport de larves.

En aquesta tesi, s'explora el transport larvari com a hipòtesi principal de les altes taxes de connectivitat genètica. Malgrat les limitacions derivades d'una manca de bibliografia sobre les característiques físiques de l'ou de la gamba vermella i les seves etapes larvàries, hem construït diversos Models Basats en Individus (o *Individual-Based Models*, IBM). Aquests IBMs s'han basat en l'acoblament de models de transport hidrodinàmics i lagrangians. Utilitzant-los, hem simulat el transport de les etapes pelàgiques pre-adultes incloent hipòtesis sobre les característiques larvàries. L'objectiu d'aquesta tesi ha estat identificar els trets larvaris significativament determinants de la connectivitat entre les poblacions de gamba vermella i, a més, estimar les principals rutes de transport larvari, tenint en compte les variacions ambientals a nivell temporal i espacial.

Els IBMs necessiten d'una correcta representació de la circulació regional. Per això, en un primer estudi, hem contrastat els resultats del camp hidrodinàmic amb dos implementacions diferents de models de circulació. Pel que fa a la part biològica, les simulacions es basen en les condicions inicials dels reproductors, com el temps de posta i la ubicació de l'alliberament inicial de partícules. Així doncs, hem ajustat la ubicació de l'alliberament dels ous mitjançant un model de distribució d'espècies establert en base a

la biomassa reproductora de la gamba.

Per estimar altes taxes de dispersió de les larves hem inclòs la migració dels ous cap a les capes superficials pel canvi de flotabilitat, ja que, sense aquest efecte, el transport tant d'ous com de larves, es dona a prop del fons marí (amb una dispersió mitjana de 27 km). En aquest context, els canyons submarins que segueixen el marge del nord-oest de la mar Mediterrània, no comporten desplaçaments verticals significatius. En aquest treball, hem pogut determinar que el comportament determinant per implementar un moviment ontogenètic dels individus és la flotabilitat dels ous i, possiblement, també la dels nauplis. Aquest és l'únic comportament compatible amb l'ascens dels ous fins als 600 m (profunditat mitjana de les zones de fresa) dins de la columna d'aigua en només uns pocs dies. Així, degut a que les larves accedeixen a les capes superiors d'aigua, càlides i dinàmiques, les taxes de dispersió augmenten malgrat la disminució del temps de deriva. La connectivitat entre localitats queda definida per la profunditat en que es troben els individus entre la fase larvària i la fase juvenil. Això és degut a l'increment de l'estratificació de la columna d'aigua durant l'època estival i a l'elevada presència en la zona de remolins de mesoescala, fet que podria retenir les larves prop de les zones de fresa o impedir que les larves puguin creuar un canal poc profund. A més, les nostres simulacions de deriva interanuals indiquen que la duració i la ubicació dels fronts de densitat superficial afecten a la retenció de larves. Hem detectat que el front de densitat superficial localitzat a la regió dels canyons submarins concentra els individus, que acaben sent alliberats en latituds més altes o per sota de la posició del front. En aquesta mateixa àrea, la simulació lagrangiana en temps invers (*backtracking*) de l'IBM mostra l'origen forà de les larves recollides en la superfície durant un mostreig de meroplàncton (molt provablement arribades d'altres caladors).

En general, els nostres resultats indiquen que en les regions del nord-oest de la Mar Mediterrània estudiades s'observarien tres rutes de connectivitat diferents com a conseqüència de l'hidrodinamisme i la hidrografia de les aigües superficials. Aquests resultats revelen però la necessitat d'anàlisis addicionals que incloguin l'esforç pesquer. Així doncs, els resultats apunten a recomanar a l'administració pesquera de dividir el marge Ibèric del nord-oest de la Mediterrània en dues unitats: una al voltant dels canyons submarins en el talús continental i l'altra la conca semitancada que delimiten el Golf de València i les Illes Balears.

Abbreviations

ADCP: Acoustic Doppler Current Profiler

BC: Blanes Canyon

CCC: Cap de Creus Canyon

CL: Carapace Length

CODE: Coastal Ocean Dynamics Experiment

CONECTA: **CONECT**ividad poblacional en la gamba rosada ***A****risteus antennatus*

DNA: Deoxyribonucleic Acid

DSWC: Dense Shelf Water Cascading

DVM: Diel Vertical Migration

eq.: equation

FAO: Food and Agriculture Organization

GFCM: General Fisheries Commission for the Mediterranean

GSA: Geographical SubArea

IBM: Individual-based model

LIW: Levantine Intermediate Water

MAW: Modified Atlantic Water

MLD: Mixed Layer Depth

MPA: Marine Protected Area

NC: Northern Current

NW: Northwestern

PC: Palamós Canyon

PLD: Pelagic larval duration

PPD: Pelagic propagule duration

ROMS: Regional Oceanic Modeling System

SVP: Surface Velocity Program

Table of Contents

CHAPTER 1

1.1. Introduction

1.1.1. Population connectivity in the oceans

In the marine system, population connectivity refers to the geographically distant subpopulations that connect through the flow of organisms (Carr et al., 2017). Either pelagic or sedentary species can roam a few to thousand kilometers throughout several life periods from the dispersal of early stages (eggs, larvae, propagules) to the active migration of individuals (juveniles, adults).

Population connectivity encompasses the scale of *inter*- and *intra*-population exchanges. On an *inter*-population level (i.e., demographic), marine populations naturally or artificially fragment by perturbations of the migration path (i.e., the flow of organisms) and habitat losses (Hillman et al., 2018). For example, both the embrittlement of the coral ecosystem by the effect of water acidification (Cerrano et al., 2013) and the reduction of aquatic meadows by coastline anthropization (Montefalcone et al., 2010) illustrate the effect of environmental deterioration on population. On an *intra*-population level (i.e., individuals), the subpopulation distance is initiated by the organism mobility over its lifetime for physiological needs or functional traits like ontogenetic migration or migration towards feeding grounds (Pineda et al., 2007). On both levels, populations connect by following three types of individual exchange: unidirectional, bidirectional, and no exchange (see Figure 1). If the exportation rate of individuals is greater than the importation rate, the population is defined as a *source.* In the reverse case, the population is defined as a *sink* (see Cowen and Sponaugle, 2009).

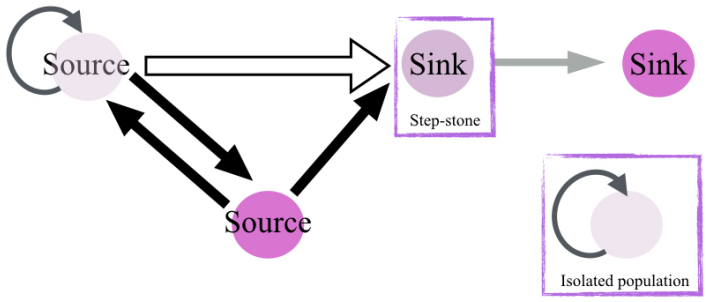

Figure 1. The complexity of the population connectivity and terminology corresponding to the direction and the rates of individual exchanges. Full circles and arrows represent populations and flows, respectively. The width of the arrows indicates an exchange rate.

Generally, the linkage of the population has positive repercussions for a given community and the ecosystem where the population resides. As one of the advantages from high connectivity rates, the genetic diversity guarantees the healthiness of population, which induces a better resilience to the various threats and stresses from the human activities, environmental changes, and water pollution (Sgrò et al., 2011). The genetic diversity takes origin in the pooling of multiple genomes during the mating of genetically different individuals (i.e., sexual reproduction). In contrast, spatially isolated population (*closed* population opposed to *open* population with high connectivity rates) are the most exposed to extinction in case of perturbations and diseases (Nichols et al., 2007; Johannesson et al., 2011). As one of the other advantages, mobile individuals favor the colonization of ecological niches (i.e., conditions that benefit their development). However, unbalanced connectivity alters the community and triggers the depletion of other marine communities blended in the ecosystem (Morel-Journel et al., 2016). If they newly settle into an already-existing ecosystem, organisms can quickly proliferate and disturb the endemic species by predation, food and "occupation" competitiveness, and diffusion of pathogen components (Gallardo et al., 2016; Pickett and David, 2018, Kough et al., 2014). Preceding the settlement and colonization of invasive species, an outlook of studies about invasive species often mentions indirect transports of pelagic organisms by ship-associated vectors (e.g., ballast, hulls, Cariton et al., 1993; Carlton et al., 2019) and by human-build channels (e.g., Lionfish by the Panama channel; Hixon et al., 2016).

Overall, connectivity studies can quantify the advantages and inconveniences of already-existing or future decision plans regarding the human activity. Knowing the conditions of a metapopulation such as the demography in *sink* and *source* populations and patchiness degree, are as important as knowing the network of individuals (i.e., flow, connection). There are several reasons for this: i) the source population can limit the quantity of exported individuals, ii) the perturbation of the flow can lead to the disappearance of a sink population, that iii) can be itself a step-stone population (i.e., population that receives and provides individuals, see Figure 1) or an important commercial resource. The knowledge about population connectivity helps create and manage protected areas (MPA) or fishery restricted areas, even though it is among the last criteria for the decision-makers (i.e., the 13th criteria out of 14 for designing protected areas; Balbar and

Metaxas, 2019). For the MPA, the connectivity studies allow verifying the replenishment of the population inside the protected grounds or beyond its boundaries (Carr et al., 2017). For fishery management, analyses can point out and define the areas on which population should be protected (Fogarty and Botsford, 2007). Connectivity studies may also interfere in decisions regarding the management of seabed mining industry (Lodge et al., 2014), the pipe network (van der Molen et al., 2018) and the building of underwater farms (fish farms, Uglem et al., 2009; windfarm, Bray et al., 2014) that can create step-stone habitats or perturb the existing ecosystem.

1.1.2. Connectivity of deep-sea shrimp *Aristeus antennatus*

Aristeus antennatus (Risso, 1816) is a commercially valuable deep-sea red and blue shrimp. This benthic decapod crustacean species lives off the continental margin from 80 m down to 3300 m depth of the Mediterranean Sea (Sardà et al., 2004) and associates with the homogeneous water masses of the Levantine Intermediate Waters (Sardà et al., 2009). Furthermore, its overall distribution spans on several management units shared among different countries and continents (Figure 2), with a decreasing abundance from the western to the eastern basin of the Mediterranean Sea (Cau et al., 2002).

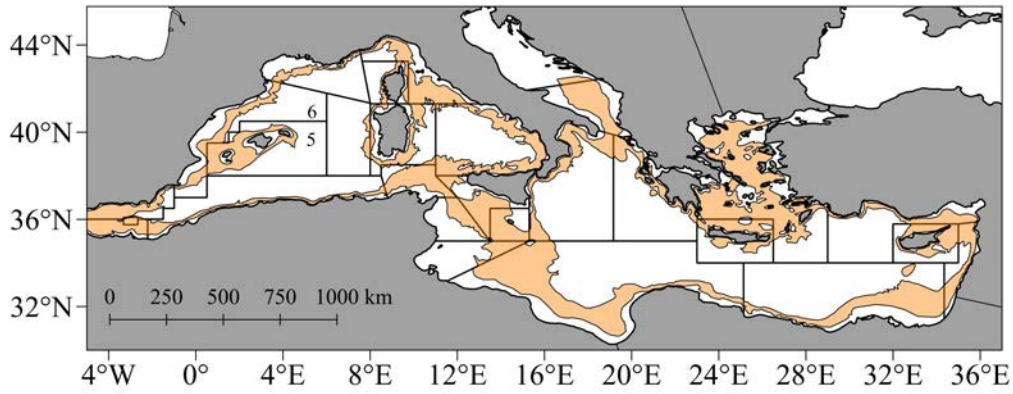

Figure 2. Distribution boundaries of the deep-sea red and blue shrimp *Aristeus antennatus* in the Mediterranean Sea (orange polygon) provided by the FAO. Geographical subareas (GSA) from management units of the General Fisheries Commission for the Mediterranean divide the sea. In the Ph. D. thesis, the studies mostly focused on the GSA6 with partial interaction on the GSA 5.

The deep-sea red and blue shrimp is one of the most targeted species for trawling boats along the Spanish coast of the Mediterranean Sea. Yearly incomes from the first sale of the shrimp reach 20% on average whereas the shrimp weight represents only 3% of total

landings. There, the fisheries are supported by favorable hydrography and the productivity of submarine canyons close to the harbors. Specifically, three submarine canyons (in the decreasing latitudinal orders: Cap de Creus, Palamós, and Blanes) are deeply indenting the continental margin. These places enhance the exchange of water and its components (sediment and organic carbon; Puig et al., 2003) providing favorable and diverse habitats for benthic species like *A. antennatus* (Fernandez-Arcaya et al., 2017). The deep-sea red and blue shrimp has a dynamic association with these structures like ontogenetic and seasonal migrations in and outside the canyons (Sardà et al., 1997; Tudela et al. 2003). Occasionally, the canyons flush superficial waters, which cause the departure of the shrimp from the fishing grounds (Company et al., 2008). Intense flushing events occur during dry and cold winters producing higher evaporation rates and cooling the sea surface, thus increasing the water density and initiating a deep-water formation event. The event cause water cascading along the margin that is, then, funneled inside the canyons (Canals et al., 2009). In the following 2 – 3 years after the event, the transport of particles (sediments, organic matters) down to about 1000 m depth by the Dense Shelf Water Cascading (DSWC) event (Canals et al., 2006) infers relatively high rates of small and young individuals in the catches.

The temporal disappearance of *A. antennatus* developed a collective conscious from the shrimp-dependent human activity toward fisheries sustainability. In the Palamós fishing ground, where the effect of the DSWC has been the strongest, a local management plan for reducing the fishing effort and protect the juveniles has been set since 2012 (BOE 2013, 2018). Therefore, since 2012, the fisheries on Palamós fishing ground have been monitoring the shrimp catches for analyzing signs of progress attributed to the management plan. Gorelli (2017) assessed the status of *A. antennatus* fishery in Catalonia in order to provide management advice. First of all, under the management plan imposing the use of 50 mm square mesh (instead of 40 mm diamond mesh), the gear better selected bigger shrimps (Gorelli et al., 2017). Additionally, the measure had an economically positive impact for fishermen from Palamós, illustrated by the increase of the yield per recruit (Y/R) and biomass per recruit (B/R). With that management strategy, the sustainability of the blue and red shrimp had positive consequences for the local shrimp population, and could be beneficial if the management plan expands to a regional scale.

Nonetheless, the sustainability of the stock is also reliant on the potential recruitment rate near the fishery ground. It is assumed that the recruitment occurs on bottoms beyond 1000 m depth (Sardà and Company, 2012), from where a ban from the GFCM forbid the use of dredge-like gear. This virgin stock is inhabited by abundant (in number) juveniles and male (Sardà et al., 2001), and constantly supports the recovery of the exploited stocks (D'Onghia et al., 2009) by the migration of individuals to upper parts of the slope. Given that the caught shrimps are potential spawners and that shrimp fecundity is size-dependent, bigger and older spawners are expected to release more offsprings (Orsi Relini et al., 2013), which could relatively rise the shrimp settlement rates over various grounds of the Catalan Sea. For a preserved population, three cases about the future settlement of offsprings are possible (see Figure 3). In Case 1, the offsprings from preserved shrimps (stock A) recruit on grounds close to another fishery exploitation stock (stock B). In Case 2, the offsprings settle close to the preserved stock. This is the most beneficial for fishermen under a local management plan. In Case 3, the recruits are provided from other external exploited stocks. For establishing how the stocks are linked among them, an effective way is to study the population connectivity.

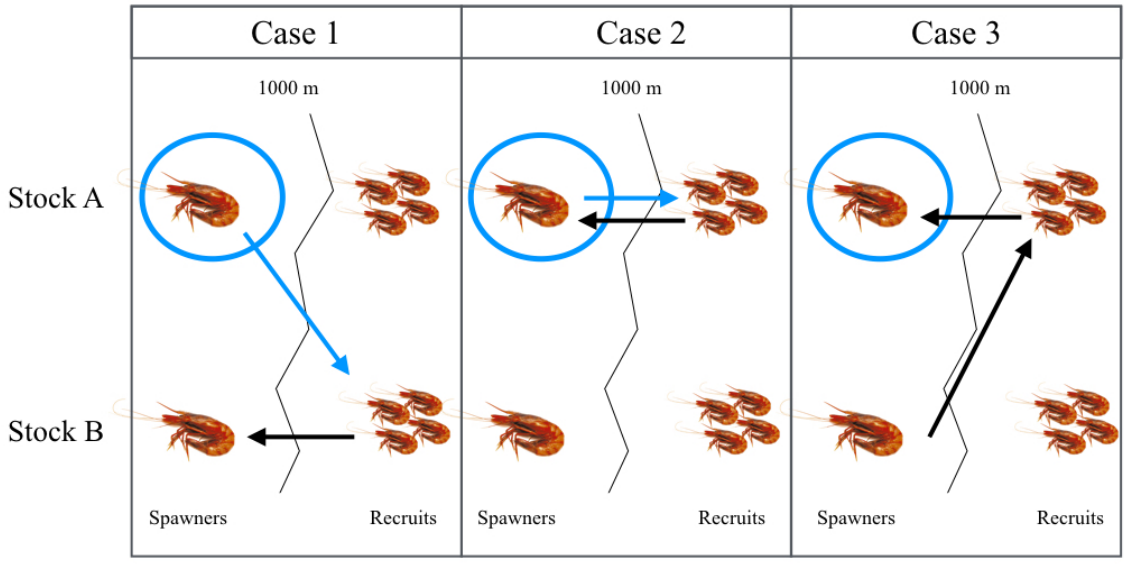

Figure 3. Relation of the spawners in a restricted fishery area (blue ellipse) with the recruits according to three different cases.

Connectivity among the populations of the deep-sea red and blue shrimp has been established on several scales in the Mediterranean Sea. Several genetic tools have been used (Mitochondrial DNA; Fernàndez et al., 2011, nuclear DNA; Cannas et al., 2012;

Sacci et al., 2011) and showed the homogeneous genetics between dispatched populations of the whole Mediterranean Sea. Between the eastern and western Mediterranean basins, it is not confirmed yet if the stocks are genetically distinct (Fernàndez et al., 2011) or not (Marra et al., 2015). However, in the western Mediterranean Sea, all the studies agreed that shrimps shared similar genetics, and consequently are (connected) open populations. On a smaller scale, studies of parental genetic between different Mediterranean Spanish harbors are to be analyzed, though preliminary results ascertained as well high connectivity rates between different Spanish stocks (Personal communication, MI Roldán, 2019). Sardà et al. (2010) also showed that the flow of genes occurs along the bathymetric gradient when juveniles from deeper layers migrate onto the upper part of the continental slope.

Genetic analyses provide good information for the stakeholders and management plan makers. However, the picture of the connectivity path has neither been described nor understood yet. Additionally, genetics is not always precise enough to retrieve the origin of the sample and to determine the connectivity path (Lowe and Allendorf, 2010). *A. antennatus* is a benthic and relatively sedentary species that do not migrate large distances, at worst, it moves a few hundred meters across the slope (e.g., juveniles migrating to adults area) and a few kilometers along the slope (e.g., seasonal displacement between open slope and canyons). Connectivity is therefore influenced by the transport of larvae. In particular, the peak of ready-to-spawn females occurs in July and August (Demestre and Fortuño, 1992) for the population in the Catalan Sea and larval transport is assumed to occur in summer by hydrodynamics processes.

1.1.3. Larval tracking

Larval tracking is a way to i) materialize the paths of drifting larvae, ii) better understand the hydrodynamic process behind the larval transport, iii) identify the barriers that modify the larval transport, iv) investigate which larval traits lead to connect known populations, and v) provide suggestion for monitoring the human activities (e.g., fishery management plans).

In general, larvae drift following currents and traveling from 10s to 100s kilometers (Cowen et al., 2006). Most marine species follow an r-selection strategy, which produce many offsprings affected by high mortality rate. For these species, the larva develops independently from the adult during a short period (compared to the lifespan of adults) in which they molt into various stages (Thorson, 1950). Free-drifting larva introduces greater consequences for sessile (like the corals) and sedentary adults (i.e., *A. antennatus*) than for oceanodromous species (e.g., migratory species like tunas, eels). Besides, paths and distances of larval transport are diverse as there is diversity of larval and adults characteristics within a species (i.e., larval morphology, larval development stages, larval behavior, spawning period and depth, see Dibacco et al., 2006, Treml et al., 2015).

Pineda et al. (2007) suggested that the larval dispersal and the post-larval survival are the components defining population connectivity. Larval dispersal is itself an outcome from the larval transport affected by survival and settlement rates. In the thesis, we were conscious that numerous rates (survival, mortality, settlement) could not be estimated and we decided to loosen up these previous definitions. We use the notion of connectivity without pretending to quantify the contribution of a population to another (i.e., also called potential connectivity in Watson et al. (2010)) and the notion of larval dispersal as equivalent to larval trajectory/transport/path.

The larval transport modeling (a demographic modeling approach) is a tool that is expected to be useful for population connectivity studies. In following such methodology, a particle can represent several tiny elements of the marine system, such as viruses, plastics, spores, eggs, or larvae, which are transported by external forces because of their size. The particle virtually follows the circulation in regions simulated by a hydrodynamic model. In opposition to the pelagic and coastal species, the study of deep-sea connectivity through larval transport modeling is scarce and challenging to approach. Yet, deep-sea species living off the floor are more likely to be greatly affected by anthropogenic activities such as fishing and deep-sea mining deteriorating the seabed (Clark et al., 2016; Jones et al., 2017).

The issues restraining models of the deep-sea larval dispersal rose from lacking knowledge on the larvae and modeling limitations. First, information about deep-sea larvae is mostly inexistent due to costly requirements for harvesting the larvae or rearing them in the laboratory (especially for non-carrying eggs species). Contrary to demersal and pelagic species, the spatial scale of deep-sea larvae dispersal accounts for the whole water column (> 200 m) and the open ocean, resulting in great amounts of meroplanktonic sampling effort (*tiny* gear for big ocean) during the reproductive cycle of the adults (if known). Larvae of deep-sea species can drift in deep water as well at the surface (Arellano et al., 2014) with different developmental strategies, like stopping or abbreviating the larval phase (Pradillon et al., 2005; Mileikovsky, 1971). Consequently, most of the deep-sea larvae are unknown and larvae can be mistaken to other species (i.e., monster larvae; Bracken-Grissom et al., 2012). Second, solved physical models mostly focus on circulation at the surface, which neglects the deep-sea flow variability. Indeed, superficial mesoscale circulation can propagate in deeper circulation (Adams et al., 2011), near-bottom flows are constrained by the topography (Vic et al., 2018) and friction of the currents in sharp topography generates deep-sea mesoscale variability (Gula et al., 2016). Last, in deep-sea, where the average water temperature is no higher than 3 ºC, the larval development takes a few days to several years depending on the species and its habitats (Hilario et al., 2015). Such long duration of larval dispersal requires multi-annual and ocean-scale hydrodynamic outputs for complying with the larval dispersal extent (Vic et al., 2018), that are not originally assigned for deep-sea studies.

Nonetheless, modeling strategies with simplistic concepts are developed for overcoming these issues. The modeled trajectories initially start at the reproductive period and from the area where the deep-sea adults spawn. Then, larvae drift passively in the water masses where they were released. So far, deep-sea larval transport studies often consider the effect of pelagic larval duration and sometimes include the vertical position variability of the larvae. If non-existent, empirical or laboratory estimates of larval duration are rare though the knowledge from similar species (i.e., genetically close species) gives approximated values for the larval transport simulation (Etter and Bower, 2015; Metaxas et al., 2019; Palmas et al., 2017; Young et al., 2012). When enough data are available, the non-linear relationship between the larval duration and the water

temperature can be developed for further hydrographic consideration in the modeled larval drifts (Yearsley et al., 2011). Among studies considering the larval position in the water column, the modeler can define a depth based on collected larvae in which the virtual organisms will passively drift (Young et al., 2012; McVeigh et al. 2017). Few numerical studies implement the interactive locomotion of the larvae according to their traits (i.e., egg size, stages) and the hydrography of the water mass (Cardona et al., 2016; Palmas et al., 2017) and a bunch of them used real or approximated values of the larval traits (Beaulieux et al., 2015; Mori et al., 2016). Eventually, larval duration or dispersal depth can be estimated by establishing sensitivity scenarios in such a way that values allow the larvae to settle at the correct place (McVeigh et al. 2017).

Overall, studies of deep-sea larval connectivity lack of sufficient information for disclosing the entire life cycle of the species including the life cycle of larvae. For the case of *A. antennatus,* before summer 2016, just a few larvae were found at the surface (Carbonell et al. 2010; Heldt, 1954; Seridji, 1971), which prevented to produce significant results about the larval ecology and potential connection with deep-sea spawners. Fortunately, during the planktonic survey from CONECTA project in summer 2016, larvae were found in abundance in the surface water of the NW Mediterranean Sea (Carretón et al., 2019). Although this collection of larvae enlightened several aspects of the early life cycle, larval behavior and biology remain unknown. Furthermore, the scientific survey targeted the capture of larvae by sampling the water columns over a large area where shrimp female gathered (i.e., mainly above the continental slope). Thus, the survey gave a small snapshot of the potential larval distribution in the Catalan Sea but more samplings is necessary to fully understand the distribution pattern of the species.

1.1.4. Objectives and structure of the Ph.D. thesis

Aiming for studying the larval transport and connectivity of *A. antennatus* requires overcoming uncertainties regarding the larval biology, larval behavior, and the influence from the Mediterranean Sea hydrodynamics. If most of shrimp larval traits can be generalized and can also apply for other similar species, the adult ecology and dynamics of the shrimp at spawning period remain species-dependent, so that even studying the larval transport with few generic environmental and biological conditions is a step forward for understanding the population connectivity.

So far, the connectivity of the shrimp by parental genetic is high but connectivity path and the contribution rate from a population to another one remain uncertain. The main objectives of this thesis are to 1) model the essential larval traits of *A. antennatus*, which would efficiently modulate the connectivity path and 2) identify the main larval trajectories and their uncertainties induced by the hydrodynamic variability.

The following chapters are dedicated to estimate the connectivity path of A. antennatus from simplistic larval dispersal simulations to complex scenarios. In every chapter, the source of uncertainty is analyzed by parametrizing a stepwise larval transport model including influential larval traits or hydrodynamics variability.

In **Chapter 1**, the passive larval transport was assessed, only advected by near-bottom currents simulated by two different hydrodynamic models. We estimated the main oceanic drivers for supporting efficiently the larval drifts and the uncertainty in the trajectories delivered by hydrodynamic models.

In **Chapter 2**, we raise the importance of the larval ecology for sustaining vertical displacement of larvae towards advantageous waters. The effect of buoyancy on the youngest larval stages and the effect of sensible changes in the hydrodynamics were tested to detect the parameters generating the largest uncertainties in the larval dispersals. Issues produced by the scarce knowledge on *A. antennatus* larvae were overcome by performing simulations and analyses on the egg buoyancy and the pelagic larval duration.

Chapter 1 and **Chapter 2** were dedicated to overcome the lack of knowledge about the shrimp larvae. They provided enough understandings for making more accurate simulations of larval transport.

In **Chapter 3**, we adjusted the place of spawning females by modeling the spatial spawner distribution along the continental margin. We focused on the spatiotemporal variability of the spawner distribution within the canyons, which provided relevant information linked to the scope of the results in Chapter 1.

In **Chapter 4**, the knowledge acquired from the previous chapters (1 – 3) allowed to run interannual simulations of the larval dispersals. This chapter highlighted the impact of temporal changes in the northwestern Mediterranean Sea mesoscale circulation on the larval dispersal and retention.

In **Chapter 5**, we took advantage of having the real distribution of larvae from the CONECTA cruise in summer 2016 to identify other potential sources of uncertainties in connectivity and to have a most realistic estimation of the population connectivity. A larval transport model was parameterized to track back in time the provenance of larvae found during the survey.

1.2. General Methodology

Larval transport is supported by several biological and physical mechanisms that are highly variable in time and space. For addressing the connectivity of *A. antennatus* and filling up the knowledge gap about the pelagic stages of the shrimp, multiple dissociated or combined steps were carried out before or during the larval tracking simulations. Firstly, the larval cycle was approached. Secondly, the larval traits having relevant influences were identified. Finally, the hydrodynamics of the studied areas were assessed. Once these steps were completed, then larval transport was simulated in the Lagrangian tracking model framework.

1.2.1. Larval cycle and characteristics

Neither information about the early-life cycle of *A. antennatus* shrimp nor the behavior during the embryonic and larval development are available from literature. However, the knowledge gaps can be alternatively filled with data from other species that are taxonomically close to *A. antennatus*. The closest species of the blue and red shrimp are within the Aristeidae family that are also from the deep-sea realm (Figure 4). Nevertheless, larvae of this family are not known or rarely collected. Another group of closest specimens is the Penaeidae family and relatives (i.e., Trachypenaeidae, Parapenaeidae), which mostly are from coastal or estuarial environments, and therefore, easier to collect and breed.

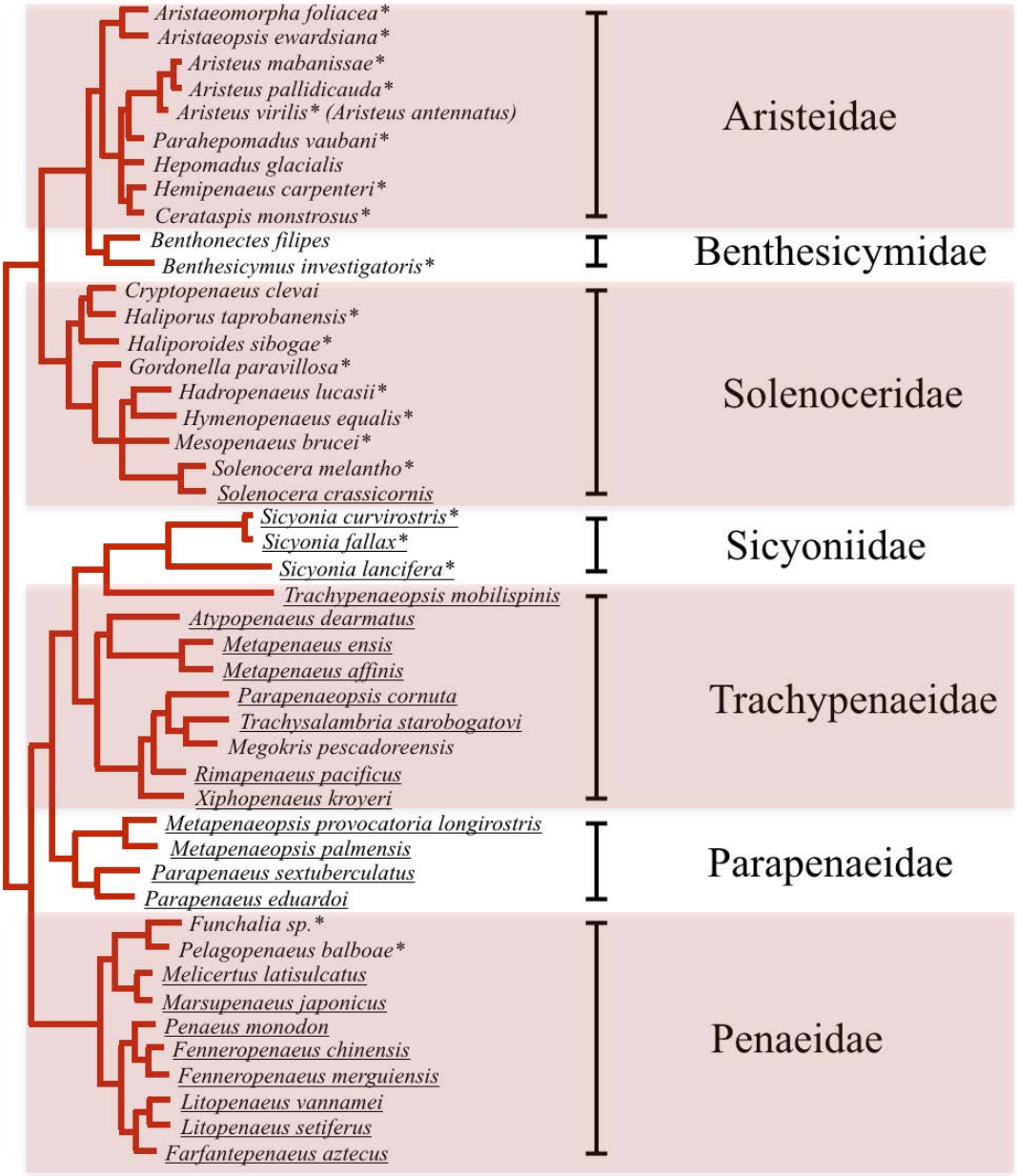

Figure 4. Phylogenetic relation of Penaeoidae species from a Bayesian Inference analysis (extracted and adapted from Ma et al., 2009. Species related by a few nodes were genetically close species. Species marked with stars are deep-sea species (see Table S1). Underlined species are species that have various larval studies (see Table S1). *Aristeus antennatus* was not in the original analysis, however, according to Fernández et al., 2013, the species is close to *Aristeus virilis*.

Assuming that coastal and estuarine species are taxonomically close to each other, we can use this information for setting larval transport models. The egg morphology is comparable and they are not carried by adults but develops and hatches in pelagic waters. Eggs are small, ranging between 160 and 720 um (Dall et al., 1990), among which the sizes of *A. antennatus* oocytes (yet-to-be-spawn eggs) belong (Demestre and Fortuño, 1992). Eggs activate when fecundated and produce a relatively large perivitelline space conferring to the eggs a potential positive buoyancy. Moreover, the larval stages show

similar morphology (Figure 5), that results in misidentification of the species with another (e.g., *A. Antennatus* with *Gennadas elegans* and *Aristomorphocea foliacea*; Carretón, M., pers. comm.) and their development is conditioned by the water temperature (Dall et al., 1990).

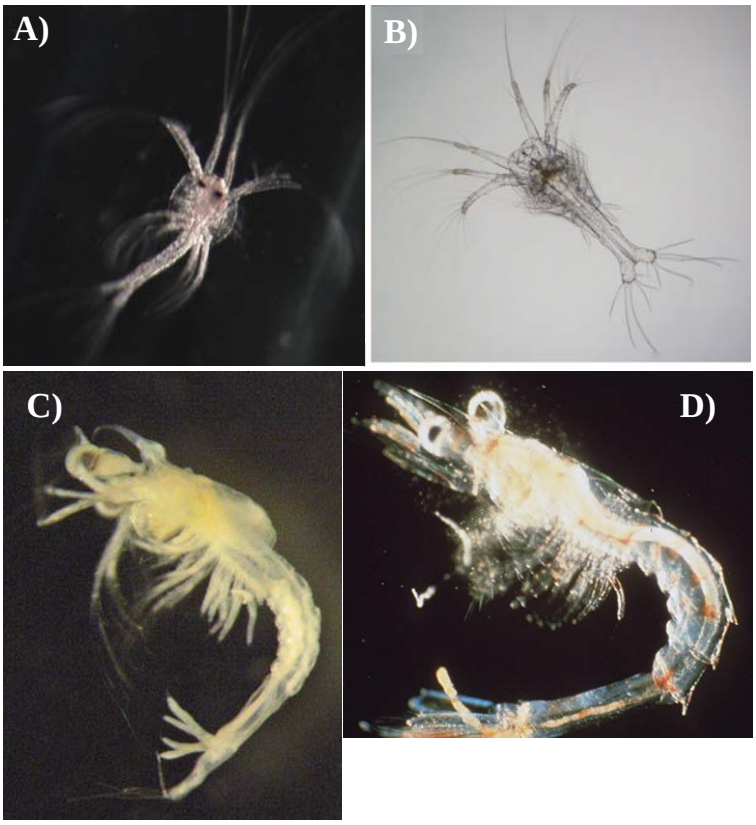

Figure 5. The larval stages of protozoea (A and B) and mysis (C and D) for *Aristeus antennatus* (A and C), *Litopenaeus vannamei* (B) and an undefined Penaeid species (D). It shows the similar appearance of larvae from the same suborder (Penaeidae). Credits: M. Carretón (*A. antennatus*); Pérez-Morales et al., 2017 (*L. vannamei*); Estévez et al., 2019 (unidentified Penaeid larva).

After hatching, Penaeid larvae develop into several stages of nauplius, protozoea, and mysis which have peculiar morphology inferring different ways of swimming. Swimming abilities are poorly known because most of the Penaeid larval studies focus on the hydrographic condition and the diets that optimize their growth instead of their behavioral ability. Nauplius is a lecithotrophic stage which swims thanks to the rowing movement of the antennas. The swimming is chaotic and not very well described. Protozoa can stabilize its position by pleopod activation but can displace bigger distance by rowing with its antennas as well. Mysis has a locomotion mechanism close to the adults by contracting the abdomens and using the telson (Chu and Wong, 1996; Martin et al., 2014).

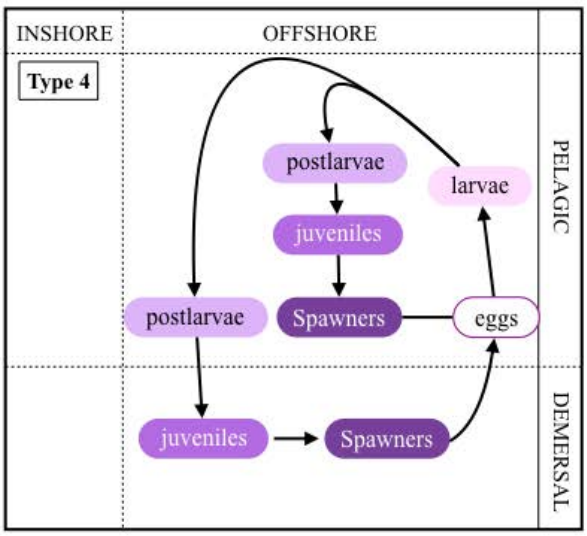

Figure 6. Type 4 of Penaeids larval cycle, extracted from Dall et al. (1990). Types are built from the vertical distribution and the ecosystem of the adults before spawning.

Besides, life cycles and behavior of Penaeid larvae depend on how close to the coast the adults are. Dall et al. (1990) resumed four types of larval cycles (see example Figure 6) which consider the spawners ecosystem (i. e., estuarine, inshore, offshore) along with its position in the water column (demersal and pelagic). One type (Type 4 in Figure 6) describes the larval cycle for deep-sea Penaeid species that represents the best assumption on the larval cycle of *A. antennatus*. It is that eggs are spawned by benthic females and hatch into larvae in pelagic waters. Larvae are then molting in several stages while drifting in the open-oceans, and then they turn into postlarvae that swim downward to the recruitment ground.

Larval characteristics, such as like the behavior and biology of the specimens, group a lot more of individual features that affect the larval trajectory (Metaxas, 2001). On the one hand, the behavior component groups the larval capacities for moving either passively with buoyancy forces or actively by random or oriented swimming in reactions related to the environment (North et al., 2009). Subsequently, the larvae can access to better water conditions (for feeding and growing, Fiksen et al., 2007), to a suitable settlement habitat (Leis and Lockett, 2005), and to be relatively less exposed to predation (Gray and Kingsford, 2003). On the other hand, the biological component clusters all the morphological aspects and physiological preference from which larvae are dependent to reach the post-larval stages. Within this cluster, we count the pelagic larval duration, the growth rate, the mortality rate, the water quality that are, most of the time, estimated

values from reared larvae. A large part of the knowledge is provided by bred species with optimal ranges of temperature and diet which allow a quick development into a viable post-larvae to improve the productivity and cost effectiveness of the farms. Yet, most of the laboratory-estimated values have to be used with precaution, as they consider optimal laboratory conditions not reflecting the high oceanographic variability. For example, Leis (2010) indicates that the *in situ* (in the ocean) larval swimming velocity can be 30% lower than the critical speed of the larvae in the lab.

Generally, swimming behavior and pelagic larval duration influence efficiently the larval dispersal on the length of the trajectories while the other larval traits are indicators of the larval status and condition the connectivity rate (Treml et al., 2015). A number of studies (e.g., Corell et al., 2012) suggested that the swimming ability of larvae has a major influence on larval dispersal on the vertical dimension. That is, water column divides into several layers having different hydrographic ranges and amplitudes of current that cause the transport to be longer in time or on distance. The same concept applies for species with free-drifting buoyant eggs that place at water column depth according to the water density and egg density. Paradoxically, the shallower water layers are also the warmest, which shortens the pelagic larval duration (O' Connor et al., 2007) and balances the distance of the larval transport in the very dynamic surface waters (Corell et al., 2012).

1.2.2. Influence of the Mediterranean Sea on larval transport

In larval transport, the principal displacement drivers are the hydrography and hydrodynamics. In fact, hydrography of water masses contains abiotic components regulating the larval metabolism, growth, development, and mortality. Water temperature and salinity may have prominent variations in the horizontal dimension (e.g., gradients between coastal and open ocean waters, at fronts, and at upwelling interfaces) and the vertical dimension (water stratification), which affects the larval transport. Last but not least, the timing and place of larval release/hatching tied to the biology of the spawners eventually modify the connectivity between subpopulations (Dibacco, 2008) because water masses and current flows change within a few days over relatively small spatial scales.

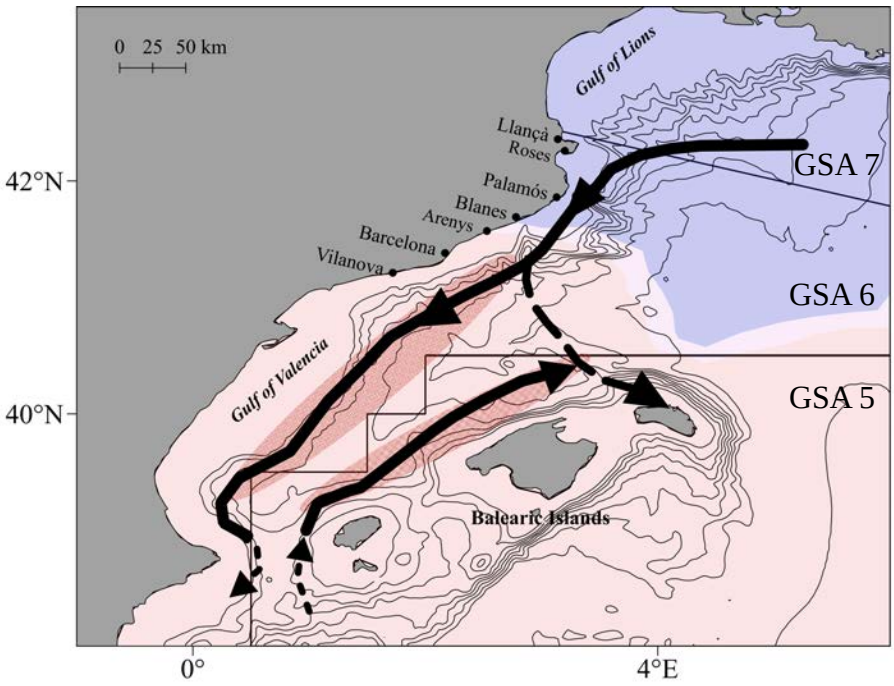

Figure 7. Map of the northwestern Mediterranean Sea and main surface regional hydrodynamic patterns. Blue and red waters colors represent the average position of the recent and old Modified Atlantic Water, respectively. Black arrows are the main current called North Current for the jet going southward and the Balearic Current along the Balearic Islands. The continental margins are places of density front (red ellipses). Eddies are not represented because of their temporal variation but are evoked in the text. Adapted from Pascual et al. (2002).

As for the western Mediterranean Sea, this basin is characterized by three vertically discretized water masses. Surface waters belong to the Modified Atlantic Water (MAW) mass, a surface layer deep to 100/200 m that is strongly stratified during summer (Salat, 1996). The summer MAW is relatively warm and saline and is exposed to high spatiotemporal variability because of the river discharges, the evaporation, and wind stress. Old and recent MAW (Figure 7) are distinguished based on the water residence time and water temperature (e.g., old MAW is distinctly warmer). The interface between old and recent MAW forms the North Balearic Front, also called the Pyrenean Front. In summer, the front is located in the northern part of the western Mediterranean Sea (López-García et al., 1994). Below the MAW and down to 600/800 m, the Levantine Intermediate Water (LIW) mass issued from the eastern Mediterranean basin, with homogeneous hydrography stabilizing at 13 – 13.8 ºC and 38.48 – 38.60 PSU (Salat and Cruzado, 1981). Deeper than the LIW, the Western Mediterranean Deep Water mass is slightly colder (12.7 – 12.9 ºC) and less saline (38.42 – 38.48 PSU) than the LIW (Béthoux et al., 1990). Overall, the deep Mediterranean Sea has elevated water temperature and salinity compared to the global and average values in the deep ocean (i.e., 0 – 3 ºC and 35 PSU).

Regarding hydrodynamic processes, the water circulation expands or reduces the larval transport at different spatial and time scales. Multiple circulation scales encompass the whole basin circulation to small perturbation features (see Figures 7 and 8) characterizing the northwestern Mediterranean Sea hydrodynamics. On relatively large time (months) and space (100 km or more) scales, strong regional geostrophic currents and jets are well-known wind-driven hydrodynamic features extending the larval transport. The main surface current of the northwestern Mediterranean Sea is called the Northern Current (NC) and flows southwardly following the continental slope. It is partially influenced by the anti-clockwise Gulf of Lions gyre and by north winds (Tramuntana and Mistral). The jet can reach up to 30 cm s^{-1} and be maximum underneath the surface, with a core 50 km wide and 250 m deep at summer (García-Ladona et al., 1996; Lapouyade and Durrieu de Madron, 2001). At the Eivissa channel, the NC splits and either crosses the channel or forms the Balearic Current, which follows a northward direction along the Balearic Islands (Castellón et al., 1990). Those currents are guided by density fronts, called the Catalan and the Balearic shelf/slope density fronts (Font et al., 1988; Salat, 1995), respectively, with short fluctuation periods (< 1 month) induced by the slope topography (Albérola et al., 1995; Jorda et al., 2013).

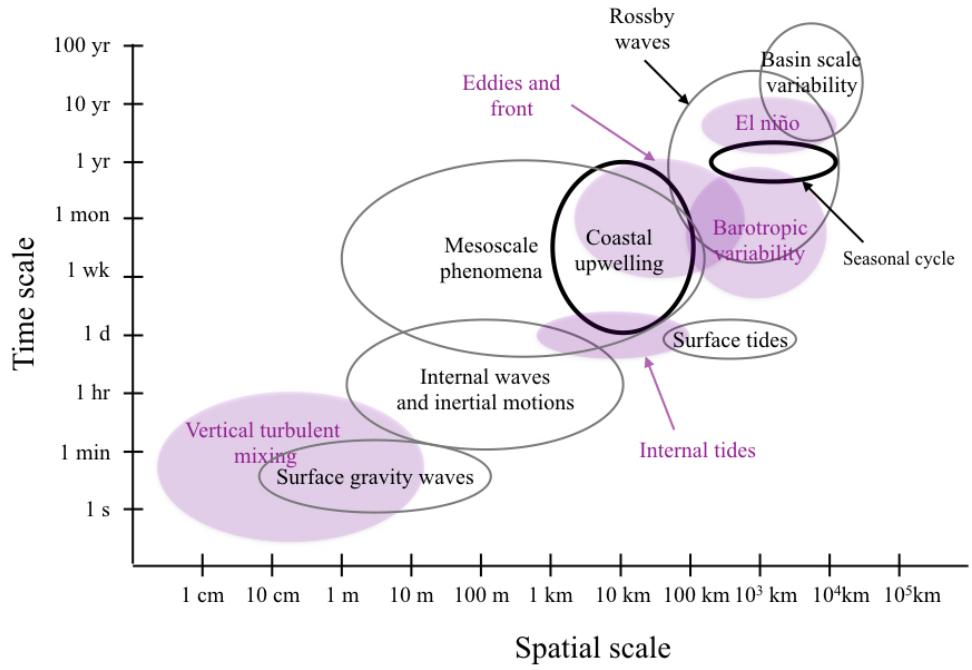

Figure 8. Spatiotemporal scales of major ocean processes and transporting the larvae. Representation adapted and accredited to D. Chelton.

On a middle time (days to a week) and space (10 to 100 km) scales, various circulation patterns may enhance or limit the larval drift such as eddies, tides, and upwellings. Tides in the Mediterranean Sea can be neglected, but several eddies form and disappear during summer. Their appearance is linked to instabilities of the NC due to the continental margin shape (e.g., where the continental shelf narrows in the western zone of the Lion Gulf (Hu et al., 2011) and widens at the northern zone of the Gulf of Valencia (Olivar et al. (2010)), or due to the interface of different water masses (e.g., at the Balearic channels; Lafuente et al. (1995) and the density fronts; Pascual et al. (2002)). Lifetime and diameters of eddies vary around couple of weeks and grow to a maximum diameter before disappearing (Condie and Condie, 2016; Rubio et al., 2009). Eddies have trajectories following the main current (i.e., NC or Balearic Current) and transport aggregated small organisms such as larvae, zooplankton, and phytoplankton (Sabatés, et al., 2013; Villate et al., 2014). The topography of submarine canyons is specifically the source of many mesoscale circulations. First, it creates meanders from the main current if it flows above the canyon rims (Ahumada-Sempoal et al., 2013). Second, NC also generates downwelling and upwelling of water masses along the canyon walls (Ahumada-Sempoal et al., 2015; Jordi et al., 2006). Third, the submarine canyons have closed circulations (Palanques et al., 2005) with relatively frequent short-term variability (Solé et al., 2016). To conclude, due to those small-scale internal circulations, larvae are bound to be retained (Ahumada-Sempoal et al., 2015).

Last, small scales of ocean processes gather the water turbulences and waves, which generally increase the dispersion of larvae around the main trajectory (North et al., 2004; Monismith and Fong, 2004). On the vertical dimension, the horizontal water dynamics is stronger at the surface than the layers a few meters below. In contrast, vertical water circulation is 10 to 100 times lower than horizontal currents, except under specific forcings such as water cascading (Canals et al., 2009) and frontal areas (Vélez-Belchí and Tintoré, 2001).

1.2.3. Modeling methods for tackling connectivity of *A. antennatus*

Model simulations are useful tools incorporated into various marine system studies and resolve more or less complex equations on different time/spatial scales. In the present thesis, statistical and numerical models are used to process and estimate the lacking data on the larval traits, the hydrography and hydrodynamics of the Mediterranean Sea, and the displacements of the larvae.

Statistical models were used to fill the knowledge gap with robust estimations. They approximate the best relationship between a dependent variable and a set of explanatory predictors. After setting a statistical model, the lacking information was estimated through a new set of explanatory predictors that become inputs for the initialization of larval tracking models. In this thesis, we modeled complex and non-linear relationships between the spawner distribution and environmental variables for defining places were releasing the eggs. Multiple linear regressions were also fitted for estimating the pelagic egg and larval duration of *A. antennatus* according to water temperature.

Modeling the larval trajectories follows the concept of individual-based models and couples hydrodynamics, particle tracking algorithm, and concepts of larval ecology. In those models, each particle represents the early life stages (eggs and larvae) and has various evolving characteristics. These particles are displaced in two or three dimensions by a Lagrangian particle tracking algorithm that estimates the movements of the particles based on the current velocity fields (meridional, zonal, and vertical components). In parallel, mathematical modules can be included in the larval tracking model, which include equations upgrading the larval states or inferring the larval behavior. Those modules lean on already-known relationships, like the growth rate and the terminal velocity due to buoyancy, or they lean on rates applied under certain environmental conditions encountered by the larvae during transport simulation, like mortality rate induced by lethal temperature. While accurate connectivity rates are expected by increasing model complexity, the implementation of influential behaviors can also be sufficient for the scope of the study (North et al., 2009). Larval tracking models quickly

provide estimations of connectivity, given that the tools are used appropriately and that the outputs are validated.

The drawbacks of modeling lay in the necessity to gather expertise from several fields (biologist, physician, oceanographers, and informatics) and to have enough information for validation of the simulations. Nonetheless, in the last two decades (1998 – 2018), several studies about the numerical modeling of larval transport emerged (e.g., 2 to 100 studies per year, setting search in Web Of Science: theme = larva* AND theme = modeling AND theme = connectivity). In those studies, various marine research categories are mixed: “Marine Freshwater Biology” (305 studies), “Ecology” (299 studies), “Oceanography” (250 studies) and “Fisheries” (102). Those entangled categories show that larval transport studies have a purpose for investigating the relation of living organisms to the ecosystem dynamics (“Oceanography”) and the impact of human activities (“Fisheries”). In the last decades, the improvement in new technologies and computational power also allowed to run the numerical models faster, to implement longer larval transports, and to consider much more complex analytic (i.e., the possible impact of larval behavior) or predictive (i.e., possible impact of a new offshore structure) scenarios.

Most of the time, models of larval transport are run offline with outputs from hydrodynamics models that provide water velocities and hydrography on three-dimensional grids. Hydrodynamic models involve the physical principles of continuity (e.g., water energy, and mass conservations), momentum conservation (fluid motions) and tracer transport (temperature and salinity) for estimating the flow dynamics in a region. Hydrodynamic models are first initialized with inputs representing coarse water circulation within the domain and forcings at the grid borders. These forcings are atmospheric (at the air-sea interface), tidal, from river runoff and from the open boundary (ocean outside the domain’s limits). Second, the spatial and the time resolution for resolving equations are essential parameters for seizing the different oceanographic processes (see Figure 8; Pineda et al., 2007) though they also compromise with the computational run time. Last, good performance of hydrodynamic models comes from selecting an adjusted discretization of the vertical layer. The models can have fixed depth (z-layer model), stretched terrain-following layers (sigma-layer model) or a hybrid of the

two according to the objectives of the modelers and the studied region. In conclusion, building and running hydrodynamic models need a number of preparation files, running time and validation effort, which means that they are not exclusively created and adapted for larval transport modeling.

1.2.4. Supplementary information

Table S1. Species (sp.) of Penaeoidae used in Figure 4. for phylogenetic tree. Depth range was extracted from Sea Life Base.

Family	Genus	species	Depth range	Studied larvae?	Reference with larvae
Aristeidae	*Aristeus*	*virilis*	188 – 1500	n/a	
	A.	*mabahissae*	475 – 1084	n/a	
	A.	*pallidicauda*	600 – 700 (1)	n/a	(1) Koamai, 1993
	Parahepomadus	*vaubani*	880 – 1200	n/a	
	Cerataspis	*monstrosus*	495 – 5060	Rare	Lira et al., 2017
	Hemipenaeus	*carpenti*	900 – 4030	n/a	
	Hepomadus	*glacialis*	Abyssal (2)	n/a	(2) Dall, 2001
	Aristaeomorpha	*foliacea*	60 – 1300	Rare	Heldt, 1955
	Aristaeopsis	*edwardsiana*	274 – 1850	n/a	
Benthesicymidae	*Benthesicymus*	*investigators*	0 – 1690	n/a	
	Benthonectes	*fillipes*	1270 – 1910 (3)	n/a	(3) Crosnier and Forest, 1973
Solenoceridae	*Cryptopenaeus*	*clevai*	300 – 540	n/a	
	Haliporus	*taprobanensis*	700 – 1200	n/a	
	Haliporoides	*sibogae*	100 – 1463	n/a	
	Gordonella	*paravillosa*	870 – 1886	n/a	
	Hadropenaeus	*lucasii*	150 – 1200	n/a	
	Hymenopenaeus	*equalis*	200 – 1362	n/a	
	Mesopenaeus	*brucei*	488 – 880	n/a	
	Solenocera	*melantho*	78 – 400	n/a	
	S.	*crassicornis*	0 – 175	Yes	Holthuis, 1980 Cheung, 1963
Sicyoniidae	*Sicyonia*	*curvirostris*	100 – 806	Other sp.	Paulinose, 1982a
	S.	*fallax*	150 – 806	Other sp.	Paulinose, 1982a
	S.	*lancifera*	8 – 250	Other sp.	Paulinose, 1982a
Trachypenaeidae	*Trachypenaeopsis*	*mobilispinis*	0 – 100	Other sp.	Paulinose, 1982a
	Atypopenaeus	*dearmatus*	0 – 274	Other sp.	Paulinose, 1982b
	Metapenaeus	*ensis*	8 – 95	Yes	Chu, 1991
	Metapenaeus	*affinis*	5 – 92	Yes	Thomas et al.
	Parapenaeopsis	*cornuta*	1 – 37	Other sp.	Hassan, 1984
	Trachysalambria	*starobogatovi*	0 – 80 (4)	Other sp.	(4) Chan et al., 2016 Matsuno and Abe, 2006
	Megokris	*pescadoreensis*	n/a	n/a	
	Rimapenaeus	*pacificus*	2 – 100	Other sp.	Ditty and Salas
	Xiphopenaeus	*kroyeri*	0 – 70 m	Yes	Maris, 1986
Parapenaeidae	*Metapenaeopsis*	*provocatoria*	60 – 480	Other sp.	Choi and Hong, 2001
	M.	*palmensis*	5 – 100	Other sp.	Chong and Sasekumar, 1993; Ronquillo and Saisho, 1997
	Parapenaeus	*sextuberculatus*	136 – 600	Other sp.	Dos santos, 1998
	P.	*eduardxoi*		Other sp.	Landeira et al., 2009 Torres, 2015 (thesis)
Penaeidae	*Funchalia*	*sp.*	0 – 2000	n/a	
	Pelagopenaeus	*balboa*	0 – 1609	n/a	
	Melicertus	*canaliculatus*	0 – 50	Yes	Choy, 1984
	Marsupenaeus	*japonicus*	0 – 90	Yes	Hudinaga, 1942
	Penaeus	*monodon*	0 – 150	Yes	Motor, 1979
	Fenneropenaeus	*chinensis*	90 – 180	Yes	Heng and Rui-yu, 1994
	F.	*merguiensis*	10 – 55	Yes	Motor and Buri, 1979
	Litopenaeus	*vannamei*	0 – 72	Yes	Kitani, 1986
	L.	*setiferus*	0 – 119	Yes	Anderson et al., 1949
	Farfantepenaeus	*aztecus*	0 – 200	Yes	Cook and Murphy, 1971

CHAPTER 2

Section 2.1.

Influence of the summer deep-sea circulations on passive drifts among the submarine canyons in the northwestern Mediterranean Sea

Morane Clavel-Henry
Jordi Solé
Miguel-Ángel Ahumada-Sempoal
Nixon Bahamon
Florence Briton
Guiomar Rotllant
Joan B. Company

Congress oral presentation: The Crustacean Society, Mid-Year Meetings 2017, Barcelona. Spain.
Conference: Pesca i Ciència - V Jornada tècnica sobre la Gamba de Palamós, 2018, Palamós. Spain.
Congress poster: Fish Forum 2018, Roma, Italia.

Published in **Ocean Sciences 15 (2019). doi: 10.5194/os-15-1-2019**

Abstract

Marine biophysical models can be used to explore the displacement of individuals in and between submarine canyons. Mostly, the studies focus on the shallow hydrodynamics in or around a single canyon. In the northwestern Mediterranean Sea, knowledge of the deep-sea circulation and its spatial variability in three contiguous submarine canyons is limited. We used a Lagrangian framework with three-dimensional velocity fields from two versions of the Regional Ocean Modeling System (ROMS) to study the deep-bottom connectivity between submarine canyons and to compare their influence on the particle transport. From a biological point of view, the particles represented eggs and larvae spawned by the deep-sea commercial shrimp *Aristeus antennatus* along the continental slope in summer. The passive particles mainly followed a southwest drift along the continental slope and drifted less than 200 km considering a pelagic larval duration (PLD) of 31 days. Two of the submarine canyons were connected by more than 27% of particles if they were released at sea bottom depths above 600 m. The vertical advection of particles depended on the depth where particles were released and the circulation influenced by the morphology of each submarine canyon. Therefore, the impact of contiguous submarine canyons on particle transport should be studied on a case-by-case basis and not be generalized. Because the flows were strongly influenced by the bottom topography, the hydrodynamic model with finer bathymetric resolution data, a less smoothed bottom topography, and finer sigma-layer resolution near the bottom should give more accurate simulations of near-bottom passive drift. Those results propose that the physical model parameterization and discretization have to be considered for improving connectivity studies of deep-sea species.

2.1.1. Introduction

Lagrangian particles coupled with three-dimensional hydrodynamic models are useful to assess the impact of ocean circulation on the drift of small elements or individuals. It allows for the exploration of various scenarios of dispersal and increases knowledge in several fields of marine systems, such as predicting the direction of oil spills (Jones et al., 2016); understanding the circulation of microplastics (Lebreton et al., 2012); estimating the impact of aquaculture (Cromey and Black, 2005); and describing the spatial

dispersion of crustaceans, fish, and other marine larvae (Ahumada-Sempoal et al., 2015; North, 2008; Ospina-Alvarez et al., 2013). Particles in the open ocean are susceptible to advection between locations, influenced by regional currents and mesoscale features such as eddies and meanders (Ahumada-Sempoal et al., 2013). The particles without implemented behavior are called passive and are efficiently used to study the inactive transport of elements. They also provide a useful approximation of larval drifts when the ecological knowledge on the early life cycle is scarce. The individual-based models (IBM) configure each Lagrangian particle with characteristics parameterized by the modeler. In marine ecological studies, IBMs provide a representation of the potential connectivity between geographically separated subpopulations, with implications for fishery management and conservation plans (Andrello et al., 2013; Basterretxea et al., 2012; Kough et al., 2013; Siegel et al., 2003).

Simulation of marine passive drifts provides a picture of the highly dynamic circulation in the vicinity of the submarine canyons. Influence of canyons on the transport of particles and living organisms has begun to raise interest, but only a few studies are dealing with the Lagrangian transport of particles specifically in those small-scale topographic structures (Ahumada-Sempoal et al., 2015; Kool et al., 2015; Shan et al., 2014). In the northwestern (NW) Mediterranean Sea, several submarine canyons, whose heads are incising the continental shelf (i.e., Cap de Creus, Palamós, and Blanes canyons), generate mesoscale features from the main circulation pattern (Millot, 1999) called the Northern Current (NC). When the NC crosses a canyon, it causes a downwelling on the upstream wall and an upwelling on the downstream wall in the 100 – 200 m layer depth (Ahumada-Sempoal et al., 2015; Jordi et al., 2006), or it causes the opposite at lower depths (Flexas et al., 2008). Within the canyons, near-bottom currents produce a closed circulation (Palanques et al., 2005; Solé et al., 2016), which loses strength with the depth (Flexas et al., 2008; Granata et al., 1999). The canyon shape enhances the downwelling of water and its components (sediment and organic carbon; Puig et al., 2003, biogenic or inorganic particles; Granata et al., 1999), and it provides favorable and diverse habitats for benthic species (Fernandez-Arcaya et al., 2017). Those exchanges proceed at different velocity rates following the condition of the waters. For example, cascading of winter water masses drives suspended substances along the funnel structure of the canyons (Canals et al., 2009). In summer, the stratification of the water column is well-established in the NW Mediterranean Sea decoupling the mixed layer

from the rest of the water column (Rojas et al., 1995) and slowing the downward sink of biogenic particles (Granata et al.,1999). During that season, the circulation of the NC is shallower (250 m deep), wider (50 km wide) and less intense than in winter (Millot, 1999).

To date, the impact of the circulation on the dispersal of particles was estimated with hydrophysical data (Ahumada-Sempoal et al., 2015; Granata et al., 1999; Rojas et al., 1995) and with sediment traps (Durrieu de Madron et al., 1999; Lopez-Fernandez et al., 2013) in shallow waters above the NW Mediterranean submarine canyons. None of the previous studies simulated the particle transport at a deeper layer or showed the particle exchanges among different water layers of submarine canyons. Information on the roles of the upper part of the canyon on both horizontal and vertical transport of particles is not clear (e.g., 0 – 300 m; Granata et al., 1999), and for deeper parts this information is rarely provided. In accordance with those facts, we questioned if the deep-sea circulation mechanism in each submarine canyons of the NW Mediterranean Sea can be generalized.

In this study, deep passive drifts along the NW Mediterranean continental slope are simulated to determine the influence of the summer circulation modulated by the presence of the submarine canyons. We partly focused on the drift sensitivity to deep circulation using the outputs of two hydrodynamic numerical models to approach the transport uncertainties. With this study, we are expecting to provide a first insight into the deep connectivity between submarine canyons to improve the management of their grounds, namely of the deep-sea shrimp *Aristeus antennatus*.

2.1.2. Materials and Methods

The influence of deep circulation on passive drifts among the submarine canyons of the NW Mediterranean Sea was analyzed through the dispersal of Lagrangian particles.

2.1.2.1. Hydrodynamic models

The sensitivity of dispersal to the circulation was generated with the use of two available hydrodynamic models, which covered the area of the submarine canyons in the

northwestern Mediterranean Sea (see Figure 9). Because of the parameterization related to the topography (i.e., bathymetric data sets and smoothing) and the vertical layer discretization in the two hydrodynamic models, small differences in morphology of the submarine canyons were expected to impact the flow circulation.

The two hydrodynamic models were climatological simulations using the Regional Ocean Model System (ROMS; Shchepetkin and McWilliams, 2005), a free-surface terrain following primitive equations ocean model. ROMS includes accurate and efficient physical and numerical algorithms (Shchepetkin, 2003). The two models were referred to by their implementation versions, ROMS-Rutgers and ROMS-Agrif (Debreu et al., 2012), for the sake of clarity. In the present paper, the ROMS-Rutgers configuration and its validations are presented, while ROMS-Agrif has already been used and validated in Ahumada-Sempoal et al. (2013, 2015).

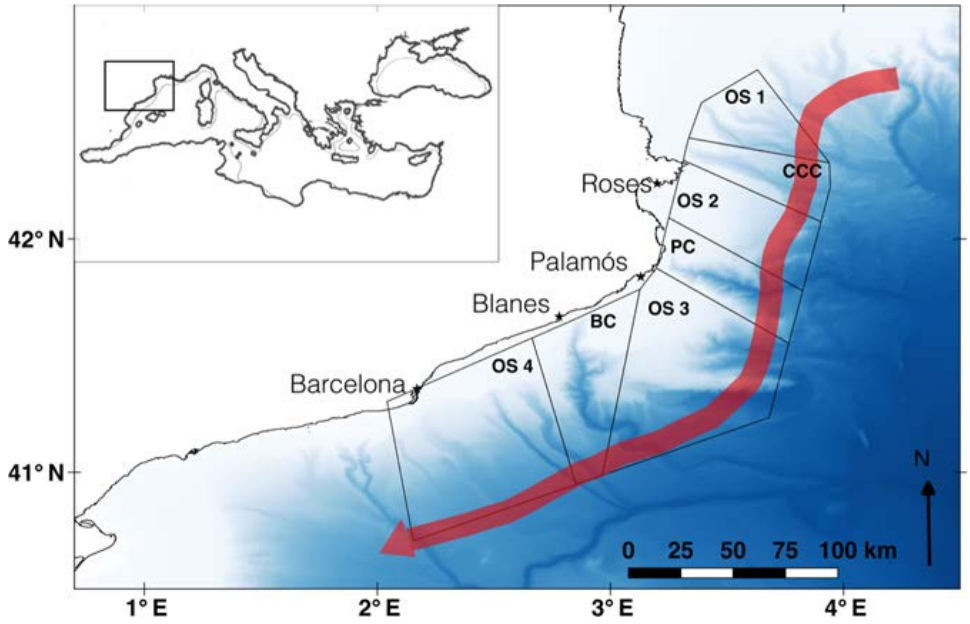

Figure 9. Map of the study area. Release zones are represented along the northwestern Mediterranean Sea: open slope (OS) 1, Cap de Creus canyon (CCC), OS 2, Palamós canyon (PC), OS 3, Blanes canyon (BC), and OS 4. The red arrow indicates the direction of the Northern Current. Bathymetry was extracted from EMODnet (http://www.emodnet-bathymetry.eu).

The ROMS-Rutgers model was forced by a climatological atmospheric forcing. The air temperature, shortwave radiation, longwave radiation, precipitation, cloud cover, and freshwater flux used to force the model came from the ERA-40 reanalysis (Uppala et al., 2005). Surface pressure came from the ERA-Interim reanalysis (Dee et al., 2011). All

these variables had a spatial resolution of 1° and a time resolution of 6 h. QuikSCAT blend data were used for wind forcing (both zonal and meridional). The wind had a spatial resolution of 0.25° and a time resolution of 6 h. The boundary conditions were obtained from NEMO (available from https://www.nemo-ocean.eu/, last access: March 2012; these simulations were reported in Adani et al., 2011) and interpolated to the ROMS grid to define a sponge layer of 10 horizontal grid points with a nudging relaxation time of 30 d. This methodology for the implementation of the model in the area followed the same procedure as the one already tested in the Alboran Sea (Solé et al., 2016). This model implementation was already used in previous publications as a hydrodynamic model coupled with a fisheries model (Coll et al., 2016).

The simulation domain ranges from 0.65° W to 6.08° E and from 38 to 43.69° N. The grid resolution is 2 km (with 256 × 384 grid points horizontally) and the vertical domain is discretized using 40 vertical levels with a finer resolution near the surface (S coordinate surface and bottom parameter are $\theta_S = 5$ and $\theta_b = 0.4$). Thus, the thickness of the near-bottom layer on the continental slopes delimited by the 500 and 800 m isobaths is 24 m (± 3.2 m). The advection scheme used in our simulations was MPDATA (recursive flux-corrected 3-D advection of particles; Smolarkiewicz and Margolin, 1998) and Large–McWilliams–Doney (LMD) mixing as a subgrid-scale turbulent mixing closure scheme (Large et al., 1994), also known as the K-Profile Parameterization (KPP) scheme. The air–sea interaction used for the boundary layer in ROMS was based on the bulk parameterization (Fairall et al., 1996). Bathymetry grid with a horizontal resolution of 100 m was provided by the Geoscience department of the Institute of Marine Sciences (ICM-CSIC, Barcelona) and fitted to the grid of the model. We ran the ROMS-Rutgers model version 3.6 using climatological atmospheric forcing and boundary conditions. The initial conditions to start the simulations were obtained using the same interpolated fields as the ones used for the boundary conditions for all variables. After an 8-year spin-up period with a baroclinic time step of 120 s, we used the ninth year as the study period.

The regional ROMS-Rutgers implementation has been daily saved and validated. First, we compared the simulations with the coarser model used for the initial and boundary conditions (NEMO). Second, the model was compared to the ARGO float vertical data

profiles of temperature and salinity to test the correct structure of the simulated water column within the year. For the ARGO tests, we selected 1900 casts in the area from October 2003 to December 2012. The data collected cover depths from the surface down to a maximum of 720 m. The ARGO vertical profile resolution was 5 m from the surface to 200 and 25 m from 200 to 720 m. We grouped the ARGO casts by months and by six subareas dividing the domain according to the Coriolis force divided by the bottom depth (Figure 10). Then, we selected the subareas that have more than 30 ARGO profiles for each month, we calculated a monthly averaged profile of ARGO, and we compared them with the modeled climatologic profile (monthly average).

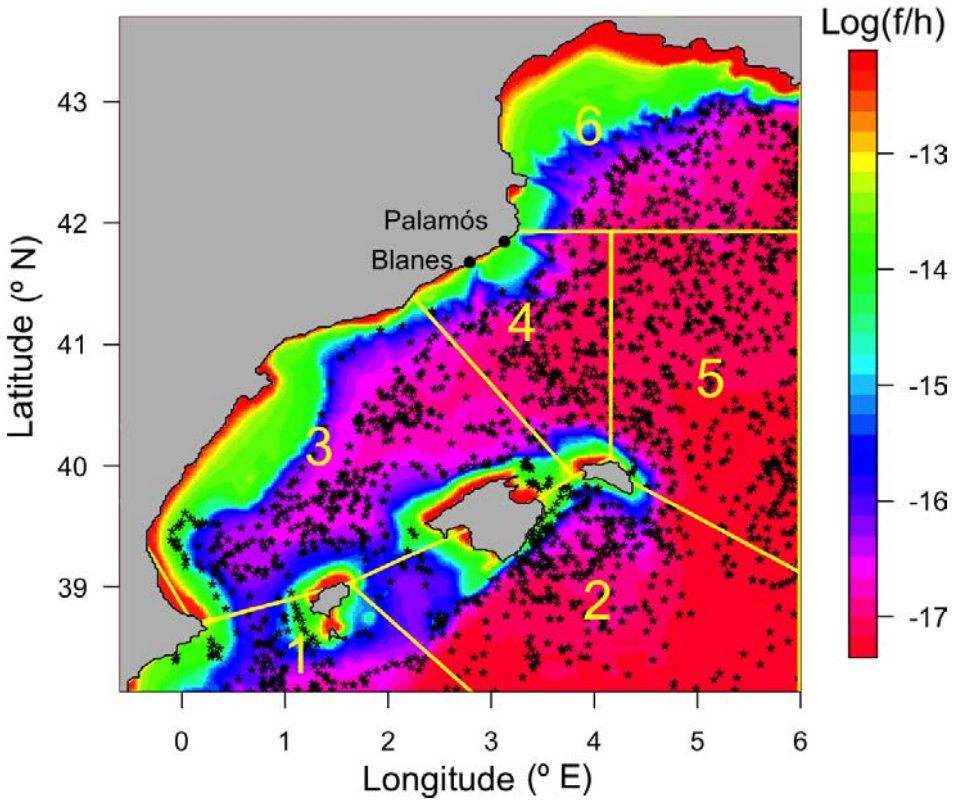

Figure 10. Map of the ROMS-Rutgers model domain and position of ARGO buoys. The color bar represents the Coriolis parameter (f) divided by the depth (h) (f / h in a zebra color palette). The six subareas selected to validate the model using ARGO float observations are shown by yellow polygons. The black dots in the domain represent all the ARGO profiles considered.

The main general behavior of the ROMS-Rutgers model simulation was coherent with the lower-resolution model (NEMO) and with the reported hydrography of the northwestern Mediterranean Sea. The model also successfully reproduced the main seasonal behavior of the different water masses. A Taylor diagram (Taylor, 2001) was used to display the correlation, root mean square error (RMSE), and standard deviation

(SD) between the monthly averages of the ROMS-Rutgers model profiles and ARGO profiles by subareas (Figure 11). The comparison showed reasonably good correlations of statistical significance. For temperature, the correlation between model and ARGO was higher than 0.7 during 10 of the 12 months, while for salinity it was higher than 0.95 for all the months. As it is shown in Figure 11, during the month of September, the correlations in the Taylor diagram for temperature and salinity were higher than 0.9 in both variables. The month of September was selected because the thermocline in our domain disappears and the mixing process at that period of the year is likely to vary the most. Consequently, it shows that the circulation over different depths has been well reproduced in the model.

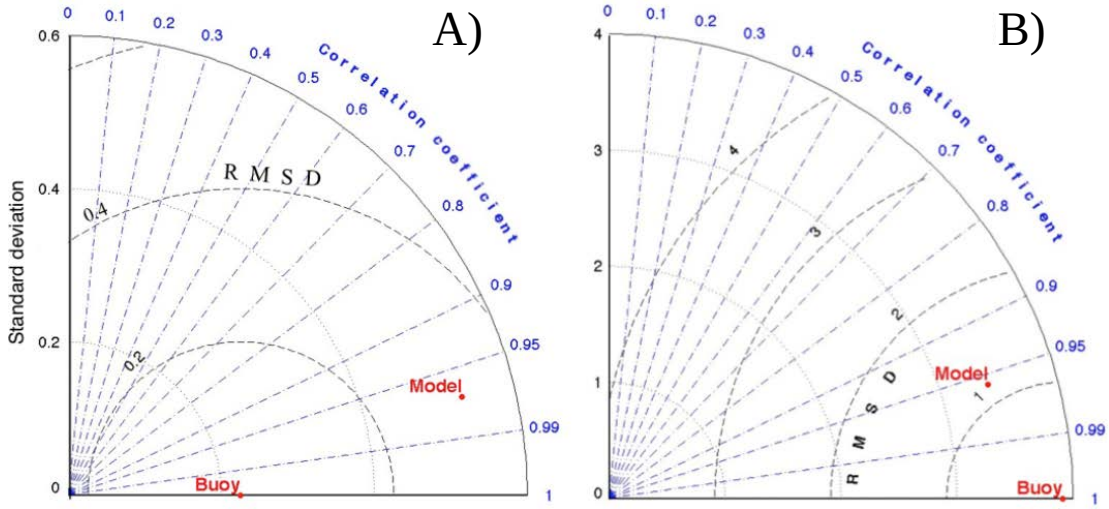

Figure 11. Taylor diagrams for validation of ROMS-Rutgers. Example of comparison between buoys (ARGO floats) and ROMS-Rutgers model simulations during September. The temperature of float versus model (A) and the salinity of float versus model (B). Radial from the origin (0, 0) are the correlation coefficients, internal circles centered on the origin are standard deviations, and internal circles centered at the buoy position are root mean square differences (RMSDs).

The second set of velocity and thermodynamic fields was provided by ROMS-Agrif, built and validated in Ahumada-Sempoal et al. (2013). The simulation domain ranges from 40.21 to 43.93° N and 0.03° W to 6° E. It has a finer horizontal resolution (~ 1.2 km), with 32 sigma levels of a finer resolution near the surface and coarser resolution near the bottom (S coordinate surface and bottom parameters are θ s = 7 and θ b = 0) than ROMS-Rutgers. The average thickness of the near-bottom layer is 54 m and is approximately 2 times thicker than the near-bottom layer from ROMS-Rutgers. The model was one-way nested from a coarse regional resolution model of 4 km. Bathymetry was derived from the ETOPO2-arcminute model (with horizontal grid resolution of 3

km) from Smith and Sandell (1997). Surface forcing and initial and boundary conditions were built with the ROMSTOOLS package (Penven et al., 2008), running a 10-year simulation of the model.

In the ROMS-Rutgers configuration, the bottom circulation followed a southward direction along the bottom slope, except in the area south of Blanes canyon (Figure 12.A). Over the bottom floor of the continental slope, the highest velocities reached 8.5 cm s^{-1} on the southern mouth of Palamós canyon. The fastest vertical velocities were at sea bottom deeper than 400 m and are mostly located among the submarine canyons. The minimum and maximum velocity values (-1.4 and 1.7 mm s^{-1}, respectively) were located in Palamós canyon. In ROMS-Agrif, the hydrodynamic model had higher near-bottom currents in the areas at the north and south of Palamós canyon. The maximum velocity reached 11.6 cm s^{-1} off the continental slope between Palamós and Blanes canyons. Higher intensities of vertical near-bottom current were also in those areas (see Figure 12.B) even though the most extreme values of vertical velocity were -1.23 and 1.11 mm s^{-1} on the bottom off the continental rise.

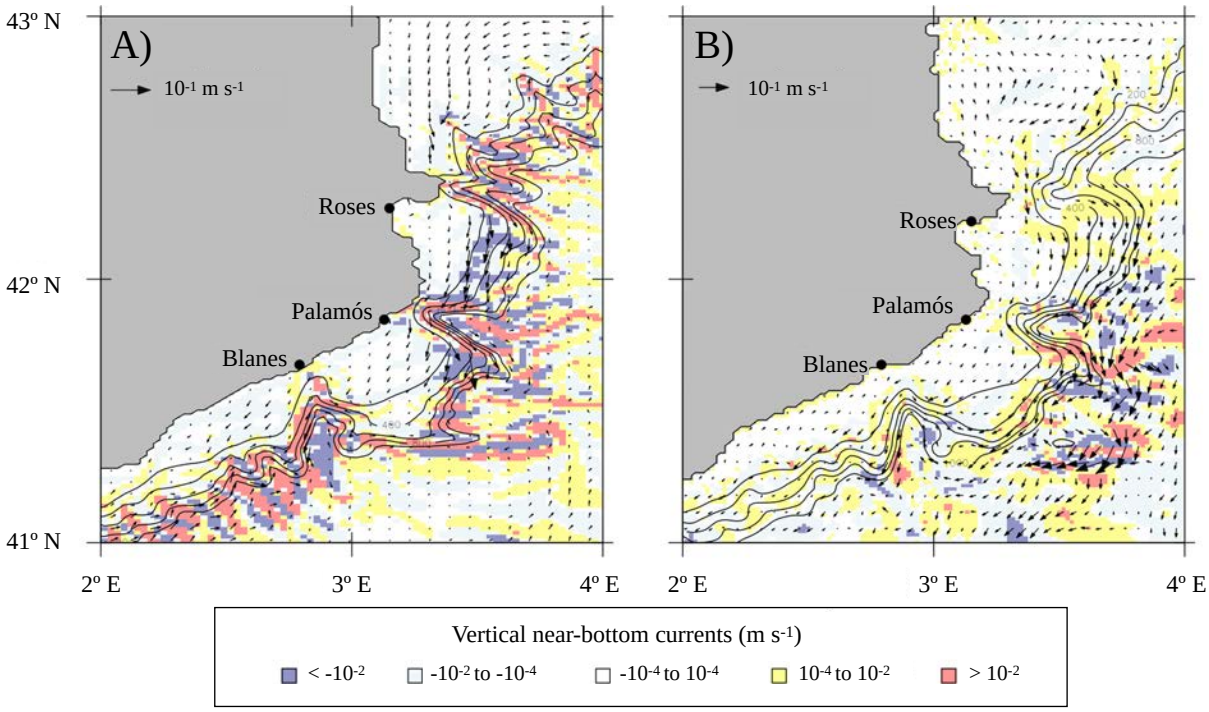

Figure 12. Vertical velocity and horizontal velocity vectors at bottom in the northwestern Mediterranean Sea in the ROMS-Rutgers (A) and ROMS-Agrif models (B). Colors from blue to red according to the downward or upward (negative or positive) vertical velocity. Continuous black lines are the isobaths adapted from the bathymetry of the hydrodynamic models.

2.1.2.2. Practical study

In this study, we considered some characteristics of the deep-sea shrimp *Aristeus antennatus* for the initial configuration of the simulated passive drifters. *A. antennatus* is a benthic commercial species distributed over the area of study (Demestre and Lleonart, 1993; Sardà et al., 1997), and it is an important source of income for the fishing harbors of the NW Mediterranean Sea (Gorelli et al., 2014).

The spawning peak of *A. antennatus* (i.e., release of particles) occurred in summer (July to September; Demestre and Fortuño, 1992) in the sea bottom delimited by the isobaths of 500 and 800 m, i.e., on average 650 m (Sardà et al., 1997; Tudela et al., 2003) at midnight (Schram et al., 2010). The ecology of the early pelagic stages (eggs and larvae) is hardly known due to the difficulty to catch the larvae in the open sea and to keep the adults in captivity alive.

For setting the duration of simulated drift, we used the pelagic larval duration (PLD) of the shrimp, i.e., the time a larva spends in the water column from spawning to the first post-larval stage. As individuals of the superfamily Penaeidae (which contains the species *A. antennatus*) release eggs in the environment before hatching (Dall et al., 1990), the PLD definition was extended to account for the duration of the embryonic stage. To overcome the situation of an unknown PLD for *A. antennatus*, we fitted a linear model to the relation between the duration of eggs developing into the post-larvae stage from 43 penaeid species by reviewing research articles (see Table S2) and the temperature of the water in which the larvae were reared. The linear model, whose initial assumptions were verified (see Figure S1) and had a coefficient of determination R^2 = 56%, was the following:

$$PLD = 64.71 \cdot exp(-0.06 \cdot T) \qquad (1)$$

where T is water temperature in degrees Celsius. Then, the effect of water temperature on the duration of the larval stage had the shape of an exponential law (O'Connor et al., 2007; Pepin, 1991). When particles were at the deep-sea bottom, we could estimate their PLD to be 31 days because the seawater temperature was approximately 13.2 °C. The duration appeared to be shorter than the PLD for other deep-sea species (Arellano et al.,

between those values according to a given factor (e.g., release zone, canyons, and hydrodynamics models) was significant.

In this study, the last position of the particles was attributed to the zone beneath the particle. The proportion of particles released from a release zone reaching a settlement zone was displayed in a connectivity matrix. Each cell represents the proportion of particles $P_{i,j}$ from a zone i that has settled into a zone j:

$$P_{i,j} = N_{i,j}/N_i \qquad (4)$$

where (i, j) is in the interval [1 : 10], $N_{i,j}$ represents the number of particles settled in the zone j which has been released in zone i, and N_i is the number of particles released in zone i. Retention proportions are assumed to be the ratio of particles that remained in the zone where they were released ($P_{i,i}$ with $j = i$) and appear on the diagonal of the matrix.

2.1.3. Results

Dispersal of particles in both configurations of ROMS had common general patterns and mostly diverged on the transport magnitude.

2.1.3.1. Lagrangian dispersal within the ROMS-Rutgers outputs

Releases in canyons generally made the drift distance larger and variable (Figure 13). Lagrangian simulations carried out with the ROMS-Rutgers model transported particles over 27 km on average and up to 111 km for the longest trajectory. First, from the canyons, passive particles drifted 33 km, 6 km more than the average distance, while from open slopes, particles drifted 25 km, which was 3 km less than the average distance. Besides, the highest average drift distance was 36.3 km (± 15.1 km) from the releases in the PC. Second, when released on the northern walls of the canyons, the particles drifted 29 km, which was 10 km less than the particles released on the southern walls. Last, the open slope 1 (OS 1) and OS 3 were the release zones with the shortest transports from which particles drifted 15.2 km (± 5.5 km) and 15.7 km (± 6.8 km), respectively.

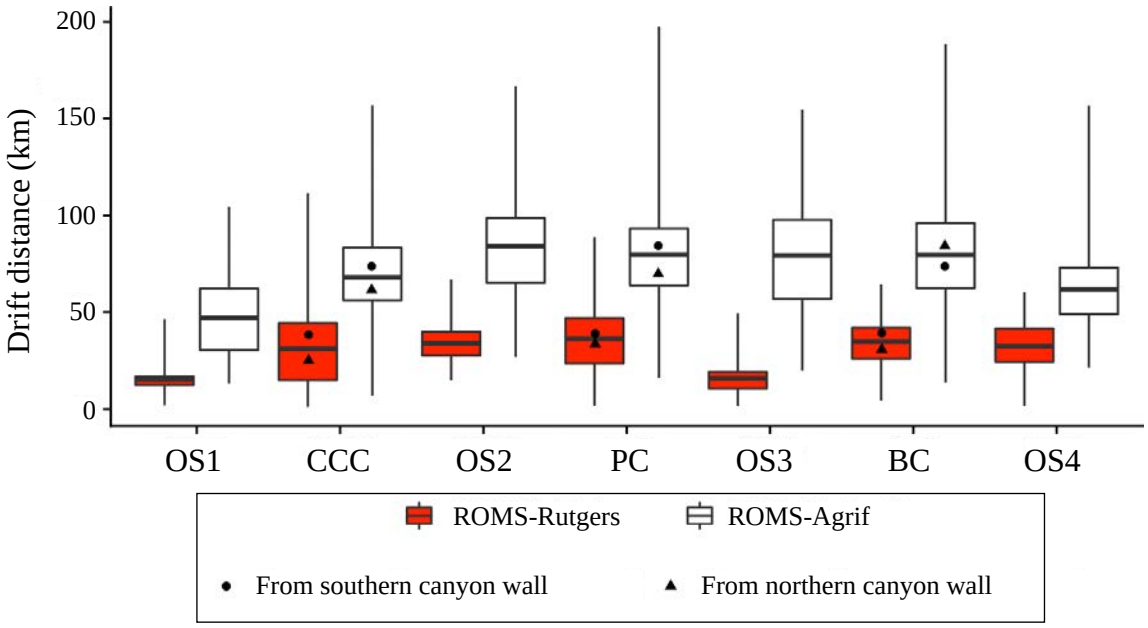

Figure 13. Horizontal transport of passive particles (km) from the release zones in the ROMS-Rutgers (red bars) and ROMS-Agrif (white bars) simulations. Boxplots represent the minimum, 25% quantile, mean, 75% quantile, and maximum. Release zone codes are as indicated in Figure 9.

Particle retentions in the release zones were high and particles from canyons generally seeded the nearby zones (see Figure 14.A). The overall retention rate was averaged at 60% (± 33%), because 42% to 100% of the particles stay in their release zones, except for the particles from the OS 2 (99% of particles drifted into the PC). Particles released in the CCC can drift up to 28% and 27% in the southern zones of OS 2 and PC, respectively. The connectivity of CCC with PC is possible for particles having drifted approximately 50 km (± 7 km) from 624 m (± 92 m) depth. The zone OS3 has received 56% of particles from the PC and has retained 96% of particles released inside. Last, we observe a drift direction opposite to the general southwestward direction of the main current in the south of our study area. Twenty-three percent of particles from the OS 4 drifted northward to the BC.

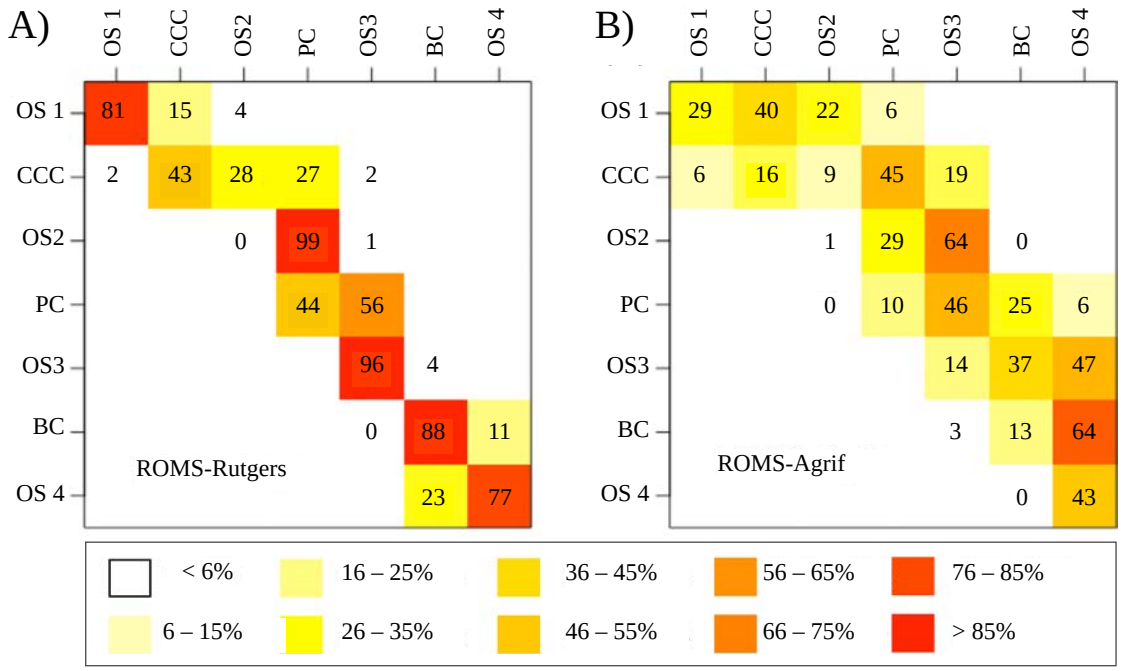

Figure 14. Dispersal rate (%) of passive particles between the zones of release (Y-axis) and settlement (X-axis). The retention rates are on the diagonal. Release zone codes are as indicated in Figure 9.

The vertical displacement of particles at the end of the 31 days simulation was relatively independent of the bottom depth at the release event (Figures 15.A–B). Generally, more than 26% of particles rise above the isobath of 500 m, around 30% of particles drifted without having vertically displaced, and 5% of particles go deeper than 800 m (see Figures 15.A–B). More specifically, 12.8% of particles released above the bottom between the isobaths of 700 and 800 m (hence, 700/800 m) arrived below 800 m. There are only 0.7% and 4.8% of bottom-released particles between the isobaths of 500 and 600 m and the isobaths of 600 and 700 m (hence, 500/600 and 600/700 m), respectively, which also reach such a depth. Moreover, the downward displacement is greater for particles released in canyons than on open slopes. From the three depth layers, 500/600, 600/700, and 700/800 m, as previously defined, 0.2%, 1%, and 11.1% of particles on open slopes and 2%, 13.5%, and 19.7% of particles on canyon slopes, respectively, go deeper than 800 m. Besides, the particles released in the middle layer (600/700 m) of the canyons were likely to be more dispersed vertically than from similar release conditions on the open slope (retention on the depth 27.3% and 36.8%, respectively).

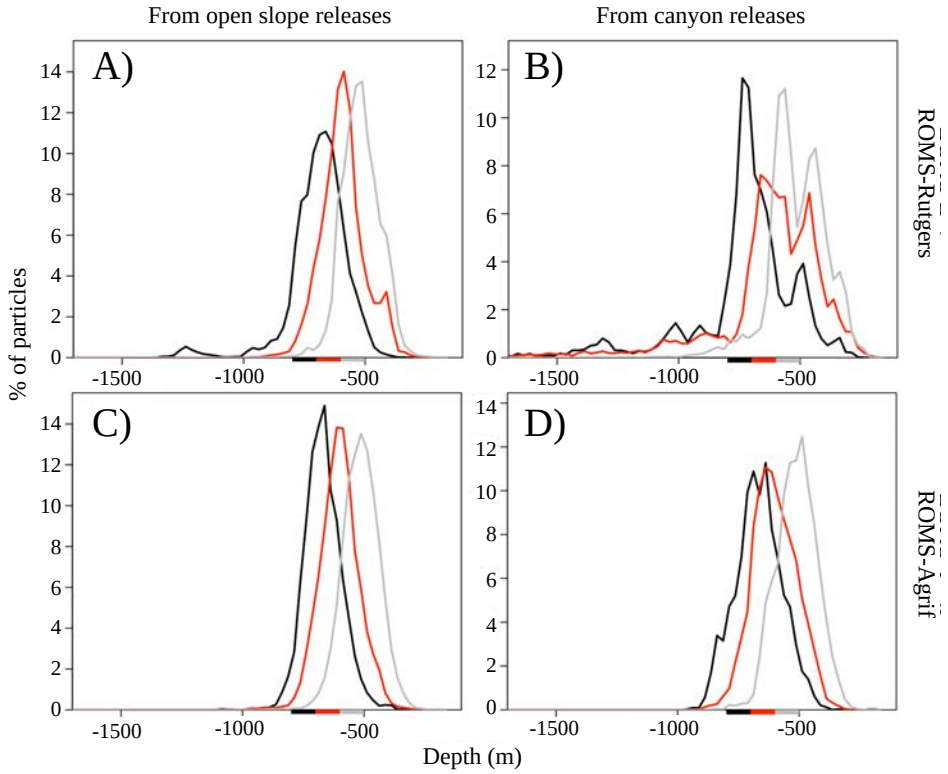

Figure 15. Depth range (m) of particles after 31 days of drift. Particles were released between the following three depth ranges: 500 – 600 m (gray), 600 – 700 m (red), and 700 – 800 m (black) denoted by colored horizontal bars on the X-axis.

In submarine canyons, the particles had a broader vertical displacement than over open slopes. Intensity and amplitudes in the vertical displacement of particles were dependent on the canyons and their walls, especially when they were released above both walls of the Blanes canyon (Figure 16). On average, the particle vertical displacements in canyons or above the open slope are ascents of 28 and 24 m, respectively. Furthermore, the variability of the vertical displacement of particles in canyons (± 154 m) is 2 times higher than on open slopes (± 67.5 m). The drifts in PC have on average the highest ascent of 133 m. The PC is also the canyon with the widest vertical displacements where the maxima upward and downward displacements are 490 and 1163 m, respectively. From its southern wall, particles averagely rise 145 m, while on the northern wall there is an ascent of 58 m. Particles from the CCC averagely rose 44 m as did particles from the PC, but the vertical displacements were limited to a small range of 86 m in the CCC compared to 170 m in the PC. The drifts from BC have on average the furthest descent (127 m down). The drifts within BC went downward by 62 m when particles were above the northern wall and went upward by 36 m when particles drift above the southern wall. Contrary to the different days of release in the other canyons, the northern and southern

walls of BC are where the temporal variability of the vertical displacements is the highest with a standard deviation of 53 and 34 m, respectively.

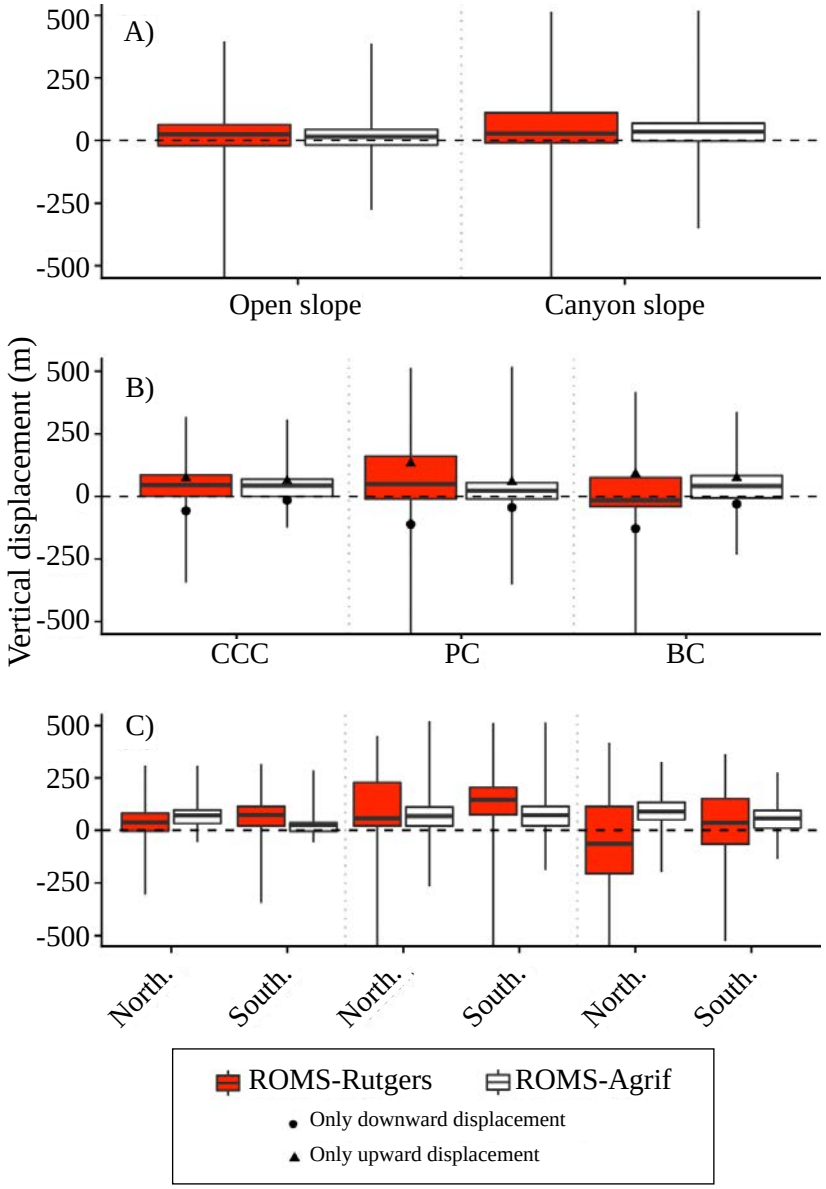

Figure 16. Particles vertical displacement. Vertical displacement according to particles drifting on the open slope or the canyon slope (A), drifting within the canyons (B), and released on the northern wall (North.) or southern wall (South.) of the canyons (C) in the ROMS-Rutgers and the ROMS-Agrif simulations. Release zone codes are as indicated in Figure 9.

The influence of submarine canyons on the transport paths resulted in a common drift direction with small divergences in the trajectories (see Figure 17). Indeed, particles southwardly followed the continental slope and spread differently according to the canyon in which they were released. To begin with, transport paths starting in the CCC and at one depth layer (500/600, 600/700, or 700/800 m) did not overlap with the ones starting at another depth layer, and they kept a linear direction when particles left the

CCC. Second, the simulated drifts that began from the PC were affected by internal circulation within the canyon (i.e., recirculation of the particles between the walls), and transport paths intersected. Last, the transport paths initialized from the BC barely left the canyon area and overlapped with the trajectories set up in a different depth layer. The overlap or intersection of the transport paths may be a consequence from the vertical displacement of the particles (see Figures 15 and 16) that were constrained by the horizontal and vertical circulation variability (see Figures 13 and 16).

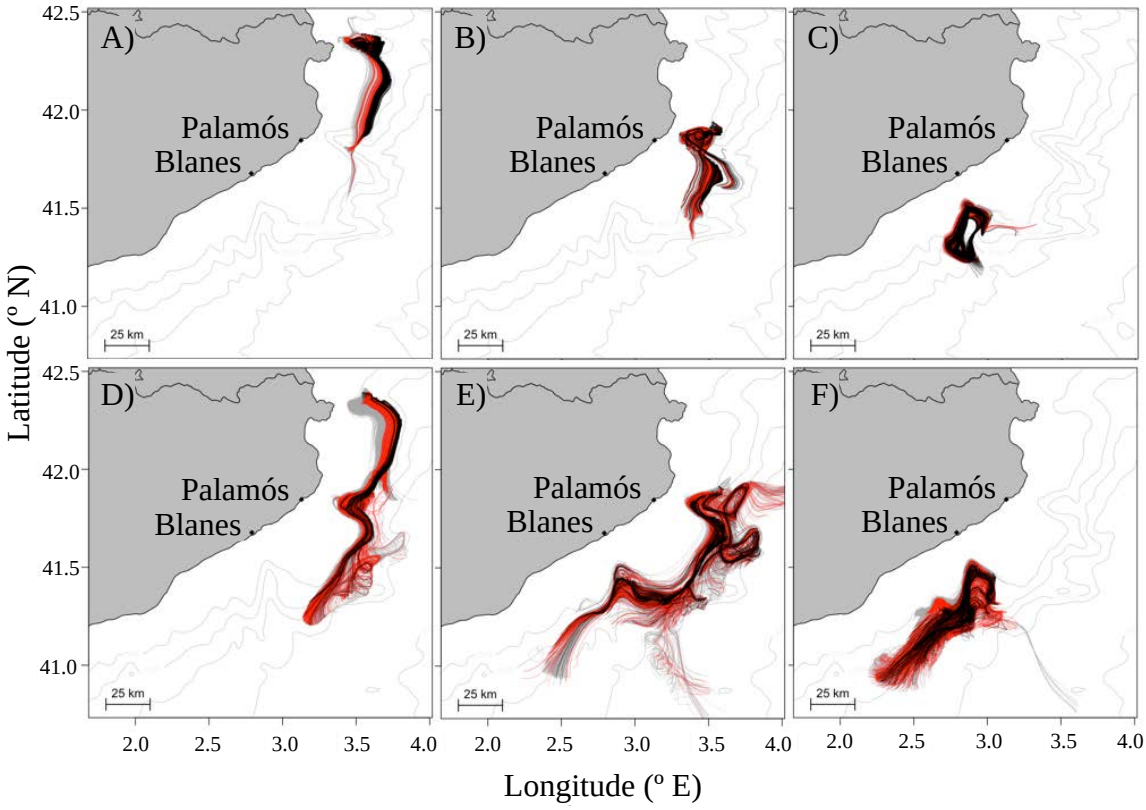

Figure 17. Estimated transport paths of passive particles during 31 d. Passive particles were released in the Cap de Creus canyon (A, D), Palamós canyon (B, E), Blanes canyon (C, F), and advected by the modeled hydrodynamics from ROMS-Rutgers (A–C) and ROMS-Agrif (D–D). Colors of the transport paths are associated with the depth ranges 500 – 600 m (gray), 600 – 700 m (red), and 700 – 800 m (black) on which particles were released.

2.1.3.2. Lagrangian dispersal within ROMS-Agrif outputs

The particles were transported further in the ROMS-Agrif configuration than in the ROMS-Rutgers configuration (Figure 13), and particles from the canyon zones had traveled slightly further than particles from the open slopes. The general drift distances of particles are approximately 70.8 km (± 26.3 km) and 44 km longer than drift in ROMS-

Rutgers. Particles could drift up to the maximum distance of 197 km, detected for particles from the PC (see Figure 13). Among the canyons, particles from CCC were transported the least distance: 47.1 km (± 21 km). Oppositely, the released particles on PC averagely travel the furthest with drifts of 84.2km (± 24.9 km). Particles from canyon slope zones or open slope zones were transported 73.7 and 68.8 km, respectively, and even though the difference of drift distances is low (5 km), it is significantly different (*p*-values < 0.05). Within the canyons, the particles from the northern walls of the CCC and PC drift 66km, which was 13km less than the particles from the southern walls. In the BC, the tendency was for particles released on the northern wall to travel 84 km, or 10 km more than particles from the southern wall.

Southern transport of particles was on a broader scope than in ROMS-Rutgers (see Figure 14.B). After a simulation period of 31 days, the retention rate by the release zones is 1% to 43% of particles (Figure 14.B), making an average of 18% (± 14%) of particles. Like in ROMS-Rutgers, the open slope OS 2 retains the least of particles (1%). Consequently, a small proportion of 29% of particles ends up in the PC, while the majority (64%) connects with open slope OS 3. The particles from the CCC also have drifted in more zones than any other release places. They were transported in four different zones, which were OS 1 at 6%, OS 2 at 9%, PC at 45%, and OS 3 at 19%. Particularly, 45% of particles connect to the PC and those particles are characterized by a drift of 70.5 km (± 9 km) from 575 m (± 77 m). A lower rate of dispersal is detected, as well, from PC to BC. On average, 25% of particles drift approximately 86.6 km (± 14.9 km) from 600 m (± 82 m) to reach BC.

The pattern of vertical particle displacements in ROMS-Agrif was similar among the different release depths and topographic structures of the NW Mediterranean Sea (see Figure 15). Overall, 37.3% of particles reaches the layer above 500 m depth, while only 0.8% of particles go deeper than 800 m. Particles released over the upper bottom depths (500/600 and 600/700 m) presented comparable but still significantly different (*p*-values < 0.05) vertical displacements even if they were released in canyons or on open slopes. Around 41% and 43% of particles drifted within the same depth layer as their releases and 44% to 48% ascended in upper depths. On the contrary and overall, from releases between isobaths 700/800 m, a majority of the particles (65%) went upward, a high

proportion of particles (6.1%) went down be low 800 m, and fewer particles were transported in the depth layer of their release (retention in the deeper layer of 29%).

The average vertical displacement of particles was a small ascent in the water column (see Figure 16), with canyons being the places of higher ascents. On average, particles rose 15 m (± 53 m) when released on open slopes, and twice that, 34 m (± 65 m), when released in canyons. Among the different canyons, particles released in the PC were vertically displaced the least (23 m on average, or half the rise of particles from the CCC and BC), but the widest vertical displacements of 352 m downwards and 519 m upwards were from PC. We furthermore notice that the average ascent and descent of particles were the highest in BC (74 m) and in PC (44 m), respectively, which are reversed directions of movement compared to the results in ROMS-Rutgers. Lastly, particles drifting above the northern wall of all the canyons significantly (p-values < 0.05) rise higher than for particles above the southern wall. In CCC, the rise of particles was 2.7 times higher on the northern wall (71 m) than on the southern wall, which represents the highest change in displacement between the walls. In contrast, in PC, the rise of particles reaches 68 m on the northern wall, which was 4 m less than for particles on the other wall. Over the different release dates, the southern wall of PC is where the vertical movement of particles temporally varies the most (standard deviation of 39 m).

With the simulation of passive drifts in ROMS-Agrif, patterns of particle trajectory were similar to the ones in ROMS-Rutgers, especially the southward drift direction and the spread of particles from the submarine canyons (see Figure 17). Nonetheless, the length of the transport paths, as demonstrated by the drift distance values (see Figure 13), was longer than in ROMS-Rutgers, and the spread of trajectories was wider. The spread was particularly amplified when particles drifted in the Palamós and Blanes canyons. For example, transport paths from the PC disclosed the advection of particles taken in two circular flows near this canyon, and the span of the transport paths from the BC widened once the particles left the canyon. Like for the simulations in ROMS-Rutgers, the variability in the transport path originated in the depth position of the particles (see Figures 15 and 16). However, the spread of the trajectory was intensified as a consequence of the current intensity estimated in the ROMS-Agrif (see Figure 12.B).

2.1.4. Discussion

Two hydrodynamic models with different implementations allowed for testing the sensitivity of particle dispersals to the Mediterranean Sea thermohaline circulation. The dispersal rates were low and similar to observations or simulations of deep larvae from other marine ecosystems like in the Baltic Sea and in another basin of the Mediterranean Sea (Corell et al., 2012; Palmas et al., 2017).

2.1.4.1. Deep-sea connectivity between submarine canyons

For the first time in the NW Mediterranean Sea, the connectivity between submarine canyons has been demonstrated through the Lagrangian transport of deep particles. The southwestward circulation having important amplitude in upper layers also predominated in the bottom drift simulation and explained the particle trajectories from the northern canyons to the southern canyons. On a local scale (i.e., canyon area), submarine canyon areas received drifters from upstream release and seeded the nearest downstream open slopes. In fact, this result is related to the flows of the NW Mediterranean Sea following the right-hand side canyon walls (Flexas et al., 2008; Palanques et al., 2005; Granata et al., 1999; Jorda et al., 2013). With this, our drift simulations supported one of the submarine canyon functions, which consisted of seeding particles in neighboring zones. Nonetheless, each submarine canyon has a singular topography and a different angle of exposure to the main circulation, resulting in different patterns of particle dispersals. In the horizontal dimension and inside each submarine canyon, particle drifts were different because they did not begin from the same depth, the same day, or with the same exposure to the current (i.e., releases on upstream or downstream canyon walls) even though the general canyon influence led to common north–south drift patterns. Those differences also appeared in analyses of sediment flux in the Mediterranean Sea (Durrieu de Madron et al., 1999; Lopez-Fernandez et al., 2013) and in simulations of passive particle drifts in different water layers (Ross et al., 2016). In the vertical dimension, our results reflected the uncorrelated currents occurring inside a canyon (Jorda et al., 2013) that could be one of the origins of the drift differences between canyons. For example, the amplitude of vertical drifts in Palamós canyon was greater than vertical drifts in the other canyons. The uncorrelated currents could also explain the general upward displacement of

bathymetric data sets chosen by the modelers. Indeed, an adequate bathymetric data set would approximate better the mesoscale structures of the water circulation (Gula et al., 2015). Then, it made the simulated drifts from the ROMS-Rutgers more appropriate for the deep passive drifts because the bathymetric data set was more precise (i.e., horizontal resolution of 100 m instead of 3 km) even though it has a lower horizontal resolution than the ROMS-Agrif. Another major difference within the drifts in the two hydrodynamic models was the northward drifts from Blanes canyon and from the open slope at its southern end (OS4) in ROMS-Rutgers. The northward particle drift is a consequence of an anticyclonic flow generated at the mouth of Blanes canyon that also affects the local deep water circulation (Ahumada-Sempoal et al., 2013; Jorda et al., 2013). The southwestward flow in ROMS-Agrif may be the consequence of the bathymetric data set used before the run of the hydrodynamic model and the hydrodynamic model parameterization of the water profile discretization. In ROMS models, the water is discretized by terrain-following sigma layers that generally have high resolution near the surface and relax the circulation variability near the bottom.

The generated drift uncertainties gave arguments for choosing one hydrodynamic model over another, above all when drifts are in deep water. In the absence of more hydrodynamic models, we encourage the deep-sea Lagrangian modeler to cross-validate the Lagrangian drifts with the existing literature. Our work evidences the importance of two major sources of uncertainty in the particle drifts from the hydrodynamic models: bathymetry and model discretization (i.e., choice of S-coordinate parameters). These two factors are shown to be particularly important in the zones near the canyons (all the water column) and open-slope areas. This is an important outcome for modeling studies. In this sense, this study shows the areas where uncertainty grows and so helps to evaluate when and where the choice of the hydrodynamic models will have a large impact on the drift results.

2.1.4.3. Relation between deep-sea circulation and larval cycle of *A. antennatus*

The association of eggs and larvae of *Aristeus antennatus* with passive particles comprised the first approach to their drift. Our study revealed interesting dispersal features which could be related to the ecology of *A. antennatus*. First, few particles in canyons were transported near 1000 m depth, where peaks of juvenile abundances have been reported at the end of fall (Sardà et al., 1997; D'Onghia et al., 2009; Sardà and Cartes, 1997). It would imply that the late larvae are helped or constrained by the vertical circulation to settle in the deep zones. Second, the low dispersal rates from the canyons highlighted that inactive larvae may be retained by those topographic structures. In fact, the morphology of the canyons facilitates the retention of pelagic particles for a few days (Ahumada-Sempoal et al., 2015; Rojas et al., 2014). In that case, it would mean that subpopulations of *A. antennatus* strongly depend on their own. Then, the surface of management plans should be structured to local shrimp fishing grounds, like the one in Palamós canyon (Boletín Oficial del Estado, 2013, 2018). Furthermore, because the submarine valley is localized between two areas of high fishing effort (Palamós and Blanes), there is an interest in its potential role for marine populations. Literature categorizes submarine valley effects as canyon influences, but, due to the exposure of the submarine valley to the current, an evaluation of whether the valley deviates or recirculates the flow is needed.

In this study, the duration of simulation corresponded to the first PLD approximation of *Aristeus antennatus* larvae generalized from penaeid larvae. Nonetheless, further studies need to explore the variability of the estimated dispersal features with longer PLDs. In the framework of the *A. antennatus* case study, the PLD length can be expanded in accordance with a plausible time range of 6 months, i.e., time between the beginning of the spawning peak in July and the period of sampled early juveniles (Sardà et al., 1997; D'Onghia et al., 2009; Sardà and Cartes, 1997). The effect of PLD length can also be estimated with water temperature changes during the larval drift, as they are likely to affect the PLD when *A. antennatus* larvae reach the warm surface waters (O'Connor et al., 2007). The larval behavior needs to be taken into account, because it can significantly

affect the vertical position of decapod larvae in the water column and may influence the larval dispersal (Cowen and Sponaugle, 2009; Levin, 2006; Queiroga and Blanton, 2004). Few studies on *A. antennatus* larvae sampled in open ocean have revealed their presence in the surface water layer (Carbonell et al., 2010; Carretón et al., 2019; Heldt, 1955; Seridji, 1971; Torres et al., 2013). Sardà et al. (2004) and Palmas et al. (2017) assumed that positive buoyancy of eggs partly underlined the presence of individuals in the shallowest water layer. The buoyancy mechanism needs to be analyzed through sensitivity tests in order to compensate for the lack of accurate knowledge about it (Hilário et al., 2015; Ross et al., 2016).

2.1.5. Conclusions

Passive drifts of particles simulated by a Lagrangian transport model coupled with two hydrodynamic models (ROMS-Rutgers and ROMS-Agrif) were compared. The particle releases used characteristics of deep-sea blue and red shrimp, *A. antennatus*, spawners and scarce knowledge of their free-living period (i.e., eggs and larvae). Then, drift simulations began in a highly disturbed circulation induced by the submarine canyons of the NW Mediterranean Sea. In general, horizontal dispersion of deep-sea passive particles was relatively short during the 31 days simulation, but their transports could establish links between the submarine canyons. Like numerous other studies, our work concludes that marine topographic features (i.e., the deep submarine canyons and submarine valleys) favored particle reception and retention. It also supports that the amplitude and variability of vertical displacement (upward and downward in the water column) are higher inside submarine canyons than on other parts of the continental slope. Besides, the variability in the particle vertical displacement was dependent on the three-dimensional distribution of particle releases in a submarine canyon. Variability in particle dispersions was also a consequence of differences between canyon topography and their exposure to the currents. This sensitivity to the topography highlighted the importance of the modeler choice before running hydrodynamic models. Having a finer bathymetry data input and a finer vertical resolution near the bottom (i.e., like in ROMS-Rutgers) is important for estimating the circulation and the passive dispersions with more accuracy, even though the hydrodynamic model has a coarse horizontal resolution (i.e., 2 km vs. 1.2 km). Therefore, the ROMS-Rutgers model was approved by better modeling the

bottom drifts, and it will be used for future studies on the benthic deep-sea species *A. antennatus*. Numerical simulations of the larval drift are one of the best approaches that allowed for approximating the unknown dispersal paths of *A. antennatus* in the NW Mediterranean Sea. This study is the first step of a work conducted with the final focus to improve fishery management of a deep-sea species. However, observation of the pelagic larval traits, validation of the dispersals, and simulation including biological behaviors (vertical migration, buoyancy, and swimming abilities) are required before involving the results in the management strategies.

2.1.6. Supplementary information

Table S2. Pelagic Larval Duration (PLD) according to the water temperature by species of the family Penaeidae.

Species	PLD (day)	T (°C)	Reference
Artemesia longinaris	24 32	24 16	Boschi and Scelzo, 1974a
	32.5 28	17 20	Boschi and Scelzo, 1974b
Litopenaeus stylirostris	15	30	Kitani, 1986a
	15	28.25	Prahl and Gardeazabal, 1977
Macropetasma africanus	14 25 21 17	25 15 18 22	Cockcroft and Emmerson, 1984
	19.5	22	Cockcroft, 1985
Metapenaeopsis barbata	10	28.4	Ronquillo and Saisho, 1997
M. dalei	15.8	25	Choi and Hong, 2001
M. stridulans	16.50	25.75	Chong and Sasekumar, 1994
Metapenaeus affinis	15.25	27.5	Hassan, 1980
	15.54	26.1	Muthu et al., 1979a
	13.41 12.56 11.70	29.7 28.8 29.7	Thomas et al., 1974
	17.25	30	Tirmizi, 1981
M. bennettae	17.07	26	Preston, 1985a
M. brevicornis	23.5	27	Teng, 1971
M. dalli	12	26	Crisp et al., 2016
M. dobsoni	15.5 13.33	26.15 30	Muthu et al., 1974
M. ensis	13 10	26 30	Chu et al.,1996
	12.5	27	Leong and al., 1992
	10.38875	29	Ronquillo and Saisho, 1993
M. joyneri	22.87 22	22.5 24	Lee and lee, 1968
M. macleayi	16.04	26	Preston, 1985b
M. monoceros	11	28	Kumlu et al.,2001
	19.16	26.1	Mohamed et al., 1979
M. moyebi	14	26.5	Kurata and Vanitchkul, 1974
	16.39 18.6	31 29	Nandakumar et al., 1989
Parapenaeopsis stylifera	15.8	25	Hassan, 1984
	20.625	26.65	Muthu et al., 1979b
Penaeus aztecus	17 12.5 11	24 28 32	Cook and Murphy, 1969
P. brevirostris	9.90	27	Kitani, 1997
P. californiensis	11.44	29	Kitani and Alvarado, 1982
	12 17	27 23.5	Rodriguez de la Cruz, 1975
	18 14 12 10	30 28 25 22	Villarreal, Hernandez-Llamas, 2005
P. chinensis	21.29	19.5	Oka, 1967
P. duorarum	11	28	Cripe, 1997
	17.9375 30	26 21	Ewald,1965
	10.32	30	Kitani, 1985
P. esculentus	9.25	26.25	Fielder et al., 1975
P. indicus	13.565	25.6	Muthu et al., 1974
P. japonicus	12	28	Hudinaga, 1942
	10	28	Hudinaga and Miyamura, 1965
P. kerathurus	12	27.5	Klaoudatos, 1978
	10.375	29.5	Türkmen, 2003
	16 16.6	24 25	Yúfera et al., 1984
P. latisulcatus	12.7 31.3 34 21 17 14	24.4 17.1 17 20 22.5 25	Roberts et al., 2012
	8	29.2	Shokita, 1970
P. marginatus	15 11	25 30	Gopalakrishnan, 1976
P. merguiensis	12 11 10 11 11	28 28 28 28 28	Beard, 1977
	9.25	27.5	Motoh and Buri, 1979
P. monodon	10.5 8 14	28 33 23	Reyes, 1985
	12.41	27.5	Silas *et al.*, 1979
	12 11 8 7 8	24 26 28 30 32	Surech Babu, 2013
	12.6	28.8	Villaluz et al., 1969
P. occidentalis	10.76	27	Kitani,1996
P. paulensis	25.5 18.5	20 25	Boff and Marchiori, 1984
	8.5	26	Lemos and Phan, 2001
P. penicillatus	8.125	31.23	Heng and Rui-Yu, 1994
	10	25.5	Pan and Yu, 1989
P. plebejus	16.48	26	Preston, 1985b
P.schmitti	12.5	28.5	Pinto and Ewald, 1974
P. semisulcatus	12.16	31	Devarajan, 1978
	16.04	28	Hassan,1982
	12 26 10 8 8 30 34	22 10 26 30 34 8 8	Kumlu et al., 2000
	12	25.5	Kungvankij et al., 1972
	9.30	29	Ronquillo et al., 2006
P. setiferus	11 19.5	30 22	Cook, unpublished
P. vannamei	11	33	Andrade-Vizcaino, 2010
Trachypenaeus curvirostris	11	26	Ronquillo and Saisho, 1995

Section 2.2

Modeled buoyancy of eggs and larvae of the deep-sea shrimp *Aristeus antennatus* (Crustacean, Decapoda) in the northwestern Mediterranean Sea

Morane Clavel-Henry
Trond Kristiansen
Jordi Solé
Nixon Bahamon
Guiomar Rotllant
Joan B. Company

This Chapter was in collaboration with Trond Kristiansen

Congress: the International MarCo (2018, Heraklion, Grecia.
Conference: Pesca i Ciència - V Jornada tècnica sobre la Gamba de Palamós, 2018, Palamós. Spain.
Poster at Congress: Fish Forum 2018, Roma, Italia.

Article accepted in **PLoS ONE 15(1) (2020). doi: 10.1371/journal.pone.0223396**

Abstract

Information on the buoyancy of eggs and larvae from deep-sea species is rare but necessary for explaining the position of non-swimming larvae in the water column. Due to embryonic morphology and ecology diversities, egg buoyancy has important variations within one species and among other ones. Nevertheless, it has hardly been explored if this buoyancy variability can be a strategy for deep-sea larvae to optimize their transport beyond their spawning areas. In the northwestern Mediterranean Sea, protozoea and mysis larvae of the commercial deep-sea shrimp *Aristeus antennatus* were recently found in upper layers, but to present, earlier stages like eggs and nauplii have not been collected. Using a Lagrangian transport model and larval characteristics, we evaluate the buoyancy and hydrodynamic effects on the transport of *A. antennatus*' larvae in the northwestern Mediterranean Sea. The transport models suggested that 75% of buoyant eggs released between 500 and 800 m depth (i.e., known spawning area), reached the upper water layers (0 – 75 m depth). Then, according to the modeled larval drifts, three spawning regions were defined in the studied area: 1) the northern part, along a continental margin crossed by large submarine canyons; 2) the central part, with two circular circulation structures (i.e., eddies); and 3) the southern part, with currents flowing through a channel. The number of larvae in the most upper layer (0 – 5 m depth) was higher if the larval transport model accounted for the ascent of eggs and nauplii (81%) instead of eggs reaching the surface before hatching (50%). The larvae reaching the most water upper layer (0 – 5 m depth) had higher rates of dispersal than the ones transported below the surface layer (deeper than 5 m depth). The results of larval dispersal simulations have implications for the understanding of *A. antennatus* larval ecology and for management decisions related to the shrimp fishery in the northwestern Mediterranean Sea.

2.2.1. Introduction

Numerous species have a pelagic larval cycle which links the spawning places to the recruitment areas. Larval cycle is a relatively short time lapse compared to the life cycle of marine animal, but it is the phase when large dispersions occur (Cowen et al., 2006). For benthic species, the distribution of the species mostly relies on the transported larvae.

Larvae have several mechanisms for positioning themselves in productive and favorable waters that optimize their growth and displacement (Rothlisberg and Church, 2013). According to those mechanisms, the larvae can be retained on the spawning places or connect to other areas that are of high interest for species with high commercial value. For that reason, many studies specifically addressed larval drifts in order to determine the efficiency of the fisheries management (Siegel et al., 2008; Criales et al., 2015).

Aristeus antennatus is a deep-sea shrimp with a high commercial value in the northwestern Mediterranean Sea. Since 1980, the reproductive cycle, biology, and the temporal and spatial dynamics of *A. antennatus* have been intensively studied based on data from commercial and scientific surveys (Demestre and Fortuño, 1992; Company et al., 2008; Maynou, 2008; Sardà et al., 2009). The acquired knowledge has contributed to shape a local management plan which restricts fishing activity on *A. antennatus* since 2012 for the harbor with the highest landings (Palamós) (BOE, 2013; BOE, 2018). The current local management plan was implemented, partly assuming that the protected population of *A. antennatus* would increase the following years on the trawling grounds, and partly based on the idea that recruited juveniles are related to the spawners living on the trawling restricted area.

Nonetheless, like many deep-sea species, knowledge about the early-life stages of *A. antennatus* and their behaviors is scarce. In the case of *A. antennatus*, knowledge can be gathered from various larvae of Dendrobranchiata species, which is the taxonomic family of *A. antennatus*, e.g., larvae molt after the hatching of eggs with the following order: nauplii, protozoea, and mysis. Lecithotrophic stages (eggs and nauplii) of *A. antennatus* have not been observed yet, but its first planktotrophic stage (protozoea) is largely found in the surface layer (Carretón et al., 2019). Because ripe females spawn on the sea bottom, the embryonic and nauplius stages are assumed to have abilities (buoyancy, swimming ability) that take them to the surface. In Clavel-Henry et al. (2019), an Individual-Based Model (IBM) study showed that the near-bottom circulation has minor effect on passive individual dispersal (encompassing neutral eggs and inactive larvae of *A. antennatus*). The study indicated that near-bottom vertical currents do not advect individuals up to shallower layers, and suggested that the vertical distribution of eggs or larvae can only be explained by their capacity of moving across the water column. To our

knowledge, the youngest stage of *A. antennatus*' larvae found in superficial waters is the first substage of protozoea (Torres et al., 2014; Carretón et al., 2019). This finding supports the hypothesis of positive buoyancy in the previous stages of *A. antennatus*' larvae.

Buoyancy adjusts the vertical egg position in the water column by the difference between egg and water densities (Lindley, 1997; Sundby and Kristiansen, 2015; Palmas et al., 2017). To date, because either some deep-sea species are gravid (i.e., eggs carried by the spawners) or egg information is unavailable, larval dispersal of deep-sea species rarely accounted for the simulation of the stages that interact with the water density. Within the Dendrobranchiata family or within other deep-sea Decapod species, diverse egg sizes and densities (Herring, 1974) were observed but were not comparable with the assumed characteristics of *A. antennatus*' eggs. In advanced stages of Decapod larvae from various ecosystems (coastal, estuarine, and deep-sea), several patterns of vertical distribution and displacements have also been described (Herring, 1974). For example, Penaeid nauplii can be found in superficial layers (Subrahmanyam, 1965; Temple and Fischer, 1967) or near the bottom (Gurney, 1942). This biodiversity translates how challenging and delicate is the generalization of the larval behavior to each unknown larval stage of the deep-sea blue and red shrimp.

Although little is known about the *A. antennatus*' larvae, and as for other deep-sea species, it is likely that the vertical position of larvae is determinant for dispersal because the surface water has stronger velocity and higher temperature than deeper water layers (Fiksen et al., 2007; Kristiansen et al., 2009). A number of hydrodynamic processes in the upper waters of the northwestern Mediterranean Sea can disperse or retain the larvae. The main circulation is driven by the Northern Current that flows southwestward between the surface and 250 m depth with maximum velocities around 0.30 m s^{-1} (Salat, 1995). Several eddies circulate in a clockwise or anti-clockwise direction and drive the distribution of larvae in the surface layer (Bakun, 2006). Those structures are unstably present during a few weeks and have different sizes and locations (Rubio et al., 2009). In summer, the Mediterranean Sea is also well-stratified by a thermocline around 15 m deep (Houpert et al., 2015). This thermocline forms a physical barrier for some small-scale

ocean processes such as water mixing (Thorpe, 2007), and therefore can limit vertical displacement of Decapod larval stages (Queiroga and Blanton, 2004; Lloyd et al., 2012).

In this paper, we analyze the impact of buoyancy variability and three-dimensional water mass circulation on the drifts of eggs and larvae between spawning and recruitment areas for the benthic deep-sea shrimp *A. antennatus* species in the northwestern Mediterranean Sea. This work was an opportunity to test for the first time a protocol to define buoyancy values for undescribed larval stages of a deep-sea species and to provide new elements for the management plan makers.

2.2.2. Materials and Methods

An Individual-Based Model (IBM) for embryonic and larval stages of the deep-sea blue and red shrimp (*A. antennatus*) was implemented with a Lagrangian particle-tracking framework. It simulated the early life-cycle behavior and dispersal patterns of shrimp larvae using 3D hydrodynamic model outputs of the northwestern (NW) Mediterranean Sea.

2.2.2.1. The hydrodynamic model

A climatological simulation of the NW Mediterranean Sea hydrodynamics was run using the Regional Ocean Modeling System (ROMS; Shchepetkin and McWilliams (2005)), a free-surface, terrain-following, primitive equation ocean model. A Mellor-Yamada 2.5 turbulence closure scheme is used for subgrid-scale mixing in the simulation (Warner et al., 2005). Different models (IBM in Clavel-Henry et al. (2019), and a spatiotemporal food web model (Ecopath with Ecosim) in Coll et al. (2016)) have successfully used the daily outputs of the ROMS model in the NW Mediterranean Sea and on the Valencian Gulf. The simulation domain ranged from 38° N to 43.69° N and from 0.65° W to 6.08° E (Figure 18), with a grid spacing of 2 km (with 256 x 384 grid points horizontally). The vertical domain is discretized using 40 vertical levels with a finer resolution near the surface (surface layer thickness between 0.49 m and 5.91 m). ROMS is built forced by a high resolution and accurate bathymetry of the western Mediterranean basin, which is

fundamental for the drift study of *A. antennatus*' eggs and larvae because adults are benthic and females spawn around 800 m depth (Sardà et al., 2003a).

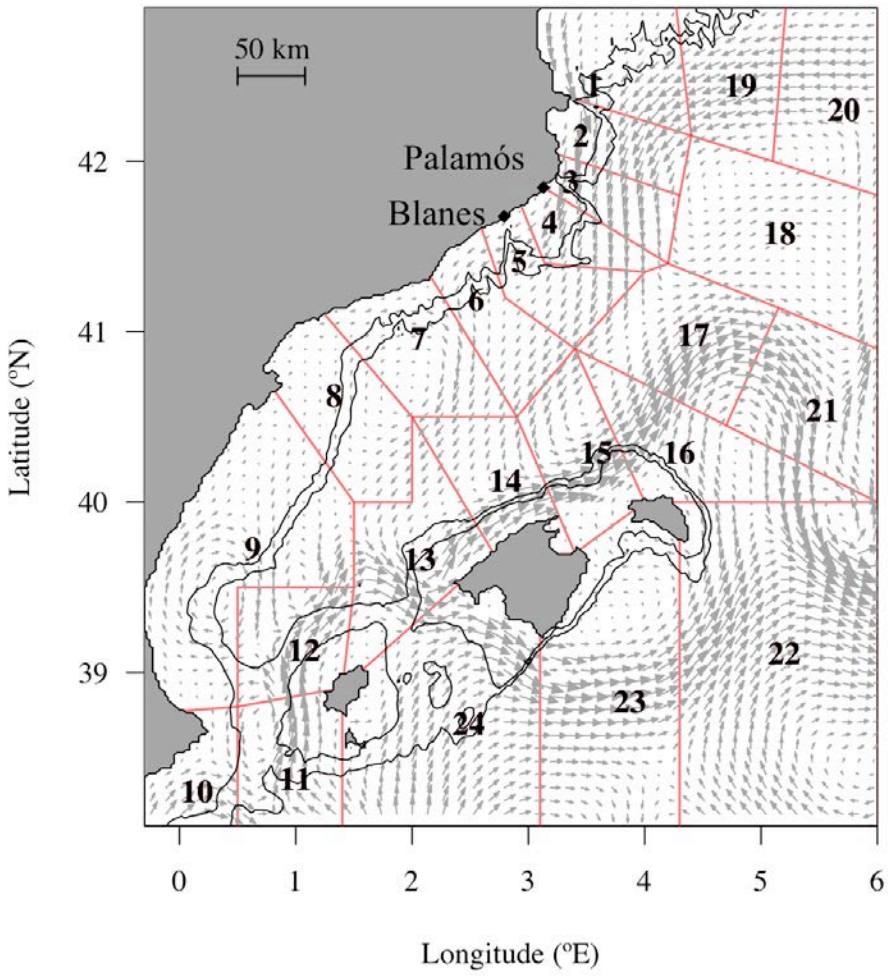

Figure 18. Release and settlement zones defined in the northwestern Mediterranean Sea for this study. The domain is divided by release zones (polygons from 1 to 12) and settlement zones (polygons from 1 to 24) along the continental margins of the management unit called Geographical Sub Area 6 (GSA 6) from the Food and Agriculture Organization. Eggs were spawned in the release zones at the seafloor between the 500 m and 800 m isobaths (black lines) where the mature female shrimp aggregates. All the zones (polygons from 1 to 24) are considered potential settlement zones of the deep-sea blue and red shrimp. Arrows represent the average surface current (m s^{-1}) over July from the hydrodynamic model used in the study.

The ROMS outputs are validated in Clavel-Henry et al. (2019) and provided realistic products of the hydrodynamic and hydrographic characteristics (current velocities, salinity, and temperature) of the NW Mediterranean Sea. The upper water layers were characterized by the main southward current (i.e., the Northern Current) following the eastern coast of Spain and by several mesoscale circulations, like eddies. We estimated eddy size and center over monthly-averaged ROMS current velocities field with an algorithm described in Nencioli et al. (2010). Seawater density is a derived product of the

salinity and temperature (eq. 13 in Fofonof and Millard (1983)). On the horizontal dimension, average estimated temperature, salinity, and seawater density in summer (i.e., July to September) are 27.6 ºC, 37.5 PSU, and 1026.3 kg m^{-3} at the surface and 13.1 ºC, 38.2 PSU and 1035.35 kg m^{-3}, at bottom, respectively. Those values are in the range of seawater measurements carried out in the NW Mediterranean Sea (Salat, 1995; Manca et al., 2004).

2.2.2.2. The Individual-Based Model

The Lagrangian drift of individuals was calculated using the Python framework OpenDrift (from Dagestad and Röhrs (2018); available on https://github.com/OpenDrift). The equation for the advection of individuals in the three dimensions is resolved by a fourth-order Runge-Kutta scheme. Particles were defined as 'stranded' when they came into contact with the coastline. The modules for turbulence and buoyancy were activated by the modeler. The number of particles, the release coordinates and the duration of the drift setting the initial conditions of the Individual-Based Model are also described in the following sections.

Horizontal and vertical components

The trajectories of individuals, representing virtual embryonic or larval stages, were based on the following equation:

$$\frac{dx}{dt} = U(X,t) + B(X,t) + D_h(X,t) + D_v(X,t) \qquad (5)$$

where dX/dt is the 3D displacement of the individuals from their geographical and vertical position X on a time step *dt*; U is the advection component composed by the meridional, zonal and vertical velocities from ROMS; B is the biological velocity vector, and D_h and D_v are the small-scaled turbulent velocities in the horizontal and vertical dimensions, respectively.

The vertical velocity of individuals due to turbulent diffusivity (D_v) is adjusted by the random displacement scheme (Visser, 1997) with an internal time step of 20 s and a 1 m vertical resolution. Values of K_v were provided from the coefficient of salinity vertical

diffusion from ROMS outputs. In our simulation, the vertical mixing was activated until individuals crossed the oceanic surface boundary layer (around 15 m deep; Houpert et al. (2015)). Because the Mediterranean Sea is well-stratified in summer, above the oceanic surface boundary layer, the turbulence was accounted by simulating the horizontal mixing.

The horizontal velocity due to turbulent diffusivity was computed by a random walk scheme:

$$D_h = rand \cdot \sqrt{2 \cdot K_h} \cdot dt \qquad (6)$$

with rand representing a random value sampled in a Gaussian distribution G(0,1), dt the time step, and K_h the horizontal diffusivity coefficient. For K_h, we used the yearly constant and average value of 10 $m^2\ s^{-1}$ estimated by Sayol et al. (2013) in the Western Mediterranean Sea from a hydrodynamic model with similar horizontal resolution than ours.

The biological component B(X, t) in eq. 5 represented the vertical terminal velocity due to the buoyancy force adjusted to the seawater density by the equilibrium of the Archimedes, gravitational, and friction forces under laminar flow (Reynolds number < 0.5) on a spherical object characterized by diameter and density. For the present study, this object size was randomly sampled in a Gaussian distribution with the average *A. antennatus*' egg diameter of $3.3 \cdot 10^{-4}$ m and its standard deviation at $0.45 \cdot 10^{-4}$ m (Demestre and Fortuño, 1992). The density of the sphere was selected after the analysis described in the sections below. The terminal velocity is computed by the equation provided in Sundby (1983), or by Dallavalle equations (Dallavalle, 1948) if the flow is transient (Reynolds number > 0.5).

Adaptation of the IBM to the shrimp larval cycle

Following the temporal and spatial spawners distribution, virtual eggs were set to be released in summer at midnight (Schram et al., 2010) on the bottom of the NW Mediterranean continental slope between 500 m and 800 m isobaths (Demestre and Fortuño, 1992; Sardà et al., 2003; Clavel-Henry et al., 2019).

The IBM included activation and deactivation of the buoyancy force according to the individual stage during the drifts. The buoyancy module was initially activated at the release of the eggs. The eggs were positively buoyant by assuming that on the one hand, young larvae of *A. antennatus* are found in the surface layer (Torres et al., 2014; Carretón et al., 2019) and on the other hand, if the buoyancy is neutral or negative, the swimming abilities of the nauplius could not explain an average vertical rise on 600 m. When individuals reached a non-buoyant stage, the module was deactivated. For simplification, and due to lack of knowledge, we neglected the temporal change of egg size and density.

The drift duration was the sum of the pelagic egg and larval stage durations approximated by the temperature-dependent Pelagic Propagule Duration (O'Connor et al., 2007; Hilário et al., 2015). Due to missing information regarding the embryonic and larval stages of *A. antennatus*, we assumed that its early-life development duration was similar to the near taxonomic Penaeid species. We reviewed 72 research articles (Table S3) in which the larval stage duration of 42 Penaeid species was associated with the rearing water temperature. Then, we fitted a multiple linear model on those data to estimate *A. antennatus* larval stage durations (*D*, in days) according to the seawater temperature, such as:

$$log(D) = T + Stage + \varepsilon \qquad (7)$$

where *T* is the rearing water temperature; *Stage*, a categorical variables characterizing the Penaeid larval stage and ε a random error (Figure S1). This model, whose initial assumptions were verified with a coefficient of determination R^2 = 96%, had the following shape:

$$D_{stage} = exp(-0.072 \cdot T + \begin{cases} 1.51, & if\ stage = eggs \\ 2.66, & if\ stage = nauplius \\ 3.68, & if\ stage = protozoea \\ 3.64, & if\ stage = mysis \end{cases}) \qquad (8)$$

We estimated egg stage duration before the beginning of the drift simulations and larval stage duration was estimated each time an individual molted into the next stage (e.g., from nauplius to protozoea). The water temperature involved in eq. 8 was extracted at embryonic or larval position from ROMS model. Molting was allowed only if the simulation time was bigger than the cumulated duration of the previous and current stages.

Number of particles

The methodology of Simons et al. (2013) adjusted in Clavel-Henry et al. (2019) was used to determine the lowest number of individuals to be released and to guarantee that 95% of the dispersal variability is considered in our results. It is based on the average of the Fraction of Unexplained Variance (Simons et al., 2013), which is got by extracting randomly 100 subsamples of N drifts from 350 000 simulated trajectories and by computing the cross-correlation between the 100 subsamples. The subsample size N ranged between 1 000 and 300 000. The drifts of 350 000 individuals directly started at the surface with underneath sea bottom estimated between 500 and 800 m. Assuming to catch the full range of dispersal possibilities for larvae, the 350 000 drifts lasted the maximum PPD (38.8 days). The PPD was predicted from the relationship as described in the previous section, considering the coldest water near the bottom of the studied area (12.6 ºC) where eggs are spawned. Turbulent diffusivity was as well included for the drifts of 350 000 individuals. To avoid the underestimation of needed individual number, the 350 000 drifts also included a horizontal turbulent random walk with the maximum value of the coefficient K_h estimated at 100 $m^2\ s^{-1}$ in Sayol et al. (2013) instead of its average at 10 $m^2\ s^{-1}$. Finally, the Fraction of Unexplained Variance was lower than 5% if 50 000 individuals are used (Figure S3) to simulate the larval dispersal.

2.2.2.3. Larval dispersions

Modeled dispersion started with buoyant stages having predicted densities (in kg m^{-3}) to rise toward upper water layers. When the stages were no more buoyant, the individuals were neutrally advected by the currents of the reached water mass layer.

Preliminary IBMs

Beforehand, considering the few biological data available on taxonomically close species to *A. antennatus* and the important differences in larval ecology of deep-sea species (see Table S4), the density for the eggs reaching the surface needed to be estimated. This estimation was carried out relying on physical explanation (e.g., forces applied on the particles) to model the egg rise instead of unknown biological values.

To obtain the estimation (hence called optimal buoyancy), the depth reached by the individuals was analyzed when the buoyant stages ended. In the early summer (July 1), 50 000 particles were released and tracked up to the end of the nauplius stage (~ 7.5 days). The Lagrangian drift simulations of eggs were repeated for every 10 kg m^{-3} increment, between 800 and 1030 kg m^{-3}. Then, for each particle reaching the surface (0 – 5 m depth layer), their densest value was kept. It represented the threshold where a denser value would not make the individual reach the surface and a lighter value would likely lead the individual to the surface. The average and standard deviation of the highest density values were kept to implement the drift simulation of the particles.

Other averages and standard deviations of the egg density were estimated by modifying one parameter in the configuration of the previous preliminary IBM. Independently, we computed those parameters i) for individuals reaching the upper boundary of the seasonal thermocline (about 15 m under the surface; (Houpert et al., 2015)) instead of the surface layer, ii) when the buoyancy was applied during egg and nauplius stages, instead of egg stage only, iii) when the turbulence was activated, and iv) when the drift began at late summer (September 1). In case i), the method used to find the seasonal thermocline depth, we used the maximum slope of difference in the temperature profile during summer days (Fiedler, 2010). In case ii), the particles were tracked up to the end of the nauplius stage (~7.5 days). In total, the preliminary experiment consisted of the analysis of simulations made with 24 values of egg density for six configurations of IBM (Table S5).

Runs and sensitivity scenarios of IBMs

We used six scenarios with different configurations of IBM. Sensitivity tests were performed introducing small or high variability due to the buoyant larvae or the hydrodynamics changes (Table 1). The scenario of reference IBM_0 started in early summer at the beginning of the peak period of spawning and with buoyant eggs. We modified the average egg density to lead the individuals to different depths (surface or mixed layer depth), to use different buoyant stages (eggs or eggs + nauplii), to include the vertical and horizontal turbulent components, and to begin the drift simulation in either early or late summer (July 1 or September 1). In the last scenario IBM_{Hot}, the

temperature in the upper 200 meters was incremented by 0.4 ºC, corresponding to the thermal increase expected in the upper layer of the western Mediterranean Sea over a decade (Calvo et al., 2011).

Table 1. Configurations of IBM scenarios for egg and larval drifts. *U*, advective component by the meridional, zonal and vertical velocities; *B*, velocity due to the buoyancy force; D_v and D_h, the velocity due to the vertical and horizontal diffusivity; *PZ*, Protozoea; *Turb*, Turbulence; *MLD*, Mixed Layer Depth; *LS*, Late Summer. Changes in parameterization with respect to the base scenario IBM_0 are in italics. The * indicates that the water temperature in the 0 – 200 m layer has been increased by 0.4 ºC.

IBM Scenario	Buoyant larval stages	Displacement schemes	Depth reached by buoyant stages	Release event	Density (kg m^{-3})
IBM_0	Eggs	U(X, t) + B(X, t)	Surface	July 1	884 ± 36
IBM_{PZ}	*Eggs + Nauplii*	U(X, t) + B(X, t)	Surface	July 1	979± 14
IBM_{Turb}	Eggs	U(X, t) + B(X, t) + *$D_h(X, t) + D_v(X, t)$*	Surface	July 1	885 ± 36
IBM_{MLD}	Eggs	U(X, t) + B(X, t)	*15 m*	July 1	887 ± 36
IBM_{LS}	Eggs	U(X, t) + B(X, t)	Surface	*September 1*	882 ± 36
IBM_{Hot}	Eggs	U(X, t) + B(X, t)	*Surface**	July 1	884 ± 36

Those scenarios were operated to consider the factors associated with larval ecology (IBM_0, IBM_{PZ}, and IBM_{MLD}) and to the hydrodynamics (IBM_{LS}, IBM_{Turb}, IBM_{Hot}). Through IBM_{MLD}, we explored the fact that the thermocline created a physical barrier for the larvae (Querioga and Blanton; 2004; Lloyld et al., 2012). In IBM_{PZ}, we explored the possibility that buoyancy was still taken into account in the vertical movements of nauplius after hatching. The swimming abilities of the spheroid nauplius of Penaeid can hardly lead them to the surface (Chu et al., 1996; Martin et al., 2014). Yet, the nauplius stages of some coastal shrimps were found in the superficial layer (Price, 1982), which means that an underlying process helps them to rise in the water column. Finally, the last scenarios allowed making a sensitivity analysis on the turbulent mesoscale impact on the main advection with the turbulent component (IBM_{Turb}), and on the temporal changes in the physical environment (late summer hydrodynamic circulation) on the drifts (IBM_{LS}). IBM_{Hot} was used to estimate the impact of a scenario of climate change on the larval drifts, through the rising of water temperature above average, which is expected to have a major impact on the larval duration and in seawater density.

For each scenario, the density (kg m^{-3}) of the individuals was randomly sampled from a Gaussian distribution (Figure 19), using the average and standard deviation density values from the preliminary analysis. The simulation duration lasted the time that an egg developed into early juvenile according to the water temperature when larvae molted. The time step to advect individuals was one hour. The characteristics of the individuals (density, egg size, stages, duration of the stage) and their spatial position (latitude, longitude, and depth) were saved on a daily basis for further analyses.

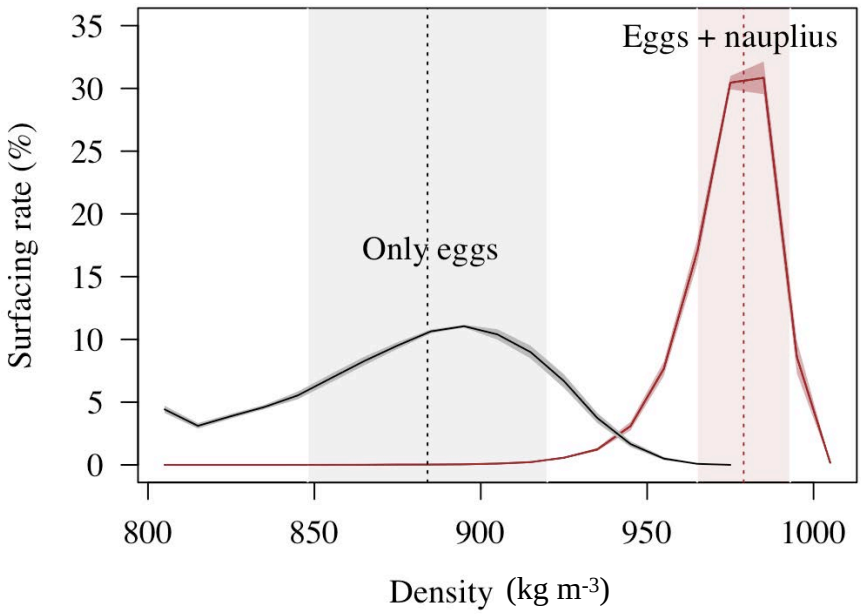

Figure 19. Modeled surfacing rates for eggs and nauplii of *A. antennatus* Surfacing rate of buoyant eggs (black line) or buoyant eggs and nauplii (brown line) related to different tested densities (kg m^{-3}). The average (vertical dashed lines) and standard deviation (colored ranges along the X-axis) of the water densities were used in different scenarios of Individual-Based Model (IBM). See details in Table 1.

2.2.2.4. Analysis of the drift simulations

The water characteristics during the drifts, the drift duration, the vertical rise of the individuals from spawning depths and the traveled distance were used to analyze the simulated drifts from the six scenarios. Distance *d* between two geographical positions given by the coordinates (X, Y) was computed by the haversine formula of great-circle distances;

$$d = arcos[sin(Y_1) \cdot sin(Y_2) + cos(Y_1) \cdot cos(Y_2) \cdot cos(X_1 - X_2)] \cdot R \qquad (9)$$

with *R* as the radius of Earth. The drift distances corresponded to the aggregated distance during the simulation. The straight distance corresponded to the distance between the beginning and the end of the drifts.

In our study, we also analyzed the individual dispersals within and among areas with the connectivity matrices. Therefore, the NW Mediterranean Sea domain was divided into 24 zones (Figure 18) shaped by the main structures of topography like the Eivissa channel, the submarine canyons (Cap de Creus, Palamós, Blanes), and the gulfs (Valencian Gulf or Lion Gulf). In creating the zones we took account of the zoning criteria provided by the General Fisheries Commission for the Mediterranean (Geographical Sub-Areas 5, 6 and 7). Then, the connectivity rates between one release zone *i* and one settlement zone *j* were computed from the ratio of individuals in the settlement zone to the initial individuals from their release zone $N_{j|i}/N_i$. The release zones were the zones 1 to 12 while the settlement zones included all the 24 zones (Figure 18). In order to focus on the most relevant results, statistical tests and principal component analyses were implemented with averaged and scaled data with the basic packages of R.

2.2.3. Results

The simulated larval drifts significantly varied with the spawning places, the number of buoyant stages, the spawning period and the depth layer reached by buoyant phase.

2.2.3.1. Larval drifts in three spawning regions

The temporal hydrodynamic and individual buoyancy variations allowed setting relevant scenarios to use for connectivity analysis. Using the characteristics of the larval drifts ant the environmental influences (PPD, drift distances, water current, and water temperature) by scenarios, a Principal Component Analysis (PCA) differentiated three clusters of scenarios (Figure 20). One gathered all the IBM parameterized by small changes with respect to IBM_0 (i.e., IBM_{Turb}, IBM_{Hot}, and IBM_{MLD}). The non-parametric Kruskal-Wallis test revealed that their PPD and drift distances were significantly different (*p*-values > 0.05). Nevertheless, their larval drifts expanded over a longer period (25.6 days) and over longer distances (118 km) even though larvae drifted at the thermocline depth (IBM_{MLD}), or within small-turbulent water (IBM_{Turb}), or in warmer water (IBM_{Hot}). The two other clusters were defined by the scenario IBM_{LS}, in which larval drifts traveled the smallest

distances (93 km), and by the scenario IBM_{PZ}, in which the surfacing of larvae had higher rates (80%) and PPDs were the shortest (23.2 days). The present analysis focused on the drifts simulated in the scenarios IBM_0, IBM_{PZ} and IBM_{LS} that were separated into distinct clusters and had important differences in their drift characteristics (Figure S4).

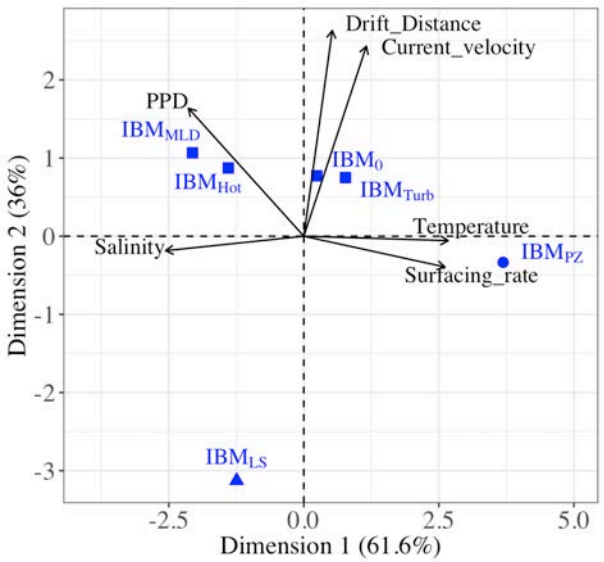

Figure 20. Scenarios of Individuals-Based Models related to the larval drift characteristics and the environmental influences. The different scenarios of Individuals-Based Models used in this study are represented by blue symbols (circle, triangle or square) and visualized with the characteristics of larval drift and environmental influences (arrow). In the Principal Component Analysis (PCA), the correlation among the characteristics is indicated by the angle between arrows (i.e., an angle of 90º indicates no correlation and an angle of 180º indicates a negative correlation). Scenarios were correlated to the larval drift characteristics and environmental influences by the closeness of their Cartesian coordinates. The PCA grouped IBM_0, IBM_{MLD}, IBM_{Hot}, and IBM_{Turb} (square), and separated IBM_{PZ} (circle) and IBM_{LS} (triangle). IBM scenarios are described in Table 1.

Generally, the larval drifts had similar trends for individuals released in specific latitudinal ranges of the NW Mediterranean Sea. For each scenario previously selected, a PCA (Figure 21) was carried out on the larval drift characteristics and environmental influences by release zones, gathering them into three regions. Besides, those three regions were driven by the same variables in each scenario. The region 1 gathered larvae released from zones 1 to 4 (approximately 41.39º N – 42.74º N) with the longest PPD and the straightest transports. The region 2 gathered individuals released between zones 5 and 10 (approximately 38.86º N – 41.39º N), which were abundant in the surface water but drifted the shortest distances. The region 3 gathered the individuals from the zones 11 and 12, and overlapped each side of the Eivissa Channel. Those individuals drifted the furthest and had low surfacing rates.

In each three regions, the individual drifts followed different circulation patterns. In region 1, Figure 22 shows an expanded and linear distribution of the individuals towards the Southwest. The dispersal of individuals from the region 2 shaped different eddies, which are almost-circular structures of the hydrodynamics. In all scenarios, those eddy-like structures were localized where the Gulf of Valencia widens (0.5º E; 39.5º N, and 2º

E; 40.5º N). These eddies had only differences in their average radius and the position of their center changed between the early and late summer releases (IBM_0 and IBM_{LS}). For instance, these eddies get 6 to 8 km larger in IBM_{LS} (Table S6) and their center displaced 9.5 km to 14.7 km further (Table S6) than eddies in IBM_0. Last, individuals from region 3 were affected by the presence of an eddy with a center averagely positioning in the Eivissa channel (0.72º E; 38.70º N, Table S6) in early summer (IBM_0).

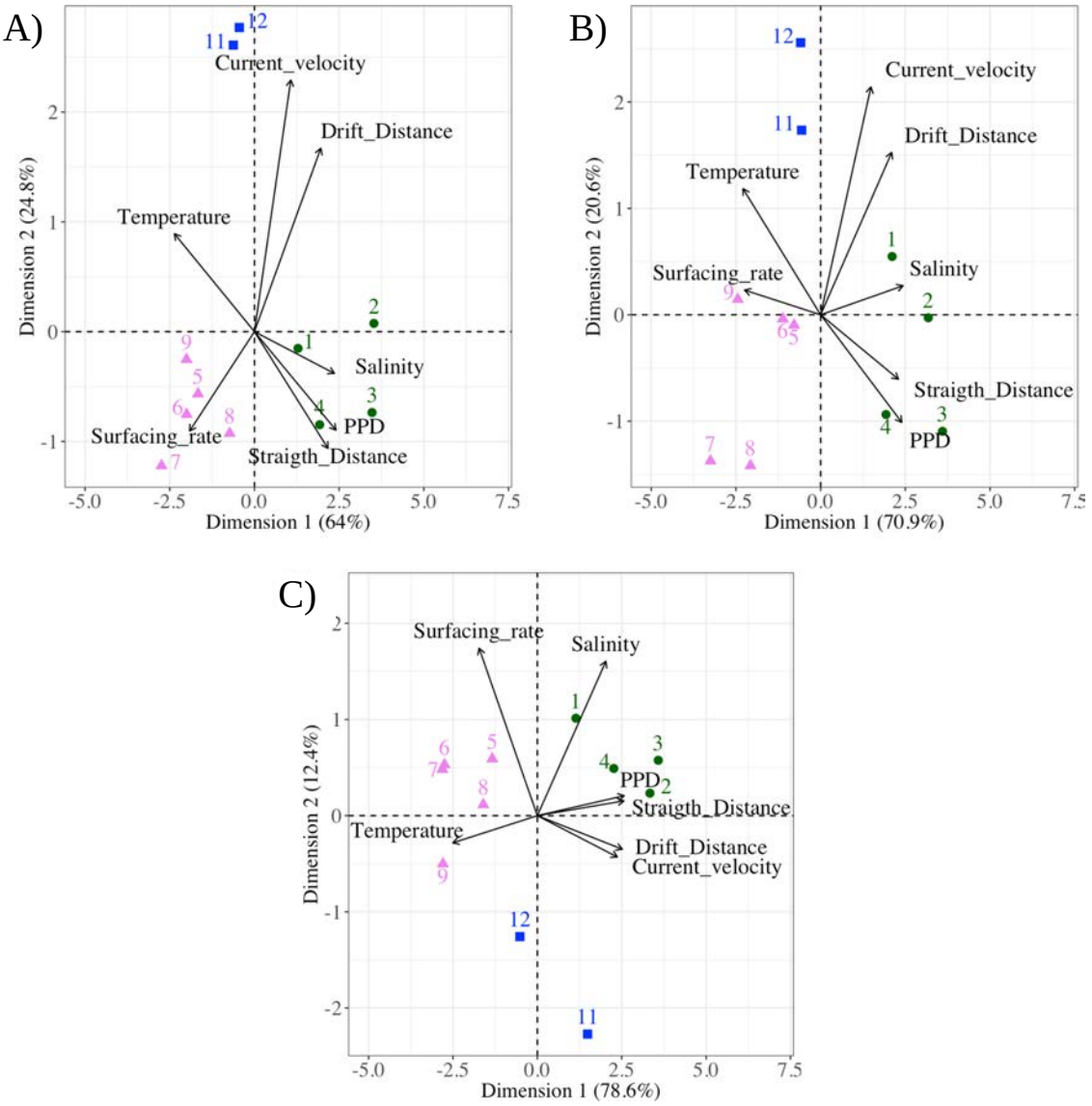

Figure 21. Larval drift characteristics and the environmental influences of the three most distinct IBM scenarios. Release zones (colored symbols and numbers) linked to characteristics of the larval drift (arrows) in a Principal Component Analysis for the base scenario IBM_0 (A), the scenario with the buoyant stages up to Protozoea IBM_{PZ} (B), and the scenario initialized at late summer IBM_{LS} (B). The correlation among the characteristics of the larval drift is indicated by the angle between arrows (i.e., an angle of 90º indicates no correlation and an angle of 180º indicates a negative correlation). Release zones were correlated to the larval drift characteristics and environmental influences by the closeness of their Cartesian coordinates. The PCA grouped three regions: the release zones 1–4 (full green circle), the release zones 5 – 9 (full pink triangle) and the release zones 11 and 12 (full blue square). IBM scenarios are described in Table 1.

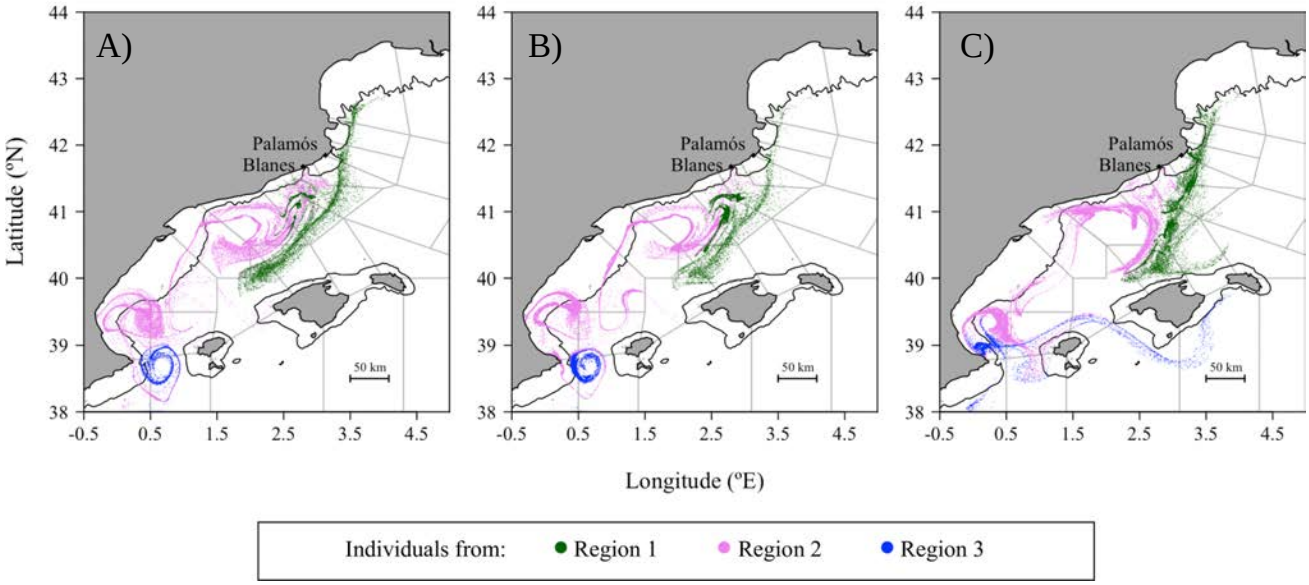

Figure 22. Settlement position of early juveniles at the end of the simulated drifts by regions and by the three selected IBM scenarios. The early juveniles are positioned after the simulation with the base scenario IBM_0 (A), the scenario with the buoyant stages up to Protozoea IBM_{PZ} (B), and the scenario initialized at late summer IBM_{LS} (C). The regions are defined according to the results of a Principal Component Analysis (Figure 21). The black line represents the shelf break at 200 m. IBM scenarios are described in Table 1.

2.2.3.2. Advantage of two buoyant stages in the larval drifts

The highest surfacing rate regardless of the regions was when the ascent of larvae occurred with two buoyant stages. With an average density of 979 kg m^{-3} in IBM_{PZ}, 93 kg m^{-3} denser than in IBM_0, 81% of the eggs and nauplii rose to the shallower water layers, while in IBM_0, 52% of the eggs reached the surface layer (Figure 23). Overall, the average time for the ascent of two buoyant stages (IBM_{PZ}) lasted 7.5 days (i.e., 5.5 days longer than in IBM_0). Nevertheless, at the end of the simulations in IBM_{PZ} and for individuals at the surface, the drift durations increased by approximately two days and the drift distances were hardly 3.6 and 4.5 km longer (regions 1 and 2) or 12.6 km shorter (region 3) than in IBM_0 (Table 2).

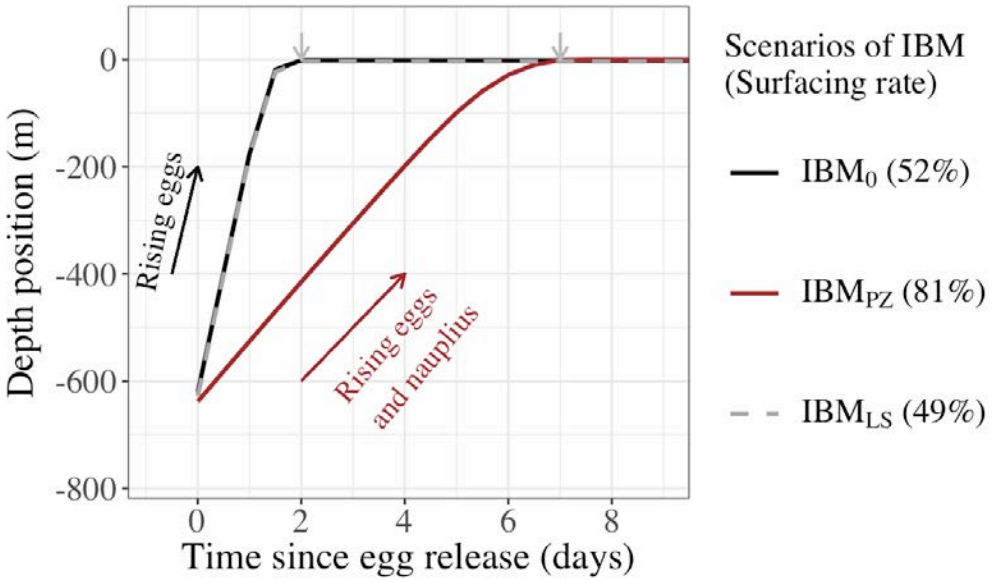

Figure 23. Depth position of eggs (IBM_0 and IBM_{LS}), and eggs and nauplius (IBM_{PZ}) after spawning. The depth position is recorded from the release day (Time = 0) to the end of the buoyant stages (grey arrow) in three Individual-Based Models. In IBM_0 (black line) and IBM_{LS} (grey dashed line), eggs were spawn at early and late summer, respectively, and buoyant eggs rose during 2 days. In IBM_{PZ} (brown line), eggs and nauplii were buoyant and rose in the water column during 7.5 days.

Table 2. Characteristics of the larval drifts by the three selected IBM scenarios, by regions of the NW Mediterranean Sea and by depth of drifts. PPD, Pelagic Propagule Duration (in days); T, the average seawater temperature (in ºC); Drift, the drift distance (in km); Surfacing rate, the percentage of individuals reaching the surface (0 – 5 m layer); PZ, Protozoea; LS; Late Summer. The regions 1 – 3 are defined in Figure 21.

				Drift in the 0 – 5 m depth water layer			Drift in the water layer below 0 – 5 m depth		
IBM Scenario	Region	Release zones	Surfacing rate	T	PPD	Drift	T	PPD	Drift
IBM_0	1	1 – 4	48.0	24.5	20.3	153.5	15.7	32.6	162
	2	5 – 9	55.6	25.9	17.6	80.1	16.5	31.2	105
	3	11 – 12	43.8	27	16.3	174.5	17.9	28.9	170.6
IBM_{PZ}	1	1 – 4	70.9	23.7	22.4	158	16.3	31.9	173.1
	2	5 – 9	85.8	24.9	20.1	83.7	17.2	30.3	102
	3	11 – 12	77.4	25.8	19.0	161.9	17.9	29.5	168.9
IBM_{LS}	1	1 – 4	45.4	22.4	20.1	147.9	16.5	30.8	145.1
	2	5 – 9	55.3	24.2	17.2	54	17.7	28.6	79.8
	3	11 – 12	26.0	25.2	15.7	57.7	18.4	27.6	113

The time lag between early and late arrival of individuals at the surface was small enough for not implying important divergences in the drift characteristics. Indeed, in the two scenarios IBM_0 and IBM_{PZ}, the surfaced larvae were not spatially exposed to different currents. When nauplii reached the upper 5 m layers in IBM_{PZ}, they were 20.5

km away from the location where the eggs have surfaced in IBM_0. However, this distance was mostly kept to the nearest kilometer between the individuals of IBM_0 with the same age (7.5 days) than the surfaced individuals of IBM_{PZ}. It illustrated that while the buoyant nauplii in IBM_{PZ} were still rising in the water column, the surface current in which the individuals from IBM_0 were advected, had not important amplitude or direction changes.

The overall consequences from late and abundant individuals at the surface were that the connectivity and retention strengthened between and within zones of the NW Mediterranean Sea. In both IBM_0 and IBM_{PZ}, the same settlement zones were connected but with different amplitudes (Figures 24.A–B). First, the dispersal rate between the release zones from the region 1 and from Blanes canyon (zones 1 to 5) and its neighboring zones (zones 5 to 7) rose from 42.6% in IBM_0 to 56.7% in IBM_{PZ}. Second, in the Gulf of Valencia's zones (zones 7 to 9), corresponding to the south of region 2, the retention rates were from 33.4% to 43.6% higher in IBM_{PZ} than IBM_0. Last, each side of the Eivissa Channel (zone 11 and 12 in the region 3) connected with the other side if the surfacing was earlier like in IBM_0. Indeed, in this scenario, the exchange of surfaced individuals between the two sides was bidirectional, with a tendency for individuals to cross northwardly the channel. A rate of 21.3% individuals from zone 11 connected to the northern zones of the Eivissa Channel (zone 9 and zone 12) and 11.5% individuals from the zone 12 crossed the channel and arrived on the southern zones of the Eivissa Channel (zones 10 and 11). While in IBM_{PZ}, the exchange of late surfaced individuals across the channel was unidirectional and it was done by the northern zones of the channel. Under the influence of an eddy (Figure 22.B), the southern zones (zone 11 and 10) of the Eivissa Channel received 63.2% individuals from zone 12 and zone 11 retained 61.4% individuals (or 55.6% individuals more than in IBM_0).

2.2.3.3. Larval drifts after early and late summer spawning

The present results distinguished the circulation in the water from the northernmost region (region 1) from the southern and warmer regions (regions 2 and 3). The drifts at the surface were exposed to higher temporal variability in the circulation fields if they started in the warmer regions of the NW Mediterranean Sea. In IBM_{LS}, 49% of

individuals (i.e., 3% fewer than in scenario IBM_0) rose to the surface (Figure 23), and drifted 24.1 days (i.e., around one day less than in scenario IBM_0). Yet, as shown in Figure 20, individuals from IBM_{LS} traveled less. The temporal current changes were measured with the differences in drifted distance per day in scenario $IBM_{LS.}$ In region 2, surfaced larvae traveled 26 km less than in IBM_0 (i.e., 3.1 km day^{-1} instead of 4.6 km day^{-1}) and in region 3, surfaced individuals traveled 96.4 km less (i.e., 3.7 km day^{-1} instead of 10.7 km day^{-1}). In contrast, the individuals in the colder region 1 had similar drifting velocity in IBM_{LS} (i.e., 7.4 km day^{-1}) and in IBM_0 (i.e., 7.6 km day^{-1}).

Besides the temporal changes in the intensity of the circulation fields, two circular structures in the NW Mediterranean Sea boosted the dispersal rates of the surface individuals. First, the diameter of an eddy-like structure between the latitudes 41º N and 42º N had modified the surface connectivity of individuals toward the Balearic Islands. In IBM_{LS}, the north side of the Majorca Island (biggest island; zone 13 and 14) received 40.9% and 37.9% individuals from the Blanes canyon (zone 4) and its southern zone (zone 5 in Figure 24.C), while in IBM_0, the reception rate of the individuals was lower than 3.5%. This new connection leaned on the changes in the current direction at the end of the summer and the size of the eddy-like structure. Individuals from the region 1 traveled a similar distance per day in IBM_0 and IBM_{LS} (7.5 km day^{-1} and 7.1 km day^{-1}, respectively), but the circulation pattern had an angle closer to the south direction, which advected the individuals more southwardly in IBM_{LS} (26º clockwise from geographical South) than in IBM_0 (36º clockwise from geographical South). Figure 22.C suggests that the eddy-like circulation over the north of the region 2 qualitatively had a bigger diameter. Second, the transport of surfaced individuals across the Eivissa Channel was limited without eddy structure. Indeed, the absence of an eddy in the Eivissa Channel (Figure 22.C) paired with the fact that all surfaced individuals from zone 11 were transported unidirectionally across the Eivissa Channel. Additionally, most of the surfaced individuals from zone 12 mostly (25.2%) were advected in the eddy-like structure located at the south of the region 2.

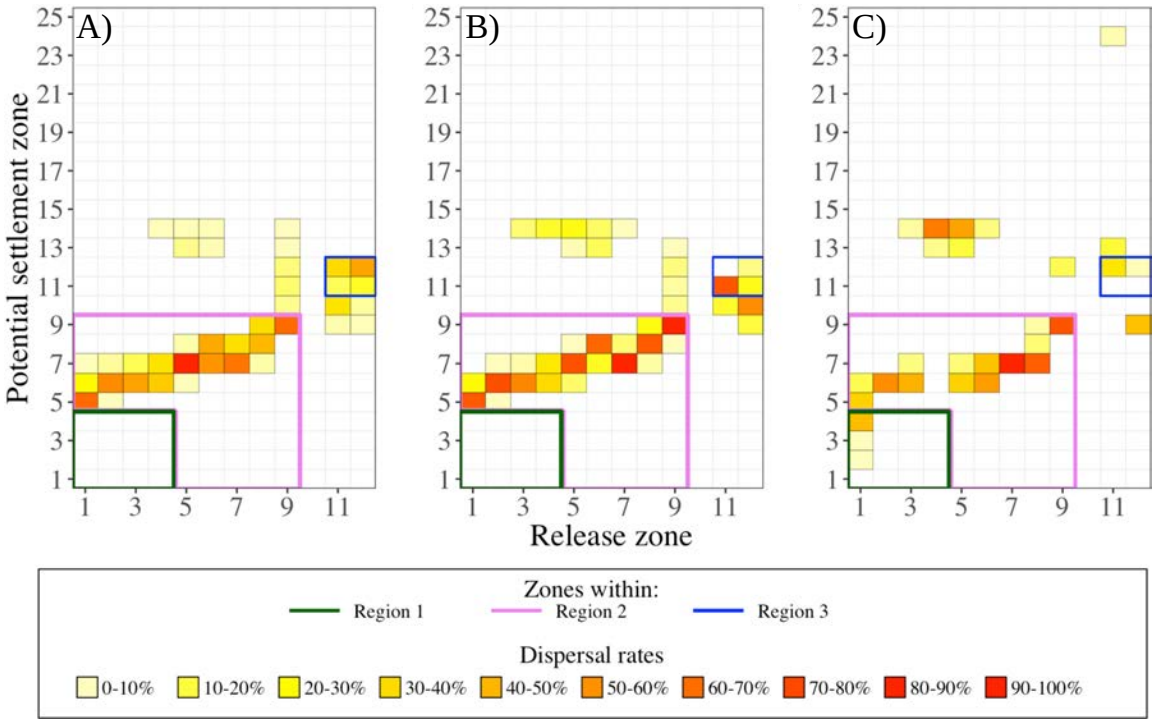

Figure 24. Dispersal rate in the upper water layers (0 – 5 m) by the three selected IBM scenarios. Dispersal rates were calculated from release zones (X-axis) to potential settlement zones (Y-axis) from simulated larval drifts in the base scenario IBM_0 (A), the scenario with the buoyant stages up to Protozoea IBM_{PZ} (B), and the scenario initialized at late summer IBM_{LS} (C). For clarity purposes, we contoured the dispersal rates in regions 1 (green lines), 2 (pink lines) and 3 (blue lines). Identification of zones and regions as defined in Figures 18 and 21, respectively. Code color is related to the dispersal rate (%). The sum of the dispersal rates over a column gives the percentage of individuals in the surface layer.

2.2.3.4. Larval drifts in different depths of water layer

A part of the individuals did not reach the surface because of the variability in egg characteristics. For example, the decrease in the rate of surfaced larvae from region 3 between IBM_0 and IBM_{LS} was related to smaller egg diameters. Nonetheless, deeper drifts brought valuable knowledge on several features that are developed below.

First, the water temperature gradient in different depth layers was advantageous for longer transports. Due to the variability in egg size and egg density, the buoyant stages stabilized at different vertical positions from zero to 75 m for more than 75% of individuals. The drifts were 20 km longer because they lasted 11 supplementary days in the deeper layers regardless of the scenario involved. The highest gradient in the drift duration occurred in the upper 100 m layer where the drift lasted 12 supplementary days at 100 m than at the surface (Figure 25). Beyond 100 m, the drift duration was stabilized at 36 – 38 days. Nonetheless, the scale of the deeper drifts by region showed that the

circulation was still stronger and weaker in the region 1 and 2, respectively, where the drifts were the longest (167.5 km) and the shortest (102.5 km), respectively and regardless the scenario. In a concrete case, the simulated drifts from region 3 in IBM_{LS} indicated that the upper and deeper layer were decoupled because individuals drifted two times longer than the individuals in the upper layer (Table 2).

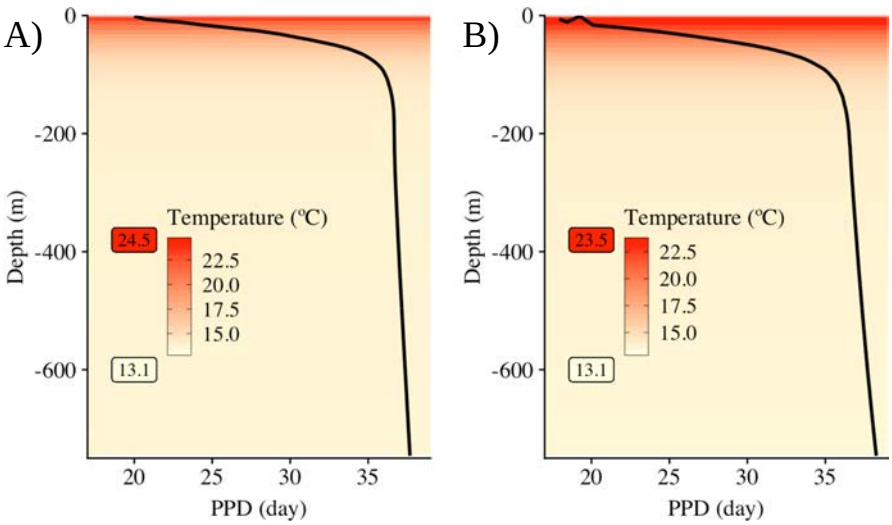

Figure 25. Pelagic Propagule Duration (PPD) according to water temperature estimated at different depths. The average duration of propagules (from eggs to early juveniles) of *Aristeus antennatus* is in relation with the decreasing temperature (color gradient, ºC) with increasing depths (Y-axis, m). In (A), PPD and water temperature from the IBM scenarios in early summer (IBM_0 and IBM_{PZ}) were averaged, and water temperature ranged between 13.1 ºC and 24.5 ºC. In (B), PPD and water temperature are from the IBM scenario in late summer (IBM_{LS}), where water temperature ranged between 13.1 ºC and 23.5 ºC. IBM scenarios are described in Table 1.

Second, longer drifts and decoupled currents underneath the five meters depth favored the connectivity with the Balearic Islands (Figure 26). In other words, the velocity fields under the surface had slightly different directions. This was particularly seen by the drifts from the region 1 that, in two cases, provided higher arrival rates of individuals on the northwestern part of the Balearic Island grounds. One case is illustrated by the drifts in IBM_0 showing 33.1% to 40% individuals from the zones 2 to 4 in the 5 – 330 m layer depth were transported toward the islands (Figure 26.A). The second case is showed by drifts in the IBM_{LS} (Figures 24.C and 26.C) where surfaced and deeper individuals reached the zones 13 and 14 but the connection with zone 15 was only established if individuals drifted in the deeper layer (8 to 381 m depth). The same concept prevailed in the region of the Eivissa Channel (Figure 26.C). Within the first 100 m layer, longer drifts (160 to 400 km) from the Eivissa Channel connected to the southern ground of the

biggest Balearic Island (Majorca Island) by 39.5% individuals from zone 11 and 13.4% individuals from zone 12.

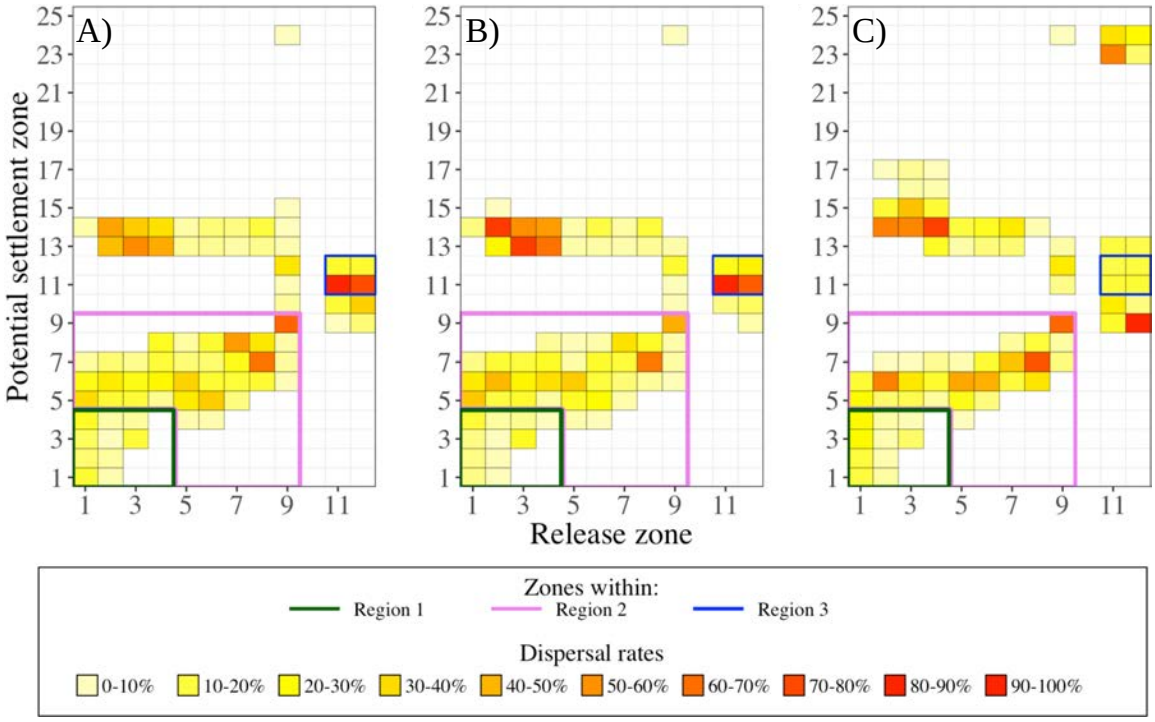

Figure 26. Dispersal rate in the lower water layers (below 5 m) by the three selected IBM scenarios. Dispersal rates were calculated from release zones (X-axis) to potential settlement zones (Y-axis) from simulated larval drifts in the base scenario IBM_0 (A), the scenario with the buoyant stages up to Protozoea IBM_{PZ} (B), and the scenario initialized at late summer IBM_{LS} (C). For clarity purposes, we contoured the dispersal rates in regions 1 (green lines), 2 (pink lines) and 3 (blue lines). Identification of zones and regions as defined in Figures 18 and 21, respectively. Code color is related to the dispersal rate (%). The sum of the dispersal rate over a column gives the percentage of individuals below the surface layer.

Finally yet importantly, the deeper and variable drifts of the individuals allowed broader connectivity. One release area could be connected up to nine other areas (see Figure 26.A). Those connections were allowed by small numbers of individuals, which remained near the release areas, like for the case of individuals from region 1, which had a northwestward dispersal and thus, an opposite direction of dispersal than particles at the surface.

2.2.4. Discussion

Model results emphasized the importance of the buoyant phases and their variability in the larval cycle of deep-sea species. In the upper water layer of the northwestern

Mediterranean Sea, the larval transport of *A. antennatus* relied on different circulation patterns and their spatiotemporal variability.

2.2.4.1. Importance of buoyant phases

The simulations of different buoyant phases in the larval drift of the blue and red shrimp *A. antennatus* emphasized the importance of the lecithotrophic stage in the drifts. In the recommendation guide for IBMs by North et al. (2009), buoyancy is a key parameter for explaining the changes in the larval drifts. However, prior to our study in the Mediterranean Sea, only Palmas et al. (2017) studied the impact of egg buoyancy on simulated drifts for the deep-sea shrimp *Aristaeomorpha foliacea* (taxonomically close to *A. antennatus*), using Atlantic anchovy egg density (Parada et al., 2003).

In our study, over half of the released individuals reached the layer where a high quantity of *A. antennatus*' larvae is found, i.e., the surface layer (Carretón et al., 2019). We estimated an average egg density of 884 kg m^{-3}, which was around 100 kg m^{-3} lighter than the ones described for other deep-sea shrimp eggs, i.e., 1025 – 1082 kg m^{-3} (Herring, 1974) and the seawater densities of the northwestern Mediterranean Sea, i.e., from 1025.3 kg m^{-3} in Cap de Creus to 1024.1 kg m^{-3} in the Eivissa channel (Salat, 1995). Nonetheless, egg density is partly species-dependent and therefore, egg density of deep-sea Decapod egg with bigger sizes than *A. antennatus*' oocyte (Herring, 1974) may not be appropriate to use in our Lagrangian model. However, the displacement of *A. antennatus*' eggs to the surface was comparable with some Penaeid eggs that were observed at the surface in laboratory water tanks and sea planktonic samples (Price, 1982; Dall et al., 1990), but this fact could not be quantitatively verified due to lack of Penaeid egg density data. To improve the next larval drift simulations with buoyant eggs of *A. antennatus*, the relationship between egg density and diameter (e.g., Herring (1974)) during the egg incubation should be considered. Indeed, when the eggs develop, several chemical reactions (i.e., the production of a perivitelline space by cortical activation of the eggs (Pongtippatee-Taweepreda et al., 2004), the egg hydration (Pandian, 2016), and embryonic development) likely modify the lipid rate, egg size, and egg density (Dall et al., 1990; Rosa et al., 2006). Nevertheless, information about egg growth of deep-sea species and Penaeid eggs needs to be provided.

Extended to the nauplius stage, the rise of individuals illustrated the important role of the nauplius for increasing the probability to reach the surface layer. However, due to lack of knowledge, two parameters were not considered in the density values of IBM_{PZ}: the loss of weight at hatching and the change of shape at hatching (Chu and Ovsianico-Koulikowsky, 1994). In the Penaeid family, the elliptical and hairy morphology of the nauplius leads to a change in the buoyancy effect (Coombs et al., 2004), which may speed up or slow down the ascent of the larvae after hatching. Furthermore, at this stage, previous studies provided the implication of the swimming behavior in the control of the larval vertical migration. Indeed, although erratically Gurney (1942), Heldt (1938), and Dobkin (1960) observed a rise of the Penaeid nauplii followed by a resting time in which the nauplii slowly sank. The velocity of Penaeus larvae is poorly informed although (Gurney, 1942) suggested that larvae rise quickly after hatching, guided by phototaxis. Nevertheless, all authors emitted doubts about the ability of nauplii to swim up to the surface. We underline the necessity to carry out studies on the locomotion of decapod shrimp larvae in the open ocean to define the potential balance between the buoyancy of the nauplii and their swimming ability.

2.2.4.2. Dispersal modulated by current variations

We noted that the main linear circulation along with eddy-like structures supported distinct dispersals of the blue and red shrimp larvae according to their drift depths. Turbulence (in scenario IBM_{Turb}) or individuals at the thermocline depth (in scenario IBM_{MLD}) introduced small variations during the drift simulation that hardly modified the final dispersals of individuals. Dominant circulation patterns particularly controlled the larval dispersal rates according to three regions in our study (instead of two in Rossi et al. (2014)). In region 1, the spatial distribution of larvae near the surface was strongly influenced by the Northern Current and winds, as reported in other drift analyses of marine larval species with egg buoyancy on our study area (Mariani et al., 2010; Ospina-álvarez et al., 2012a). In regions 2 and 3, the larval drift was limited by local mesoscale eddies, which have high importance in retaining larvae (Cowen et al., 2000). Near Blanes Canyon, the beginning of Ebro shelf, and the Eivissa Channel, previous studies identified eddies potentially trapping larvae of various species such as *Engraulis encrasicolus* and

Sardinella aurita close to the northern side of the Ebro shelf (Pinot et al., 2002; Rubio et al., 2005; Escudier et al., 2013; Sabatés et al., 2013; Karimova, 2016). Decapod larvae have never been reported trapped in eddies in our study area, but Torres et al. (2014) and Hill et al. (1996) showed that decapod larvae were also aggregated by eddies south of the Balearic Islands and on the Norway lobster (*Nephrops norvegicus*) in the Irish Sea.

New connection or reinforcement of connection between zones by larval transport and resulted from the temporal changes of the eddy characteristics (i.e., if present, the diameter and the spatial position). During summer, the displacement and intensity changes in eddies along the Iberian Coast (Rubio et al., 2005; Escudier et al., 2013) modified the simulated drifts, and therefore, the connectivity between areas. The drifts were influenced by a cyclonic eddy in the western part of the Eivissa Channel, as described previously by Lafuente et al. (1995). Its presence changed the larval dispersal by preventing the larvae from crossing the channel. However, during our late summer simulation, the fishing ground of *A. antennatus* near the Cabrera Harbor of Majorca Island (Carbonell et al., 1999), was supplied by individuals from the Eivissa Channel. The present study modeled and described for the first time how the Palamós canyon or the southern Eivissa Channel fishing grounds could connect to the fishing grounds of Majorca Island. Nonetheless, exploring the temporal evolution of eddies and their influence on the larval drift is needed to consider the possibility of persistent connectivity.

2.2.4.3. Dispersals related to the location and position of larvae

Larval duration of surface *A. antennatus*' individuals depended to the Modified Atlantic Water mass dynamics. In our study, the PPD of larvae drifting at the surface varied along with a latitudinal gradient of near-surface temperatures of the NW Mediterranean Sea, which were colder in the vicinity of Cap de Creus and warmer at the Eivissa Channel (La Violette, 1995). This gradient has already been outlined by the interface of the old and cold Modified Atlantic water with the hot and recent Modified Atlantic water (López-García et al., 1994). Additionally, it conveyed that larvae spawn from one of those regions will have distinct drifts from the other and partially explained the delimitation of the three zones in our study. The late summer dispersal enlightened a change of seawater

temperature, which, besides the change in atmospheric conditions, can be related to the position of those two water masses. Indeed, the old Modified Atlantic water goes southward driven by wind and the southern entrance of the recent Modified Atlantic water is modulated by the water circulation in the channels of the Balearic Sea (López-García et al., 1994).

The larval drift in deeper layers can be a positive strategy induced by the buoyant stages. First, it implied that when the hatching occurred in deeper water layers, the PPD was longer. Second, the larvae drifted in the core of the North Current, which is maximal between 10 and 100 m (García-Ladona et al., 1996; Macías et al., 2014). Third, the underneath surface is advantageous to larval dispersal because it may provide a good growth environment with nutrients located near the deep chlorophyll maximum (Gorelli et al., 2014) and protection from predators (Lloyd et al., 2012). Fourth, the dispersal rate was wider and revolved round close settlement zones as well as far away zones. Consequently, for the first time, our study presents a potential connectivity between the two distant fishing grounds of Palamós and Soller (in Majorca Island from the Balearic Islands) areas and the expected drift conditions to link those places, where catches of *A. antennatus* are relatively important (Carbonell et al., 1999; Gorelli et al., 2014).

2.2.5. Conclusions

Our study analyzed the larval drift of *A. antennatus* under the hypothesis that either the nauplius stage or the protozoea stage is in the upper water masses. We considered concurrently the effects of two main factors on the connectivity that both contribute to the dispersal strategy of this benthic deep-sea species: buoyancy and water mass circulation. The buoyancy linked the eggs spawned at sea bottom to the larvae in the upper layers of the ocean. A consequence of the buoyancy was the split of the Lagrangian drifts into three latitudinal spawning areas in accordance with similar larval dispersal. Simultaneously, we found that connectivity patterns and retention rates were influenced by the presence of mesoscale structures such as meanders above the head of Blanes Canyon and eddies along the Valencian Gulf and in the Eivissa Channel. The drift of larvae in early and late summer followed the persistent main circulation pattern of the NW Mediterranean Sea, with temporally variable mesoscale structures adjusting the

connectivity between the different zones. The application of buoyancy on different larval stages also highlighted that positions of the larvae in the water column influenced the dispersal direction and the intensity of connectivity between zones of the NW Mediterranean Sea. This study contributes to increasing the knowledge of *A. antennatus*' egg and larval ecology, and illustrates the potential dispersal paths of the individuals during their pelagic life. The spatiotemporal influence of mesoscale circulations in the larval dispersal should be tackled in further studies to better understand the blue and red shrimp population connectivity, and to upgrade advice towards fishing practices and fisheries management.

2.2.6. Supplementary information

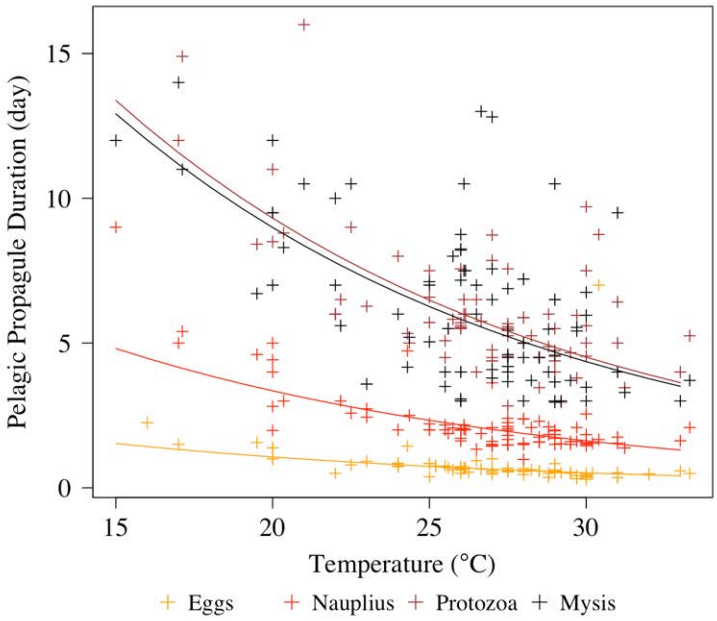

Figure S2. Decreasing Pelagic Propagule Duration (PPD) with increasing water temperature. Continuous lines are the fitted exponential curves on reviewed data (cross) for each stage: eggs (orange), nauplius (red), protozoa (brown), and mysis (black). Reviewed data of PPD and temperatures were extracted from published articles and referenced in Table S3.

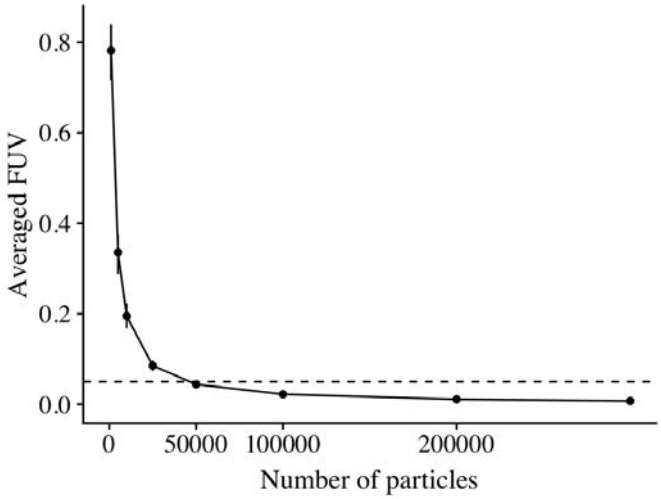

Figure S3. Number of particles needed to decrease the Fraction of Unexplained Variance (FUV) below the statistical threshold of 0.05. The FUV expressed the bias created by a low number of particles (FUV > 0.05) after dispersal simulation. Whiskers show the minimum and maximum of the 100 FUV calculated for each number of particles tested (1 000, 2 000, 5 000, 10 000, 50 000, 100 000, 200 000, 300 000). Horizontal dashed line is the statistical threshold of 0.05.

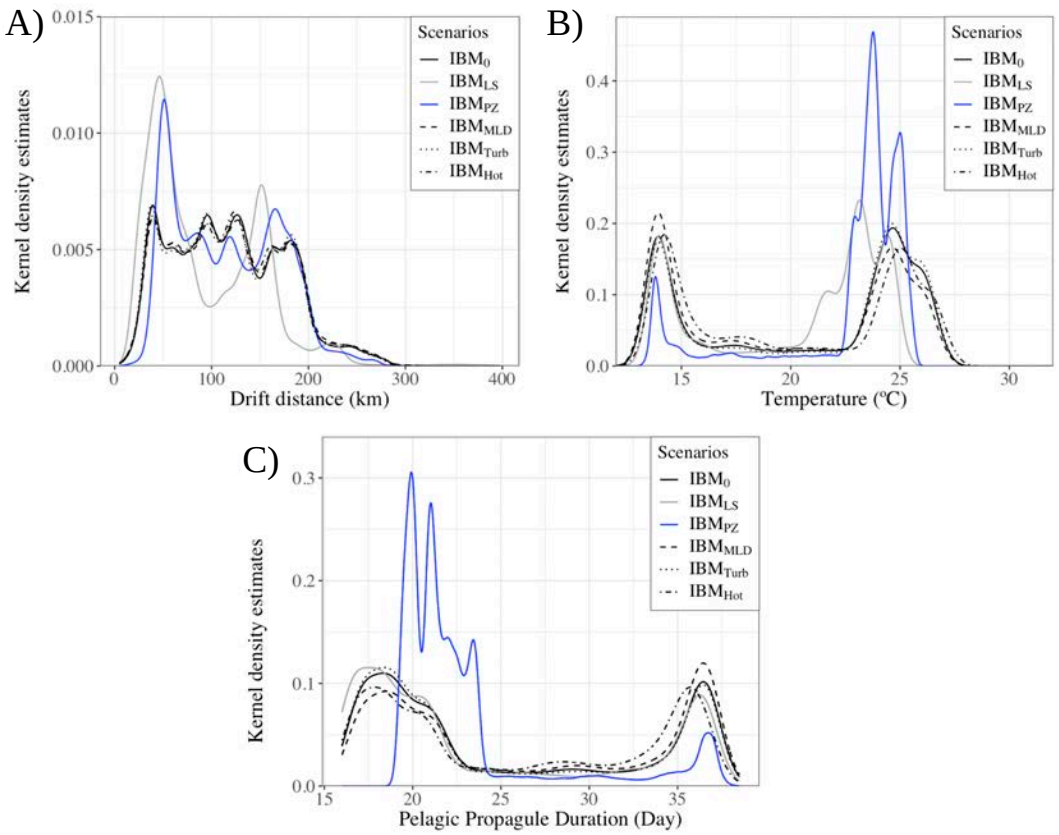

Figure S4. Kernel density estimates from 50 000 simulated individuals in different scenarios. The simulated transport characteristics were the drift distances (A), the Pelagic Propagule Duration (B), and the water temperature during the drifts (C). Black lines indicate the scenarios grouped together by the PCA (see Figure 20) with IBM_0, IBM_{MLD}, IBM_{Diff} and IBM_{Hot} in four different line types. Blue line indicates the scenario IBM_{PZ}, and grey line indicates the scenario IBM_{LS}. See Table 1 for a description of the IBM scenarios.

Table S3. Duration of embryonic and larval (propagules) stages according to the water temperature by Penaeid species.

Species	T (ºC)	Stage duration (d)	Stage	Reference
Artemesia longinaris	20.00	1.00	eggs	Boschi *et al.*, 1974
	17.00	1.50	eggs	
	20.00	4.00	Nauplius	
	17.00	5.00	Nauplius	
	20.00	11.00	Protozoa	
	17.00	12.00	Protozoa	
	20.00	12.00	Mysis	
	17.00	14.00	Mysis	
Macropetasma africanus	22.00	0.50	eggs	Crockcroft, 1985
	22.00	6.00	Nauplius	
	22.00	6.00	Protozoa	
	22.00	7.00	Mysis	
Metapeanopsis dalei	25.00	0.84	eggs	Choi and Hong, 2001
	25.00	2.00	Nauplius	
	25.00	6.58	Protozoa	
	25.00	5.04	Mysis	
Metapeanopsis stridulans	25.75	0.62	eggs	Chong and Sasekumar, 1994
	25.75	2.06	Nauplius	
	25.75	5.82	Protozoa	
	25.75	8.00	Mysis	
Metapenaeus affinis	27.50	0.58	eggs	Hassan, 1980
	27.50	2.12	Nauplius	
	27.50	5.67	Protozoa	
	27.50	6.88	Mysis	
	27.50	1.48	Nauplius	Hudinaga,1941
	26.10	0.67	eggs	Muthu *et al.*,1979a
	26.10	2.04	Nauplius	
	26.10	6.00	Protozoa	
	26.10	7.50	Mysis	
	29.70	0.31	eggs	Thomas *et al.*, 1974
	28.80	0.36	eggs	
	29.70	0.42	eggs	
	29.70	1.60	Nauplius	
	28.80	1.84	Nauplius	
	29.70	2.08	Nauplius	
	29.70	3.79	Protozoa	
	28.80	4.88	Protozoa	
	29.70	5.42	Mysis	
	28.80	5.48	Mysis	
	29.70	5.54	Mysis	
	29.70	5.96	Protozoa	
	30.00	0.45	eggs	Tirmizi *et al.*, 1981
	30.00	2.55	Nauplius	
	30.00	6.75	Mysis	
	30.00	7.50	Protozoa	
Metapenaeus bennettae	26.00	0.62	eggs	Preston, 1985a
	26.00	2.00	Nauplius	
	26.00	5.70	Protozoa	
	26.00	8.75	Mysis	
Metapenaeus brevicornis	30.00	0.40	eggs	Rao, 1979
	30.00	1.83	Nauplius	
	30.00	5.00	Protozoa	
	27.00	0.48	eggs	Teng,1971
	27.00	1.48	Nauplius	
	27.00	8.73	Protozoa	
	27.00	12.81	Mysis	
Metapenaeus dalli	26.00	2.00	Nauplius	Crisp *et al.*, 2016
	26.00	4.00	Protozoa	
	26.00	4.00	Mysis	
Metapenaeus dobsoni	26.15	0.69	eggs	Muthu *et al.*,1979b
	26.15	2.00	Nauplius	
	26.15	6.00	Protozoa	
	26.15	7.50	Mysis	
	30.00	0.35	eggs	Thomas *et al.*, 1974
	30.00	1.45	Nauplius	
	30.00	5.60	Protozoa	
	30.00	5.96	Mysis	

Species	T (ºC)	Stage duration (d)	Stage	Reference
Metapenaeus ensis	27.00	1.00	eggs	Leong *et al.*, 1992
	27.00	1.50	Nauplius	
	27.00	4.50	Protozoa	
	27.00	6.50	Mysis	
	29.00	0.53	eggs	Ronquillo and Saisho, 1993
	29.00	1.99	Nauplius	
	29.00	3.66	Mysis	
	29.00	4.74	Protozoa	
Metapenaeus joyneri	22.50	0.79	eggs	Lee and Lee, 1968
	22.50	2.58	Nauplius	
	22.50	9.00	Protozoa	
	22.50	10.50	Mysis	
	22.00	10.00	Mysis	
Metapenaeus macleayi	26.00	0.67	eggs	Preston, 1985b
	26.00	1.62	Nauplius	
	26.00	5.50	Protozoa	
	26.00	8.25	Mysis	
Metapenaeus monoceros	24.00	0.75	eggs	Aktas and Çavdar, 2012
	28.00	0.56	eggs	
	32.00	0.47	eggs	
	28.50	1.58	Nauplius	Courties, 1976
	27.50	1.48	Nauplius	Hudinaga,1941
	26.10	0.67	eggs	Mohamed *et al.*,1979
	26.10	2.17	Nauplius	
	26.10	6.50	Protozoa	
	26.10	10.50	Mysis	
	26.50	0.94	eggs	Khafage *et al.*, 2009
	26.50	1.33	Nauplius	
	26.50	6.00	Mysis	
	26.50	6.50	Protozoa	
Metapenaeus moyebi	26.50	4.00	Protozoa	Kurata and Vanitchkul, 1974*
	26.50	7.00	Mysis	
	31.00	0.35	eggs	Nandakumar *et al.*, 1989
	29.00	0.83	eggs	
	31.00	1.54	Nauplius	
	29.00	1.83	Nauplius	
	31.00	5.00	Protozoa	
	29.00	5.50	Protozoa	
	31.00	9.50	Mysis	
	29.00	10.50	Mysis	
Parapenaeopsis stylifera	25.00	0.38	eggs	Hassan, 1984
	25.00	2.21	Nauplius	
	25.00	5.71	Protozoa	
	25.00	7.12	Mysis	
	26.65	0.65	eggs	Muthu *et al.*,1979c
	26.65	1.88	Nauplius	
	26.65	5.75	Protozoa	
	26.65	13.00	Mysis	
	30.00	0.29	eggs	Thomas *et al.*, 1974
	30.00	1.54	Nauplius	
	30.00	9.71	Protozoa	
	30.40	7.00	eggs	
	30.40	1.67	Nauplius	
	30.40	8.75	Protozoa	
Parapenaeus longirostris	16.00	2.25	eggs	Heldt, 1938
Penaeus aztecus	30.20	0.50	eggs	Kitani, 1986a
	30.20	1.54	Nauplius	
	27.50	2.25	Nauplius	Krantz and Norris, 1976
	27.00	3.63	Nauplius	
	27.50	5.44	Mysis	
	27.50	7.56	Protozoa	
	27.00	7.56	Mysis	
	27.00	7.85	Protozoa	

Table S3. (Continued)

Species	T (ºC)	Stage duration (d)	Stage	Reference
Penaeus brevirostris	27.00	0.54	eggs	Kitani, 1997
	27.00	1.44	Nauplius	
	27.00	4.08	Mysis	
	27.00	4.38	Protozoa	
Penaeus californiensis	29.00	0.61	eggs	Kitani and Alvarado, 1982
	29.00	1.71	Nauplius	
	29.00	4.54	Protozoa	
	29.00	4.58	Mysis	
Penaeus chinensis	24.30	1.44	eggs	Oka, 1967
	19.50	1.56	eggs	
	24.30	4.17	Mysis	
	19.50	4.60	Nauplius	
	24.30	4.73	Nauplius	
	24.30	5.33	Protozoa	
	19.50	6.71	Mysis	
	19.50	8.42	Protozoa	
Penaeus duorarum	28.00	0.58	eggs	Dobkin,1961
	26.00	7.17	Mysis	Ewald, 1965
	26.00	7.56	Protozoa	
	21.00	10.50	Mysis	
	21.00	16.00	Protozoa	
	30.00	0.50	eggs	Kitani, 1985
	30.00	1.56	Nauplius	
	30.00	3.47	Mysis	
	30.00	4.54	Protozoa	
	27.50	1.81	Nauplius	Krantz and Norris, 1976
	23.00	2.73	Nauplius	
	23.00	3.58	Mysis	
	27.50	3.67	Mysis	
	27.50	5.56	Protozoa	
	23.00	6.27	Protozoa	
Penaeus esculentus	26.25	0.54	eggs	Fielder *et al.*, 1975
Penaeus indicus	25.60	0.69	eggs	Muthu *et al.*, 1974
	25.60	1.88	Nauplius	
	25.60	5.50	Protozoa	
	25.60	5.50	Mysis	
Penaeus japonicus	28.00	0.58	eggs	Hudinaga, 1942
	28.00	1.54	Nauplius	
	28.00	5.00	Protozoa	
	28.00	5.00	Mysis	
	28.00	1.50	Nauplius	Hudinaga and Miyamura, 1962
	28.00	3.00	Mysis	
	28.00	5.00	Protozoa	
Penaeus kerathurus	25.20	0.75	eggs	Heldt,1938
	24.00	0.85	eggs	
	20.00	1.38	eggs	
	20.00	2.81	Nauplius	
	27.50	2.04	Nauplius	Klaoudatos, 1978
	27.50	4.00	Mysis	
	27.50	5.50	Protozoa	
	27.00	2.08	Nauplius	Lumare and Gozzo, 1973
	20.00	4.42	Nauplius	
	29.50	0.50	eggs	Türkmen, 2004
	29.50	1.50	Nauplius	
	29.50	3.71	Mysis	
	29.50	4.67	Protozoa	
	24.00	2.00	Nauplius	Yufera *et al.*, 1984
	24.00	6.00	Mysis	
	24.00	8.00	Protozoa	

Species	T (ºC)	Stage duration (d)	Stage	Reference
Penaeus latisulcatus	24.36	2.50	Nauplius	Roberts *et al.*, 2012
	20.35	3.00	Nauplius	
	22.17	3.00	Nauplius	
	24.36	5.00	Protozoa	
	24.36	5.20	Mysis	
	17.12	5.40	Nauplius	
	17.12	11.00	Mysis	
	17.12	14.90	Protozoa	
	22.17	5.60	Mysis	
	22.17	6.50	Protozoa	
	20.35	8.30	Mysis	
	20.35	8.80	Protozoa	
	29.20	0.52	eggs	Shokita, 1970
	29.20	1.52	Nauplius	
	29.20	2.96	Protozoa	
	29.20	3.00	Mysis	
Penaeus marginatus	25.00	0.83	eggs	Gopalakrishnan, 1976
Penaeus merguiensis	27.50	0.55	eggs	Motoh and Buri, 1979
	27.50	1.67	Nauplius	
	27.50	2.83	Protozoa	
	27.50	4.19	Mysis	
	29.00	4.00	Protozoa	Zacharia and Kakati, 2004
	29.00	3.00	Mysis	
	33.00	3.00	Mysis	
	33.00	4.00	Protozoa	
	27.00	0.48	eggs	Teng,1971
Penaeus monodon	28.00	0.46	eggs	Motoh, 1979
	28.00	1.50	Nauplius	
	28.00	4.50	Mysis	
	28.00	5.00	Protozoa	
	25.20	0.75	eggs	Motoh, 1981
	24.00	0.85	eggs	
	20.00	1.38	eggs	
	33.00	0.58	eggs	Reyes, 1985
	28.00	0.67	eggs	
	23.00	0.92	eggs	
	28.00	0.98	Nauplius	
	33.00	1.63	Nauplius	
	23.00	2.43	Nauplius	
	27.50	1.98	Nauplius	Silas *et al.*,1979
	27.50	4.50	Mysis	
	27.50	5.25	Protozoa	
	27.50	0.68	eggs	
	28.80	0.50	eggs	Villaluz *et al.*, 1969
	28.80	2.10	Nauplius	
	28.80	4.00	Mysis	
	28.80	6.00	Protozoa	
Penaeus occidentalis	27.00	0.60	eggs	Kitani,1996
	27.00	1.60	Nauplius	
	27.00	3.79	Mysis	
	27.00	4.76	Protozoa	
Penaeus paulensis	30.00	1.50	Nauplius	Boff and Marchiori, 1984
	25.00	2.00	Nauplius	
	30.00	3.00	Mysis	
	20.00	5.00	Nauplius	
	25.00	7.00	Mysis	
	25.00	7.5	Protozoa	
	15.00	9.00	Nauplius	
	20.00	9.50	Protozoa	
	20.00	9.50	Mysis	
	15.00	12.00	Mysis	

Table S3. (Continued)

Species	T (ºC)	Stage duration (d)	Stage	Reference
Penaeus paulensis	26.00	0.50	eggs	Lemos and Phan, 2001
	26.00	2.00	Nauplius	
	26.00	3.00	Protozoa	
	26.00	3.00	Mysis	
Penaeus penicillatus	31.23	1.38	Nauplius	Heng and Rui-Yu, 1994
	31.23	3.29	Mysis	
	31.23	3.46	Protozoa	
	25.50	2.00	Nauplius	Pan and Yu, 1989
	25.50	3.50	Mysis	
	25.50	4.50	Protozoa	
Penaeus plebejus	26.00	0.73	eggs	Preston, 1985
	26.00	2.00	Nauplius	
	26.00	5.54	Protozoa	
	26.00	8.21	Mysis	
Penaeus schmidti	28.50	2.29	Nauplius	Pinto and Ewald, 1974
	28.50	3.46	Protozoa	
	28.50	4.50	Mysis	
Penaeus semisulcatus	24.00	0.73	eggs	Aktas *et al.*, 2004
	28.00	0.60	eggs	
	32.00	0.48	eggs	
	31.00	0.52	eggs	Devarajan, 1978
	31.00	1.75	Nauplius	
	31.00	4.00	Mysis	
	31.00	6.42	Protozoa	
	28.00	0.58	eggs	Hassan,1982
	28.00	2.38	Nauplius	
	28.00	5.88	Protozoa	
	28.00	7.21	Mysis	
	25.50	0.75	eggs	Kungvankij *et al.*, 1972
	25.50	2.17	Nauplius	
	25.50	4.00	Mysis	
	25.50	5.08	Protozoa	
	28.00	0.59	eggs	Ronquillo *et al.*, 2006
	29.00	1.97	Nauplius	
	29.00	2.96	Mysis	
	29.00	4.38	Protozoa	
Penaeus setiferus	27.50	2.40	Nauplius	Krantz and Norris, 1976
	27.50	4.54	Protozoa	
	27.50	4.60	Mysis	
Penaeus stylirostris	29.00	0.57	eggs	Kitani, 1986b
	29.00	1.50	Nauplius	
	29.00	6.50	Protozoa	
	29.00	6.50	Mysis	
	28.25	0.63	eggs	Prahl and Gardeazabal, 1977
	28.25	2.08	Nauplius	
	28.25	3.71	Mysis	
	28.25	5.25	Protozoa	
Penaeus vannamei	33.30	0.50	eggs	Andrade-Vizcaino, 2010
	33.30	2.08	Nauplius	
	33.30	5.25	Protozoa	
	33.30	3.71	Mysis	
	29.50	0.53	eggs	Kitani, 1986c
	29.50	1.60	Nauplius	
Trachypenaeus curvirostris	26.00	0.63	eggs	Ronquillo and Saisho, 1995
	26.00	1.71	Nauplius	
	26.00	3.07	Mysis	
	26.00	5.60	Protozoa	
Pleoticus muelleri	20.00	1.00	eggs	Iorio *et al.*, 1990
	20.00	1.98	Nauplius	
	20.00	7.00	Mysis	
	20.00	8.50	Protozoa	

Table S4. Ranges of egg sizes and available egg buoyancy for deep-sea crustaceans and Penaeid species.

Species	Type	Eggs diameter (µm)	Density (kg m^{-3})	Reference
Acanthephyra acanthitelsonis	Deep-sea	640 – 1920	1068	Herring, 1974
A.acutifrons	Deep-sea	760 – 1920	1050 – 11066	Herring, 1974
A.curtirostris	Deep-sea	620 – 1900	1057 – 11066	Herring, 1974
A. pelagica	Deep-sea	680 – 11000	1063	Herring, 1974
A. purpurea	Deep-sea	520 – 11120	1048 – 11075	Herring, 1974:
Chaceon affinis	Deep-sea	585 – 1655	n/a	Espinosa *et al.*, 2011
Ephyrina bifida	Deep-sea	3520 – 14700	1026	Herring, 1974
E. hoskynii	Deep-sea	3120 – 14000	1027	Herring, 1974
Farfantepenaeus aztecus	Penaeus	180 – 1280	n/a	Velazquez and Gracia, 2000
F. paulensis	Penaeus	304	n/a	Peixoto *et al.*, 2008
Heterocarpus ensifer	Deep-sea	540 – 1400	1081	Herring, 1974
H. grimaldii	Deep-sea	520 – 1640	1075	Herring, 1974
Hymenodora gracilis	Deep-sea	2000 – 12300	1026 – 11030	Chace,1940; Herring, 1974
Litopenaeus occidentalis	Penaeus	197 – 1238	n/a	Rojas and Alfaro, 2006
L.setiferus	Penaeus	200 – 1340	n/a	Perez and Gracia, 2000
L. stylirostris	Penaeus	219 – 1262	n/a	Rojas and Alfaro, 2006
L. vannamei	Penaeus	228 – 1274	n/a	Rojas and Alfaro, 2006
Meningodora miccyla	Deep-sea	720 – 1940	1054	Herring, 1974
M. vesca	Deep-sea	620 – 11100	1047	Herring, 1974
Metapenaeus ensis	Penaeus	260 – 1310	n/a	Ronquillo and Saisho, 1993
M. monoceros	Penaeus	145 – 1261	n/a	Nandakumar, 2001
Nematocarcinus cursor	Deep-sea	540 – 1420	1075	Herring, 1974
N. exilis	Deep-sea	640 – 1500	1082	Herring, 1974
Notostomus auriculatus	Deep-sea	640 – 1980	1054	Herring, 1974
N. elegans	Deep-sea	740 – 1800	1051	Herring, 1974
Oplophorus spinosus	Deep-sea	3140 – 13210	1025 – 11031	Herring, 1974; Sudnik 2017
Paralomis verrilli	Deep-sea	2000	n/a	Komai and Amaoka, 1989
Parapasiphaea sulcatifrons	Deep-sea	3200 – 14400	1026	Herring, 1974; Sudnik and Falkenhaug, 2015
Paromola cuvieri	Deep-sea	585 – 1655	n/a	Triay-Portella *et al.*, 2014
Pasiphaea hoblocerca	Deep-sea	2240 – 11600	1041	Herring, 1974
P. multidendata	Deep-sea	2600 – 12000	1038	Apollonio, 1969; Herring, 1974
Penaeus duorarum	Penaeus	230 – 1320	n/a	Velazquez and Gracia, 2000
P. monodon	Penaeus	270 – 1280	n/a	Pongtippatee-Taweepreda *et al.*,2014
P. vannamei	Penaeus	271	n/a	Palacios *et al.*, 1999
Pleisionika edwardsii	Deep-sea	440 – 1340	1079	Herring, 1974
Pontophilus talismani	Deep-sea	740 – 1520	1076	Herring, 1974
Systellaspis cristata	Deep-sea	2720 – 14120	1028	Herring, 1974
S. brauerei	Deep-sea	3120 – 14640	1027	Herring, 1974
S. debelis	Deep-sea	1880 – 1412	1028 – 1031	Herring, 1974

Table S5. Frequence of surfacing individuals (in percentage) in the preliminary experiments. Percentage of buoyant stages reaching the surface or the Mixed Layer Depth (MLD) for a given density (kg m^{-3}) in Individual-Based Model modified by the release period (early summer and late summer) and by the activation of random turbulences.

Release period	Early summer						Late summer	
Buoyant stage	eggs		eggs		eggs and nauplius		eggs	
Turbulence	No		Yes		No		No	
Water depth	Surface	MLD	Surface	MLD	Surface	MLD	Surface	MLD
800	4.39	4.12	4.78	4.24	0.00	0.00	4.78	4.24
810	3.10	2.92	3.38	2.94	0.00	0.00	3.38	2.94
820	4.03	3.67	4.06	3.74	0.00	0.00	4.06	3.74
830	4.54	4.39	4.82	4.56	0.00	0.00	4.82	4.56
840	5.55	5.21	5.90	5.32	0.00	0.00	5.90	5.32
850	6.86	6.53	7.33	6.71	0.00	0.00	7.33	6.71
860	8.38	7.86	8.66	8.05	0.01	0.02	8.66	8.05
870	9.48	9.14	9.82	9.40	0.03	0.03	9.82	9.40
880	10.66	10.39	10.80	10.60	0.02	0.04	10.80	10.60
890	10.97	10.88	11.06	11.17	0.05	0.09	11.06	11.17
900	10.36	10.91	9.91	10.65	0.11	0.20	9.91	10.65
910	9.02	9.62	8.37	9.25	0.24	0.54	8.37	9.25
920	6.70	7.30	6.03	7.01	0.61	1.14	6.03	7.01
930	3.70	4.28	3.28	3.95	1.32	2.85	3.28	3.95
940	1.66	1.98	1.38	1.78	3.34	7.25	1.38	1.78
950	0.51	0.68	0.36	0.56	8.07	16.26	0.36	0.56
960	0.09	0.12	0.07	0.09	17.64	30.08	0.07	0.09
970	0.00	0.00	0.00	0.00	30.83	31.76	0.00	0.00
980	0.00	0.00	0.00	0.00	29.93	9.50	0.00	0.00
990	0.00	0.00	0.00	0.00	7.66	0.22	0.00	0.00
1000	0.00	0.00	0.00	0.00	0.14	0.00	0.00	0.00

Table S6. Characteristics of eddies involved in the larval dispersals. Three eddies were shaped by the larval dispersal simulation (see Figure 22). Coordinates of the eddy center were estimated with an algorithm from Nencioli et al. (2010). The edge of eddies was got from the streamlines. Computation of the eddy radius is based on the circle surface (Area= pi*$Radius^2$) and approximated the estimated eddy size.

Regions	**Month**	**Coordinates eddy center**	**Area (km^2)**	**Radius (km)**	**Rotation**
Northern part of the Valencian Gulf	July September	1.96 ºE; 40.67 ºN 2.04 ºE; 40.61 ºN	2550 4231	29 37	Clockwise Clockwise
Southern part of the Valencian Gulf	July September	0.35 ºE; 39.46 ºN 0.32 ºE; 39.33 ºN	3353 4897	33 39	Clockwise Clockwise
Eivissa Channel	July	0.72 ºE; 38.70 ºN	2977	31	Anticlockwise

Section 2.3

Modeling the spatiotemporal distribution of the deep-sea shrimp *Aristeus antennatus* (Crustacea: Decapoda) on the northwestern Mediterranean continental margin crossed by submarine canyons

Morane Clavel-Henry
Nixon Bahamon
Jordi Solé
José A. Garcia del Arco
Giulia Gorelli
Marta Carretón
Guiomar Rotllant
Joan B. Company

Congress poster: The Crustacean Society, Mid-Year Meetings 2017, Barcelona, Spain.

Article Submitted to **Journal of Marine Systems** (2019)

Abstract

Submarine canyons aggregate numerous marine species and can affect the structure of benthic communities. However, analyses dedicated to assess the spatial distribution variability among several canyons are rare. In the northwestern Mediterranean Sea, three major submarine canyons consecutively indent the narrow margin. There, the abundance of deep-sea blue and red shrimp *Aristeus antennatus* (Crustacea: Decapoda), one of the most important fishery-targeted species in the western and central Mediterranean Sea, sustains relatively high incomes for the nearest fishing harbors. To date, the spatial distribution of this shrimp species has only been assessed on known fishing grounds, but it has neither been modeled simultaneously covering several submarine canyons nor according to the environmental conditions. In this study, we aimed to look over the spatiotemporal shrimp distribution in a region of the northwestern Mediterranean Sea with a particular interest on variations in the three submarine canyons. From summer landing data between 2005 and 2014, we implemented a species distribution model with georeferenced catches linked to environmental data of the shrimp habitats. The model showed that the bottom topography was one of the most essential variables to explain the spatial distribution of the catches and that the highest catch rates were between 475 m and 575 m depth. Overall, two canyons (Blanes and Palamós) sheltered higher estimates of catches on the shallower and narrower part of their margins (at 510 and 565 m depth). Among them, 60% of estimated summer catches came from Palamós canyon, but this estimate shifted to Blanes canyon in summer 2008, probably due to variations in fishing fleet behavior. Modeled hypothetical warmer temperature scenarios suggested the shrimp catches would decrease less in Blanes canyon (3% fewer catches) than in Palamós canyon (20% fewer catches). The information produced by the species distribution model allowed setting spawning locations and depths, which is useful to better understand the canyon influence on benthic communities and to parameterize larval transport models.

2.3.1. Introduction

Good knowledge of species distribution is helpful to assess the impact of human activities and the environment and to set management or conservation plans (Brown and Yoder, 2015). In marine systems, the distribution and abundance of populations are

altered by fishery activities (Montero et al., 2016), climate change (Jones and Cheung, 2015), and the effectiveness of implementing marine protected areas (Krüger et al., 2017). Marine species aggregate in highly productive near shore, in upwelling systems, and particular topographic areas such as submarine canyons (Leo et al., 2010; Sigman and Hain, 2012). In relatively low productive continental margins, canyons are rugged geomorphological structures gathering multiple favorable ecological conditions for marine community development, i.e., nutrient and food availability, and habitats (Fernandez-Arcaya et al., 2017), including commercial species that are often over-exploited (Danovaro et al., 2010).

In the Catalan Sea, a region of the NW Mediterranean Sea between the latitudes 40.8º N and 43º N, three major submarine canyons (Cap de Creus, Palamós, and Blanes) cross a continental margin geographically close to fishing harbors. These canyons shorten the access of the fishing fleets to abundant resources, like the deep-sea blue and red shrimp *Aristeus antennatus* (Risso, 1816), one of the most targeted species of the western Mediterranean Sea. This shrimp has a distribution modulated by seasonal migrations across the continental margin (Sardà et al., 2003a; Tudela et al., 2003) and interactions with submarine canyons (Sardà et al., 1997; Tudela et al., 2003).

Most landings of *A. antennatus* take place in the fishing harbors of Palamós and Blanes that are located nearby eponymous submarine canyons (Company et al., 2008). There, the waters conditions are mostly determined by the stable Levantine Intermediate Water (LIW), with water temperatures between 13.0 and 13.8 ºC and salinity ranges between 38.48 and 38.60 PSU (Salat and Cruzado, 1981) and match with the physiological preferences of the shrimp (Carbonell et al., 2017). In summer, shrimp landings are particularly high because female spawners aggregate at fishing ground depths between 400 and 900 m (Sardà et al., 2003b). In contrast, winter waters are turbulent and sometimes funneled inside the canyons, which chase the shrimps off the fishing grounds. However, these intense perturbations issued from Dense Shelf Water Cascading (DSWC) events only occur during very cold and dry winters (Company et al., 2008).

Information about the population dynamics of *A. antennatus* originates from different local analyses in canyons (Sardà et al., 2009; Gorelli et al., 2014) and in areas over the open slope (Maynou, 2008; Amores et al., 2014; Carbonell et al., 2017; Cartes et al., 2018). To date, some studies have focused on the spatial distribution of the shrimp by data interpolation (i.e., Maynou et al., 1996; Palmas et al., 2015) or by estimation with environmental variables (i.e., Paradinas, 2017; Masnadi et al., 2018). Nonetheless, the spatial variability of shrimp distribution has not yet been tackled over the whole fishing areas in the NW Mediterranean Sea, including the submarine canyons.

In the present study, we aim to estimate the location of *A. antennatus* spawning sites in the Catalan Sea, their characteristics related to the topography and water masses, and their spatiotemporal variability in various submarine canyon conditions. Spawning sites were modeled by a species distribution model based on summer georeferenced catches of *A. antennatus* linked to bottom topography and other near-bottom water characteristics.

2.3.2. Materials and Methods

Geo-referenced daily catch data of *A. antennatus* on trawling grounds over the Catalan slope, seafloor characteristics, and environmental variables were processed by a statistical model to estimate the shrimp distribution of their spawning sites. The implementation of the model was based on summer data because it focused on the spawning places of mature females, it neglected the temporal effect from shrimp mobility and seasonal variability of environmental data, and it corresponded to the peak of shrimp catches (Sardà et al., 2003b).

2.3.2.1. Catch per unit effort data

Standardized CPUEs were used as the response variable for fitting the species distribution model. Beforehand, a total of 1 645 569 daily geo-referenced catch data of *A. antennatus* were provided by the General Direction of Fishing and Maritime Affairs (DGPAM) of the Autonomous Catalan Government for the spawning period of the species (June to September) between 2005 and 2014. Each catch data are arranged by

shrimp size-category, which differentiates the small shrimps (i.e., < 30 mm at carapace length) from the large ones (i.e., > 30 mm at carapace length). Analyses were conducted on large size-category catches, which have higher rates of ready-to-spawn females (Sardà *et al.*, 1997). Catches per unit of effort (CPUE; in kg day^{-1} vessel^{-1}) were linked to the fishing location recorded by the Vessel Monitoring System (VMS, see Additional File) since 2005 (Martín et al., 2014). The data were provided for the most important shrimp fishing grounds of the Catalan Sea: Llançà, Roses, Palamós, Blanes, Arenys de Mar, Barcelona, Vilanova i la Geltrú, and Tarragona (see Figure 27). However, we omitted some data from the analysis to avoid biasing by artifactual regional variability because preliminary analyses suggested that CPUEs from Tarragona, Llançà, and Barcelona fishing harbors were unreliable.

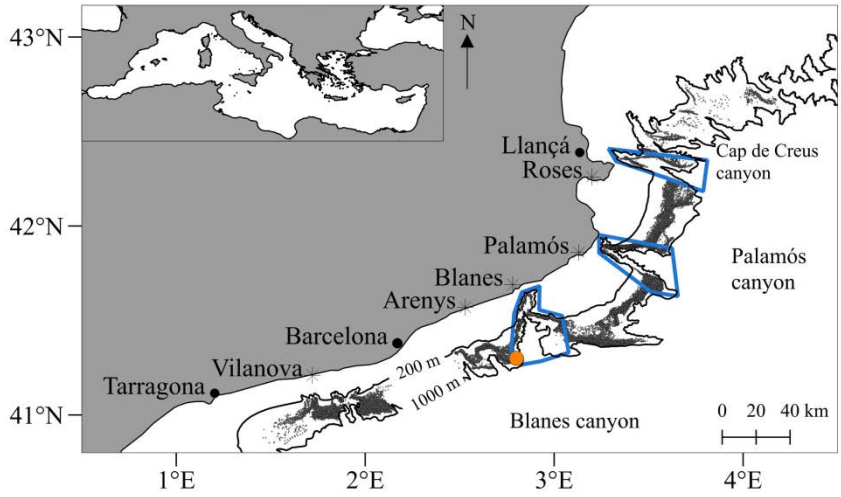

Figure 27. Location of fishing harbors, VMS data (small black dots), and shelf-indenting submarine canyons (blue polygons) along the Catalan slope of the northwestern Mediterranean Sea. The location with the highest standardized CPUE is indicated by the orange dot. The 200 and 1000 m depth isobaths represent the bathymetric limits of *A. antennatus* catches. Fishing harbors with data used in the analyses are indicated by stars, while data from fishing harbors located by a full circle were omitted.

Adapting the method by Mamouridis *et al.* (2014), CPUE data were standardized by fitting a multiple linear regression:

$$log(CPUE) = year + month + harbor + year|harbor + GRT + \varepsilon \quad (10)$$

where log*(CPUE)* represents log-transformed CPUE, *GRT* is the vessel Gross Registered Tonnage, *year|harbor* represents the effect of yearly landings by the harbor, and ε the unknown error. This model explained 33.2% of the data variability and was appropriate according to the residuals analysis (Figure S5).

2.3.2.2. Environmental variables and seafloor characteristics

For fitting the species model distribution, we selected environmental variables and seafloor characteristics relevant to the preferences of *A. antennatus* such as salinity, temperature (Guijarro et al., 2008), bathymetry (Sardà et al., 2004), dissolved oxygen (Cartes et al., 2018).

Monthly gridded environmental data from 2005 to 2014 were provided by outputs from the open-source biogeochemistry and physics reanalysis of the model NEMO-OPA (http://marine.copernicus.eu) with a spatial resolution of 0.06º. The gridded bathymetry was provided by outputs from EmodNET (http://www.emodnet-bathymetry.eu) with a spatial resolution of 0.021º. Additionally, other environmental and seafloor variables were derived from the previous outputs, as they may contribute to shape the shrimp CPUEs distribution (Maynou, 2008; Sardà et al., 2009; Amores et al., 2014). The kinetic energy (*KE*) was computed from the meridional (*u*) and zonal (*v*) velocities, such as:

$$KE = 0.5 \cdot (u^2 + v^2)\,. \qquad (11)$$

The rugosity of the floor and the slope were estimated from the gridded bathymetry following the methods of Wilson et al. (2007) and Horn (1981), respectively, on a window of nine grid cells. Rugosity and slope were supplementary topographic data that characterized the three-dimensional relief around the fishing depth. For instance, rugosity values around zero represented an even topography, while rugosity values above zero denoted topography steepness increasing on a relatively short distance (Figure 28).

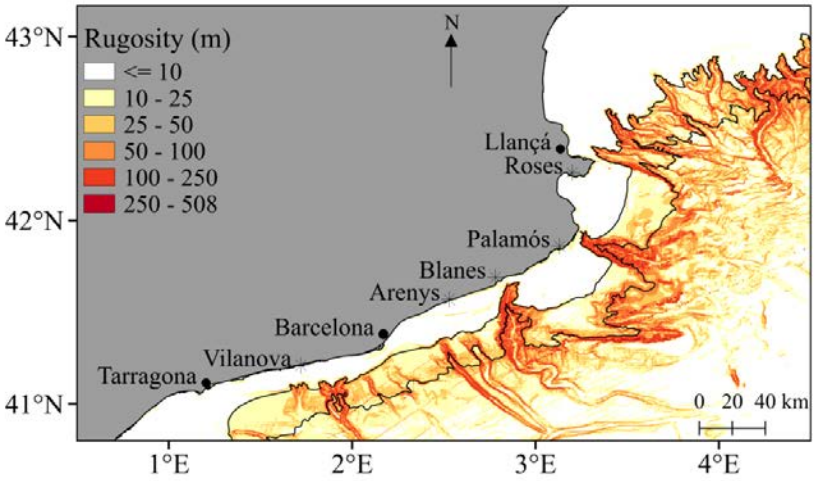

Figure 28. Rugosity of the Catalan Sea seafloor. The 200 and the 1000 m depth isobaths are represented by continuous black lines. Fishing harbor's symbols are indicated in Figure 27.

Before fitting the model, we summed up monthly standardized CPUE values to grid cells of 0.015 º spatial resolution covering a domain between 40.6 – 43º N and 1 – 5º E. With this resolution and domain borders, four CPUE grid cells fitted in one grid cell of environmental data. Then, the near-bottom environmental variables (e.g., salinity and water temperature) and seafloor characteristics (e.g., bathymetry, rugosity, and slope) were interpolated to monthly CPUEs location.

2.3.2.3. Modeling the link between CPUEs and environmental data

The random regression forest method (R-package *randomForest* by Liaw and Wiener (2001)) was used to adjust the species distribution model. This method was selected for being able to deal with the expected non-linear relationships between the response variable (log-transformed CPUE of *A. antennatus*) and predictors (Sardà et al., 2009).

Random forest is a stable algorithm with a good predictive capacity (Šiaulys and Bucas, 2012; Luan et al., 2018) though it is rarely used for marine species distribution models. Described in Breiman (2001), the algorithm starts by randomly sampling several subdatabases (called bootstrap sample) with replacement from the main dataset (i.e., bagging's method). The size of each subdatabase is approximately two-thirds of the dataset. Then, a regression tree is fitted on each subdatabase. One tree grows with nodes that are the best split of the subdatabase from randomly selected predictors. Last, all the regression trees are averaged to obtain the final estimates. The number of decision trees (i.e., the size of the forest and the number of subdatabases) and the number of randomly selected predictors splitting the tree were fixed to 500 and 4, respectively. Those values were both selected for stabilizing the error rate between the predictions and the observations. After building the random forest, the out-of-bag data (the remaining one-third of the dataset) were used to evaluate the performance of the model (i.e., the proportion of variance explained by the model) and helped for the model validation.

The random forest model was fitted with datasets of non-collinear predictors (i.e., the environmental and topographic variables). In the case of high collinearity (r-value > 0.60), we selected the predictors that explained greater variability in the model. Thus, dissolved oxygen or salinity was disregarded because of their relatively high collinearity

(*r*-value = 0.62). We proceeded similarly for slope and rugosity, as they had very high collinearity (*r*-value = 0.99). The combination of predictors to yield the best model was kept after a stepwise criteria methodology, based on i) the proportion of variance explained by the model, ii) their importance in the model based on mean squared error (MSE) method (Breiman, 2001), and iii) the verification of model residuals (Figure S6). Spatial projection of the residuals and semi-variograms were built on the residuals to detect and correct eventual spatial bias created by the data distribution (Dormann et al., 2007). Besides, we verified the model performance by ten-fold cross-validation for which ten Root Mean Square Errors (RMSE) were calculated by:

$$\frac{\sqrt{\sum \left[CPUE_{estimated} - CPUE_{observed}\right]^2}}{n} \qquad (12)$$

where *n* is the number of CPUE data.

2.3.2.4. Spawning sites distribution

Estimation in the Catalan Sea

Using estimates from the best-fitted random forest model, the spawning sites were characterized according to predictor values and located in the Catalan Sea. For better featuring the variations of standardized and model-estimated CPUEs, we scaled them to the percentage of their respective maximum CPUE values. Thus, the scale ranged from 0% (the minimum CPUE) to 100% (the highest CPUE).

With these scales, we compared the fluctuation of standardized and model-estimated CPUEs and estimated the optimized predictor ranges on which the CPUEs were relatively high (e.g., > 75% of CPUE maximum). The locations of spawning sites were hindcast by the best-fitted random forest on a gridded domain with a grid resolution of 0.015º and the borders between 40.6 – 43º N and 1 – 5º E from 5 m to 2380 m depth. In total, 40 spatial estimations of CPUEs were predicted based on the monthly values of gridded environmental and topographic variables rescaled on grid resolution of 0.015º (i.e., June, July, August, and September between 2005 and 2014). Then, the spatial shrimp distribution in a specific summer was the summing up of the four-month

estimates of CPUEs per grid cell.

Estimation in the submarine canyons

To compare the species distribution between the three submarine canyons, we extracted the model-estimated CPUEs per canyon area (see Figure 27). The three canyon areas were shaped by a polygon overlaying head and walls of the canyons as indicated by the isobaths 200 and 1000 m depth. On one hand, we approached the variability of the maximum CPUE percentages across the continental slope (i.e., around 200 to 1400 m) per summer between 2006 and 2014. On the other hand, we estimated the summer contribution of the canyons to the total model-estimated CPUEs, in other words, we evaluated which canyons yielded the highest catches by summer. A ratio of the canyon surface to the biggest canyon surface (i.e., Blanes canyon with 436 km^2) corrected the total model-estimated CPUEs per canyon in order to account for the canyon size differences.

Additionally, we hindcast CPUEs while increasing and decreasing water temperature by 0.1º up to 1 ºC above (warmer water) and below (cooler) the canyon-averaged temperature. Simulations of CPUE values with water temperature below 13 °C were closer to potential scenarios related to persistent-in-time events of dense shelf water cascading (DSWC), even though the events may not last to summer. For example, in winter 2005/2006, a very strong DSWC event lowered the near-bottom water temperature in winter and spring from 13 °C to 10.5 °C (Canals et al., 2006). On the contrary, warmer scenarios above 13 °C are in line with the reported warming trend of the Western Mediterranean Sea (Schroeder et al., 2016) and with global warming trends (Penuelas et al., 2017).

2.3.3. Results

The most suitable environmental conditions and seafloor characteristics for spawning females of *A. antennatus* in the whole Catalan Sea were identified with the Random Forest model and explained 60.1% of the variability. Overall, the performance of RF was stable, as indicated by RMSE from the 10-fold cross-validation (1.669 ± 0.009 kg km^{-2}

day^{-1}). Residuals analyses indicated that there was no significant spatial correlation and residual normality was followed (Figure S6). Because the model had good performance ability, we analyzed the predictor ranges associated with high catches and the spatial model-estimated CPUEs in the Catalan Sea with details per canyon.

2.3.3.1. Predictor ranges and optimized CPUEs estimates

In order of importance, the predictors included in the model were the combination of summers, bathymetry, seafloor rugosity, CPUEs coordinates, water temperature, kinetic energy, and salinity (Figures S7 and S8).

The fitted random forest model proved its predictive capacity for capturing the temporal variations of cumulated standardized CPUEs for summer periods during the decade 2005 – 2014 (Figure 29). The landings had two local maxima in summers 2008 and 2012. Particularly, in summer 2012, the CPUE standardized and model-estimated landings reached maxima of 70.7 T and 43.4 T, respectively (Table 3).

Table 3. Value of the predictors with CPUE maximums from both the standardized dataset and the model prediction. The column Figure indicates the figure index and panel on which the value of maximum CPUE rescaled the datasets.

Predictors	Predictors value at the maximum CPUE	Value of the maximum CPUE	CPUE from:	Figure
Summer year	2012	70 742 kg	Dataset	29
		43 466 kg	Prediction	29
Bathymetry	-506 m	20.2 kg day^{-1} km^{-2}	Dataset	30.A
		13.3 kg day^{-1} km^{-2}	Prediction	30.A
Temperature	12.97 ºC	21.1 kg day^{-1} km^{-2}	Dataset	30.B
		13.7 kg day^{-1} km^{-2}	Prediction	30.B
Salinity	38.52	31.0 kg day^{-1} km^{-2}	Dataset	30.C
		19.6 kg day^{-1} km^{-2}	Prediction	30.C
Rugosity	29.24	22.7 kg day^{-1} km^{-2}	Dataset	30.D
		14.6 kg day^{-1} km^{-2}	Prediction	30.D
Coordinates	2.80º E; 41.30º N	333.6 kg km^{-2} summer^{-1}	Dataset	27
	3.36º E; 41.88º N	142.6 kg km^{-2} summer^{-1}	Prediction	32

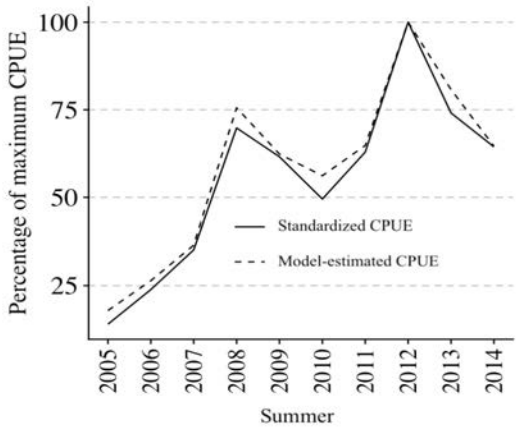

Figure 29. Interannual variation of the summer CPUE (percentage of the maximum) from standardized (continuous line) and model-estimated (dashed line) CPUEs.

Except for the kinetic energy predictor, *A. antennatus* CPUEs (i.e., standardized and model-estimated) had a comparable Gaussian-like relationship, which, therefore, described the optimal environmental variation for the shrimp distribution (Figure 30). CPUEs were maximum at 506 m depth with 12.97 ºC water temperature, 38.5 PSU salinity, and seafloor rugosity of 29.2% (Table 3), thus providing environmental boundaries for spawning areas. CPUEs near the maximum (i.e., above 75% CPUE) were related to temperature variations of $\Delta T = 0.30$ ºC, while the range for salinity was much narrower ($\Delta S = 0.026$ PSU).

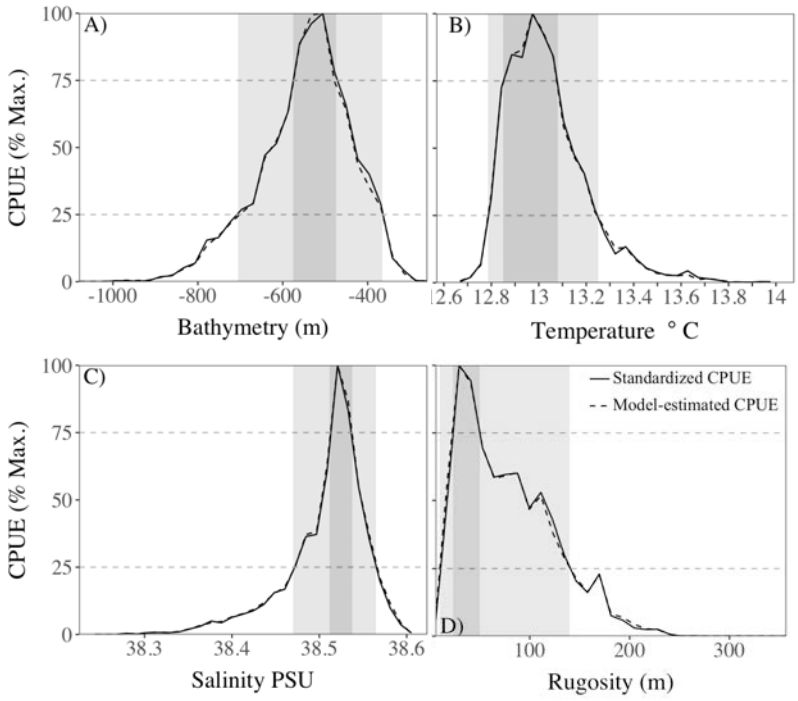

Figure 30. Distribution of the CPUE (percentage of the maximum) from the standardized (continuous line) and the model-estimated (dashed line) CPUEs, according to A) bathymetry, B) water temperature, C) salinity, and D) rugosity. The shadowed areas represent the range of predictor values for which the CPUE percentage is higher than 25% (light grey) and 75% (dark grey). See Table 4 for the maximum CPUE values.

2.3.3.2. Spawning sites in the Catalan sea and the submarine canyons

Over the Catalan Sea, percentages of maximum CPUE were high over a limited bathymetric gradient and in the submarine canyons. Higher CPUEs occurred on a narrow band of the bathymetry in the rugged canyons. On average, the bathymetry between 475 and 575 m depth sheltered more than 75% of the maximum predicted CPUE (13.3 kg day^{-1} km^{-2}, Figure 30.A). This bathymetric range narrowed in the canyons where the distribution of the highest CPUEs was estimated between 510 and 565 m depth (see Figure 31). In Palamós canyon, high estimations of CPUEs were as well distributed at the bottom between 575 and 625 m depth. Those patterns were related to the rugosity, the fourth more important predictor, because higher CPUEs were expected between 23 and 50% (Figure 31) while in canyons, rugosity averaged around 68, 100, and 101% for Cap de Creus, Palamós, and Blanes canyons, respectively (Table 4). Opposingly, on the open slope with rugosity ranging from 38 to 66%, higher CPUEs were estimated on a larger bathymetric band (i.e., between 480 and 840 m depth).

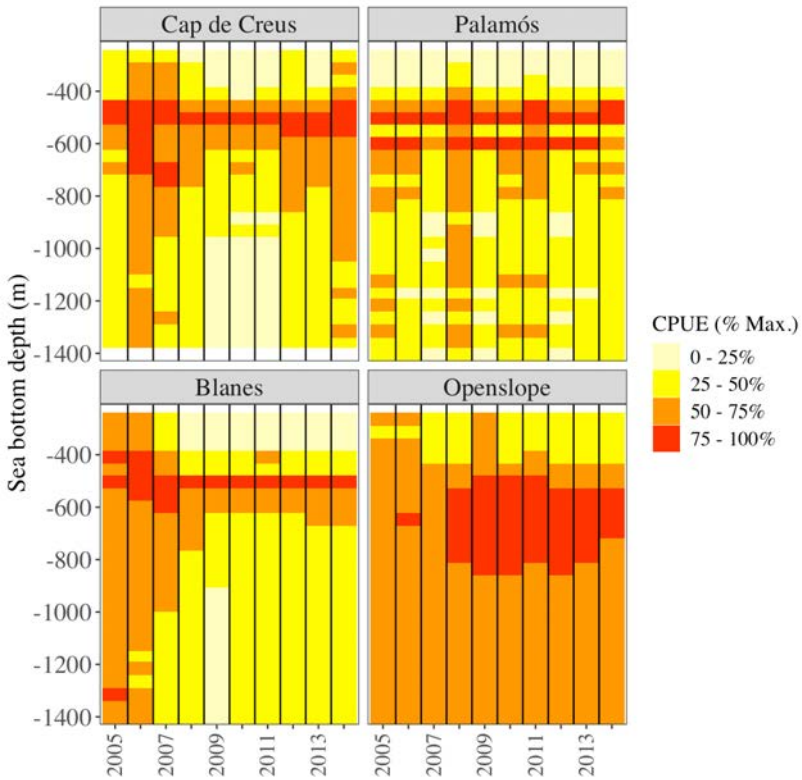

Figure 31. Summer distribution of the model-estimated CPUE (percentage of maximum) over the continental margin (200 m to 1400 m) in the submarine canyons of Cap de Creus, Palamós, and Blanes (see Figure 27) and on the open slope. Percentages of maximum were computed based on the maximum CPUE of each summer between 2005 and 2014.

Table 4. Average values and ranges (minimum/maximum) of the predictors associated with Vehicle Monitoring System positions on the open slope and within the areas of Cap de Creus, Palamós and Blanes canyons.

Variable (unit)	Open slope	Cap de Creus	Palamós	Blanes
Bathymetry (m)	533 (249/1069)	775 (127/1358)	1019 (84/2095)	845 (56/1954)
Temperature (ºC)	13.0 (12.7/14.0)	13.1 (12.8/13.8)	13.0 (12.6/14.6)	12.9 (12.6/15.3)
Salinity (psu)	38.5 (38.2/38.6)	38.5 (38.3/38.6)	38.5 (38.1/38.6)	38.5 (38.2/38.6)
Rugosity (m)	59.2 (2.60/353)	66.9 (8.3/216)	94.5 (2.4/296.3)	89.4 (0.4/ 251.8)
KE ($cm^2\ s^{-2}$)	1.85 (0/ 132)	1.57 (0/161)	3.96 (0/161)	1.38 (0/52.9)

The model estimated relatively high catches (> 40% of maximum CPUE) in the canyon zones of the Catalan Sea (Figure 32). On average, higher CPUEs (> 60% of maximum including the maximum estimate of CPUE of 142 kg km^{-2} $summer^{-1}$; Table 3) were located in the Palamós canyon head and middle upstream wall. Lower values of CPUEs (i.e., 20 – 60% of maximum CPUE) were situated on the downstream wall of the Blanes canyon where the highest standardized catches (i.e., 333 kg km^{-2} $summer^{-1}$; Table 3) were located before the model fitting. In the two canyons, estimated CPUE showed important temporal variability (Figure S9), as expected from the interannual variations shown in Figures 29 and 31. The CPUEs estimated in the Cap de Creus canyon were barely higher than estimates on the open slope (< 20%, Figure 32). The estimated CPUEs were low (< 5% of maximum CPUE) on bottom depth below 500 m.

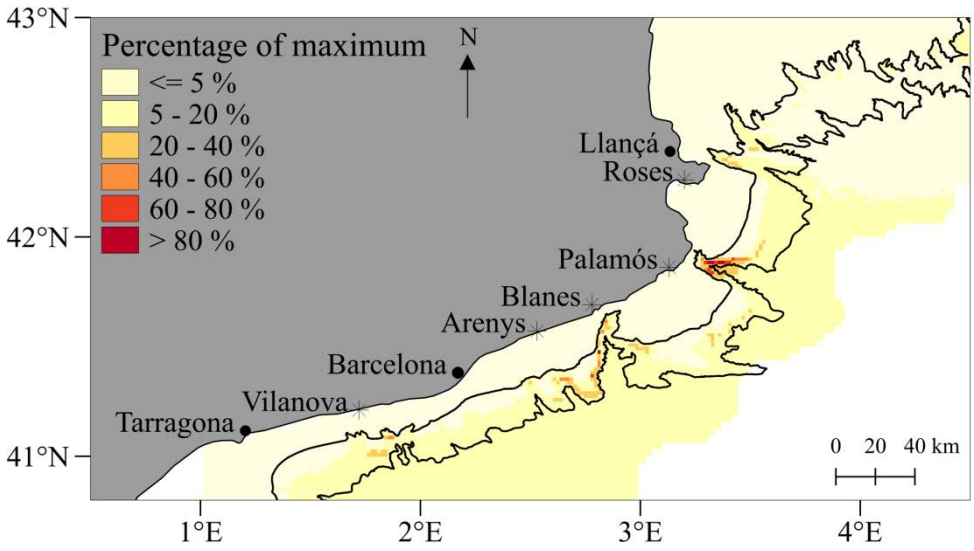

Figure 32. Average model-estimated CPUE (percentage of the maximum) in the Catalan Sea over the decade 2005 – 2014. Isobaths at 200 and 1000 m depth are represented by continuous black lines. Fishing harbors indicated by a star provided model input data. Fishing harbor's symbols are indicated in Figure 27.

2.3.3.3. Evolution of the spawning sites in the submarine canyons

The contribution of the Blanes canyon to the catches within the three main canyons (Blanes, Palamós, and Cap de Creus) increases with time (see Figure 33). Between 2005 and 2007, higher catches from Palamós Canyon prevailed in the total catches from all canyons (> 60% of the catches), but in 2008 and from 2011, the relative contribution of catches from Blanes canyon (50 to 60% of the CPUE) was dominant. This shift was also identified in the gridded CPUEs estimates (Figures S10.A-J) with contributions lower than 50% from the Blanes canyon for the years 2005, 2006, and 2007 but then, with contributions greater than 50% for the next years. The contribution to the total catches by the Cap de Creus canyon remained relatively stable over time, with an average CPUE of 20%, ranging from 11% in 2007 to 25% in 2008.

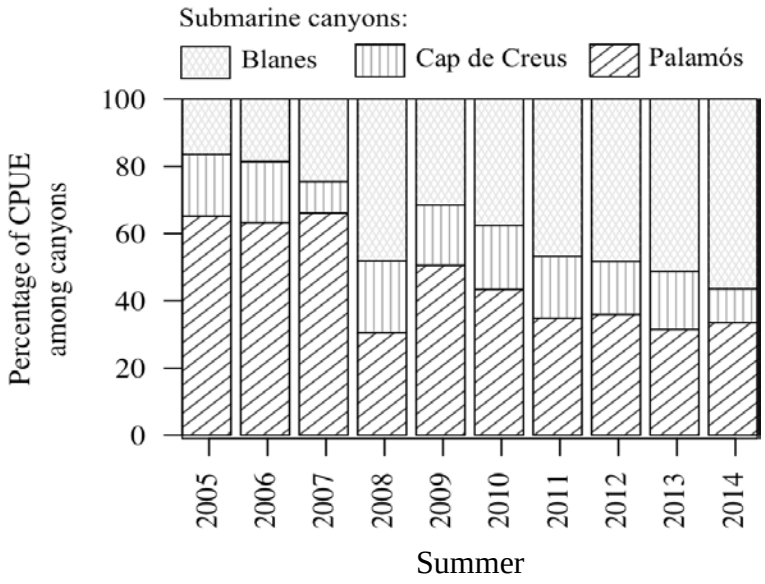

Figure 33. Variation of annual CPUE contributions (in percentage) from the three submarine canyons. Model-estimated CPUEs in each canyon were divided by the sum of CPUEs in all canyons (200 to 1000 m depth). The variability in canyons sizes (Cap de Creus 350 km2; Palamós 372 km2; Blanes 436 km2) was accounted by rescaling the CPUEs to the size of Blanes canyon (i.e., multiplying the CPUE by 1.25, 1.17, and 1, respectively).

Except for the seafloor characteristics (i.e., rugosity and bathymetry) and the KE, the remaining environmental conditions in each canyon were barely different (see Table 4). In particular, the near-bottom temperature linked to maximum catches ranged from about 12.9 ºC to 13.1 ºC. Nonetheless, the hindcast CPUE after changing water temperature differed among canyons (see Figure 34). In the Blanes Canyon, the estimated CPUE was

maximum at 13 ºC and a decrease or a rise of temperature would barely change the CPUE. In Palamós canyon, the rise of temperature would decrease the catches by 20% below the maximum CPUE at 13ºC, whereas the colder temperature would decrease the catches by 7%. In Cap de Creus canyon, cold temperatures (<12.8 ºC) would generate maximum CPUE values, but from 12.8ºC to 13.5ºC, the CPUE would decrease by 15%.

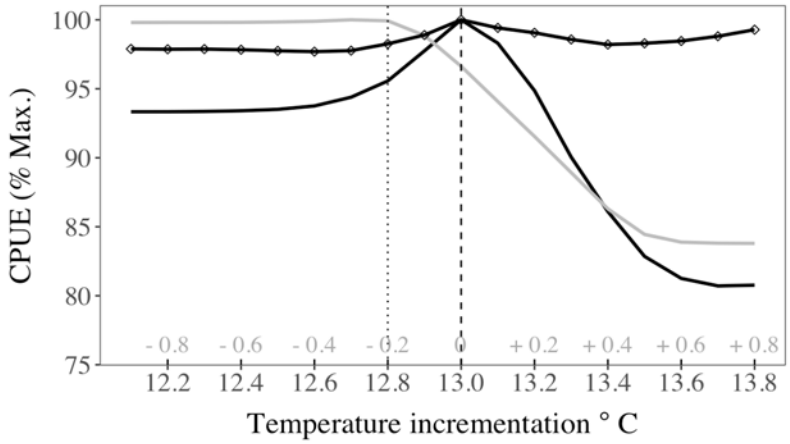

Figure 34. Model-estimated CPUE (percentage of the maximum) in the canyons of Cap de Creus (grey lines), Palamós (black line), and Blanes (black line with diamond tick marks) by artificially decreasing and rising the average water temperature by 1 ºC. The dashed line indicates the average near-bottom sea temperature (13 ºC) for which the CPUEs are maximum in the canyons of Palamós and Blanes. The dotted line is the sea temperature (12.8 ºC) at which the CPUEs in the canyon of Cap de Creus begins to decrease.

2.3.4. Discussion

For the first time, the summer spatial distribution of the blue and red deep-sea shrimp over the entire continental slope in the Catalan Sea has been modeled. Boundaries of spawning areas in the Catalan Sea and inside submarine canyons were set by analyses of optimal environmental and seafloor conditions. Then, potential effects of water warming, following the current trend of water temperature (Bethoux et al., 1990; Schroeder et al., 2016) and water cooling due to eventual strong and long-lasting deep-water formation events on spawners catches were tested.

Overall, ranges of optimal environmental and seafloor conditions found by species distribution modeling overlapped with the ranges estimated from several methods. Bottom ranges where the shrimp distributed agreed with previous studies (400 – 900 m, in Demestre and Martín (1993), Cau et al., (2002) and Rinelli et al. (2013), except that

relatively high CPUEs of shrimps were particularly concentrated on a narrow and shallow bathymetric band in the canyons. Though this pattern was described in previous studies (Demestre and Martín, 1993, Sardà et al., 1994, 1997), this aggregation was not previously related to the seafloor rugosity. We remained aware that other environmental factors could influence the shrimp distribution at spawning time. For example, the prey distribution (Cartes et al., 1994) and the relatively high availability of food, suspended organic particles, and chlorophyll caused by inner canyon circulation (Company et al., 2008) may explain higher catch rates inside the canyons. In fact, those data are hardly available on the spatial gridded-domain tackled in our study. Besides, shrimp-related biological factors like its physiology (e.g., average size, reproduction stages, and sex rates) across the continental margin (Orsi Relini et al., 2013) may also help to precisely defined the predicted spawners distribution. Therefore, for improvement of the spawner modeled distribution, this information should be associated with the georeferenced catches for future studies.

In the Catalan Sea, summer estimated landings of large shrimp from Palamós and Blanes fishing grounds were greater than any other fishing grounds of the basin, which is in line with studied observations in Demestre and Martín (1993), Gorelli et al. (2016) and Sardà et al. (1997). Between these two canyons, a shift in the location of high CPUEs set off from summer 2008 was estimated for the first time and showed that fishery over the Blanes canyon supported most landings than fishery over Palamós canyon. This shift likely came from georeferenced CPUE that were discontinuously provided over summers (e.g., CPUEs from Arenys harbor were available starting 2008 while from Blanes harbor, it was from 2005). In that context, comparisons of the canyons capacity using georeferenced CPUE only provided by their most close fishing harbor (e.g., Palamós and Blanes) neglected the information recorded in other harbors sharing the same fishing ground. Thus, with our estimations, we inferred that Blanes canyon could sustain the fisheries from several harbors (e.g., Palamós, Blanes, and Arenys) and was a potent resource of the deep-sea shrimp.

Within and among the canyons, the shrimp distribution had relatively small but significant spatial variations. First, spatial estimation of shrimp distribution completed and corrected existent maps built by VMS data from ships affiliated to Blanes and

Palamós in (Gorelli et al., 2014). For instance, the distribution of the catches over the canyons walls in the present study differed from those provided by Gorelli et al. (2014). This is likely because we included VMS data from Roses and Arenys fishing fleets that were localized over the fishing ground in Palamós and Blanes canyons, respectively. Second, comparing the shrimp distribution in various canyons during the same summer period improved our understanding of the shrimp dynamics and showed that their structures and locations shape the distribution of benthic communities. In fact, the method for estimating spawning areas in the Catalan submarine canyons can be exported to other Mediterranean canyons where *A. antennatus* is present e.g., Italy (Orsi Relini and Relini, 1998) and Sardaign (Sabatini et al., 2007). Additionally, this can help identify other ranges of environmental values supporting the shrimp distribution within the canyons.

Estimation of spawning sites can be of great use for modeling studies implied with egg dispersal and population connectivity and for supporting integrated management plans for the species. Spatial modeling analyses must focus on the shrimp fishery region unit, taking into account all the important triggers of abundance (i.e., the three canyons in our study), and avoiding the limitations of a local approach. Indeed, our study showed relatively high spawner aggregation on the slopes of Catalan canyons and suggested that aggregations do not only take place on the open slope (Sardà et al., 1994). This illustrated that results from previous studies dealing with single and small areas (like in Sardà et al. (1994)) can be nuanced when they are related to wider areas. On a wider scale, the study of Cau *et al.* (2002) found variations of the spatial distribution of the shrimp in the western Mediterranean Sea, but the scale was too broad to show the variability in our study zone.

The aspect of our study covering eventual temperature change effect on spawner distribution showed that catches would not drop with hindcast warmer bottom temperatures. Indeed, the deep water of the Mediterranean Sea is expected to warm by 0.2 °C per decade (Borghini et al., 2014), which would imply at least 30 years before dropping the spawner biomass by 20%. Nevertheless, a biomass decrease of 20% in the Palamós fishing grounds, may seriously affect the economy of the harbors, where 40% of the income depends on the sales of *A. antennatus*. The biomass is not only directly

affected by global warming, but could also be indirectly influenced by the changes in the trophic chain due to expected biodiversity loss (Yasuhara and Danovaro, 2016; Sweetman et al., 2017). With this in mind, future scenarios hindcasting the shrimp distribution should consider the interaction with its prey and the prey's sensitivity to environmental changes.

2.3.5. Conclusions

The summer distribution of the blue and red shrimp biomass on the continental slope indented by three major canyons in the Catalan sea was estimated from random forest regression tree models in the summers between 2005 and 2014. Based on optimal environmental conditions, the present modeling study achieved an adequate spatial representation of the distributed CPUE and allowed to identify expected spawning areas with significant higher CPUEs. The species distribution modeling indicated that seafloor characteristics explain most of the shrimp distribution variability and suggested that shrimps aggregate on shallower and narrower parts of the canyon margin rather than on the open slope. In these three canyons, the bathymetric distribution of the shrimp is comparable over the summers of 2005 – 2014. Nevertheless, small changes in temperatures induced a different response in catches per canyon. In addition to spatially estimate higher catches in the canyons, these results conveyed the suggestion that spatial shrimp dynamics is specific in each canyon. In short, this study provides valuable information about spawning areas required in further numerical Lagrangian drift experiments. In particular, this estimation can be used to adjust the location for a higher quantity of egg releases in larval drift models. Last but not least, the spatial distribution of the shrimp CPUE can support strategies for developing fishery management plans for the species.

2.3.6. Supplementary information

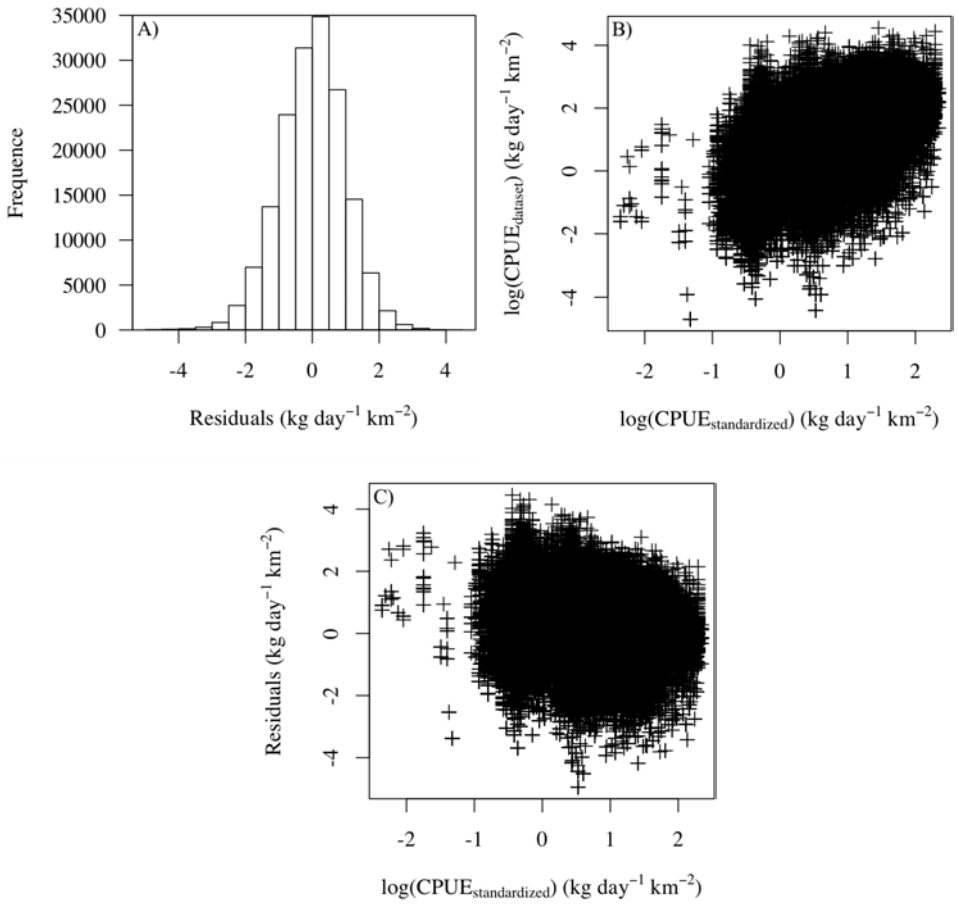

Figure S5. Residuals diagnostics for the standardization of catches, histogram of deviance residuals (A), log-transformed observed CPUE against log-transformed standardized CPUE (B), and residuals against log-transformed standardized CPUE (C).

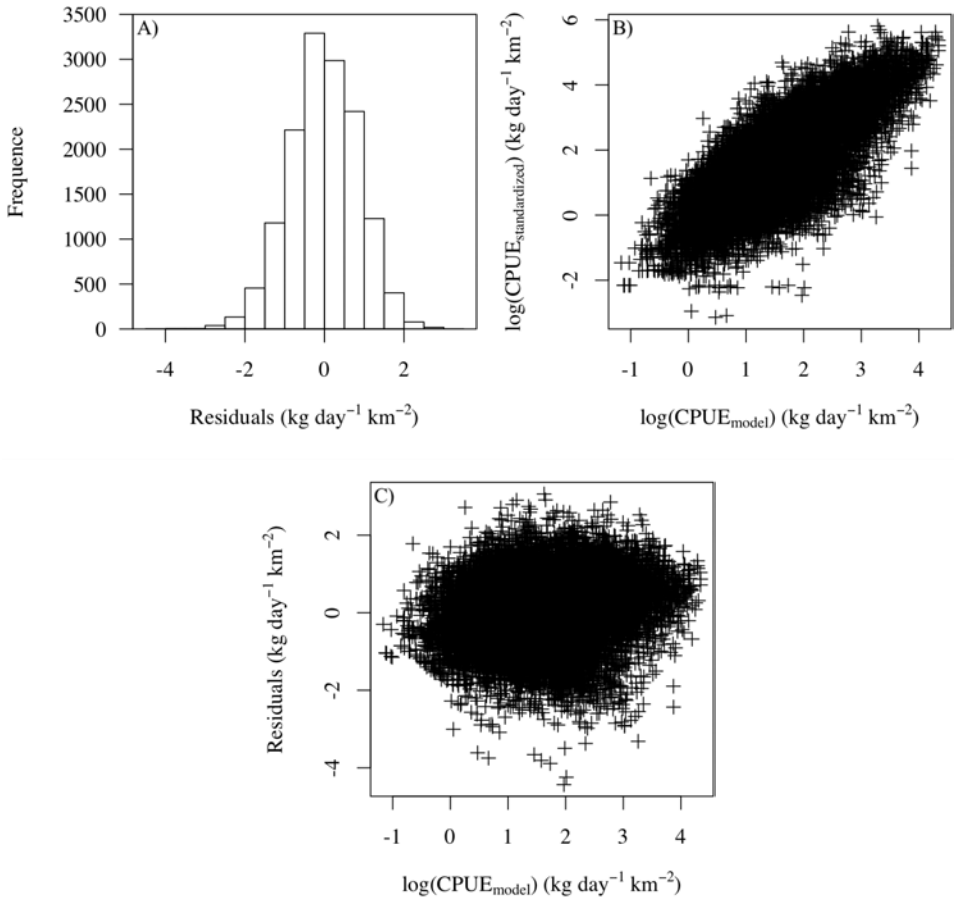

Figure S6. Residuals diagnostic for the random forest model histogram of model residuals (A), log-transformed standardized CPUE against log-transformed modeled CPUE (B), and residuals against log-transformed modeled CPUE (C).

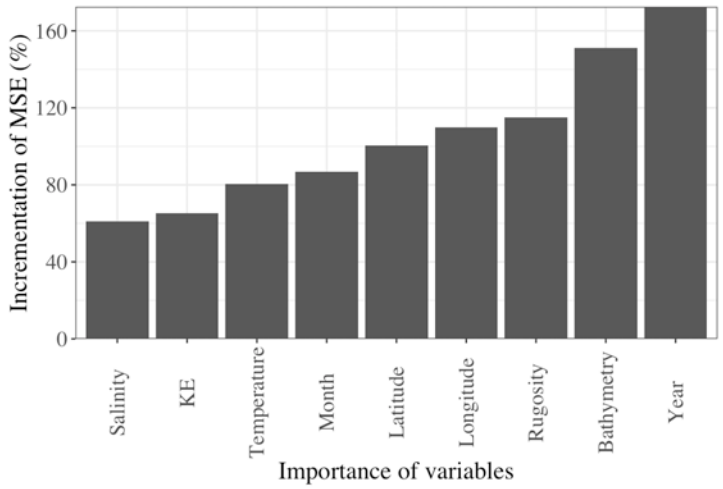

Figure S7. Importance of the variables in the random forest model relative to the incrementation (in percent) of the Mean Squared Error (MSE). The MSE incrementation was obtained by permuting randomly a variable in the dataset, predicting the CPUE based on the permuted dataset, and comparing the MSE from the original dataset and the permuted dataset.

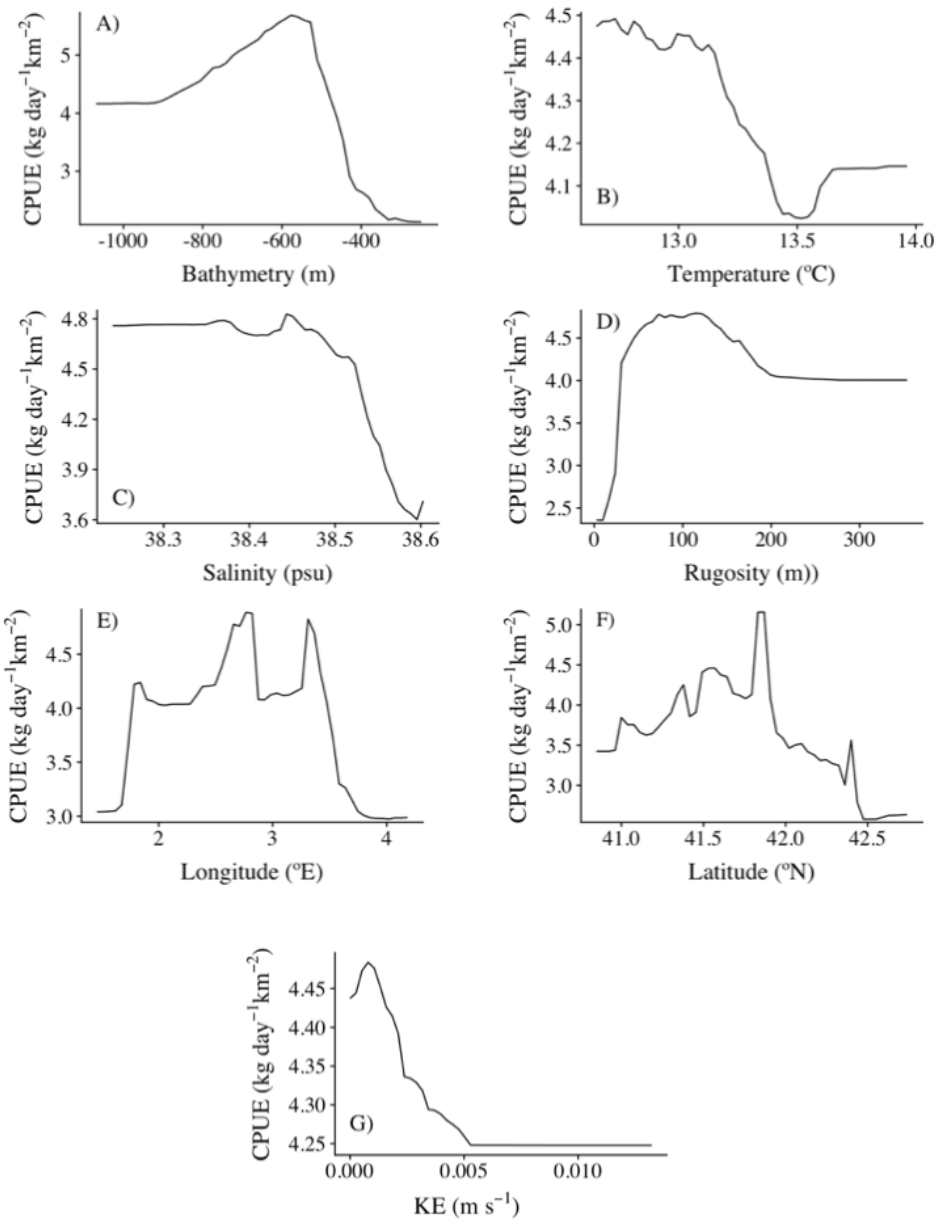

Figure S8. Partial effects of the predictors bathymetry (A), seawater temperature (B), salinity ©, rugosity (D), longitude (E), latitude (F), and Kinetic Energy (KE) (G) on the CPUE.

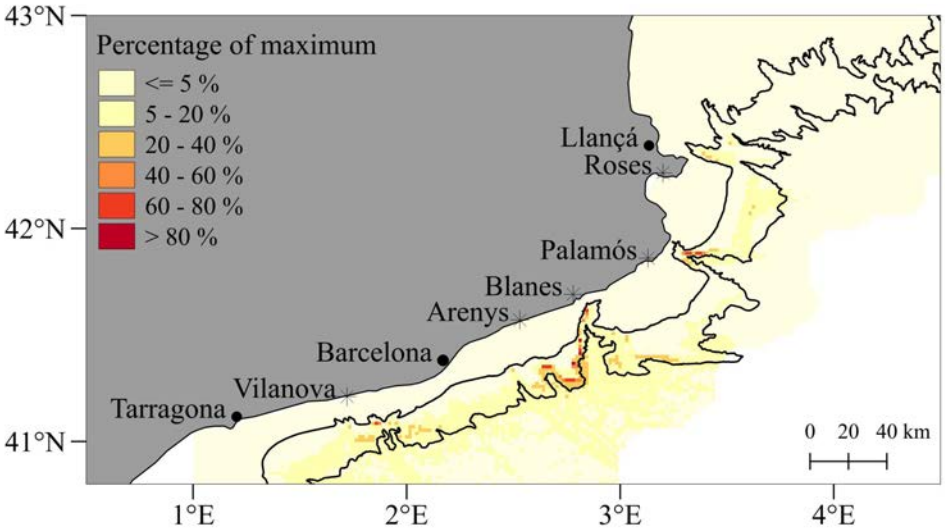

Figure S9. Map of the standard deviation CPUE (as a percentage of the maximum) from the random forest model in the Catalan Sea over the decade 2005-2014. Isobaths at 200 and 1000 m depth are represented by continuous black lines.

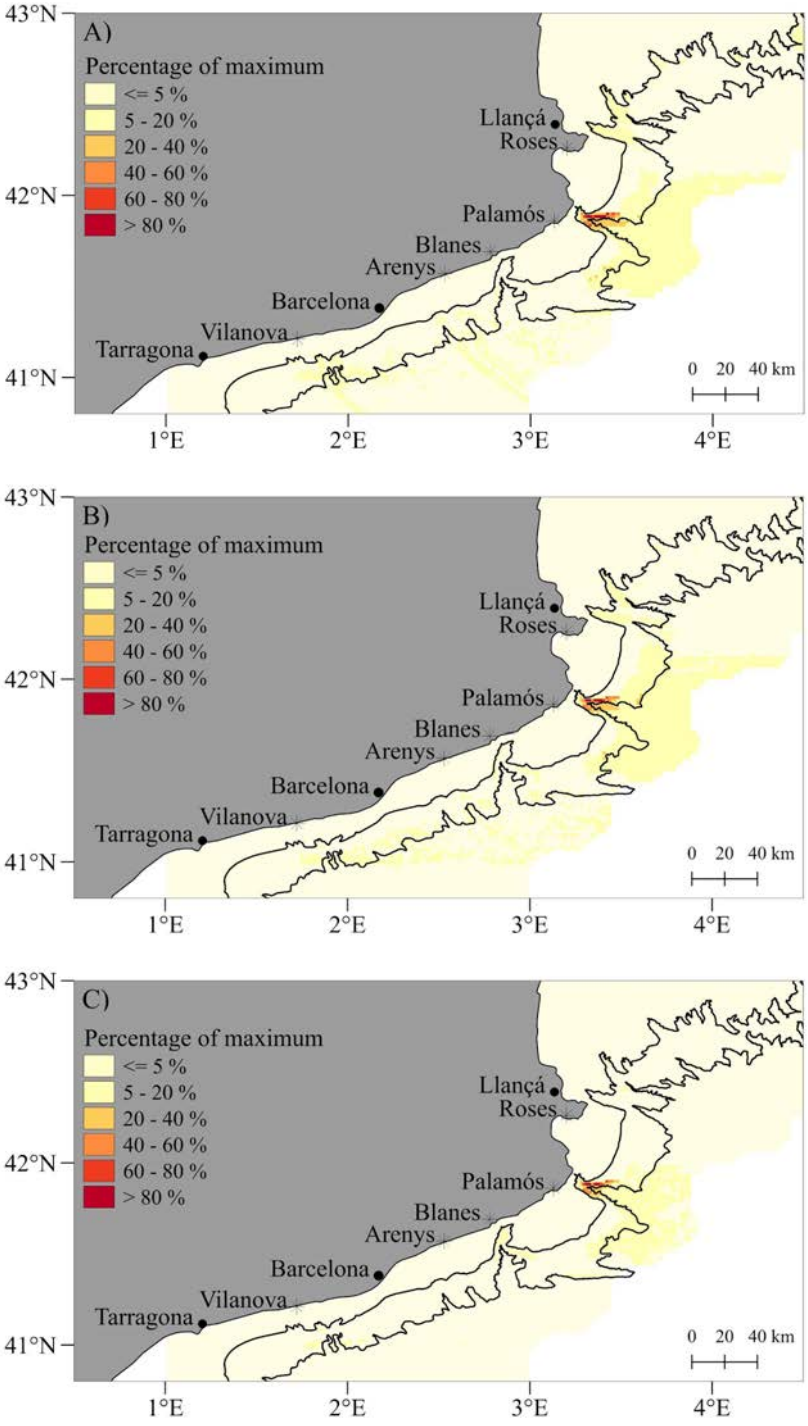

Figure S10. Map of the estimated CPUE (as a percentage of the maximum) from the random forest in summer 2005 (A), 2006 (B), 2007 (C), 2008 (D), 2009 (E), 2010 (F), 2011 (G), 2012 (H), 2013 (I), and 2014 (J) in the Catalan Sea. Isobaths at 200 and 1000 m depth are represented by continuous black lines. Fishing harbor's symbols are indicated in Figure 27.

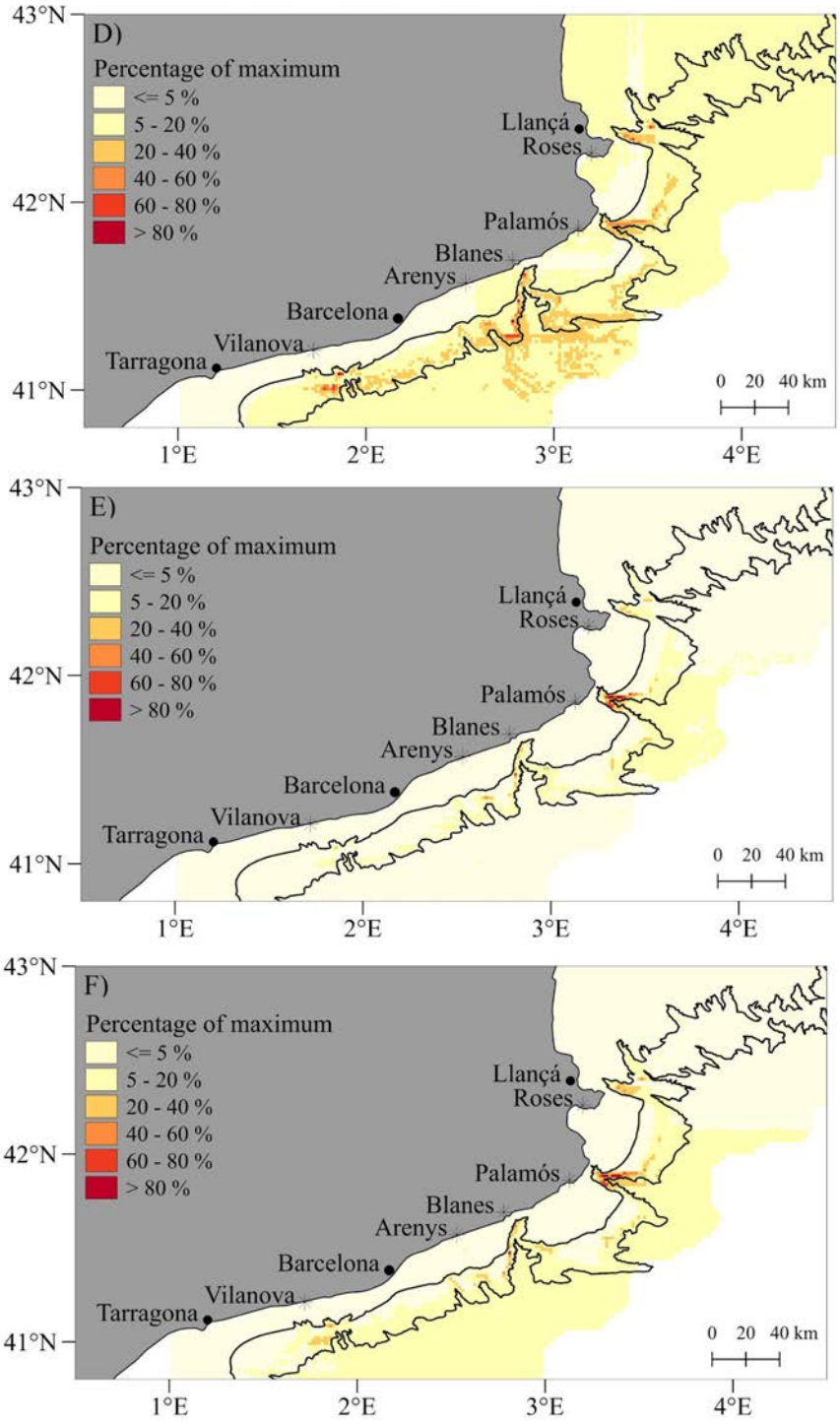

Figure S10. (Continued)

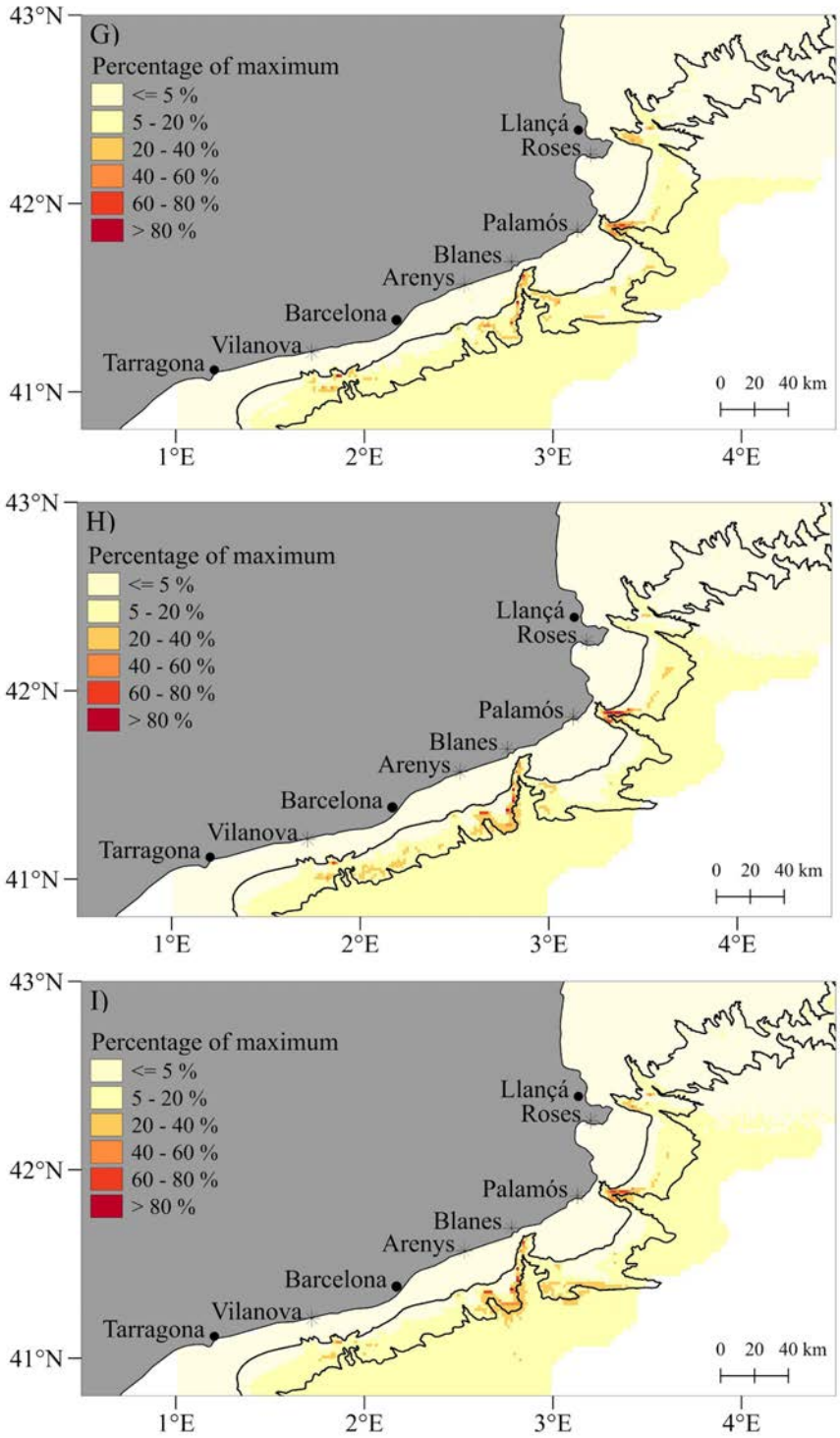

Figure S10. (Continued)

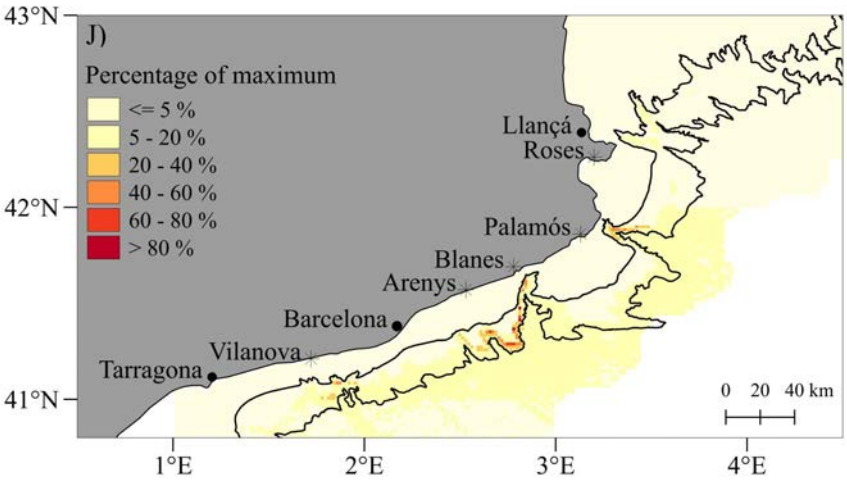

Figure S10. (Continued)

2.3.7. Additional file

Georeferencing the catches

Courtesy of J. A. Garcia *et al.* (2016)

In this appendix, the method to georeference the catch to coordinates is schemed and illustrated.

General methods

Over the period from 2005 to 2014, two sets of data (i.e., the Vessel Monitoring Systems (VMS) data and landings data) were daily recorded by regional administration and public institutions. The VMS data record the fishing boat position per time unit. Then, fishing boat speed is calculated by the distance between two records and we can filter the records for which the fishing boat is trawling according to the boat velocity (i.e., < 4 knots). Landings data are recorded by the fish auction and the fishermen logbooks. They informed about the weight of shrimp catches and their size-category (i.e., commercial size with small and large carapace length) per trawlers and date.

Then, SQL queries assign catch weight from the landing dataset to the trawlers position at rising activity by fishing boat's ID and date.

Main results

Catches are georeferenced and can be projected on maps like in Figure 1.

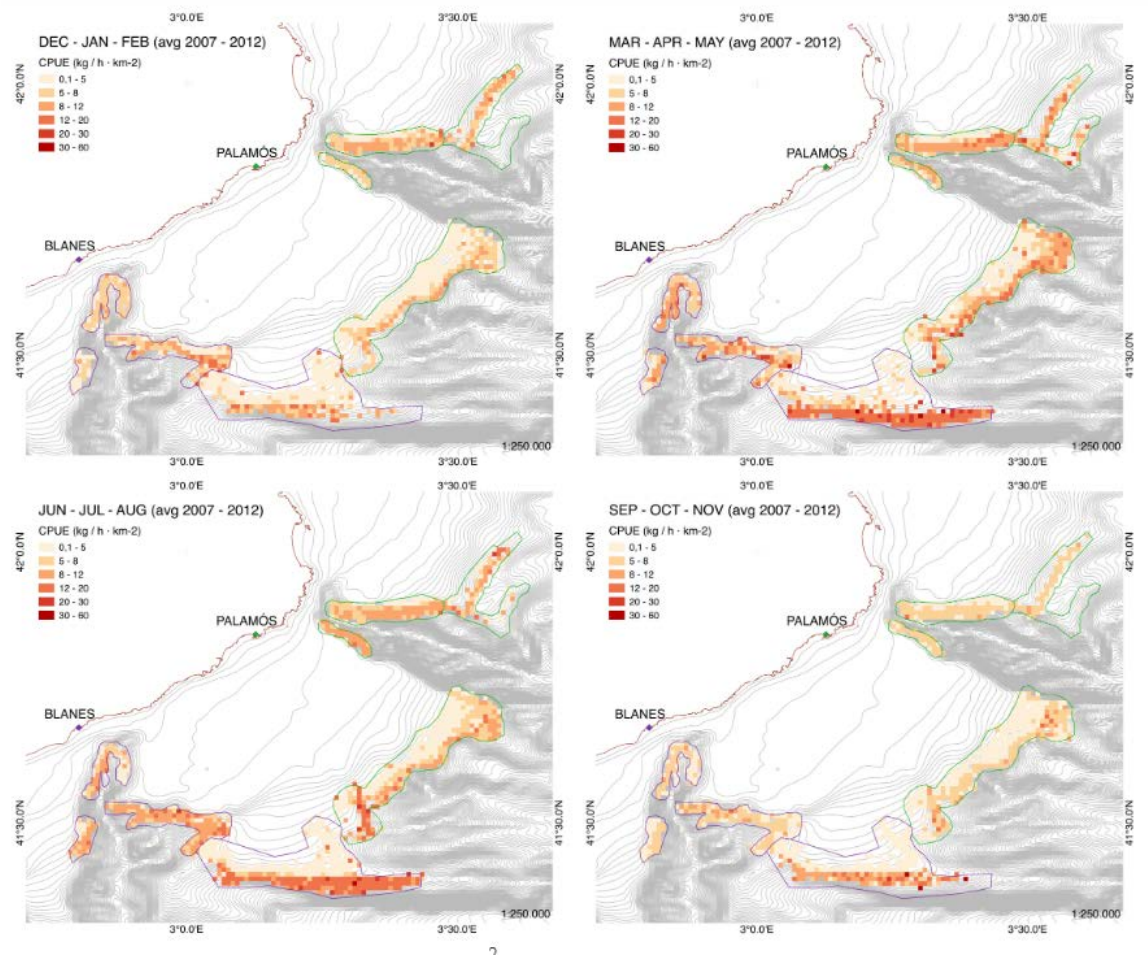

Figure 1. Catch Per Unit of Effort (CPUE) maps in total kg h^{-1} km^{-2} of *Aristeus antennatus* per trimester for the trawling fleets from Blanes and Palamós (Credits to Gorelli e*t al.*, 2014)

Section 2.4

Larval drifts of *A. antennatus* shrimp (Crustacea: Decapoda) linked to the North Balearic Front of the NW Mediterranean Sea

Morane Clavel-Henry
Jordi Solé
Nixon Bahamon
Marta Carretón
Joan B. Company

Conference: Pesca i Ciència, VI Jornada tècnica sobre la gamba vermella a Catalunya. Palamós, Spain.

Article submitted to **Progress in Oceanography** (2019)

Abstract

Marine fronts are oceanographic drivers for marine species dispersal, especially for their pelagic organisms like the larvae. Larvae can aggregate at the front and consequently have a limited dispersal, which in turn reduces the connectivity between marine populations. Due to the high variations in the ocean, the front also has annual changes (i.e., its formation period, gradient, and position), which have poorly-documented effects on larval retention. In the northwestern Mediterranean Sea, a surface density front is localized across a continental margin which is also indented by submarine canyons. There, an abundant population of the commercial deep-sea blue and red shrimp *Aristeus antennatus* (Crustacea: Decapoda) inhabits the seafloor. Each summer, the shrimp offspring are released in pelagic deep-sea and access the superficial waters divided by the density front. In this study, we focused on the interannual influence of the density front on the larval transports of shrimps and its repercussions on the potential connectivity between shrimp populations at each front side. A particle-tracking model simulated the larval transport of *A. antennatus* in interannual (years 2006 to 2016) hydrodynamics of the northwestern Mediterranean Sea. Larval transport and seawater density were correlated by 70%. Over the years 2006 – 2016, the front region retained 86% of larvae, but this rate yearly varied due to changes in density gradient and position of the front. For example, in 2010, 48% of larvae connected to zones south of the front when the density gradient was relatively low. In 2015, 99.2% of larvae were retained in the front region when the latitudinal front position and density gradient were relatively high. Interannual variations of the front position were potentially related to the strength and position of mesoscale circulation patterns. Our findings suggest that the larval retained on habitats favored by canyon productivity because of the front could explain the persistent abundance of *A. antennatus* population. This information is important to set or improve the fisheries management in zones with strong interannual variations of the hydrodynamics.

2.4.1. Introduction

The sustainable management of fish and crustacean stock is based on the balance of favorable environmental conditions, a viable renewal of the population, and good

practices from multiscale fishery activity. Most commercial stocks are assessed yearly considering an estimate of the present biomass, their reproductive potential, and the mortality by fishery (Cooper & Weir, 2006). However, ecology, distribution, and dispersal of invertebrates and fish larvae are of great interest for research in population dynamics and the management of marine resources. Numerous studies have described the spread of larvae from plankton sampling and analyzed the larval ecology under several hydrodynamic conditions (McManus and Woodson, 2012). These studies have allowed understanding the interaction of larvae with their ecosystem, which, in turn, has improved our knowledge for estimating the paths of larval dispersal and the connectivity between subpopulations. Consequently, we can estimate the subpopulations that replenish by themselves and the ones that continuously or temporally supply other marine communities with recruits. Then, it supports the fishery management plans for preserving both the fishery interests and the resource for commercial species (Ospina Álvarez et al., 2015; Nicolle et al., 2017).

In the northwestern Mediterranean Sea, this information is sought for the fishery management of the highly valuable and commercial deep-sea shrimp *Aristeus antennatus* as the one applied on the fishing grounds off Palamós (BOE 2013; 2018). From the moment of spawning to metamorphose into juveniles, the variability of the larval trajectory depended to the hydrodynamics and several biological traits, themselves conditioned by the water masses and the larval ecology (i.e., duration in pelagic water, egg buoyancy (Clavel-Henry et al., 2019; Clavel-Henry et al., 2020). For example, the particles drifted short distances over a month in the deep cold waters with low currents (Clavel-Henry et al., 2019) whereas surfaced particles were carried out on long distances over a small amount of time in warm waters with intense currents (Clavel-Henry et al., 2020). In this study, differences in the drift distance, duration, and trajectories were also estimated because of spatial differences in the hydrography and hydrodynamics in the surface water. But overall, the spatial position of the larvae is an important factor found in most larval transport modeling analyzes (e.g., Metaxas, 2001, Nicolle et al., 2017).

The seasonal and yearly changes in the hydrography and water circulation also contribute to the larval dispersal variability (Criales et al., 2005; Snauffer et al., 2014), providing that species reproduction occurs on specific (e.g., once a year) or episodic periods (e.g.,

several times per year). Analyzing this variability gives insights to establish the larval path constancy over time and to identify the hydrodynamic changes which improve or hamper the recruitment on fishing grounds (Ospina-Álvarez et al., 2015; Snauffer et al., 2014; Tiessen et al., 2014). Numerous larval dispersal studies have estimated that yearly changes in atmospheric conditions like the wind (e.g, Tiessen et al., 2014) and the North Atlantic Oscillation (e.g, Peck et al., 2008) were responsible for interannual variability of larval dispersal. For instance, for certain years when the prevailing wind is strong, the main current is enhanced and transports cooler or warmer influxes (Tiessen et al., 2014).

Additionally, the mesoscale circulation (i.e., eddy, front, meander, and upwelling) resulting from the water hydrography or current instabilities also have a physical role in the interannual larval dispersal variability (Galarza et al., 2009; Woodson et al., 2012). In many larval dispersal studies, eddies have a significant and variable influence on larval dispersion over months, seasons, or years because of their lifetime, strength, size, and position (Bakun, 2006; Condie and Condie, 2016). For example, this influence monthly changed the dispersion of surfaced *A. antennatus* larvae in climatological circulation (Clavel-Henry et al., 2020). Unlike with eddies, the impact of the front strength and position on larval dispersal has never been addressed, although a few studies were interested in their retentive effect. Yet, the fronts are major ocean processes having the same spatiotemporal scales than eddies, but with different dynamic features impacting the larval development (e.g., interfaces between water masses with different temperatures (Sabatés and Olivar, 1996; Woodson et al., 2012)).

In the NW Mediterranean Sea, many studies deeply investigated the front position influence on adults and larval distribution (Amores et al., 2013; Gannier and Praca, 2007; Galarza et al., 2009; Sabatés and Olivar, 1996) but their retentive role on larval dispersal has been restricted to a few Lagrangian modeling studies (Branicki et al., 2008; Mancho et al., 2008; Ospina-Álvarez et al., 2012b). In a climatological year, cold and warm water masses localizing the North Balearic Front (NBF) in the NW Mediterranean Sea influenced the duration and the length of *A. antennatus* larval drifts (Clavel-Henry et al., 2020). Yet, linking the interannual front variability to the larval dispersal has some interesting consequences for the zone affected by the front. Indeed, the western part of the NBF is perpendicular to a continental margin incised by three submarine canyons and

overexploited by the fishery activity. There, the high productivity of canyons influences the distribution of *A. antennatus* larvae and adults (García del Arco et al., 2016, Carretón et al., 2018, Chapter 3), but research projects are still led to understand the mechanisms contributing to the constancy of the shrimp abundance and justifying the high parental genetic rates between subpopulations (Sardà et al., 2010).

In this context, this study aims to 1) estimate the interannual contribution of the NBF to *A. antennatus* larval transport, 2) assess the eventual larval retention in the vicinity of the submarine canyon grounds and 3) describe the oceanographic mechanisms leading to interannual variability of larval dispersal. Simulations of larval transport were modeled in the interannual circulation of the northwestern Mediterranean Sea. We first analyzed the characteristics of larval transport and then, we related those characteristics to the oceanographic conditions. Lastly, we discussed the potential influence of the NBF in the management of the shrimp resource.

2.4.2. Materials and Methods

The estimation of interannual larval drift variability used summer circulation between 2005 and 2016 from an ocean circulation model coupled with a Lagrangian tracking model. Simulated particles represented *A. antennatus* larvae released in the northwestern Mediterranean Sea regions affected by the North Balearic Front. We investigated the interannual changes in the larval drifts and linked their features to the dynamics of the region affected by the front.

2.4.2.1. Interannual hydrodynamics

The three-dimensional circulation of the NW Mediterranean Sea was modeled by the Regional Ocean Modeling System (ROMS; Shchepetkin and McWilliams, 2005) between 2006 and 2016. The model domain was defined from 0.65º W to 6.08º E and from 38º N to 43.69º N with a horizontal resolution of 2 km (256 x 384 cells) and 40 sigma vertical levels with a finer resolution close to the surface (more details in Clavel-Henry et al., 2019).

The interannual hydrodynamic circulation was implemented by forcing the climatological runs of the NW Mediterranean Sea circulation model described Macías *et al.* (2011) and Clavel-Henry et al. (2019a) with interannual gridded atmospheric conditions. All atmospheric forcings came from ERA-Interim reanalysis (Dee et al., 2011) and had a spatial resolution of half a degree. The air temperature, cloud cover, freshwater flux, wind and surface pressure had a time resolution of 6 hours. The shortwave radiation, long-wave radiation, and precipitation had a time resolution of 12 hours. The forcing files were processed to fit the ROMS grid using the python package Romstools (https://github.com/trondkr/romstools). Daily climatological discharge of two important rivers (Ebro and Rhone) was included as s forcing and supplied the hydrodynamic model with fresh water.

The interannual model implementation was used for the first time in this study and was validated using the same methodology as in Clavel-Henry et al. (2019a). Real observation of temperature and salinity came from 4 850 ARGO buoys from January 2006 to December 2016. The domain was divided into 6 sectors (see Figure S11), within which we averaged at least 20 ARGO profiles per year and month. Then, we compared them with the average profiles made within the same month, year and sector from the interannual model. The Root Mean Square Error (RMSE), the standard deviation and the correlation were displayed in Taylor diagrams (Taylor, 2001). The comparison generally showed good results; with the correlation between the average ARGO profile and the interannual model higher than 0.8 for 84% temperature profiles and 98.5% salinity profiles (see Figures S12 – S20 for validation in summer estimations).

2.4.2.2. Larval transport model

We used the framework of OpenDrift (Dagestad *et al.*, 2018) to simulate the offline displacement of larvae within the three-dimensional interannual ROMS model. The particle-tracking model spatially and temporally interpolated the ROMS model outputs (e.g., velocities, temperature) to the individual positions. The displacement equation corresponded to:

$$dX = U \cdot dt + B \cdot dt + S \cdot dt \qquad (13)$$

where *dX* is the 3D displacement of the individuals after the time step *dt* from their previous position (i.e., longitude, latitude, and depth), *U* the 3D velocity vector from the hydrodynamic model, B the vertical velocity induced by positive egg buoyancy and S the vertical velocity induced by swimming of nauplius (with $S = 0$ m s^{-1} by default). The time step *dt* for the advection of individuals was 1 hour and the output of the simulation was saved every 12 hours. The displacement equation was resolved with a fourth-order Runge-Kutta scheme and particles reaching the coast, or reaching the postlarval stage were stranded.

The vertical velocity from egg buoyancy was computed by one of two schemes adapted for spherical objects in different water regimes (i.e., the laminar regime, eq. 1 in Sundby (1983); the transient regime, eq. 2-11 in Dallavalle (1948)). These schemes relied on water characteristics (viscosity, density) and embryologic information (density, size). Due to lack of data on the embryonic ecology of *A. antennatus*, the egg densities were randomly selected in a Gaussian distribution having a mean of 984 kg m^{-3} and a standard deviation of 36 kg m^{-3}. Egg diameters were randomly selected in a Gaussian distribution having a mean of 330 µm and a standard deviation of 40.5 µm. Both values were selected from an estimation of the surfacing egg density values and the size of the oocytes provided Clavel-Henry et al. (2020), and Demestre and Fortuño (1992), respectively.

After the eggs hatched, we set $B = 0$ m s^{-1} in eq .13. In case the eggs did not hatch in the upper 15 m depth, the value of the velocity *S* was computed such as the distance between the depth of the newly hatched nauplius and the 15 m layer was overcome during the nauplius stage. By implementing this, we complied with the high quantity of first protozoea stages collected near the surface (Carretón et al., 2019) and we also focused our interest on the hydrodynamics in waters above the thermocline.

2.4.2.3. Initialization of the drifts

Larval drift was modeled using Lagrangian particles with biological and behavioral components that were estimated from the adult and larval ecology.

The individual releases corresponded to the period of the spawning peak of *A. antennatus* in July and August (Demestre and Fortuño, 1992). The releases of individuals started on July 1, July 15, August 1 and August 15 of years between 2006 and 2016. The drifts started from sea bottom between 360 and 710 m where an abundant distribution of deep-sea blue and red shrimp has been estimated from real catches in Chapter 3. The number of individuals over the canyon slope between 480 and 590 m was 120 particles per grid cell and 90 particles per grid cell outside of this range. On the open slope, 60 particles per grid cell were released between 480 and 590 m; and 30 particles per grid cell outside this range. Based on the estimated distribution of the shrimp mentioned in the previous section, we had 56 970 individuals per simulation, making a total of 2.5 million simulated drifts in the interannual implementation of ROMS. The number of particles per simulation was above the limit set in Clavel-Henry et al. (2020), and consequently, we prevented biases induced by low particle numbers in the analyses of the drift simulations.

The drift duration corresponded to the pelagic larval duration (called Pelagic Propagule Duration; PPD), and included the embryonic and larval durations. Due to a lack of information on *A. antennatus* larvae, we used a multiple linear regression fitted on stage duration of Penaeid larvae according to the water temperature that was described in Clavel-Henry et al. (2020). The larval stage duration of the *A. antennatus* was computed every time a stage molted into a new one during the drift simulations. Then, the drift duration corresponded to the sum of the larval stage duration.

Due to the lack of knowledge, swimming, growth rate, and mortality were not included among the behavior and biological components.

2.4.2.4. Contribution of the NBF in the larval dispersal

The relation between the NBF and the larval dispersal was estimated by analyzing the modeled transport from individuals released in the front zone. To do so, the domain of the NW Mediterranean Sea was divided into 8 zones according to the water density gradients (Figure 35) and larval drifts starting from the area of Palamós Canyon were mainly analyzed (zone 2 in Figure 35). This zone contained the NBF which was

delimited by the homogenous sea surface density of the Gulf of Lions and the recent Modified Atlantic Water.

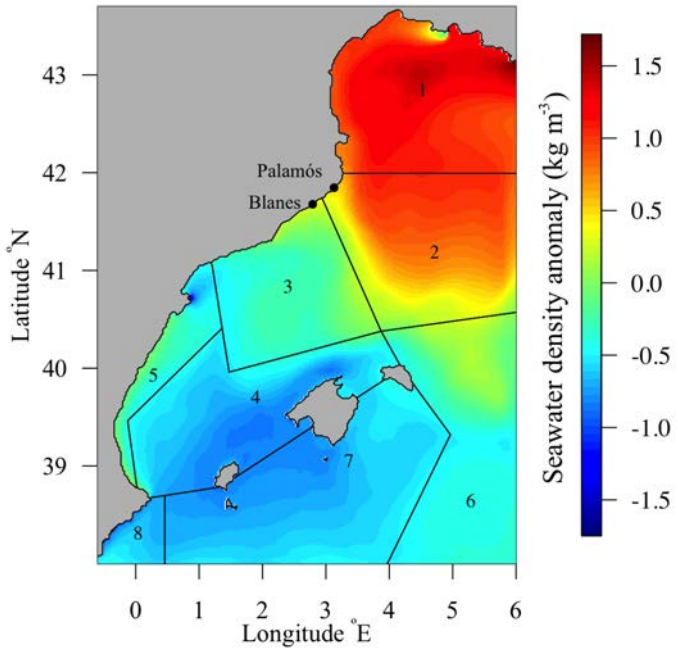

Figure 35. Spatial density anomaly in the surface waters of the northwestern Mediterranean Sea. The anomaly is the climatological seawater density (average between 2006 and 2016) from the Regional Ocean Modelling System minus the average surface water density of the studied area (1025 kg m^{-3}). Eight zones (1 to 8) were defined according to the density gradient changes. In our analysis, we focused on simulated drifts initialized in zone 2. Landings of *Aristeus antennatus* in two fishing harbors (Palamós and Blanes) are the highest of the NW Mediterranean Sea. These harbors are situated on each side of the density front (i.e., at seawater anomaly around 0 kg m^{-3}).

To estimate the contribution of the NBF in the interannual larval transport of *A. antennatus*, we analyzed the dispersal of individuals by measuring their drift distance, duration (PPD) and residence time within the front zone over time (i.e., 2006 – 2016) and space (i.e., latitudes of the spawning site in zone 2 bracketed by ~41.4º N and 42º N). We used the temperature and density of the water masses crossed during the transport simulations to better understand the correlation between the larval drifts and the water masses.

To assess the larval retention in the front zone, we estimated the connectivity rate (i.e. the percentage of individuals reaching a neighborhood zone from the release zone 2) and the retention rate (i.e., the percentage of individuals being retained on the release zone). We also considered the supply of individuals from zone 1 and 3 into zone 2 to have an overview of the circulation beyond our studied zone.

Finally, to establish the oceanographic processes affecting the larval transport variability, we related the results from the larval drift (i.e., drift distance and duration) to the latitudinal position of the front and its sharpness. The front position was approximated by the gradient change of seawater density on northeast-southwest transects and was close to the pycnocline of 1025.5 kg m^{-3}, on average. We indexed the interannual change of the front position by computing the distances between a climatological front (i.e., the density front in the average of the seawater density fields between 2006 and 2016) and the interannual fronts. For this purpose, we made 50 parallel transects between the climatological and annual fronts, and we made an average of the transect lengths (see Figure S21). Similarly, the strength of the front (i.e., how the gradient change over a certain distance) was approximated by the difference of seawater densities estimated at each end of a 20 km segment centered on the front (see Figure S22).

Afterward, we selected three years in which the estimated connectivity rates were extreme (minimum and maximum rates) and illustrated them with featured mesoscale circulation patterns (eddy position and size, isopycnal near the fronts). We detected the position of large eddies and meanders through a vector geometry-based algorithm developed in Nencioli et al. (2010) and adapted in R. The detection worked and complied with four conditions applied on the zonal and meridional velocity. The algorithm considered the change of velocity direction (west/east or north/south) and the rotational circulation around potential eddy centers. We retained the center position of closed circular circulation (eddy) and semi-closed circular circulation (meanders) near the NBF for the monthly persistent and strong structures. Later, as defined in Nencioli et al. (2010), the area of those structures was the biggest circular contour from the streamlines around the eddy center position (see Figure S23).

2.4.3. Results

The front zone corresponded to a zone of temporary intense and variable hydrodynamics (zone 2 in Figure 35). The drift of individuals was rather dominated by the circulation intensity than the water temperature (see Figure 36). The Pelagic Propagule Duration lasted between 19.3 days and 21.1 days and was correlated to the seawater temperature

(Pearson correlation: 70%) varying up to 1 ºC around an average at 24.1 ºC. The PPD was not strongly correlated to the drift distances (Pearson correlation: 40%), which had no trend or periodicity detected over the decade. In the summers of 2009 and 2012, two local maxima in drift distances rose to 141 km and 158 km. On the contrary, drift simulations had two local minima at 90 km and 92 km in the summers of 2006 and 2014. The drift distance was also uncorrelated (Pearson correlation: 33%) to the residence time of the individuals within the studied zone. These results implied that the hydrodynamics generated interannual uncertainty on the larval drifts that had other origins that the warmth of the water and the intensity of the velocity fields. For example, larvae could be transported across long distances (i.e., 135 km in 2010, and 160 km in 2012) and either stayed in our studied zone (residence time of 20 days in 2012) or left it (residence time of 15 days in 2010).

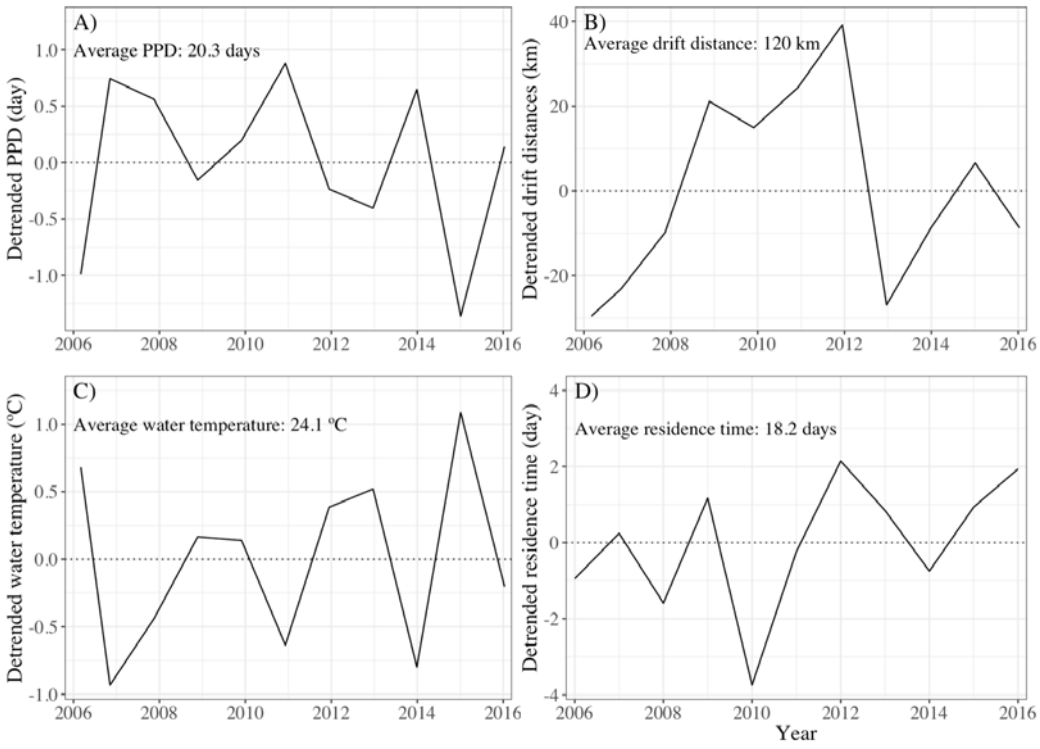

Figure 36. Yearly variations of detrended environmental and drifts characteristics. Detrends of environmental and drifts characteristics are their yearly deviation from the average over the years 2006 – 2016. The X-axis is the years from 2006 to 2016. The Y-axis are the Pelagic Propagule Duration (PPD; A), the drift distance (B), the water temperature at individual coordinates (C), and the residence time (D) for individuals released from zone 2 (see Figure 35).

However, according to the latitudinal releases of individuals, the characteristics of the larval drift presented high correlations with the water conditions during the larval drifts (see Figure 37). The drift distances and the seawater density were correlated by 98%; the

drift distance and the residence time by 93% and the water density and the residence time by 91%. In particular, when the individual releases occurred at latitudes lower than 41.65º N, the residence time, as well as the drift distances, became shorter (i.e., by 5 days and by 40 km) and the water density decreased by 0.5 kg m^{-3}. Between 41.65º N and 41.9º N, the water density presented a local maximum and minimum at 41.7º N and at 41.85º N where the density values were 0.15 kg m^{-3} higher and 0.1 kg m^{-3} lower than the average, respectively. These variations were also detected in the drift distances at the same latitudes and the transport rose of 19 km and decreased by 4 km, respectively. Beyond 41.9º N, larval drifts were up to 24 km higher than the average. Overall, transport drifted 56 km less if they were released near the southern border of zone 2 than if the drifts started around the northern border. These analyses showed that the density front had split the zone of release with a northern part under strong advection and with a southern part under less intense current, which transported individuals outside of the studied zone.

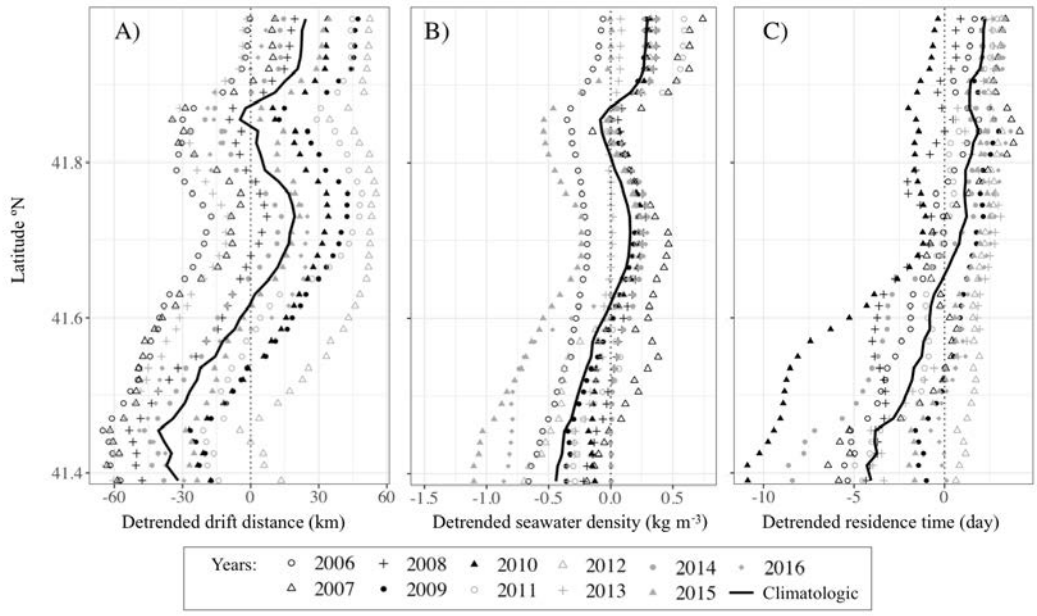

Figure 37. Latitudinal variations of detrended environmental and drift characteristics. Detrends of environmental and drifts characteristics are their yearly deviation from the average over the years 2006 – 2016. The X-axis are the drift distance (A), the water density at individual coordinates (B), and the residence time (C). The Y-axis is the range of released latitudes for individuals from zone 2 (see Figure 35).

Overall, the dispersal of individuals toward other zones was rather limited and the retention rate within the zone 2 reached 85.9% (Figure 38). Except for simulations in the summers of 2010 and 2014, the retention rates varied between 81.7% and 99.8% and

reached maximum in 2012 and 2015. During these summers, zone 2 received 19.6% and 24.8% of individuals from the nearest southern zone (zone 3 in Figure 35). The dispersal simulations in the summers of 2010 and 2014 had not only the lowest rates of retention but also a southern dispersal rate (i.e., to zone 3), which reached 23.5% and 51.5% respectively. All along the years, the northern zone 1 has abundantly supplied the zone of interest, with a range between 56% and 81.3% of its individuals arriving on it.

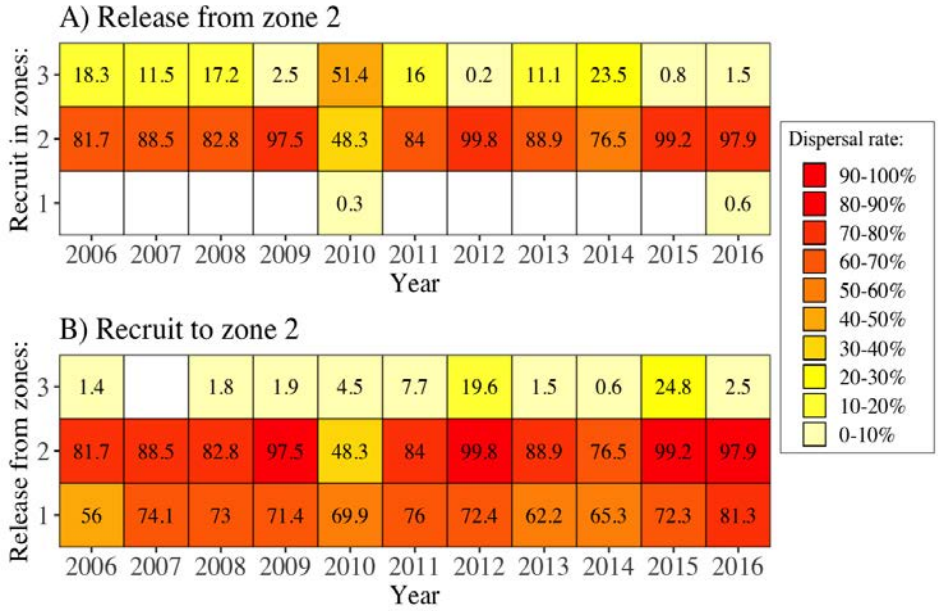

Figure 38. Dispersal rates over the period 2006 – 2016. Estimation of the dispersal rates from the release zone 2 (A), and from the northern zone 1 and the southern zone 3 to zone 2 (B). The dispersal rates on the middle row correspond to retention rates in zone 2. See Figure 35 for the spatial representation of zones.

The previous findings indicated that the front zone was mainly a retention zone. Nonetheless, the temporal variability of the front strength, represented by the density gradient near the front, as well as its spatial position affected larval dispersal (Figures 39 and 40). More precisely, they were correlated by 58% and 71% (Pearson correlation) to the retention of larvae in the front zone, respectively. On one hand, we observed that during the summers of high retention rates like in 2012 and 2016, the front strength was high: the water density increased by 0.88 to 0.90 kg m^{-3} over 20 km northeastward transects centered on the front position (see Figure 39). For those years, the front was slightly further north than the climatological front (7 to 20 km, see Figure 40). On the other hand, lower retention rates in 2010 and 2014 were combined with low raises of density; around 0.41 and 0.28 kg m^{-3}, respectively. Additionally, the fronts were located more than 30 km to the south of the climatological front, which were consequently the highest anomalies in the front positions.

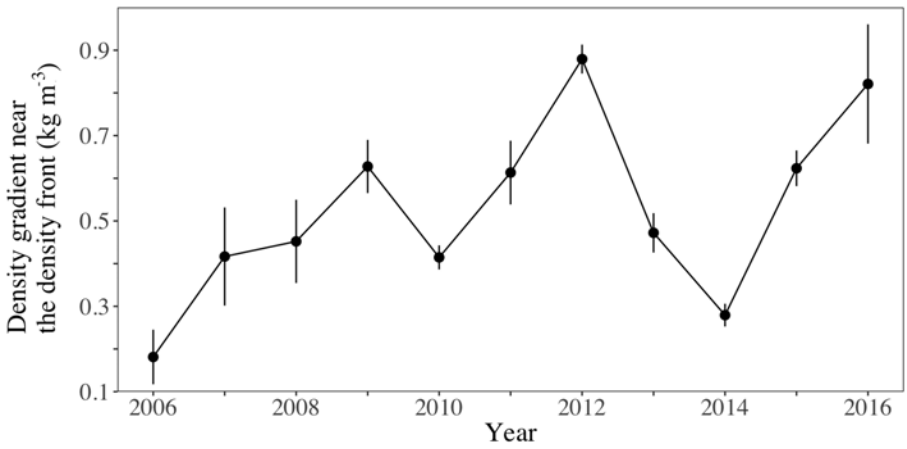

Figure 39. Interannual variability of the density gradient across the NBF. The X-axis is years from 2006 to 2016. The Y-axis is the average density gradient computed between two coordinates, each 10 km away from the density front.

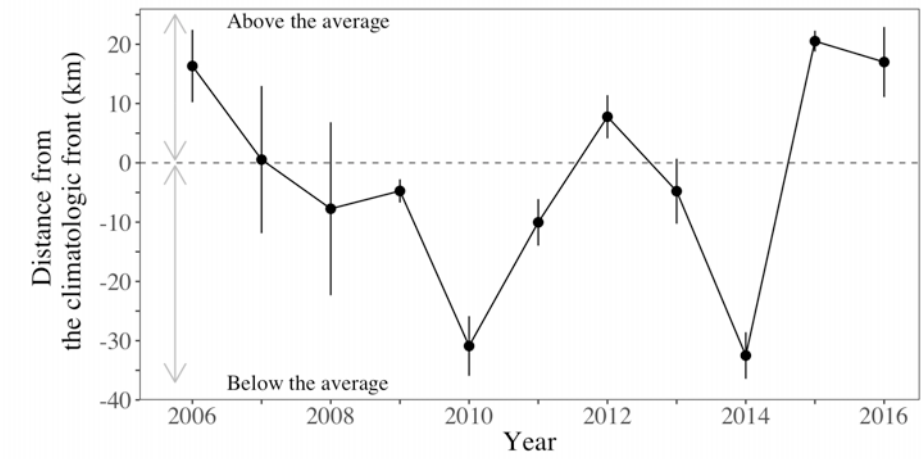

Figure 40. Interannual variability of the front position related to its climatological position. The X-axis is years from 2006 to 2016. The Y-axis is the average distance between fronts from interannual and climatological (average between 2006 and 2016) seawater density fields estimated in the ROMS model. Positive/negative distances correspond to fronts above/below the climatological front. The horizontal dashed line represents a distance of 0 km.

Larval retention was the consequence of distant mesoscale structures of the NW Mediterranean Sea. The variability of the density front was related to the proximity of the anticyclonic and cyclonic circulation structures (see Figure 41), which contribute to the convergence of water masses. As shown previously, the density front was correlated to the drift distances, the residence time (Figure 36.D), and dispersal rates (Figure 38). The circulation in years with sharp fronts and strong retention (2012, 2015 and 2016) was furthermore related to the Northern Current and a southern anticyclonic eddy close to the density front. Especially in 2012, 2015 and 2016, the edges of large eddies restrained the

dispersal of individuals towards the south, and also transported a significant number of individuals released in a southern zone (see Figure 38.B). These dispersals can be observed as well with large meanders that gather similar circulations (i.e., edge close to our studied zone and negative vorticity as in 2009 and 2011, see Figures S24.D and S24.F). Oppositely, in some years (e.g., 2010), the convergence of the flows was weaker and the density gradient at the front was not sharp, with persistent large eddies detected far from the studied zone, or with no detection of eddies. In those cases, larval dispersal increased toward the South, such as in 2010, when the retention rate was the lowest, but the drift distance was among the highest (135 km). With these observations, we related the front variability to the position and size of southern eddies or large meanders that were persistent and emerged in the monthly average of the ROMS hydrodynamics (see Figure 41).

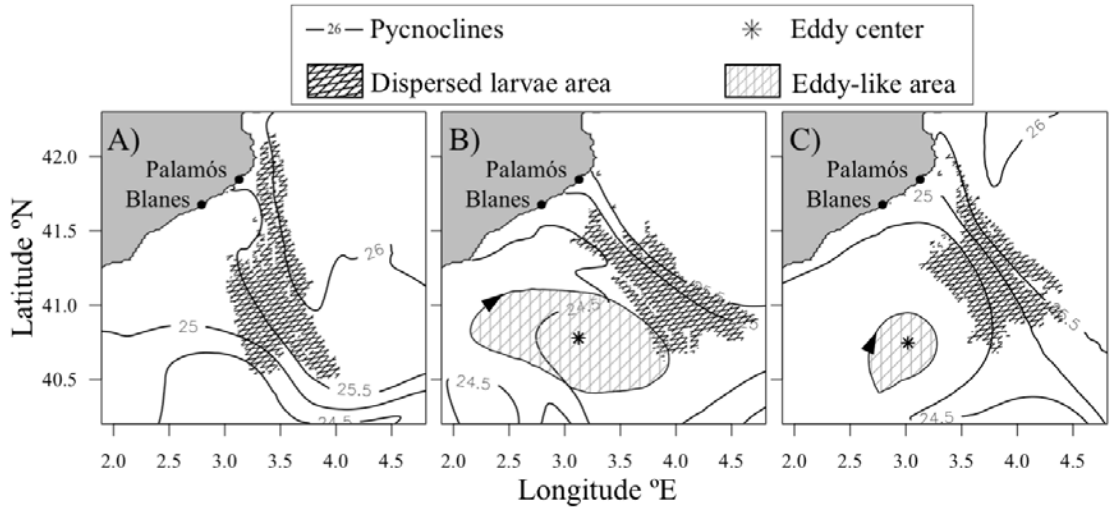

Figure 41. Maps of the dispersed larvae after drift simulations. Individuals were initially released within the zone impacted by the density front (zone 2 in Figure 35) in 2010 (A), 2012 (B), and 2015 (C). Those years were selected because individuals had extreme dispersal rates (see Figure 38). Pycnoclines at the surface ranged between 1024.5 (24.5) to 1026 (26) kg m^{-3}. Other maps per year are provided in the supplementary files (Figures S24.A-K).

2.4.4. Discussion

Interannual simulation of larval drifts in the area of three major submarine canyons represented how the variability of the hydrodynamics near the NBF could limit the population connectivity of *Aristeus antennatus* with southern zones. Among diverse mesoscale circulation structures around the front, influences from southern anticyclonic eddies and large meander have substantially driven larval transport.

2.4.4.1. Front and larval transport

Larval transport of *A. antennatus* and dispersal to southern zones depended on the position of the NBF. Evidence about the front impact on larval distribution in the NW Mediterranean Sea has been provided by several studies before, notably the shelf-slope fronts along the continental and insular coastlines of the Catalan Sea. In Sabatés and Olivar (1996), the geographical position of the front had a role in the distribution of shelf and mesopelagic fish larvae. The more the front was above the continental slope, the more the larvae from coastal species spread over the shelf and the shelf break. The NBF is perpendicular to the coast and does not have the same origin as shelf-slope front, but we estimated that it had a similar limitation on the larval distribution according to the geographical position of the fronts, like in 2012 and 2015. Generally, our results suggest that for some summers, the position of the NBF was favorable for higher retention and reception of larvae in the vicinity of the Palamós Canyon, and in other years, it was favorable for a higher dispersal in the southern zones. Mariani et al. (2010) had a similar conclusion about the role of a displacing front on the recruitment of tunas in a southern area of the NW Mediterranean Sea. Our results are in agreement with Mancho et al. (2008), who defined the NBF as a Lagrangian barrier and a limitation to larval connectivity.

2.4.4.2. Front and main circulation

The circulation along the density front was influenced by the strong and interannual variable Northern Current, i.e., the southeastward current associated with the Lions' gyre. Two facts are considered for understanding how summer atmospheric forcings on the Lions' gyre could have impacted the larval dispersal. First, larvae in the surface layer are most likely to be transported by wind-driven currents (Snauffer et al., 2014). Second, the Lions' gyre is a cyclonic gyre whose strength and position are modulated by the seasonal and interannual variability of winds and heat fluxes (Echevin et al., 2003; Herbaut et al., 1997; Korres et al., 2000; Molcard et al., 2002). Under those atmospheric changes, the larval supply from the northern part of the Mediterranean Sea to the study area would decrease, like in 2006, 2013 and 2014. Additionally, the larval transport from the study

zone would expand less towards the open ocean, like in 2006 and 2013. The importance of the current jet near a front on either the larval accumulation or on larval distribution has already been demonstrated (Sabatés and Olivar, 1996; Munk et al., 1999; Perry et al., 1993). Our study, in agreement with these previous findings, illustrated for the first time the role of the hydrography from the Lions' gyre along the NBF on the *A. antennatus* dispersal.

2.4.4.3. Front and mesoscale circulation

Along the NBF, the advection of the larvae was also reinforced with the proximity of anticyclonic eddies and large meanders. In the summer, anticyclonic eddies are generated by the dominant thermohaline circulation (Pascual et al., 2002), and move along the continental slope (Rubio et al., 2005). The intrusion of recent Modified Atlantic Water through the Balearic channels also contributes to the formation of eddies and large northeastward meanders (López García et al., 1994). These mesoscale structures had two effects in our study. First, the vorticity can transport the larvae (Landeira et al., 2009). In our study, larvae released south of the NBF were transported northeastward because of an eddy edge made possible the dispersal of larvae from Blanes fishing grounds towards Palamós fishing ground as in 2012, 2015 and 2016. Second, the proximity of an eddy with the frontal zone and the strong current jet enhances the offshore advection of larvae. Along with the NBF, Branicki et al. (2011) supported the idea that eddies near a front can influence the transport across the Lagrangian barrier. In our analysis, the larval drift of *A. antennatus* did not last long enough time to be influenced by this mechanism. However, the extent of larval transport revealed that eddy close to the frontal zone could contribute to the acceleration of the flows by squeezing convergent water masses of old and recent Modified Atlantic Water. With this, our study agrees that the NBF is an important delimitation of two dynamically different regions as established in Rossi et al. (2014), and its variability explains interannual differences in the recruitment. We underline that due to spatiotemporal variability of the mesoscale circulations or their origins (i.e., wind and hydrographic gradient), parameters or indexes that could characterize the link between the front and the larval drifts, could not go further than the descriptive phase.

2.4.4.4. Front and consequences on larval ecology

The estimated larval distribution due to their transport near the surface showed that the Palamós area is at an advantageous location for recruitments above the average. First of all, the frontal zones are advantageous as well as inconvenient regions in which larvae have a better growing and feeding rates due to the favorable and enriched waters as well as mortality by predation (Bakun, 2006; Granata et al., 2004). For example, tuna larvae whose pelagic life overlaps with *A. antennatus* larvae accumulate in fronts and feed on unidentified shrimp larvae (Catalán et al., 2011; Medina et al., 2016). This is an important insight for the shrimp larval dispersal and features a potential interaction with other commercial species. In that sense, we encourage the research community to narrow the taxonomic identification of prey in the stomach contents. Second, within the front, the larvae are transported offshore and are expected to recruit on the bottom floor outside of the fishing activity ground. This is in agreement with the fact that small shrimps, juveniles, and a part of the population that has not been estimated yet, are also distributed on the seafloor ranging between 1000 and 3300 m (Sardà et al., 2004; Sardà and Company, 2012). Last, given the fact that the larvae in our study zone were supplied by Cap de Creus or Blanes areas, we observed a consistent and occasional connectivity pattern with non-restricted fishery areas from those two areas. Considering the variability in the NBF position and larval dispersal, the impact of intense fisheries on the spawning biomass, e.g. from Palamós or Blanes fishing grounds, would be mostly transferred on the same or neighboring fishing grounds. A further step would be to explore how the larval swimming behavior of the larvae can affect larval drift and consequently alter the species connectivity. In particular, larvae can modify their vertical position, and consequently modify the transport (Robins et al., 2013). This question, already postulated in Clavel-Henry et al. (2020) may deserve more attention in further studies. However, the uncertainty of the larval dispersal is expected to only have minor variations because the frontal and eddy structures are relatively persistent in the upper 200 m depth layer.

2.4.5. Conclusion

The coupling of modeled hydrodynamics of the Mediterranean Sea and Lagrangian individuals representing the larvae of *A. antennatus* has shown that the North Balearic Front affected the larval drifts. Three important aspects of the front shaped the dispersal of the larvae. First, the larvae were mostly advected by strong currents along the density front. Second, the interannual variation of the front position conditioned the dispersal of particles to southern zones. Last, the position of an anticyclonic eddy, at south of the average front location, implied an expansion of the larval transport toward the open sea. Above all, these findings showed that the connectivity relationship between shrimp subpopulation is complex, and thereafter, diverse biotic and abiotic factors need to be considered at a small and large scale. In our study, we show that the front contributed to sustain the abundant population over the most important Spanish blue and red shrimp fishery ground. This can support the improvement of local management plans like in Palamós by considering the impact of the NBF and its interannual dynamic to define the surface with restricted fishery activity. This study is in line with other studies suggesting that the frontal zone is an enriched system and has interesting hydrodynamics modulating the local marine populations. However, further in-situ and lab studies on larval ecology are required to better adjust the Lagrangian transport model.

2.4.6. Supplementary information

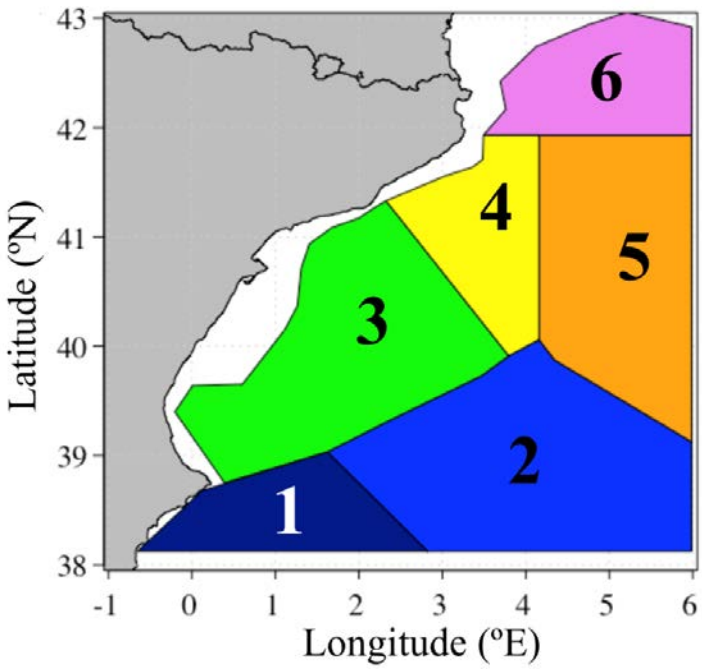

Figure S11. Map of the ROMS model domain and sectors used for ROMS validations. The validation of the hydrodynamic model compared the ROMS outputs to ARGO data. Results of the comparisons are given in Taylor diagrams (Figures S12 - S20), with focus on July and August data in sectors overlapping our study area (4, 5, 6).

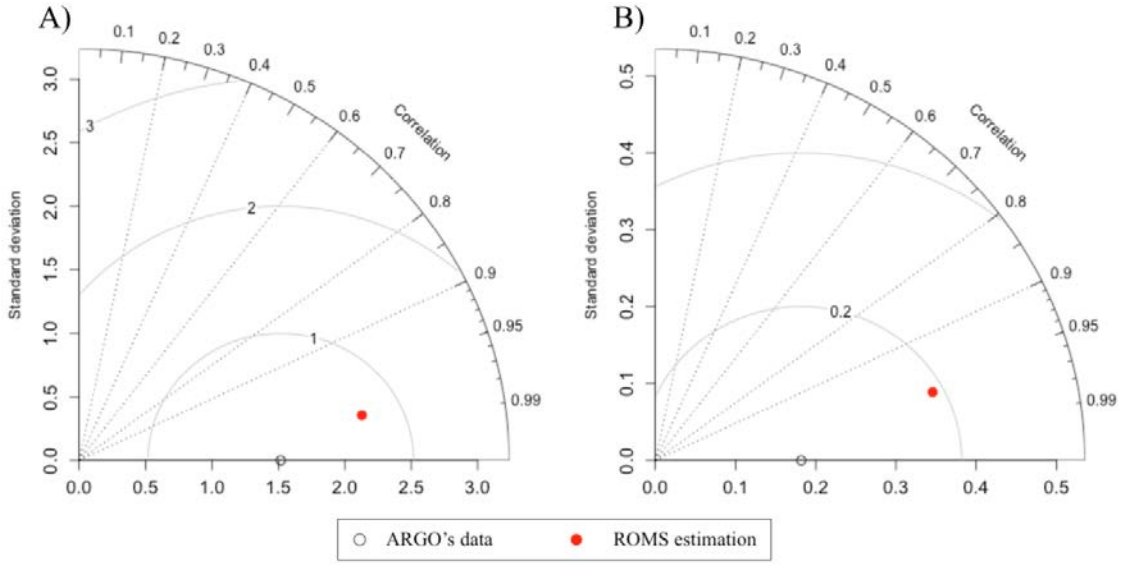

Figure S12. Taylor diagram for sector 6 in July 2008. Comparison between estimated and observed data used seawater temperature (A) and salinity (B). X-axis and Y-axis, circles centered on ARGO averaged profile and radial from the origin (0,0) represent the standard deviation, the correlation and the Root Mean Squared Error, respectively, between the data from ARGO and the ROMS model. Polygon of sector 6 is represented in Figure S11.

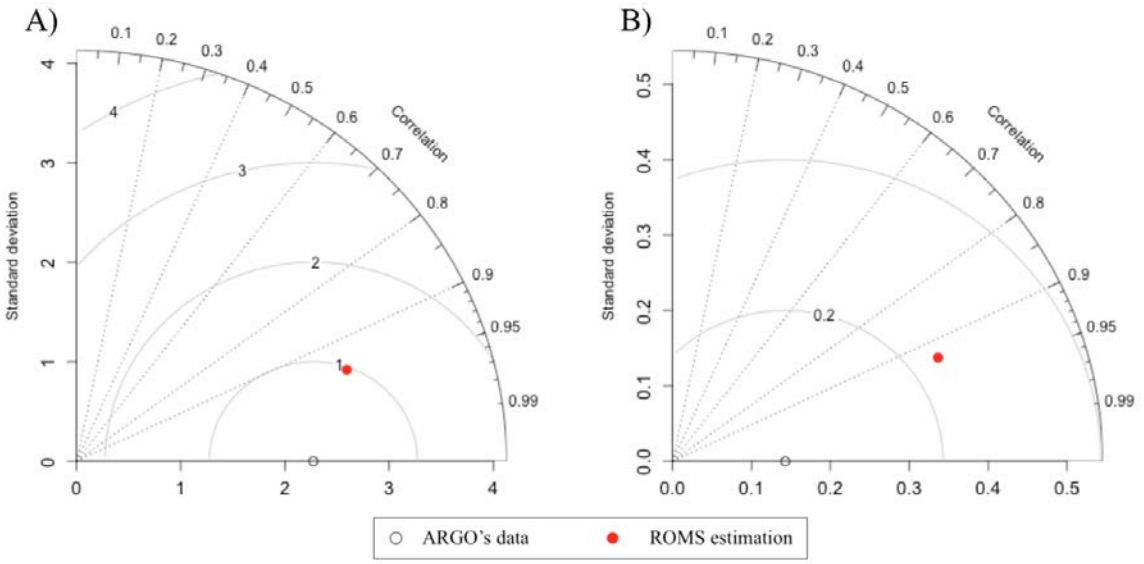

Figure S13. Taylor diagram for sector 6 in August 2008. Comparison between estimated and observed data used seawater temperature (A) and salinity (B). X-axis and Y-axis, circles centered on ARGO averaged profile and radial from the origin (0,0) represent the standard deviation, the correlation and the Root Mean Squared Error, respectively, between the data from ARGO and the ROMS model. Polygon of sector 6 is represented in Figure S11.

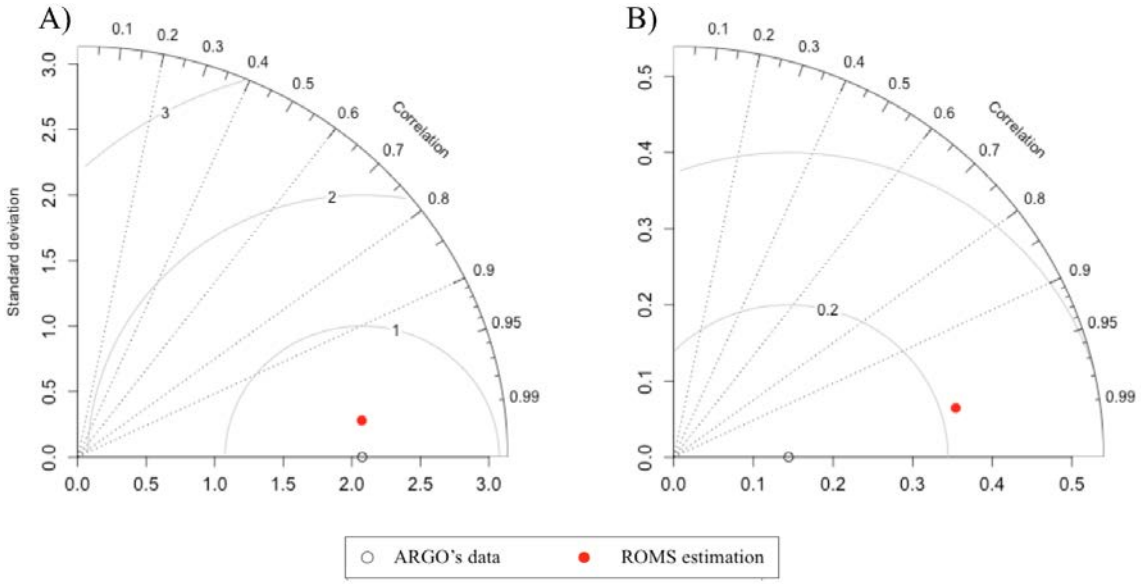

Figure S14. Taylor diagram for sector 5 in June 2012. Comparison between estimated and observed data used seawater temperature (A) and salinity (B). X-axis and Y-axis, circles centered on ARGO averaged profile and radial from the origin (0,0) represent the standard deviation, the correlation and the Root Mean Squared Error, respectively, between the data from ARGO and the ROMS model. Polygon of sector 5 is represented in Figure S11.

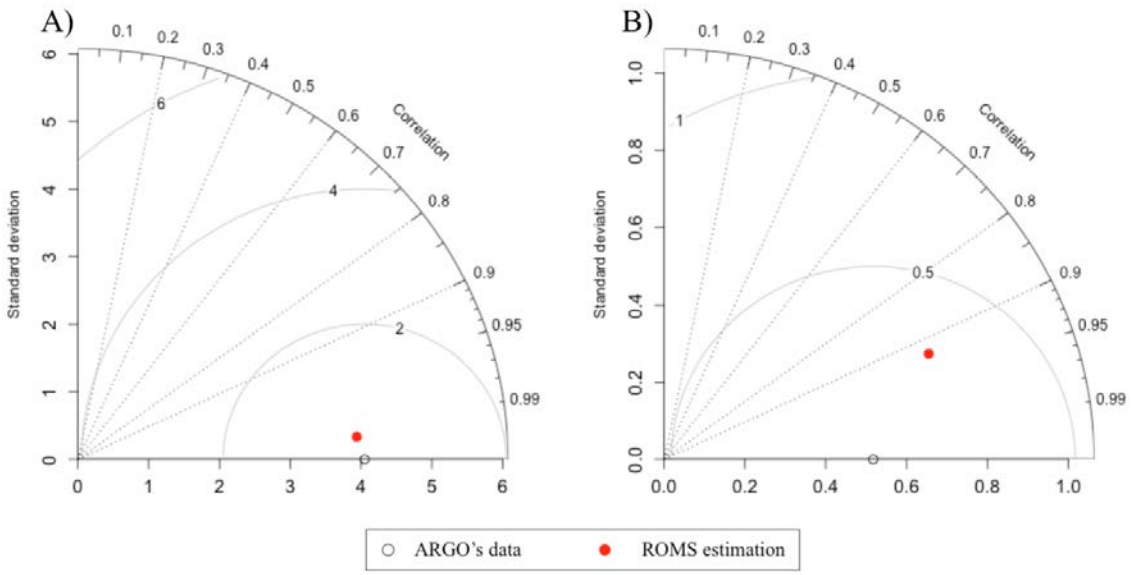

Figure S15. Taylor diagram for sector 5 in July 2014. Comparison between estimated and observed data used seawater temperature (A) and salinity (B). X-axis and Y-axis, circles centered on ARGO averaged profile and radial from the origin (0,0) represent the standard deviation, the correlation and the Root Mean Squared Error, respectively, between the data from ARGO and the ROMS model. Polygon of sector 5 is represented in Figure S11.

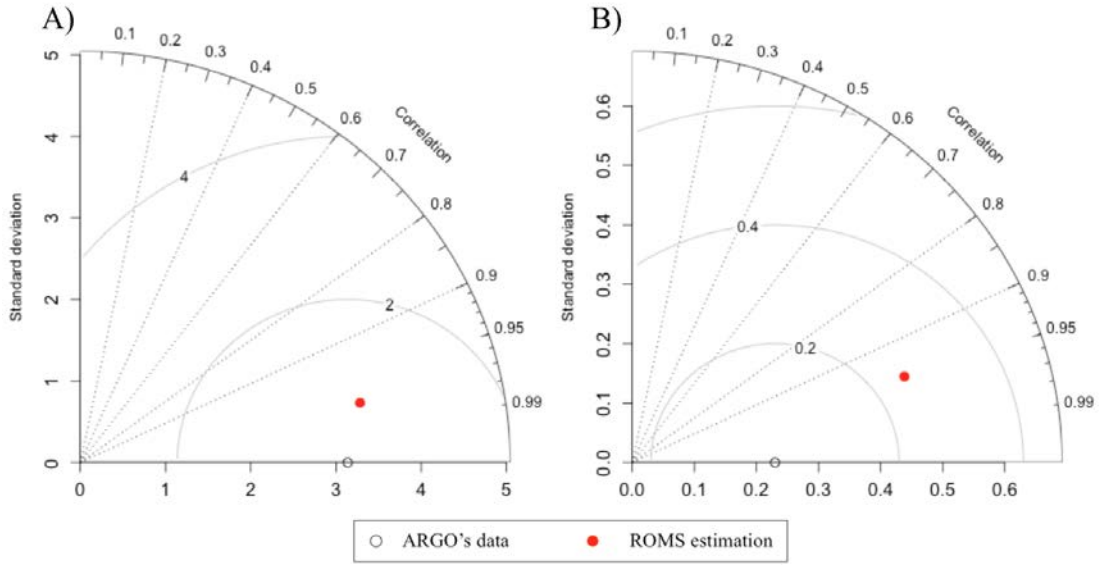

Figure S16. Taylor diagram for sector 5 in August 2014. Comparison between estimated and observed data used seawater temperature (A) and salinity (B). X-axis and Y-axis, circles centered on ARGO averaged profile and radial from the origin (0,0) represent the standard deviation, the correlation and the Root Mean Squared Error, respectively, between the data from ARGO and the ROMS model. Polygon of sector 5 is represented in Figure S11.

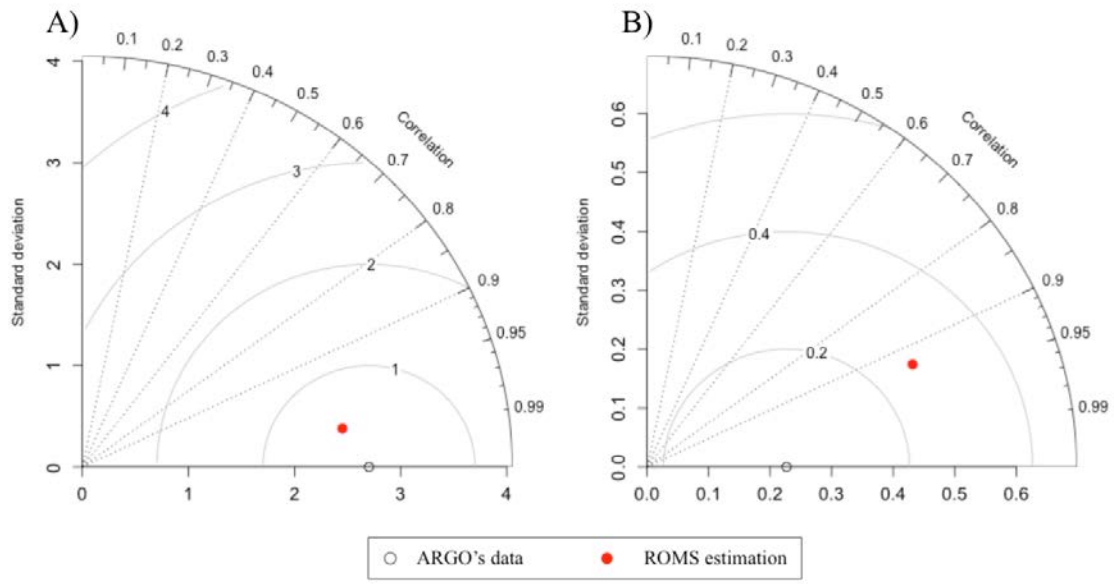

Figure S17. Taylor diagram for sector 6 in July 2014. Comparison between estimated and observed data used seawater temperature (A) and salinity (B). X-axis and Y-axis, circles centered on ARGO averaged profile and radial from the origin (0,0) represent the standard deviation, the correlation and the Root Mean Squared Error, respectively, between the data from ARGO and the ROMS model. Polygon of sector 6 is represented in Figure S11.

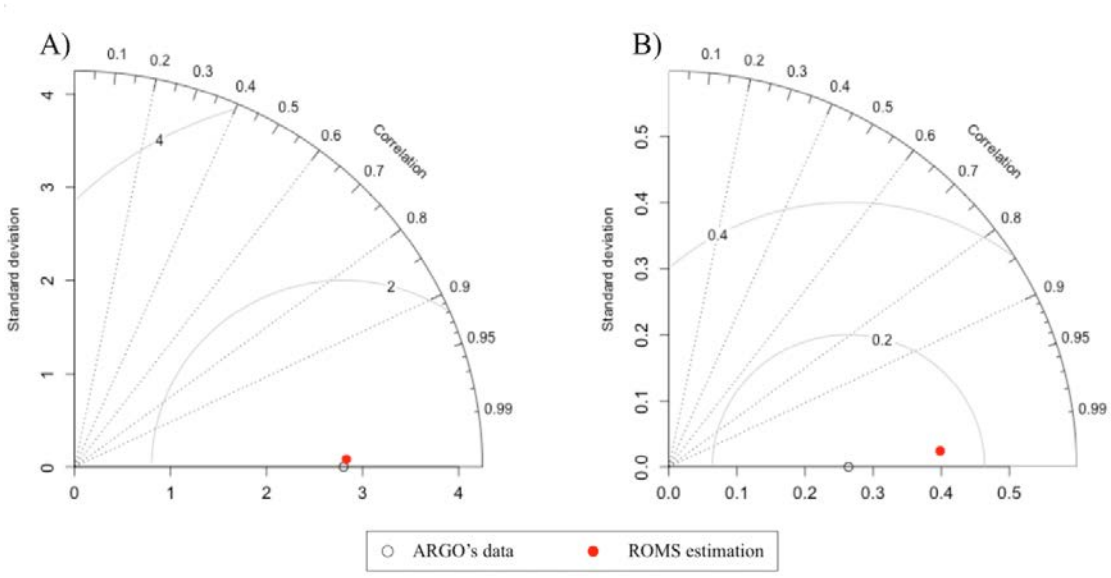

Figure S18. Taylor diagram for sector 5 in July 2015. Comparison between estimated and observed data used seawater temperature (A) and salinity (B). X-axis and Y-axis, circles centered on ARGO averaged profile and radial from the origin (0,0) represent the standard deviation, the correlation and the Root Mean Squared Error, respectively, between the data from ARGO and the ROMS model. Polygon of sector 5 is represented in Figure S11.

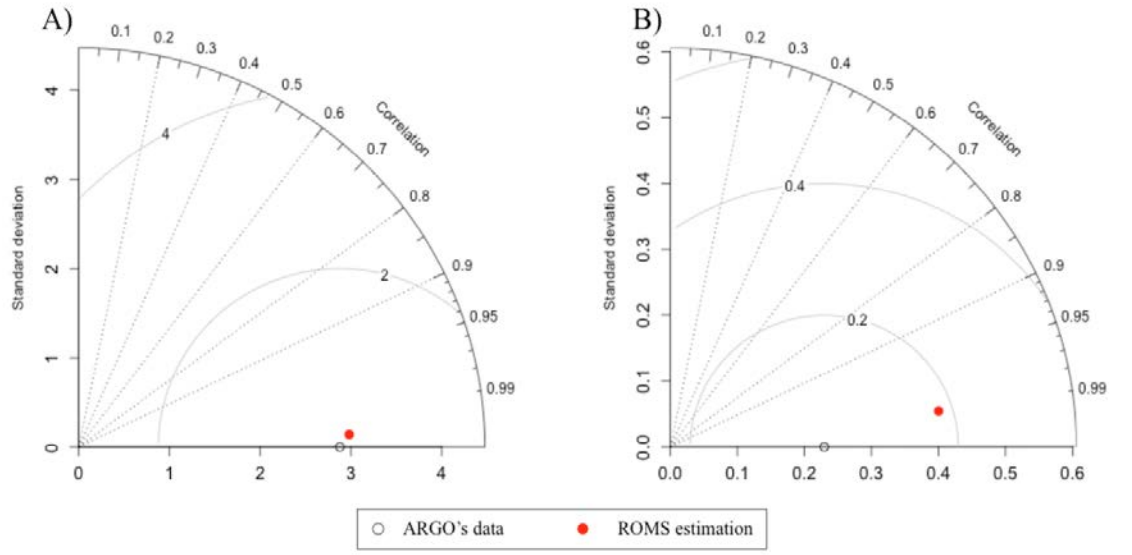

Figure S19. Taylor diagram for sector 5 in August 2015. Comparison between ROMS estimated and ARGO observed data used seawater temperature (A) and salinity (B). X-axis and Y-axis, circles centered on ARGO averaged profile and radial from the origin (0,0) represent the standard deviation, the correlation and the Root Mean Squared Error, respectively, between the data from ARGO and the ROMS model. Polygon of sector 5 is represented in Figure S11.

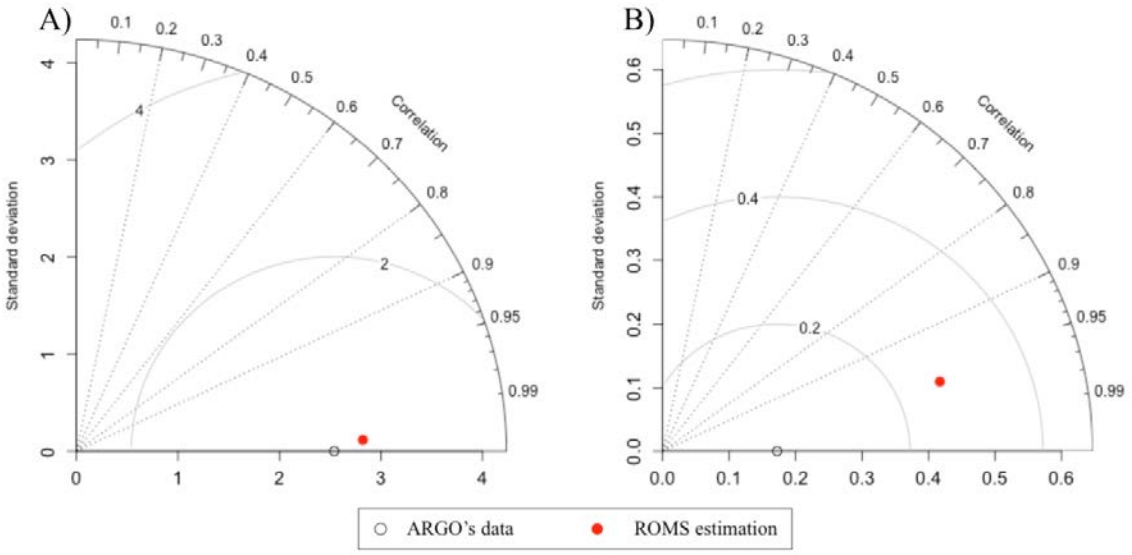

Figure S20. Taylor diagram for sector 5 in July 2016. Comparison between estimated and observed data used seawater temperature (A) and salinity (B). X-axis and Y-axis, circles centered on ARGO averaged profile and radial from the origin (0,0) represent the standard deviation, the correlation and the Root Mean Squared Error, respectively, between the data from ARGO and the ROMS model. Polygon of sector 5 is represented in Figure S11.

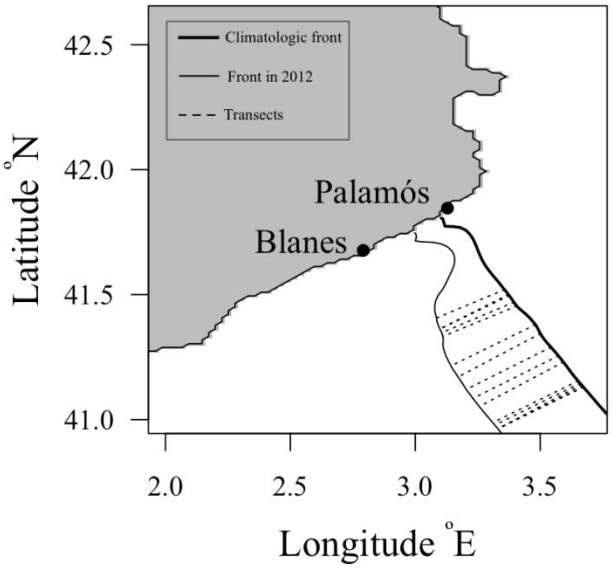

Figure S21. Method for estimating the distance between the climatological and interannual fronts. The graphic represents the positions of the climatological front and the front in 2012. A total of 50 transects perpendicular to the front(here only 15 are drawn, dashed lines) were used to compute the average distance between the fronts.

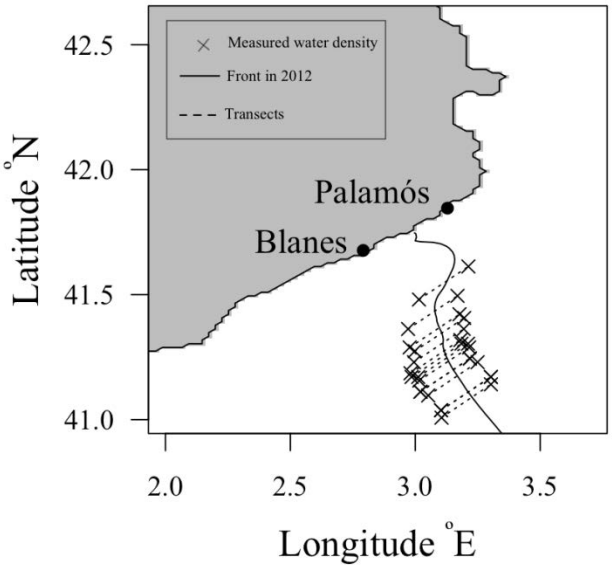

Figure S22. Method for estimating the density front strength. Seawater density was extracted 10 km away at both sides of the density front. A total of 50 segments perpendicular to the front (here only 15 are drawn, dashed lines) were used to localize the coordinates where the water density was extracted.

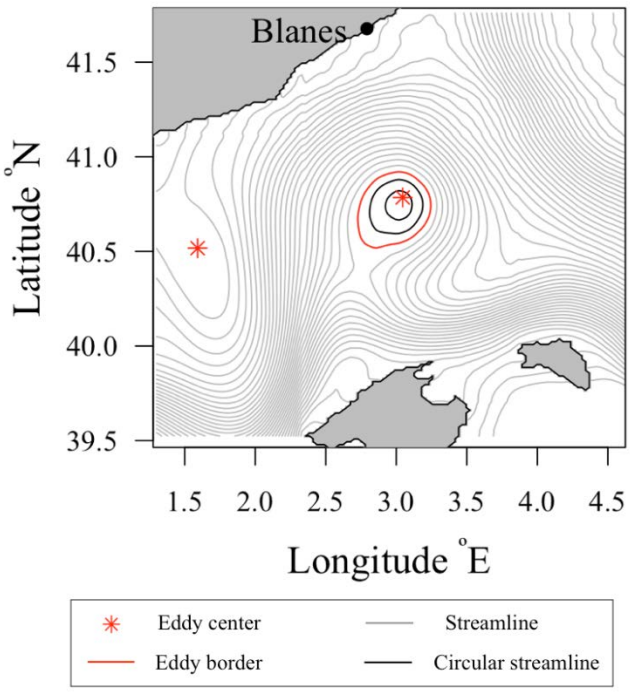

Figure S23. Method for estimating the area of the anticyclonic eddy. The graphic represents the eddy size and center in modeled hydrodynamics of 2015. After computing the streamlines, the eddy border was estimated according to the maximum area delimited by circular streamlines.

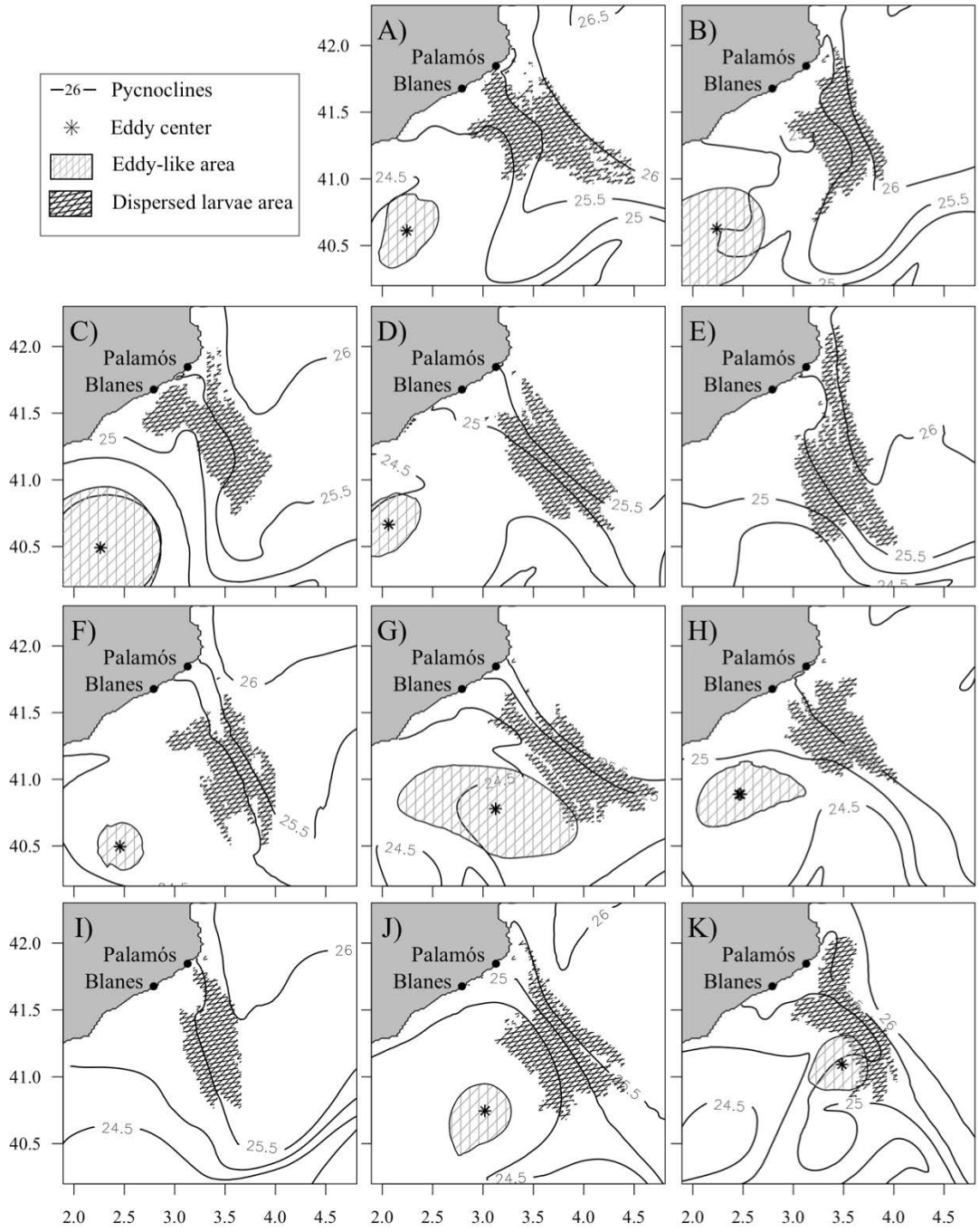

Figure S24. Maps of the dispersed larvae after drift simulations. Individuals were initially released within the zone impacted by the density front (zone 2 in Figure 35) in 2006 (A), 2007 (B), 2008 (C), 2009 (D), 2008 (E), 2011 (F), 2013 (G), 2013 (H), 2014 (I), 2015 (J), 2016 (K). The shaded black area represents the distribution of the dispersed larvae after the simulation of their transport. The shaded grey polygon and the star represent the anticyclonic eddy coverage and its center, respectively. Pycnoclines at the surface ranged between 1024.5 (24.5) to 1026 (26) kg m^{-3}.

Section 2.5

Estimating spawning locations of the deep-sea red and blue shrimp *Aristeus antennatus* (Crustacea: Decapoda) in the NW Mediterranean Sea with a backward trajectory model of the larvae

Morane Clavel-Henry
Elizabeth W. North
Jordi Solé
Nixon Bahamon
Marta Carretón
Joan B. Company

This chapter was in collaboration with Elizabeth W. North

Congress poster: Ocean Sciences Meeting 2020, San Diego (CA), USA.

Conference: Horn Point Laboratory seminar 2019, Cambridge (MD), USA.

Article submitted to **Deep-sea Research - Part I** (2020)

Abstract

The deep-sea red and blue shrimp *Aristeus antennatus* is a commercially valuable species for the Spanish fishing harbors of the northwestern Mediterranean Sea. Since 2012, some fishermen of the deep-sea shrimp follow a local management plan which restricts fishing in certain areas to sustain the resource. However, little is known about the dispersal of larvae; specifically it is not known how far larvae can be transported from spawning areas and if there could be mixing of larvae from different fishing grounds. The objective of this study was to estimate the spawning sites of collected larvae, evaluate the uncertainty of the estimates, and determine if these larvae could have come from the restricted fishing areas. Using a 3-dimensional coupled hydrodynamic and Lagrangian transport model, the spawning sites of the larvae were estimated by backwards simulation of larval trajectories from the sampling stations. The backtracked larvae were assigned temperature-dependent stage durations based on a literature review of similar species. Larvae were backtracked to spawning sites, with median distances from collection locations of 11 and 38 km when minimum and maximum Pelagic Larval Durations were implemented, respectively. Uncertainty analysis of backward trajectories showed that distance estimates could vary by as much as 27, 3, and 8 km due to differences in simulated Pelagic Larval Durations, turbulent mixing, and advection, respectively. Of the 35 sampling stations from which larvae were backtracked to fishing grounds, 13 were tracked back to multiple fishing grounds, suggesting that mixing of larvae from different fishing grounds does occur. For example, for the sampling stations on the restricted area of Palamós, on average 35% of simulated larvae came from the restricted area itself, and 0.9% and 10% of larvae came from the northern and southern neighboring areas, respectively. These results support the idea of multiple connectivities between the subpopulations of the *A. antennatus* and may help inform regional management plans.

2.5.1. Introduction

Because dispersal is a fundamental characteristic of marine systems, some populations can span multiple fishery grounds with different management policies (Kough et al.,

2013). The dispersal of many marine species occurs in pelagic larval phase, during which larvae can travel 10s to 100s of kilometers (Cowen et al., 2006). In pelagic waters, larvae can be transported by the currents and establish connections between physically distant populations, ensuring population renewal and the genetic heterogeneity needed for the stock stability (Bendsten and Hansen, 2013). Knowledge of larval dispersal and connectivity can help elucidate environmental and physical conditions that promote successful settlement and identify habitats that are important to protect and restore (Cowen and Sponaugle, 2009). In addition, linking larval distributions to spawning sites can provide information to support management plans (Bauer et al., 2014) and improve our understanding of stock dynamics (Everett et al., 2017).

With the increase of computational power, tools for studying connectivity have developed which allow larval trajectories to be simulated within a Lagrangian model framework. These numerical models can predict transport trajectories either back or forward in time through advective regimes, mesoscale circulation patterns, and turbulence in marine systems (Christensen et al. 2007; Holliday et al., 2012; Landeira et al., 2017). Additionally, transport is influenced by larval biology (e.g., pelagic larval duration, egg buoyancy) and larval behavior, which can cause larval drifts to differ from mean currents and increase uncertainty around the origins or the settlement locations of the larvae (Siegel et al., 2008; Robins et al., 2013). Lack of information about larval biology is challenging for connectivity research, especially when information on the location of larvae is scarce and the habitats of the adults is less accessible.

In the NW Mediterranean Sea, the pelagic drift of larvae of the deep-sea red and blue shrimp *Aristeus antennatus* (Crustacea: Decapoda) is assumed to establish connections between different subpopulations. The shrimp is a valuable species in the economies of Spanish harbors, particularly for the ports of Palamós and Blanes, where catches represent up to 40% of the annual income from landings (Official fishery statistics from the Autonomous Government of Catalonia, www.idescat.cat) and the fishery is regulated by fishery management plans (BOE, 2013; 2018).

The deep-sea red and blue shrimp occupies the continental slope in waters 400 m to more than 2 000 m deep (Sardà et al., 2003a) and are abundant near submarine canyons which

incise the continental margin. Some spawning sites have been identified which overlap with fishing grounds (Sardà et al., 2003b). From these, females are assumed to release eggs near bottom, which then develop into nauplius, protozoea, and finally into mysis stages in pelagic waters, similar to the larval cycle of the taxonomically close genus of Penaeid shrimps. Until 2016, little was known about the distribution of *A. antennatus* larvae because a rare few individuals were found occasionally near the surface (Held, 1954; Carbonell et al., 2010). In 2016, the CONECTA project (Spanish reference: CTM-2014-54648-C2-1-R) sponsored a cruise which used multiple gears and sampled multiple water layers from the border between Spain and France to the Eivissa Channel. More than 2 000 larvae of *A. antennatus* were caught near surface (Carretón et al., 2019), providing new and significant insight into larval distributions.

Although previous studies have estimated the drift of individuals from known spawning sites and have shown the importance of hydrodynamic variability and larval ecology on their transport (Palmas et al., 2017; Clavel-Henry et al., 2019, 2020), modeling research has not yet incorporated the latest findings on *A. antennatus* larval distributions. With this new understanding, the spawning locations of collected larvae could be estimated and could provide valuable information to support local fisheries management plans like the one on Palamós fishing grounds. Understanding the larval transport distance as well as the connectivity between fishing grounds can contribute to decisions about the size and locations of restricted areas.

In the present study, the overarching goal was to estimate the spawning locations of shrimp larvae found near the surface during the *A. antennatus* survey in the NW Mediterranean Sea on July and August 2016. A three-dimensional coupled hydrodynamic and larval transport model was used to address three specific objectives: 1) to estimate potential spawning locations for larvae captured at each station, 2) to assess sources of uncertainty in model estimates, and 3) to approximate the potential larval supply from fishery management areas as spawning locations for the larvae which were captured on the CONECTA research cruise. These analyses were intended to integrate the latest knowledge of *A. antennatus* life history and the NW Mediterranean Sea hydrodynamics, and provide information that could support fishery management of this deep-sea red and blue shrimp.

2.5.2. Materials and Methods

To address the objectives, a hydrodynamic and Lagrangian larval transport model were coupled and used to predict the trajectories of larvae collected backwards in time (i.e., from larval stage to spawning) from the collections during the CONECTA program in July-August, 2016. A series of model scenarios and analyses were conducted to understand the influence of advection, mixing and larval biology on the trajectories. Model predictions were applied to estimate the potential larval supply from different fishing grounds to the larvae collected as part of the CONECTA program.

2.5.2.1. Fishing grounds

Five fishing grounds for *A. antennatus* in the northwestern Mediterranean Sea were delimited on the Catalan continental margin. These zones were based on the distribution of daily Vehicle Monitoring System (VMS) data, provided by the Spanish government from January 2005 to December 2014 (Martín et al., 2014), which recorded the position of fishing boats and their harbors. The five fishing grounds and their sizes (km^2) were: Cap de Creus (2 802 km^2), Roses-Palamós (853 km^2), Palamós (1 158 km^2), Blanes (1 434 km^2), Barcelona to Vilanova (3,044 km^2).

2.5.2.2. Hydrodynamic model

We used a three-dimensional circulation model of the NW Mediterranean Sea implemented with the Regional Ocean Modelling System (ROMS; Shchepetkin and McWilliams, 2005). The circulation model has been run with both climatology (Clavel-Henry et al. 2019) and with interannual atmospheric conditions from 2006 to 2016. Daily outputs were stored and then validated with hydrographic profiles from ARGO buoys (Chapter 4). The model domain ranged between 0.65º W and 6.08º E, and between 38º N and 43.69º N with a horizontal resolution of 2 km (Figure 42). The water column was divided into 40 sigma layers, with increasing vertical resolution near the surface. More details on the interannual implementation and its validation are given in Chapter 4.

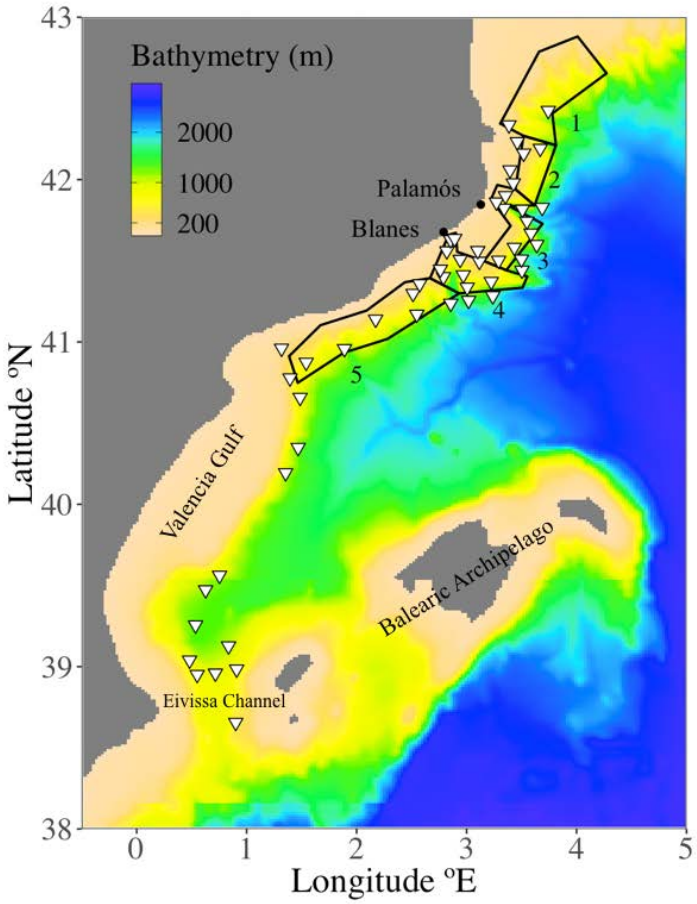

Figure 42. Spatial distribution of the sampling stations where *A. antennatus* protozoea were collected at surface in July-August 2016. Black polygons delimit known fishing grounds according to the distribution of the Vessel Monitoring System (see Figure S25) in the following north to south order: 1 - Cap de Creus, 2 - Roses and Palamós, 3 - Palamós, 4 - Blanes, and 5 - Barcelona to Vilanova.

2.5.2.3. Lagrangian larval transport model

The backtracking model was run in the framework of OpenDrift, which is an offline Lagrangian transport model that is programmed in python (Dagestad and Röhrs, 2018). OpenDrift interpolated three-dimensional outputs of ROMS to the position of the larvae in space and time using an Euler interpolation scheme. The time step was set at 900 seconds, which was the time step selected for maintaining fidelity between backward and forward tracking predictions after preliminary simulations.

In addition to advective transport, turbulent mixing (i.e., small-scale perturbations) were simulated and included in the displacement of simulated larvae. Mixing on the horizontal dimension was computed with a random walk scheme which was added to the OpenDrift code following this equation:

$$D_h = rand \cdot \sqrt{2 \cdot K_h} \cdot dt \qquad (14)$$

where D_h represented the displacement of the individual (in m), rand was a random value sampled from a Gaussian distribution G(0,1), *dt* was the time step, and K_h was the horizontal diffusivity coefficient. The coefficient of horizontal diffusivity was assigned a constant 10 m^2 s^{-1}, which was the average coefficient in the surface waters of the western Mediterranean Sea estimated in a modeling study by Sayol et al. (2014).

Vertical turbulence was calculated by a random displacement scheme (Hunter et al. 1993; Visser 1997) which is part of the OpenDrift package. This scheme used the vertical diffusion coefficient of salinity (hence vertical coefficient of diffusivity) provided in the ROMS hydrodynamic outputs. In the runs with vertical turbulence, the internal time step was set to 20 seconds.

In addition, in the vertical dimension, displacement due to the buoyancy force applied on eggs was simulated. Terminal velocity (i.e., the speed achieved by buoyant eggs) was calculated based on the spherical egg diameter and density and on the water density. Egg diameter and densities were drawn from a Gaussian distribution. For egg diameter, the distribution was implemented with a mean of 330 (± 46) µm based on observations of *A. antennatus* eggs (Demestre and Leonardo, 1992). For egg density, the mean of 884 (± 34) kg m^{-3} was used, an estimate based on the density needed for the vertical displacement of eggs to travel from the bottom to the surface during the egg stage (Clavel-Henry et al., 2020). The scheme used the equations 1 of Sundby (1983) and 2-11 of Dallavalle (1948) when the water regime was laminar or transient, respectively. This vertical displacement due to buoyancy was activated when the nauplius retrograded into eggs and was calculated with water density predicted by the ROMS model that had been interpolated in time and space to the egg position. More information about how egg buoyancy was parameterized can be found in Clavel-Henry et al. (2020).

2.5.2.4. Base model runs

Two base backtracking model runs were conducted with advection (U), egg buoyancy, vertical (V) and horizontal mixing (H), and different pelagic propagule durations (PPD; min and max) (see Table 5).

Table 5. List of model runs and information about model parameterizations for the two types of model scenarios conducted. In the plankton backtracking scenarios (A), particles were released from 55 stations (see Figure 42 and Table S7 for coordinates) and larval molting and egg buoyancy were simulated. In the Okubo backtracking scenarios (B), particles were released from 5 stations (labeled 10, 16, 25, 42, 48 in Table S7) and were assigned passive drift.

A) Plankton backtracking

Model runs	Transported by	PPD	Larval stages	Particles per station	Stations
U+HV - Min	Advection, and vertical and horizontal turbulences	Minimum	Nauplius, Egg	100	53
U+H - Min	Advection and horizontal turbulence	Minimum	Nauplius, Egg	100	53
U+V - Min	Advection and vertical turbulence	Minimum	Nauplius, Egg	100	53
U - Min	Advection	Minimum	Nauplius, Egg	1	53
U+HV - Max	Advection, and vertical and horizontal turbulences	Maximum	Protozoa, Nauplius, Egg	100	53
U+H - Max	Advection and horizontal turbulence	Maximum	Protozoa, Nauplius, Egg	100	53
U+V - Max	Advection and vertical turbulence	Maximum	Protozoa, Nauplius, Egg	100	53
U - Max	Advection	Maximum	Protozoa, Nauplius, Egg	1	53

B) Okubo backtracking

Scenario	Transported by	PPD	Larval stages	Particles per station	Stations
U+HV - Okubo	Advection, and vertical and horizontal turbulences	Maximum	none	100	5
U+H - Okubo	Advection and horizontal turbulence	Maximum	none	100	5
U+V - Okubo	Advection and vertical turbulence	Maximum	none	100	5
U - Okubo	Advection	Maximum	none	100	5

The base model run started from the day, position, and depth that larvae were collected with a Neutson sledge from July 18 to August 28, 2016 during the CONECTA research cruise (CTM 2014-54648-C2-1-R). Sampling was conducted in surface waters (0.75 m average depth of sampling) and occurred where seafloor depths were between 129 m and 1840 m in the geographical subarea (GSA) 6 of the Food and Agricultural Organisation (FAO). In the plankton samples, 2 319 protozoea of *Aristeus antennatus* were identified in 53 stations (Figure 42) of the 120 that were sampled. For model simulations, 100 individuals were released from each of the 53 stations to simulate multiple possible paths of larvae backwards in time. The number of particles per station (100) was set based on a

prior sensitivity study that examined the number of particles needed to resolve variability in Lagrangian drifts (Clavel-Henry et al., 2020). Simulated protozoea were released near-surface (0.75 m) where CONECTA collections occurred and were assumed to drift passively until retrograding into the egg stage during which density-dependent buoyancy influenced particle motion.

The drift duration lasted according to the pelagic propagule duration (PPD), which corresponded to the sum of stage durations from protozoea through the nauplii stage to the release of eggs. Stage durations were calculated based on water temperature at the larval position by a relationship described in Clavel-Henry et al. (2020) and were computed when larvae molted. The retrogradation of a larval stage occurred when the sum of the time steps in that stage was equal to the stage duration. When nauplii retrograded into eggs, the embryonic duration was computed with the bottom water temperature because eggs are assumed to be released near the seafloor where benthic females aggregate (Sardà et al., 1994) and where water temperatures are ~13 ºC (Salat and Cruzado, 1981).

Because the age of the collected larvae was unknown, two base model runs were conducted: one with minimum drift durations for the protozoea and one with maximum drift durations. Maximum and minimum durations were temperature-dependent and based on multiple regression models that had been constructed with observations of Penaeid shrimp larvae from laboratory studies (eq. 8 in Section 2.2). For the minimum PPD base run (U+HV-Min), the collected protozoea were assumed to have just molted into their current stage and the duration of the nauplius stage was used to compute the PPD. For the maximum PPD base run (U+HV-Min), the collected protozoea were assumed to be ready to transform into the mysis stage. In this case, the stage durations of the protozoea and nauplii stage were used to compute the PPD. By computing minimum and maximum PPDs, the two base model runs bracketed the expected range in PPD.

Before applying the base models to calculate connectivity, series of analyses were conducted to better understand uncertainty associated with the simulations, as described below.

2.5.2.5. Uncertainty studies

Three types of uncertainty studies focused on advection, diffusion, and PPD were undertaken to better understand the sources and relative magnitude of uncertainty in the base run model predictions.

Advection

Uncertainty from advection was expected because of the challenges associated with simulating observed current velocities using a hydrodynamic model. The magnitude of the divergence between modeled and observed current velocities was assessed by comparing model predictions with measurements at one location, the only available time-series of current velocities in the studied area. Meridional and zonal velocities were measured every 30 min with an Acoustic Doppler Current Profiler at a fixed buoy in the head of the Blanes canyon (see Figure 43) in 7-m depth intervals. Daily averages of the 48 measurements were calculated centered on noon of each day. Data were processed by the Operational Observatories of the Catalan Sea (OOCS; Bahamon et al., 2011).

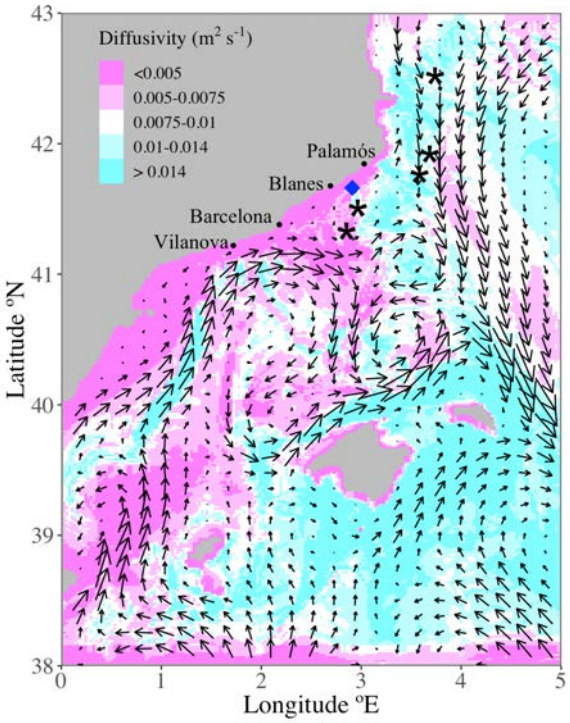

Figure 43. Average current velocities (arrows, m s^{-1}) and average vertical diffusivity coefficient (color contours, m^2 s^{-1}) in the NW Mediterranean Sea from July 18 to August 28, 2016, as predicted by the ROMS model. The averages were computed with grid points in the upper 20 m. The position of the Ocean Observatories of the Catalan Sea (OOCS) buoy where current velocities were measured during this time period is indicated by the blue diamond. The position of five sampling stations used in the uncertainty studies is indicated by the black stars. These stations were selected because they had the highest rates of return of particles to a fishing ground (see Table S7 and Figure 42).

Outside the framework of Lagrangian tracking modeling, simple backward trajectories were computed using the daily mean of recorded current velocities from the OOCS's buoy and using the ROMS model predictions that were interpolated in time and space to the buoy location. The trajectories were estimated at 7 m, 14 m and 21 m from August 28, 2016 to 15 days backwards in time. At the 15th day, the distance between the end locations of the observed and predicted trajectories was computed for each depth interval to evaluate the magnitude of the potential discrepancy in drift trajectories caused by divergence between actual velocities and those simulated by the hydrodynamic model.

Diffusion

To better understand the uncertainty associated by divergences between observed and simulated mixing, supplementary model scenarios were conducted to compare the spread of passive particles with observations from dye-release studies that were summarized in the Ocean Diffusion diagram by Okubo (Okubo, 1971). The spread of passive particles was calculated as the mean squared displacement (D_p; eq. 15), which was the average of the squared distance (d) between an individual particle locations $(X,Y)_i$ and the average position (X,Y) of the 100 particles released at the same station:

$$D_p = \sum_{i=1}^{100} d[(X,Y)_i, (\overline{X}, \overline{Y})]^2 \div 100. \qquad (15)$$

After preliminary runs of the base model (U+HV-Max), five CONECTA sampling stations were selected for model simulations. These stations had the highest rates of particle return to fishing grounds (Figure 42, zones described in section 2.5). From the five stations, 100 passive particles were released in a 1 m^2 surface, at 0.75 m below the surface and backtracked with no turbulence (advection only) and three types of turbulence: advection plus horizontal mixing (U+H), advection plus vertical mixing (U+V), and advection plus horizontal and vertical mixing (U+HV) or only with advection (U) (see Table 5). The backtracking began at the same time as the plankton backtracking scenarios and lasted the maximum PPD which had been estimated at each selected station in preliminary model runs.

We quantified the differences among model runs and Okubo's equation by estimating and comparing the values taken by the exponent q of the following power-law:

$$D_p = p \cdot t^q \qquad (16)$$

where t is the time and p the coefficient of the power-law. To do so, after each model runs, we fitted a simple linear regression model on log-transformed values of D_p and simulation time t from all five selected stations after linearizing (3):

$$log(D_p) \approx q \cdot log(t) + log(p) + \epsilon \qquad (17)$$

where ε is the random error.

PPD

In the base model run, two PPD were simulated, max and min, because the age of the protozoea was not known when they were collected. To better understand the influence of these different PPDs on backtracking predictions, the base run simulations were analyzed by calculating median drift duration and drift distances for all particles. In addition, to determine how parameterization of diffusivity interacted with PPD, the base model was re-run with different types of diffusion (advection only (U), U+H, U+V, and U+HV) and then the drift duration, drift distance, and mean squared displacement of particles was calculated (eq. 15). We also computed the distance (*D*, in km) between the average position of spawning sites in model run with advection only (U; $(X,Y)_U$) and those with different types of diffusion ($(X,Y)_n$ with n = U+H, U+V or U+HV) such that:

$$D = d[(\overline{X}, \overline{Y})_U, (\overline{X}, \overline{Y})_n] \qquad (18)$$

where d is distance (km) calculated using the great circle formula derived from the spherical law of cosines:

$$d = 6378 \cdot arcos(sin(\overline{Y_U}) \cdot sin(\overline{Y_n}) + cos(\overline{X_U} - \overline{X_n}) \cdot cos(\overline{Y_U}) \cdot cos(\overline{Y_n}) \qquad (19)$$

The distance between the spawning sites predicted by backtracking under advection only and by backtracking with different mixing parameterization was plotted versus latitude to explore the potential role of PPDs and the diffusion parameterizations on spawning site estimates in different hydrodynamic conditions which varied across the model domain.

Additional analyses were conducted to examine the uncertainty in spatial predictions introduced by the different parameterizations of PPD and diffusion. These analyses were conducted using the five stations selected for the diffusion uncertainty analysis (see above). For these stations, the location of estimated spawning sites was visualized in

relation to fishing grounds run to better understand the influence of model parameterization on the spatial distribution of model predictions.

2.5.2.6. Larval supply from fishing grounds

To estimate the potential larval supply from fishery grounds as spawning locations for the larvae captured on the CONECTA cruise, results of the base model runs (U+HV-Min and U+HV-Max) were combined and used to calculate the percent of particles which were released from each CONECTA station and backtracked to each fishery ground or to none of the fishery grounds.

2.5.3. Results

2.5.3.1. Base model

In the base model runs, backward trajectories of particles were estimated for all CONECTA sampling stations (Figure 42) and showed notable differences between runs with minimum (U+HV-Min) and maximum (U+HV-Max) PPDs (Table 6). For example, pelagic duration differed from a median of 3.9 days to 10.3 days, distance traveled changed from a median of 10.9 km to 37.6 km, and the spread of particles varied from a median of 5.0 km^2 to 26.0 km^2 when PPD was minimum and maximum, respectively. These model runs were designed to bracket possible spawning locations given uncertainty in the age of the collected larvae, and show the difference in spatial distribution that could result from this uncertainty (Figure 44).

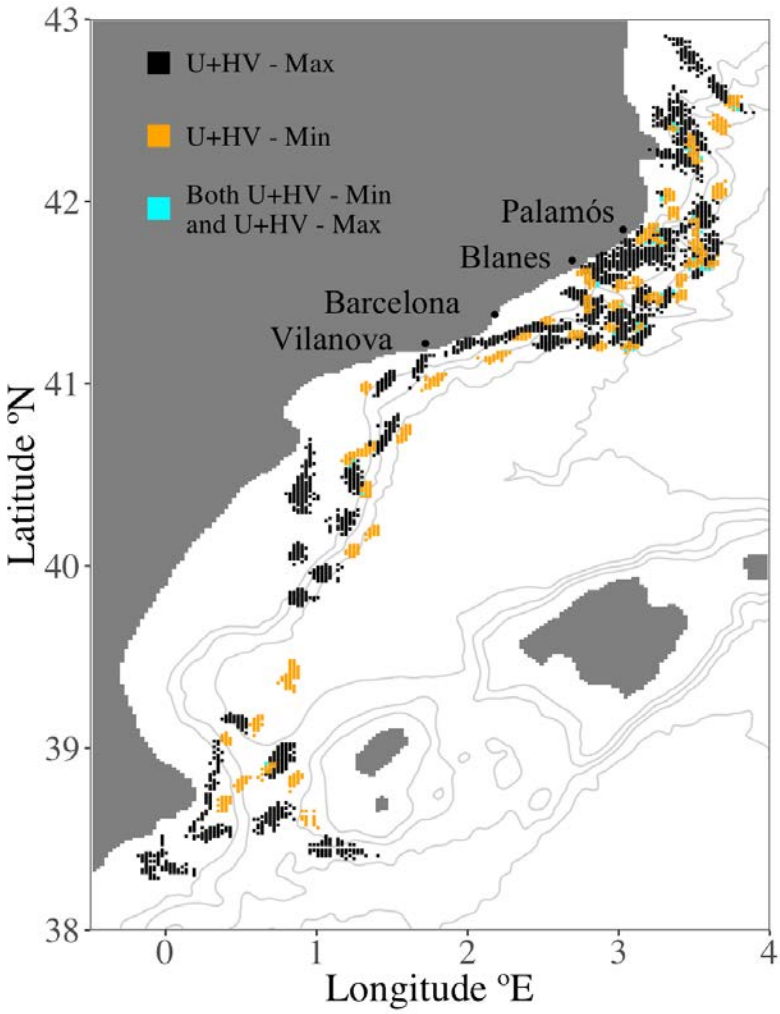

Figure 44. Spatial distribution of grid cells that contained individuals after backtracking as computed the base model run (U+HV = advection plus horizontal and vertical turbulence) with maximum Pelagic Larval Duration (black grid cells) and minimum Pelagic Larval Duration (orange grid cells). The blue grid-cells contained individuals from both minimum (U+HV - Min) and maximum (U+HV - Max) Pelagic Larval Duration. Lines gray lines are the isobaths at 200 m, 500 m, and 1000 m.

Table 6. Median duration (day), median distance from the starting location (km), median square displacement (km²), median depth (m), and number of particles in plankton backtracking scenarios with A) maximum and B) minimum Pelagic Larval Durations. Medians (25th/75th quantiles) were computed over all sampling stations (i.e., 53 particles in U, and 5 300 particles in U+H, U+V, U+HV). Distance (from the starting location) is the drift length from the beginning location to the end location for each particle. Mean squared displacement of each particle was calculated as the average of the squared distances of each particle from the center location of all particles at the end of the backtracking. Depth represents the median vertical position of the particles from the time of release to just before the egg stage. The * indicates that the value was significantly different from the value in the model run U+HV (Wilcoxon statistical test, see Table S8 for statistics).

A) Maximum Pelagic Larval Duration

Model runs	Duration (day)	Distance (km)	Mean squared displacement (km²)	Depth (m)	Number of particles
U+HV - Max	10.3 (9.9/10.8)	37.6 (15.9/62.4)	26.0 (15.4/60.4)	-9.1 (-13.3/-5.5)	5 300
U - Max	10.1 (9.7/10.4)*	40.5 (22.0/62.7)*	n/a	-0.8 (-1.0/ -0.6)*	53
U+H - Max	10.1 (9.7/10.5)*	42.2 (22.7/62.4)*	14.6 (9.1/22.8)*	-0.8 (-1.2/-0.6)*	5 300
U+V - Max	10.3 (9.9/10.7)	38.2 (16.4/62.5)	11.7 (6.6/29.4)*	-9.1 (-13.5/ -5.5)	5 300

B) Minimum Pelagic Larval Duration

Model runs	Duration (day)	Distance (km)	Mean squared displacement (km²)	Depth (m)	Number of particles
U+HV - Min	3.9 (3.8/ 4.0)	10.9 (6.4/21.2)	5.0 (3.4/7.5)	-6.0 (-9.2/-4.4)	5 300
U - Min	3.9 (3.8/ 4.0)	13.5 (6.9/21.4)*	n/a	-0.8 (-1.0/-0.7)*	53
U+H - Min	3.9 (3.8/ 4.0)*	14.0 (7.0/22.0)*	3.3 (2.5/5.0)*	-0.8 (-0.8/-0.7)*	5 300
U+V - Min	3.9 (3.8/ 4.0)	10.4 (6.2/20.7)	1.8 (0.8/3.8)*	-5.9 (-10.9/-4.5)	5 300

In the horizontal dimension, both the predicted spawning sites of backtracked particles (Figure 44) and the location of intense sampling effort (Figure 42) were concentrated in the submarine canyon areas (polygons 3 and 4 in Figure 42). Model runs suggest that other spawning sites were located on the northern part of the Valencia Gulf (40-41º N) and the middle of Eivissa Channel (39.5º N, Figure 44). The spread of backtracked particles were characterized predominantly by two patterns. One was a stretched ellipsoid found, for example, in the northernmost part of the studied area, especially in simulations with maximum PPD. The other pattern had a rounded shape with limited particle spread found, for example, in the fishing ground areas and the margin of the Valencia Gulf.

In the base model runs, the particles passively drifted close to the surface during the larval stages with a median depth of 6 m and 9 m below the surface when PPD was

minimum and maximum, respectively (Table 6). The deeper median depth in the runs with maximum PPD was likely a result of particles being vertically mixed longer than particles in the minimum PPD model run. Once retrogressing into the egg stage, the particles migrated downward for a median of 2.6 and 2.3 days before the end of backtracking and traversed a median depth of 191 m and 247 m in the PPD-maximum and PPD-minimum model runs, respectively. Although the egg stage duration was similar between model runs, the larval stage duration differed, with a median of 7.9 and 1.6 days for the PPD-maximum and PPD-minimum model runs, respectively, indicating that larvae with maximum PPD were subjected to the highly dynamic circulation of the surface layer during most of their pelagic duration.

2.5.3.2. Uncertainty studies

Three types of uncertainty studies, focused on advection, diffusion, and PPD, were undertaken to better understand the sources and relative magnitude of uncertainty in the base run model predictions. While the base model runs were used to estimate the location of the spawning sites of collected larvae, the model runs for the uncertainty analysis were used to quantify the possible effects of model parameterizations on the spawning site estimates.

Advection

The uncertainty introduced by differences between modeled and observed current velocities was assessed by comparing model predictions with OOCS measurements (Figure 45). Overall, the displacement induced by current velocities estimated by ROMS were generally compatible with the estimated displacement of ADCP velocities provided by the OOCS buoy (see Figure 45), with all trajectories moving toward the Northwest at all depths. At 7 m depth, trajectories estimated by the ADCP velocities from the OOCS buoy and by the current velocities from ROMS covered 60 km and 69 km, respectively. However, the last coordinates of those trajectories were 8 km apart and this difference increased to 23 km and 33 km in trajectories estimated at 14 m and 21 m depth, respectively. This discrepancy arose from the fact that predicted current velocities were weaker at depth than those measured at the OOCS buoy. Because simulated larvae in the base model runs had a median depth of 9 m or less, model predictions of spawning site

locations could have differed by 8 to 23 km from actual spawning locations in the area of the OOCS buoy due to uncertainty in predicted advection.

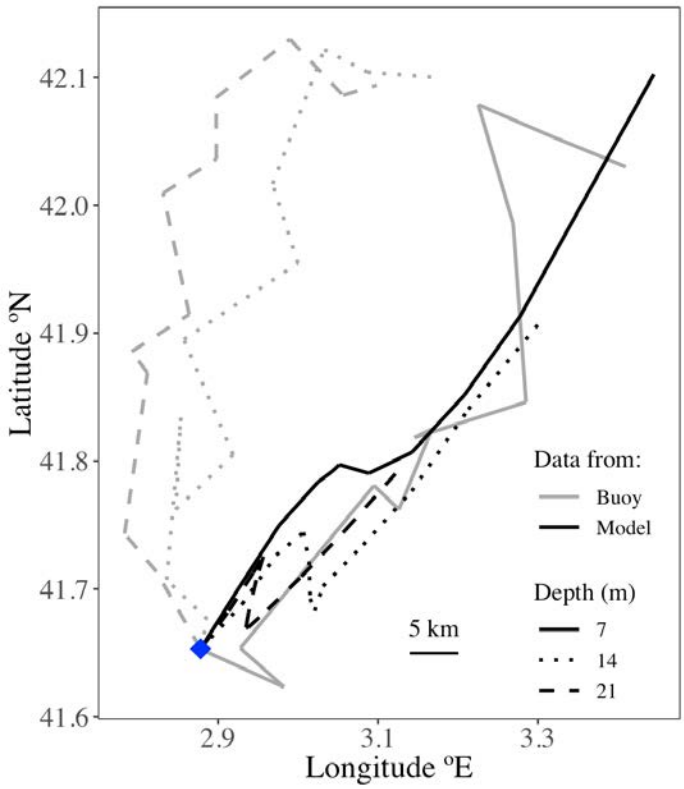

Figure 45. Estimate of backward trajectories from velocities recorded by the Operational Observatory of Catalan Sea's buoy (grey lines) and estimated by the ROMS model (black line) at the buoy position (blue diamond). Velocity profiles at 7 m (—), 14 m (···) and 21 m (- -) depths were used to compare modeled and observed velocities.

It is important to note that this uncertainty analysis was restricted to one location that had relatively low current velocities compared to the rest of the study area because current velocity observations in other places were not available. In fact, plankton sampling stations were located in areas with various current amplitudes and directions (see Figure 43). Over July 18 to August 28, the estimated current had strong southeastern velocities (around ~0.3 m s^{-1}) from around 41º N to 43º N. Below 41º N, strong northeastern currents also were predicted in the semi-enclosed basin between the continent and Balearic Archipelago (see Figure 42). One jet was parallel to the shoreline (0.40 m s^{-1}) between 40º N and 41.3º N and another (~0.30 m s^{-1}) crossed the Eivissa channel. In comparison with those jets, the currents estimated at the OOCS buoy location were low (< 0.1 m s^{-1}) .

Diffusion

The uncertainty introduced by the parameterization of mixing in the horizontal and vertical dimensions was assessed using ocean diffusion diagrams constructed by releasing passive particles from five of the CONECTA sampling stations. These stations were located in different hydrodynamic regimes (see Figure 43). The northernmost three stations were located in the Northern Current where there were high coefficients of vertical diffusivity and strong surface current velocities. The two southernmost stations were in waters with low current velocity and low diffusivities. Hence the five stations together encompassed a range of hydrodynamic conditions which were observed in the NW Mediterranean Sea during the time period of backtracking (Figure 43). During this time, the upper 20 m depth of the NW Mediterranean Sea had turbulent flows with spatial and temporal variations in the vertical diffusivities (Figure 43). Near the Palamós and Blanes canyons, the coefficient of vertical diffusivity was higher than 0.01 m^2 s^{-1} in the upper 20 m water layer whereas the diffusivity tended to be lower than 0.01 m^2 s^{-1} at other stations.

The comparison of the backtracked particle spreads with Okubo's (1971) relationship indicates that the parameterization of mixing influenced model predictions (Figure 46). Model runs without turbulent particle motion had orders of magnitude lower particle spreading than those predicted by Okubo's ocean mixing diagram (Okubo 1971) and were orders of magnitude lower than simulations that included turbulent particle motion (compare the advection-only scenarios (U-Okubo) with all other scenarios and Okubo's predictive relationship in Figure 46). For the scenarios that included turbulent particle motion, the base-case parameterization with both vertical and horizontal turbulence (U+HV-Okubo) had the best correspondence with Okubo's relationship. In this model run, the power-law relationship fit to model data had an exponent of 2.27, which was close to the exponent in Okubo's equation ($q = 2.34$). In the other model runs, the exponent was either too low (i.e., $q = 1.06$ in U-Okubo and $q = 2.05$ in U+H-Okubo) or too high (i.e., $q = 2.68$ in U+V-Okubo). Hence, parameterizations with both horizontal and vertical turbulent particle motion best reflected diffusion in the ocean, and were appropriated implemented in the base-model runs.

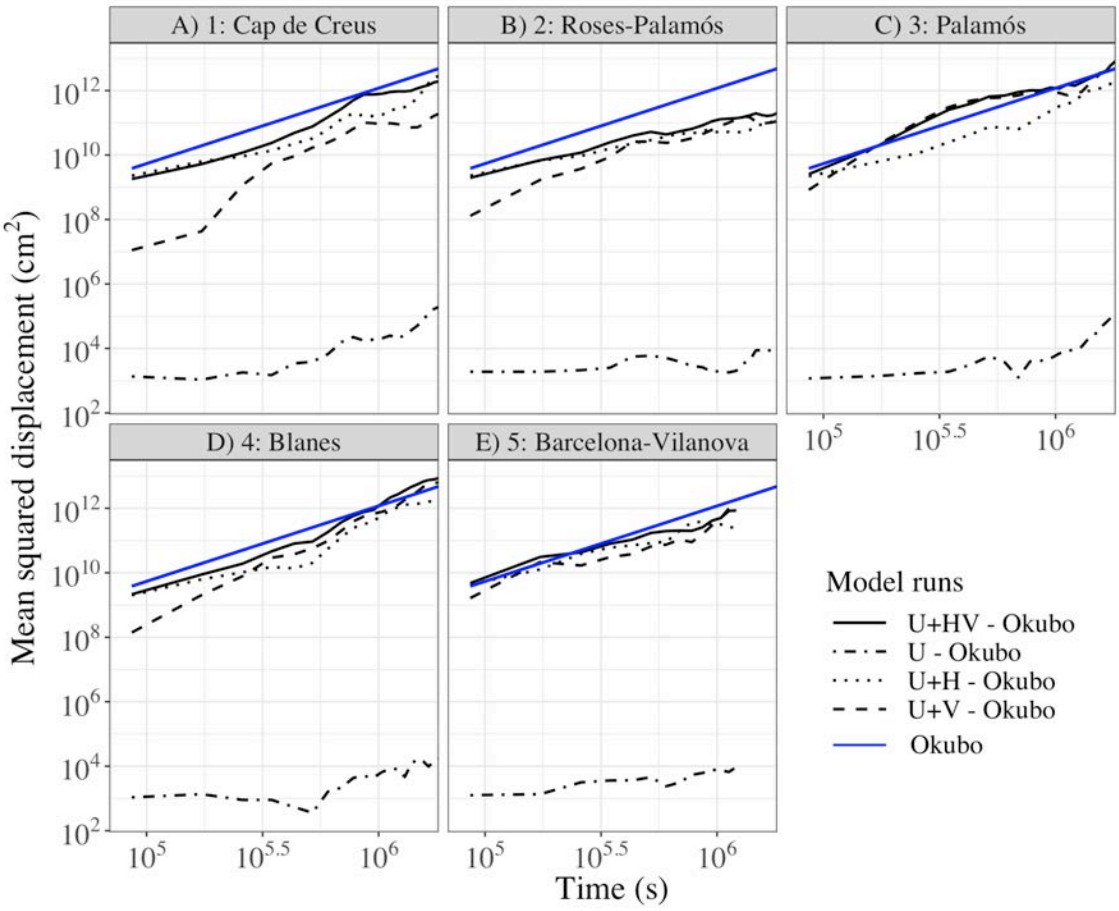

Figure 46. Diffusion diagram based on backward simulations of 100 passive drifts from 5 stations near one of the five fishery grounds of *A. antennatus* in the northwestern Mediterranean Sea (panels A – E; see Figure 42 and Table 5). Particles were released from a 1 m² area centered at the station location and tracked backwards in time. Okubo's equation for estimating mixing in the ocean, $\sigma = 0.0108 \cdot t^{2.34}$, is represented by the blue line, where σ (cm²) is variance in the spread of patches of dye released in the ocean and t (s) is time (Okubo 1971). For this plot, variance was calculated as the mean squared displacement (cm²) of particles from their centroid location. Axis are scaled with the logarithmic function as in Okubo (1971).

In plankton model simulations (Table 5.A), parameterization of vertical mixing influenced the particles dispersal. Without vertical mixing, larval transport was shallower, median of 0.8 m depth, and larvae were backtracked a median of 2 to 4 km further than those with vertical mixing (Table 6). With vertical mixing, particles drifted deeper (median of 6 to 9 m, Table 6) into depths where current velocities decreased with depth (Figure 45), resulting in slightly shorter distances travelled than simulations without vertical mixing (Table 6). The presence or absence of vertical mixing also influenced the area (km2) of the spawning sites, which was measured by the horizontal spread (mean squared displacement) of the backtracked larvae at the end of the base models runs (Table 6). The estimated area of the spawning sites was larger in the model runs with vertical and horizontal turbulence (5 km² and 26 km² in U+HV-Min and U+HV-Max) compared to those with vertical turbulence (1.8 km² and 11.7 km²; Table 6).

PPDs

The use of a short and long PPD in the base model runs U+H,V-Min and U+HV-Max, respectively, resulted in major differences in the distribution of predicted spawning sites across the continental shelf and slope. In U+HV-Min, 50.7% of particles drifted back over bathymetric depths where adults have been captured (200–1000 m) while only 40.6% of simulated individuals were backtracked to those depths in the base model run U+HV-Max (see Figure 43). Overall, minimum PPD resulted in predicted spawning site of fewer particles (26.4%) on the continental shelf (depths < 200 m) in U+HV-Min than in U+HV-Max (44.1%). This difference was likely explained by the six-day shorter duration of the larval transport simulation in U+HV-Min (median 4 days) run compared to the median duration of 10-days in the U+HV-Max run (Table 6). Additionally, this difference in distribution of spawning sites likely caused the difference in median depth of particles between the runs with different PPD (Table 6).

The influence of PPDs and diffusion parameterizations varied across the model domain, with greater divergence in spawning site locations north of Blanes and south of the Eivissa Channel where strong currents were located (Figure 47). For example, the spawning sites in U+HV-Max could be up to 36 km apart from the ones in U-Max in the canyon areas (latitudes between 41.2 – 42º N), likely due to the hydrodynamic differences in subregions of the northwestern Mediterranean Sea (see Figure 44). These differences in hydrodynamics interacted with PPD to influence the divergence between model predictions: the median distances between predicted spawning locations of model runs U and U+HV was 3.2 km and 8.6 km when drift durations were minimum or maximum, respectively, and larger differences occurred in regions with strong currents (e.g., north of the canyons area and south of Eivissa Channel in Figure 47).

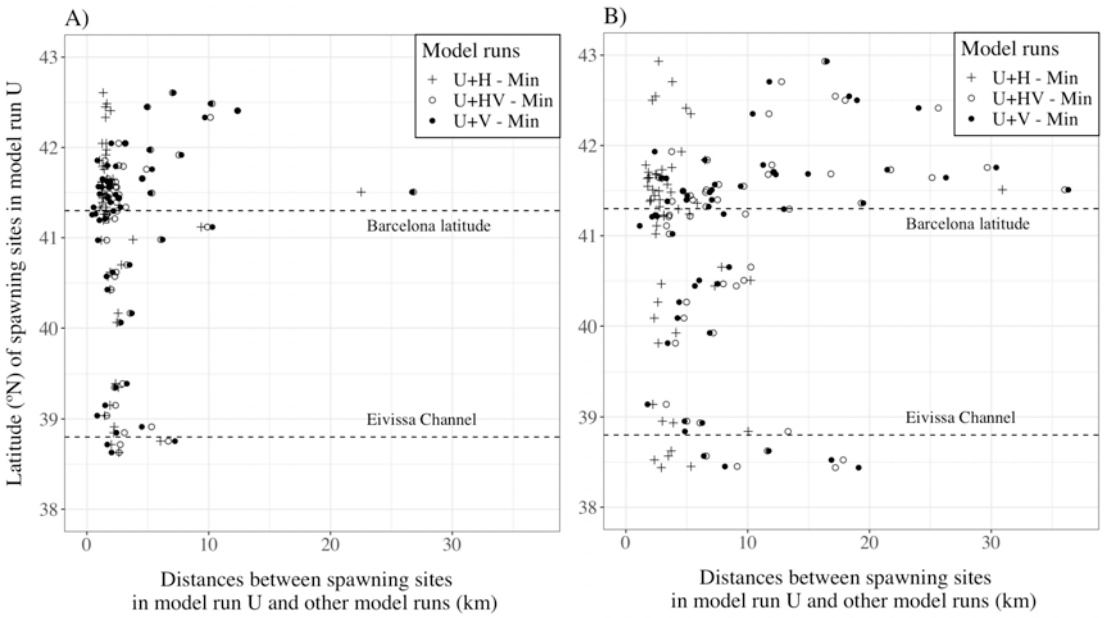

Figure 47. Distance (km) between estimated spawning sites from the advection-only model run (U) and model runs with different diffusion parameterizations in simulations with maximum Pelagic Larval Durations (A) and minimum Pelagic Larval Durations (B), plotted versus the mean latitude of the estimated spawning location in the advection-only model run (U). The different diffusion parameterizations were: advection plus horizontal turbulence (U+H), advection plus vertical turbulence (U+V), and advection plus horizontal and vertical turbulence (U+HV).

The PPD had a strong influence on the area of spawning grounds in base model runs (Table 6) and on the location of the predicted spawning grounds from the five base model stations which corresponded to those used in the Okubo analysis (Figure 48). The area of the estimated spawning sites was 4.4 to 6.5 times smaller for model runs with minimum drift durations compared to those with maximum drift durations (see Table 6). This difference in area can be seen clearly in plots of spawning locations (Figure 48) in which ending particle distributions had median areas of 3.3 and 48.0 km^2 with minimum and maximum PPDs, respectively. In addition, the final location of spawning areas differed between minimum and maximum PPDs in two of the five simulations (see Figures 48B and 48E). Also, PPD influenced the amount of overlap between model runs with different turbulence parameterizations. With minimum PPD, predicted spawning sites overlapped by more than 97% in model runs with vertical turbulence (see U+HV and U+V in Figure 48). In contrast, the overlapping rates were lower (from 17% to 94%) when spawning sites were estimated from model runs with maximum PPD (see U+HV-Max and U+V-Max in Figure 48), most likely because any divergence in trajectories between model runs were more pronounced when model runs had longer durations.

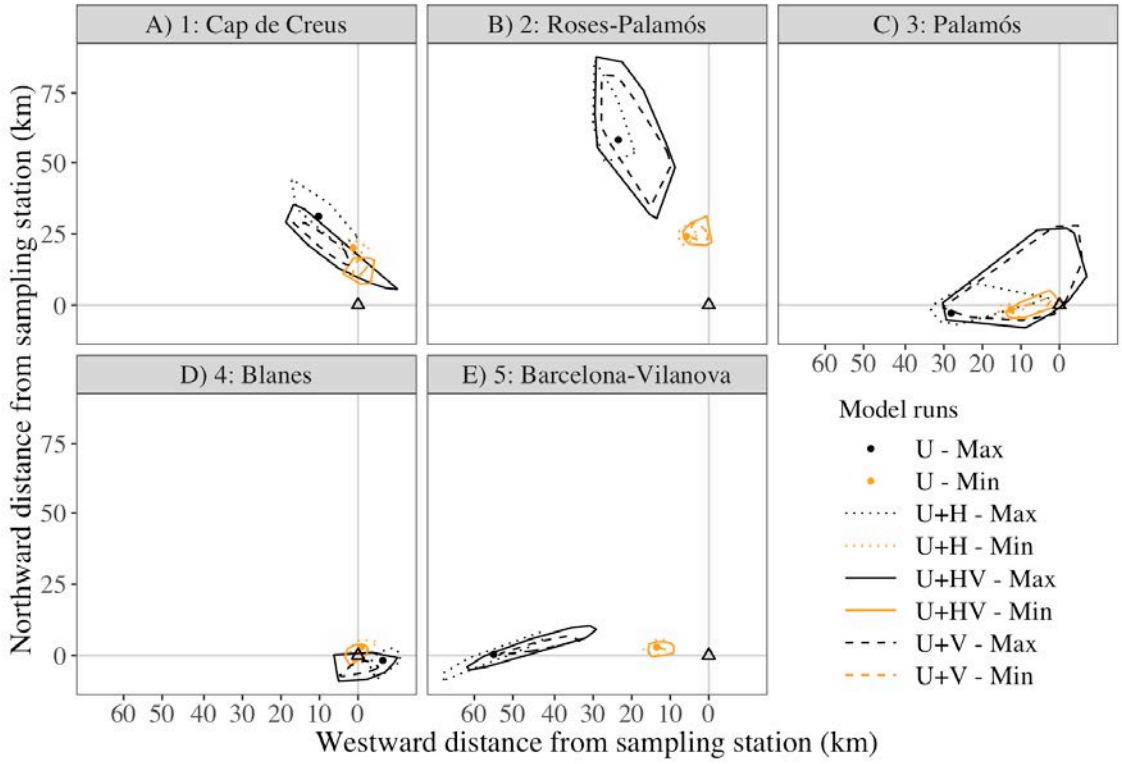

Figure 48. Estimated spawning areas of individuals after backward simulations from a sampling station (open triangles) near each fishery ground (panels A – E; see Figure 42). Results are presented for model runs with different physical parameters (U = advection only, U+H = advection plus horizontal turbulence, U+V = advection plus vertical turbulence, and U+HV = advection plus horizontal and vertical turbulence) and different Pelagic Larval Durations: Minimum (Min, orange) and Maximum (Max, black) (see Table 5). Station coordinates are in Table S7. Light grey lines indicate the X- and Y-axes with the starting location for backtracking (open triangles) at the origin (0,0).

In summary, the uncertainty analysis indicated that divergences in estimates of spawning site locations could be as much as 8 – 23 km due to differences in observed versus modeled advection, 0.1 – 21 km due to differences in turbulence parameterizations (comparing centroid locations within each PPD and site in Figure 48), and 7 – 43 km due to uncertainties in PPD (comparing of distances between spawning sites estimated in model runs U-Min and U-Max in Figure 48). Importantly, the uncertainty analysis on turbulence underscored the importance of using both horizontal and vertical mixing schemes (i.e., model runs U+HV) to simulate mixing in the ocean.

2.5.3.3. Estimates of larval supply from the fishing grounds

Base model runs (U+HV-Min and U+HV-Max) showed that protozoea released from sampling stations were backtracked in different directions depending upon the location of the release. Protozoea released from sampling stations overlaying the fishing grounds in

the submarine canyons (Palamós and Blanes, zones 3 and 4 in Figure 49) were backtracked in high proportions to those same fishing grounds (76.5 – 78% in zone 3 and 55.5 – 100% in zone 4). For the southernmost fishing ground (zone 5 in Figure 49), protozoea were backtracked from sampling stations within the fishing ground or east of the fishing ground (i.e., the protozoea moved westward as they retrograded). For the northernmost fishing grounds (zones 1 and 2), protozoea that were backtracked to those fishing grounds tended to be released south of the fishing grounds (i.e., protozoea moved northward as they retrograded). For example, 44.5% to 68.5% of larvae collected in stations above the Roses-Palamós fishing ground (zone 2 in Figure 49) were backtracked to the Cap de Creus fishing ground (zone 1).

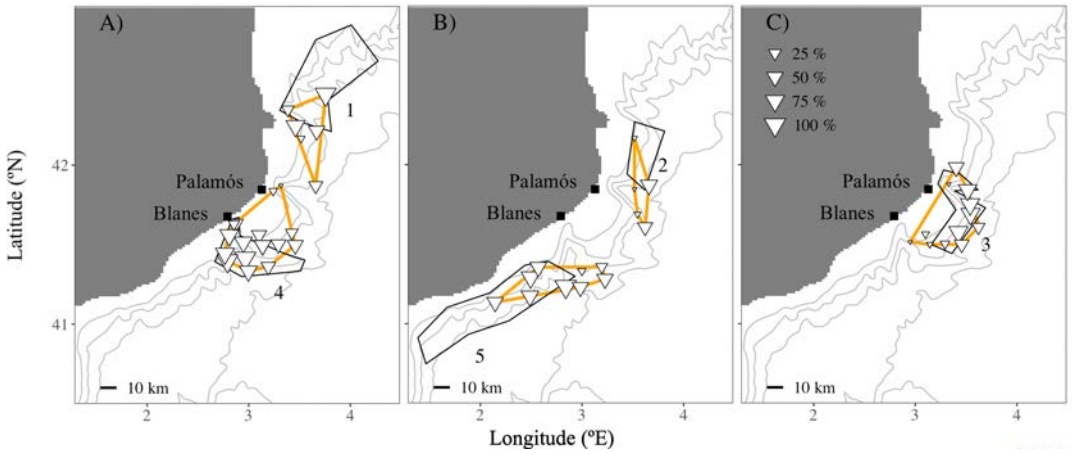

Figure 49. Sampling stations (open triangles) within sampling areas (orange polygons) from which larvae were backtracked to spawning locations that were within the fishing grounds (black polygons): Cap de Creus (polygon 1) and Blanes (polygon 4) fishing grounds (A), Rose and Palamós (polygon 2) and Barcelona to Vilanova (polygon 5) fishing grounds (B), and Palamós fishing ground (polygon 3) (C). The size of the triangle represents the averaged percent of larvae backtracked to the fishing ground from that sampling station (key in panel C). Results are pooled from the model runs with minimum and maximum Pelagic Larval Durations and advection and horizontal and vertical turbulence (U+HV-Min and U+HV-Max). The grey lines are the isobaths at 200 m, 500 m, and 1000 m.

Additionally, base model runs (U+HV-Min and U+HV-Max) indicated that multiple fishing grounds could have supplied larvae caught at one sampling station. In this region of intense shrimp fishery activity, 15 of the 27 sampling stations were supplied by two fishing grounds and two-thirds of the stations (i.e., 10 of the 15) were above or near the canyon zones (Figure 50). For example, near the Palamós canyon, the fishing grounds of Palamós-Roses and Palamós supplied 40.5% and 27.5% of larvae caught at the sampling station where the highest number of larvae (1 200 individuals, Station 19 in Table S7) were collected during the cruise.

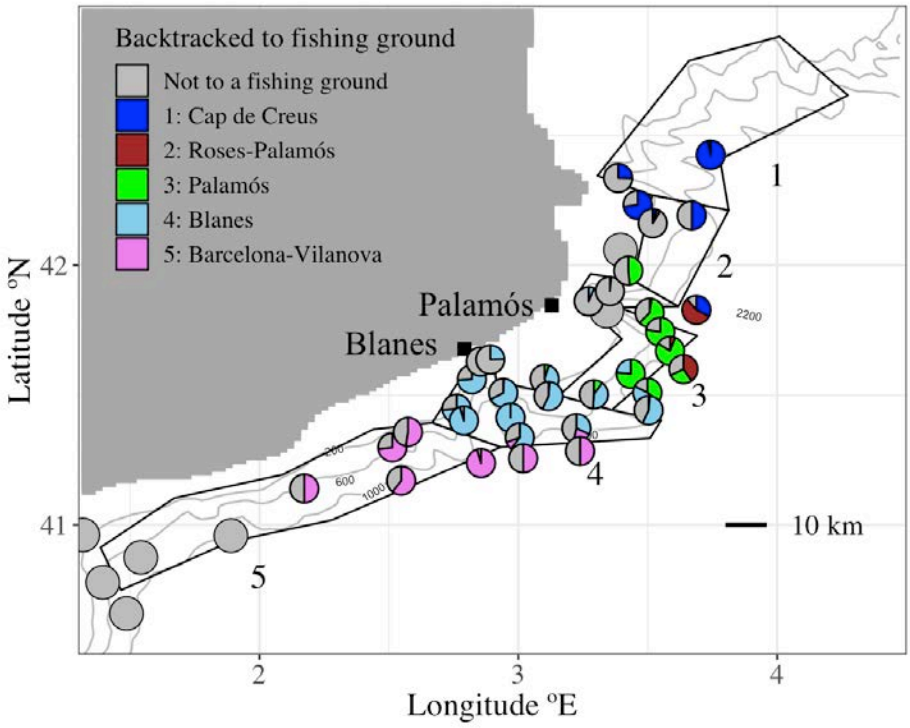

Figure 50. Proportion of protozoea backtracked from each sampling station to specific fishing grounds. Each circle represents a station where protozoea were captured and the colors within the circle correspond to the proportion of larvae backtracked to the fishing grounds: Cap de Creus (blue), Roses-Palamós (brown), Palamós (green), Blanes (light blue) and Barcelona-Vilanova (pink). The grey lines are the isobaths at 200 m, 500 m, and 1000 m.

2.5.4. Discussion

For the first time, spawning sites of the deep-sea shrimp *Aristeus antennatus* in the northwestern Mediterranean Sea were estimated by numerical backtracking of larvae. Model results suggest that larvae collected during the CONECTA cruise came from spawning sites approximately 40 km away (median, Table 6.A). The reliability of the backtracking results was examined by assessing the potential sources of errors due to predictions of advection and the parameterization of turbulence and PPD, which indicated that both horizontal and vertical turbulence parameterizations (U+HV) were necessary to correctly simulate mixing, and that PPD had the largest uncertainty (up to 43 km) of the factors examined. Consequently, the base model runs used both horizontal and vertical turbulence parameterizations (U+HV) and included both minimum and maximum PPD to account for this uncertainty. Hence, the estimates of larval supply from the fishing grounds presented herein did account for major sources of uncertainty within

the larval transport model, although it is important to acknowledge that divergences between observed and predicted current velocities were not included in estimates. The unaccounted uncertainty in hydrodynamic model predictions at one location was estimated to be on the order of 8 – 23 km, which were relatively small distances within the 853 to 3 004 km^2 fishing grounds.

Simplifications that were made in the model parameterizations should be noted. First and foremost, larvae were assumed to be passive particles. Because Penaeid larvae and post-larvae are motile and can display complicated behaviors (e.g., Forbes and Benfield 1986, Chu et al. 1996, Ogburn et al. 2013), and because the behavior of *A. antennatus* larvae is not known, model results should be viewed as the first of multiple steps needed to advance knowledge of the dispersal of this species. A second simplification was the fact that egg stage was prescribed a fixed buoyancy and duration based on a substantial literature review of other similar species. To improve confidence in model predictions, new information on the life history and behavior of *A. antennatus* is needed.

2.5.4.1. Backtracking implication for the fishery management

With acknowledgement of the uncertainty and assumptions of the model, model results do provide useful new information about *A. antennatus*, with implications for the fishery. Model predictions indicate that connectivity of larvae between fishing grounds is likely, given that a portion of the larvae that were released from every CONECTA sampling stations within the fishing grounds were backtracked to areas outside of the fishing ground over which the larvae were captured (Figure 50). In addition, in 15 of 27 stations over fishing grounds, at least one larvae was backtracked to a neighboring fishing ground (Table S7). The existence of connectivity between neighboring spawning sites is supported by observed genetic analyses (M. Roldán, pers. comm.) and by estimates of forward larval trajectories (Clavel-Henry et al., 2019, 2020).

Model results suggest that backtracking simulations could provide useful analyses to support the management of marine protected and exploited areas in a similar manner as forward larval transport studies (e.g., Basterretxea et al., 2012; Mariani et al., 2010). In

the case of *A. antennatus*' fishery, a local management plan indirectly improved the quality of the catches over the Palamós fishing ground (e.g., increase of the mean carapace length; Gorelli et al., 2017). If this exploited population is connected with others, as suggested by these model results, the local management plan may benefit the quality of catches if spatially extended to other fishing grounds. In addition, future backtracking simulations could be run to identify set other spawning areas if all pelagic larval stages (i.e., eggs, nauplius, protozoea, mysis, and early pelagic juveniles) were included. Another beneficial use of backtracking larvae transport models would be to account for the hydrodynamic variability in the region where fisheries management plan are set to understand how circulation and mixing patterns could influence larval transport in relation to the size of the protected area.

2.5.4.2. Oceanographic and biological influences on uncertainty

Hydrodynamics in the NW Mediterranean Sea influenced prediction of spawning site locations. In the horizontal dimension, two nearby sampling stations could be supplied by different spawning sites due to the changes in the surface current intensity and direction, which varied over depth and could advect larvae to different places depending on their depth position (Clavel-Henry et al., 2020). In the vertical dimension, vertical mixing was the main reason (except for the buoyancy at egg stages) that larvae were displaced in vertically. It repositioned larvae within the 0 – 15 m depth layer, the main mixing layer of the NW Mediterranean Sea in summer (D'Ortenzio et al., 2005).

Vertical mixing varied in space, likely related to atmospheric conditions (Moum and Smyth, 2001) and submarine canyons and channels (Flexas et al., 2008; Pinot et al., 2002; Rojas et al., 1995) where complex turbulent dynamics are generated. Model results also suggest that dispersal, and the role of turbulence, varied between waters with different amounts of vertical mixing (Figure 47). Hence, spawning sites of larvae transported in waters with low vertical mixing may be defined with more accuracy (Serra et al., 2003) than those in high-mixing areas. Thus, effort in to understand and simulate dispersion would improve backtracking models and predictions of connectivity.

Beyond the vertical turbulence and hydrodynamic variability, larval pelagic duration was the source of the most uncertainty in predictions of spawning sites locations. Drift duration is an important factor in the larval transport of deep-sea species (Hilário et al., 2015). In our study, backtracking of larvae with different PPD resulted in two distinct spawning sites in some cases, depending on whether the drift duration was short or long. Because estimated spawning sites of some larvae with long PPD were located over the continental shelf, which is out of the spawners depth range (Sardà et al., 1997; Company et al., 2003; Tudela et al., 2003), it is likely that either the larvae were younger than assumed or exhibit a behavior that was not included in the model.

In summary, numerical backtracking of larvae was used to provide the first estimates of the spawning sites of *Aristeus antennatus* larvae collected in surface waters of the northwestern Mediterranean Sea. Model results indicated that larvae collected at a single sampling site could have come from multiple spawning locations, and that many of the simulated larvae could have come from spawning sites within ~ 40 km. Having knowledge of larval origins is useful for determining connectivity between fishing grounds. Hence, this study provides new information which could support decision-making regarding fishery management plans in some areas. To better support management, future studies could include a wider temporal range in hydrodynamic conditions to fully resolve patterns in connectivity.

2.5.6. Supplementary information

Table S7. Coordinates of the sampling stations and estimated percentage (%) of protozoa larvae that were backtracked to specific fishing ground which are depicted in Figure 42. Sampling stations with the ID (identification number) 10, 16, 25, 42, and 48 were selected for the Okubo backtracking scenarios (see Figure 46) because of their high estimated percentage in the fishing ground (bold font) and are marked by a grey grid cell. The * indicates the sampling station over a fishing ground.

ID	Coordinates	Date (m/d)	Hour	Cap de Creus	Roses - Palamós	Palamós	Blanes	Barcelona - Vilanova	Not to fishing grounds
1	1.35483ºE; 40.19367ºN	8/10	10 pm	0	0	0	0	0	100
2	1.4685ºE; 40.34917ºN	8/12	3 am	0	0	0	0	0	100
3	1.3945ºE; 40.77767ºN	8/15	2 am	0	0	0	0	0	100
4*	1.8895ºE; 40.958ºN	8/15	11 pm	0	0	0	0	0	100
5*	2.173ºE; 41.1395ºN	8/16	5 am	0	0	0	0	50	50
6*	2.51333ºE; 41.298ºN	8/16	8 pm	0	0	0	0	73	27
7*	2.54733ºE; 41.17017ºN	8/16	10 pm	0	0	0	0	60.5	39.5
8*	2.5735ºE; 41.3575ºN	8/17	5 am	0	0	0	0	52.5	47.5
9*	2.7615ºE; 41.44733ºN	8/17	9 am	0	0	0	73.5	0	26.5
10*	**2.85567ºE; 41.2375ºN**	**8/17**	**7 pm**	0	0	0	0	**95.5**	**4.5**
11	3.01867ºE; 41.25567ºN	8/18	2 am	0	0	0	0	50	50
12	3.23833ºE; 41.28383ºN	8/19	5 am	0	0	0	0	50	50
13*	3.22417ºE; 41.372ºN	8/19	12 am	0	0	0	32	21.5	46.5
14*	3.29183ºE; 41.50217ºN	8/20	3 am	0	0	10	41	0	49
15*	2.94167ºE; 41.508ºN	8/20	8 am	0	0	1	66.5	0	32.5
16*	**2.9698333ºE; 41.41267ºN**	**8/19**	**7 pm**	0	0	0	**100**	0	0
17	3.10133ºE; 41.562ºN	8/23	9 am	0	0	5	41	0	54
18*	3.4341667ºE; 41.58200ºN	8/23	8 pm	0	0	76.5	23.5	0	0
19	3.6378333ºE; 41.59967ºN	8/24	7 am	0	40.5	27.5	0	0	32
20*	3.3415ºE; 41.82317ºN	8/24	7 pm	0	0	0	0	0	100
21*	3.27167ºE; 41.861ºN	8/25	10 am	0	0	0	6.5	0	93.5
22*	3.35383ºE; 41.9002ºN	8/25	12 am	0	0	1	0.5	0	98.5
23*	3.3855ºE; 42.33617ºN	8/27	9 am	25.5	0	0	0	0	74.5
24	3.66967ºE; 42.19167ºN	8/28	8 am	50	0	0	0	0	50
25*	**3.68783ºE; 41.828ºN**	**8/28**	**9 pm**	32.5	**56**	0	0	0	11.5
26	0.71583ºE; 38.95933ºN	8/4	0 am	0	0	0	0	0	100
27	0.83583ºE; 39.12717ºN	8/5	6 pm	0	0	0	0	0	100
28	0.48117ºE; 39.0395ºN	8/7	6 am	0	0	0	0	0	100
29	0.5355ºE; 39.25633ºN	8/7	1 am	0	0	0	0	0	100
30	0.62733ºE; 39.47283ºN	8/8	1 am	0	0	0	0	0	100
31	0.7535ºE; 39.56217ºN	8/9	7 am	0	0	0	0	0	100
32	1.48617ºE; 40.65783ºN	8/14	6 am	0	0	0	0	0	100
33*	1.5415ºE; 40.874ºN	8/14	1 am	0	0	0	0	0	100
34	1.31733ºE; 40.96067ºN	8/15	7 am	0	0	0	0	0	100
35*	2.78967ºE; 41.40117ºN	8/17	10 am	0	0	0	95.5	0	4.5
36*	3.0055ºE; 41.33667ºN	8/18	9 am	0	0	0	60.5	9	30.5
37	3.50317ºE; 41.44117ºN	8/18	0 am	0	0	1.5	55.5	0	43
38*	3.1165ºE; 41.49567ºN	8/19	0 am	0	0	1.5	55.5	0	43
39*	2.82033ºE; 41.5606ºN	8/22	1 am	0	0	0	74	0	26
40*	2.89167ºE; 41.63667ºN	8/23	5 am	0	0	0	24.5	0	75.5
41	3.49867ºE; 41.50933ºN	8/23	1 am	0	0	36	46.5	0	17.5
42*	**3.58617ºE; 41.66967ºN**	**8/25**	1 am	0	6	**78**	0	0	16
43*	3.5483333ºE; 41.74333ºN	8/26	8 am	0	0	77.5	0	0	22.5
44	3.507ºE; 41.817ºN	8/26	1 pm	0	2.5	60	0	0	37.5
45	3.42483ºE; 41.97883ºN	8/26	11 pm	0	0	48.5	0	0	51.5
46	3.39483ºE; 42.05917ºN	8/26	1 am	0	0	0	0	0	100
47	3.46093ºE; 42.23267ºN	8/27	6 am	73	0	0	0	0	27
48*	**3.743ºE; 42.42533ºN**	**8/27**	**10 pm**	**97**	0	0	0	0	3
49	0.90083ºE; 38.65583ºN	8/3	9 pm	0	0	0	0	0	100
50	0.55017ºE; 38.95117ºN	8/4	7 pm	0	0	0	0	0	100
51	0.90917ºE; 38.98433ºN	8/5	6 am	0	0	0	0	0	100
52*	2.85467ºE; 41.629ºN	8/23	3 am	0	0	0	17	0	83
53*	3.51907ºE; 42.16177ºN	8/27	4 am	4.5	4.5	0	0	0	91

Table S8. Results of Wilcoxon statistical tests for differences between model runs in the plankton backtracking scenarios (see Table 5) with A) minimum Pelagic Larval Duration and B) maximum Pelagic Larval Duration. Differences in the median drift distances (km), particle depths (m), pelagic larval durations (day), and mean squared displacement (km^2) were tested. U = advection only, U+H = advection plus horizontal turbulence, U+V = advection plus vertical turbulence, and U+HV = advection plus horizontal and vertical turbulence. "n/a" stands for non available. The *** indicates a *p*-value < 0.001.

A)

	U+HV	U	U+H	U+V
	Drift distance (km)			
U+HV		0.57	***	0.25
U			0.66	0.46
U+H				***
U+V				
	Pelagic Larval Duration (day)			
U+HV		0.59	***	0.91
U			0.99	0.58
U+H				***
U+V				
	Depth (m)			
U+HV		***	***	0.90
U			0.40	***
U+H				***
U+V				
	Mean squared displacement (km^2)			
U+HV		n/a	***	***
U			n/a	n/a
U+H				***
U+V				

B)

	U+HV	U	U+H	U+V
	Drift distance (km)			
U+HV		0.5	***	0.82
U			0.86	0.53
U+H				***
U+V				
	Pelagic Larval Duration (day)			
U+HV		0.01	***	0.89
U			0.91	0.01
U+H				***
U+V				
	Depth (m)			
U+HV		***	***	0.72
U			0.08	***
U+H				***
U+V				
	Mean squared displacement (km^2)			
U+HV		n/a	***	***
U			n/a	n/a
U+H				0.50
U+V				

Section 2.6. Main results

Section 2.1

Bottom drift of passive particles

Bottom drifts of particles followed a southwest direction along the continental slope and the shrimp Pelagic Larval Duration lasted 31 days at 13 ºC. Within the hydrodynamic model called ROMS-Rutgers, the modeled particles dispersed 27 km on average and were mostly retained in the release zones (77-96% in 4 of the 7 release zones; Figure 14.A). Within the hydrodynamic model called ROMS-Agrif, the modeled particles dispersed 70.8 km on average and were mostly advected towards southern neighbored zones (low retention rates: 1-43%; Figure 14.B).

Dispersal variability from submarine canyons

In ROMS-Rutgers, particle dispersal from canyons featured significant changes in comparison with dispersal from open slope zones. These changes included: the connectivity between canyons (27% between Cap de Creus and Palamós canyons, 0% between Palamós and Blanes canyons; Figure 14.A), the vertical displacement of particles according to the release depth (e.g., 13.5% of particles from 600/700 m set up at depths <800 m but only 1% of particles from the open slope; Figure 15.A–B), the canyon (e.g., 44 m and 133 m up in Cap de Creus and Palamós canyons, respectively; Figure 16.B), and its walls (e.g., 62 m down and 36 m up in northern and southern walls of the Blanes canyon, respectively; Figure 16.C). Therefore, various contiguous submarine canyon impacts should be processed on a case-by-case basis and compared to better understand the dispersal variability. In ROMS-Agrif, the dispersal variability from the canyon was not as different as the dispersal from the open slope. However, dispersal rates between canyons were higher (45% between Cap de Creus and Palamós canyons, 25% between Palamós and Blanes canyons; Figure 14.B).

Selection of the hydrodynamic model

ROMS-Rutgers, a hydrodynamic model with an adapted terrain-following vertical discretization and a good topography grid, has been selected over ROMS-Agrif that had a finer resolution (1.2 km vs 2 km). The use of ROMS-Rutgers reduced the drift

uncertainty of particles tracked close to the sea bottom and provided better estimations of the circulation within the submarine canyons (Figure 17). It used and run with a good bathymetric representation of submarine canyons and the resolution of the vertical layers (σ_b = 0.4 in ROMS-Rutgers vs σ_b = 0 in ROMS-Agrif) was also finer near the bottom.

Section 2.2

Three spawning regions of the NW Mediterranean Sea

Matrix of connectivity rates between zones and analyses of drifts characteristics clustered the NW Mediterranean Sea in three regions. In region 1, delimited by latitudes around 41.39 ºN – 42.74 ºN, larval drifts at surface lasted 20.1 – 20.3 days and individuals were transported 147.9 – 153.5 km on a southern direction (Table 2). Consequently, almost all particles were connected to a southern region (Figure 24). In region 2, delimited by latitudes around 38.86 ºN – 41.39 ºN, larval drifts were 17.2 – 17.6 days and individuals were transported 54 – 80.1 km (Table 2), most of the time advected by eddies. In region 3, delimited by latitudes around and below 38.86º N, larval drifts were 15.7 – 16.3 days and individuals were transported 57.7 – 174.5 km (Table 2) either crossing the Eivissa Channel if they were no eddies to recirculate the individuals (Figure 22).

Dispersal variability by late surfacing

With the late surfacing of individuals (i.e., including the nauplius as a buoyant phase), 81% of particles reached the surface (instead of 52% if only eggs were buoyant). The consequence of higher surfacing rates was reflected in the dispersal rates that were strengthened. For example, the retention rates of surface particles from region 2 were stronger (it rose by 10.2% to 43.6%; Figures 24.A and 24.C).

Dispersal variability by difference of drifting depth

Individuals that did not reach the surface layer (i.e., <5 m) were advected in colder water temperatures (15.7 – 18.4 ºC instead of 22.4 – 27 ºC), which implied longer drifts in space (20 km more) and time (11 days more) (Table 2). Vertical profile of the current changed such as new dispersal paths were modeled by individuals like 33.1 – 40% individuals released in region 2 within the 5 – 381 m depth layer reached the Balearic Archipelago zones or like 39.5% individuals released in region 3 that reached the southern part of the Majorca Island (see Figures 22 and 26).

Dispersal variability by early and late summer circulation

Differences in dispersal in early and late summer were introduced by the temporal variation of the current velocity fields and mesoscale patterns. The impact of the velocity field changes was estimated by the individuals, which drifted 5.4 to 96.4 km less in the late summer drift simulations (Table 2). The impact of the mesoscale patterns was indicated by the dispersal rates between different zones of the NW Mediterranean Sea. As for the most evident example, an eddy in the Eivissa Channel limited the individuals to cross it in early summer drift simulation. However, the absence of this eddy in the late summer drift simulation resulted in connectivity between zones at each side of the channel.

Section 2.3

Spatial estimations over the NW Mediterranean Sea bottom

Summer model-estimated catches were higher in the submarine canyons (> 40% of the maximum CPUE). These estimates were likely due to the bathymetric variations in these geomorphological structures (bathymetry and rugosity predictors; Figure S7) where the predictor values were 7.7 to 35.3 m higher and 242 to 486 m deeper than the open slope (rugosity = 59.2 m, bathymetry = 533 m, see Table 4).

Spatial estimations over the bathymetric gradient

The estimates of high catches were on a narrower range over the continental slope in the submarine canyons (510 – 565 m depth; Figure 31) than on the open slope (480 – 840 m depth; Figure 31). The bathymetric distribution of high catch rates was stable over the studied decade (2005 – 2014).

Evolution of the shrimp catch distribution in the submarine canyons

Model-estimated shrimp catches were bound to decrease with the deep-sea temperature rising by 1ºC as forecasted for the next decades. Nonetheless, the estimation of decrease was 20% in Palamós canyon while in Blanes and Cap de Creus canyons, the decrease is around 3% and 15%, respectively (Figure 34).

Section 2.4

Dispersal drifts limited by a density front

In the productive area of the submarine canyons, interannual variation of the drift distance and the time larvae kept within their release zone were correlated to the seawater density variations by 98% and 91%, respectively.

These correlations were also demonstrated by the drift characteristics variations over the latitudinal gradient (i.e., drift distance and residence time, Figures 37.A and 37.C). Besides, between latitudes 41.65º N and 41.9º N, value shifts were observed and linked to the North Balearic Front that is the interface between old and recent Modified Atlantic Water.

Larval retention related to the front characteristics

Over the zone affected by the NBF (i.e., zone 2 in Figure 35), 85.9% larvae were retained. Interannual simulations indicated that during some summers (e.g., 2010, 2012, and 2015), the retention rates significantly dropped or rose (Figure 38). These variations were correlated with the latitudinal position of the front by 71% and its strength by 58% (i.e., density gradient that characterized how stretched is the density front). Short analyses assumed that the presence of southern clockwise eddies could modify the front characteristics (Figure 41).

Section 2.5

Estimates of spawning areas by backtracking of collected protozoea

Spawning sites of larvae were estimated at close distance (10.9 – 37.6 km, Table 6) from sampling stations, over the continental margin (200 – 1000 m depth) for 40.6% of backtracked larvae if they had a long pelagic duration and for 50.7% if they had a short pelagic duration (Figure 44).

Uncertainty of the spawning sites because of the larval age

The backtracking of larvae with a short pelagic duration (i.e., backtracking implying the nauplius and egg stages) limited the larval dispersion in high hydrodynamics of the upper water layer (< 20 m depth). Larvae drifted 6 days less than the ones with long pelagic duration (i.e., protozoea, nauplius, and egg stages), which resulted in shorter drift distances (e.g., 10.9 km instead of 37.6 km; Table 6) and less larval diffusion (e.g., 5 km^2

instead of 26 km²; Table 6). This favored the hypothesis that collected protozoea were relatively young (i.e., around 4 days).

Uncertainty of the spawning sites because of mixing

Among different model runs implying water turbulence, the entrance of uncertainty was implied by the vertical turbulence. Larvae were backtracked 6 to 9 m deeper and 2 to 4 km less than larvae transported by advection only or by advection and horizontal turbulence (Table 6). Moreover, the spawning sites were localized a few kilometers away from the one estimated without effect from water turbulence. Yet, among model runs using the vertical mixing, the model run that had also horizontal mixing had the closest similitudes with sea measurement of dye-patches diffusion ($q = 2.27$ vs $q = 2.34$; Section 2.5 in paragraph 3.2.*Diffusion*).

Mixed origins of collected larvae

Collected larvae at sampling stations over submarine canyons were largely provided by the underneath fishing ground (76.5 – 78% in Palamós canyon zone and 55.5 – 100% in Blanes canyon zone, Figure 49). Collected larvae in these sampling stations were also provided by neighboring fishing grounds, which implied the mixing of larvae from different fishery grounds in the upper water layer.

CHAPTER 3

General discussion

All the previous chapters provided important outputs for approaching the connectivity of *A. antennatus* in the NW Mediterranean Sea. The following sections will firstly debrief about the methodology used in this Ph.D. thesis. Then, the results will be related to the main objectives of the thesis, namely the influence of the larval traits and the main connectivity path, and examine future lines of research that remain in the objectives' frame. Detailed discussions can be found in the previous chapters. Eventually, our findings will be contextualized with the management perspective that the scientific project CONECTA expects.

3.1. Evaluation of the larval transport modeling method

Analyzing the transport of larvae can be done directly by collecting samples in the sea and indirectly by modeling. In this thesis, the larval transport of *A. antennatus* was approached following general concepts from well-known larval cycles and assumptions aligned with the available information on the shrimp. Consequently, with pieces of knowledge about the spawner distribution and the support from hydrodynamics models, simulations of larval drift brought up relevant elements agreeing with parental genetics studies and recent findings of larvae. With chapters 1 to 5, the Lagrangian Tracking model was stepwise implemented by adding new sources of uncertainty and has set new assumption on the larvae traits. In the future, this stepwise approach can be helpful for larval dispersal modelization of *A. antennatus* in other regions (e.g., Tyrrhenian and Ionian seas) and similar commercial deep-sea species (i.e., non-carrying eggs like *Aristomorphocea foliacea* and *Penaeopsis serrata*). Throughout the larval transport simulations, we explored multiple scenarios that aimed to find the most likely behavior or biological components, and that fitted with the available observations on the larvae.

The field works provided handful snapshots of the larval distribution that were compared with the modeled larval dispersal (i.e., North et al., 2006; Zhang et al., 2015). In our studies, fieldwork shows that assuming behaviors during the first two stages after spawning (eggs and nauplius) was coherent for modeling/observing larvae of the third stage (i.e., protozoea) at the surface. Moreover, the collected larvae aggregated in regions

with peculiar geomorphology (canyons) and with mesoscale hydrodynamic features (i.e., eddies and fronts). Indeed, the snapshot of *A. antennatus* larvae collected in August 2016 showed the importance of the canyon areas, the widening of Valencia Gulf and the Eivissa Channel (Figure 51; Museu de la Pesca, 2019a). Nonetheless, with only one month of fieldwork, numerous aspect of the larval traits could not be clarified, and the places with or without collected larvae could have also corresponded to a sampling schedule overlapping with favorable conditions (e.g., current, recent spawning events).

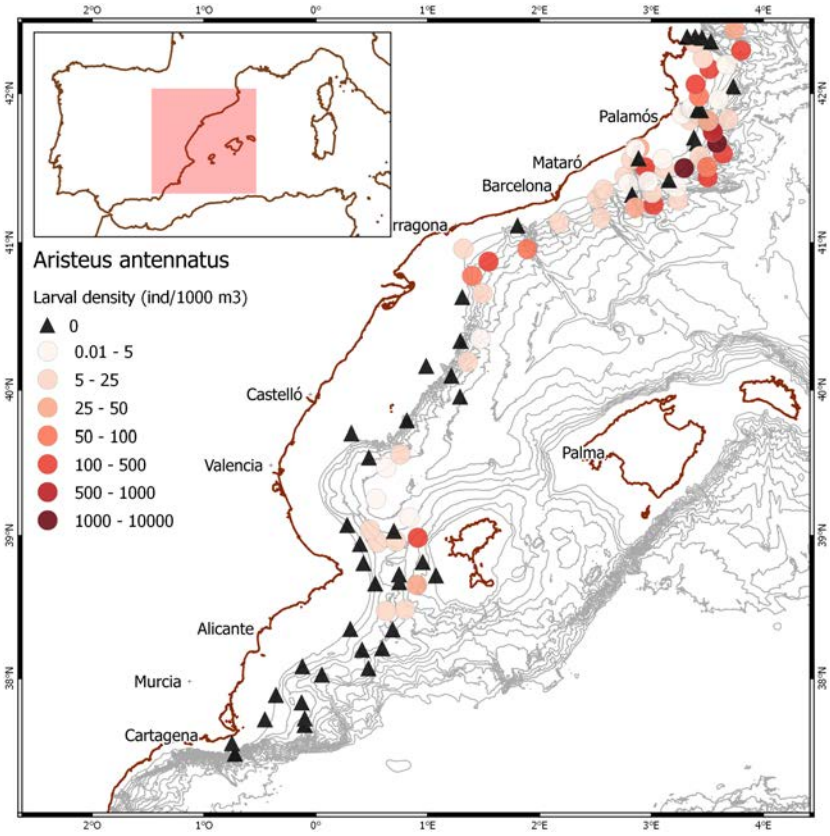

Figure 51. Larval density of *A. antennatus* larvae at the surface of the NW Mediterranean Sea in sampling stations from the CONECTA survey. Larval density gradient is sorted from light red to dark red colors. No larvae at the sampling station is symbolized by a full black triangle. Figure kindly provided by M. Carretón (Carretón et al., *in preparation*).

Fieldwork and genetics studies from the literature (Bode et al., 2019) allowed partial validation and provided reliability to the present modelling results of larval transport. For *A. antennatus*, preliminary analyses of parental genetics presented high rates of connectivity between close fishing harbors such as Palamós and Blanes (Museu de la Pesca, 2019b). Those analyses were lead on juveniles (12 mm CL) and adults (40 mm CL) sampled on the fishing grounds at two different seasons (winter and summer 2016).

Nonetheless, before validating the interannual IBMs done in Chapter 4, the results were processed considering that juveniles and adults may have different ages.

The tracking of free-drifters is a method that provides reliable trajectories for validation (see Tiessen et al., 2014). Data from free-drifters (e.g., ARGO's buoys (www.argo.ucsd.edu/How_Argo_floats.html) and buoys released during the sampling period in 2016) were used for the present work. The free-drifters suggested that the model reproduces the general trend of the dispersal (Tiessen et al., 2014). During CONECTA survey, six drifters were released at three different dates and positions (Figures 52 and 53). One type drifted at the surface (Coastal Oceanic Dynamics Experiment drifters, CODE, Figure 52) and another type drifted 5 to 10 m below the surface (Surface Velocity Program drifters, SVP, Figure 52). The trajectories during several weeks showed the presence of a dynamic barrier (i.e., front in Chapter 4) close to the surface (Figure 53.A), eddies that are anticlockwise (Figure 53.C) or clockwise (Figure 53.D), the Lion's gyre (Figures 53.B and 53.C) and reverse currents (Figure 53.B). All those structures were as well identified in the larval trajectory implemented in climatologic and interannual hydrodynamic simulations.

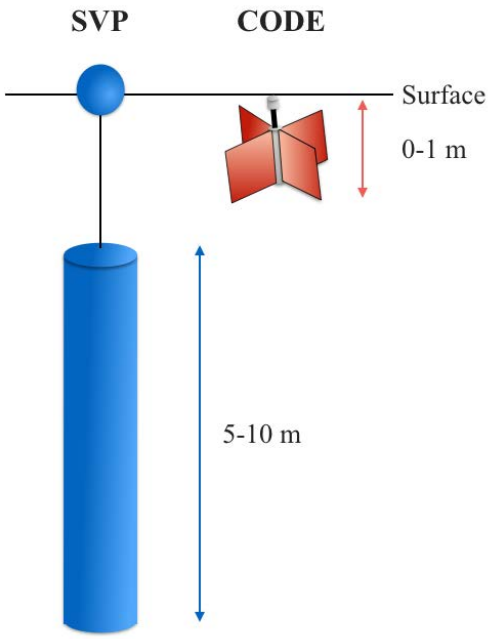

Figure 52. Free-drifters released during the CONECTA survey in summer 2016. Surface Velocity Program (SVP) drifters measure the first upper meter. Coastal Oceanic Dynamics Experiment (CODE) drifters measure the depth interval between 5 to 10 m.

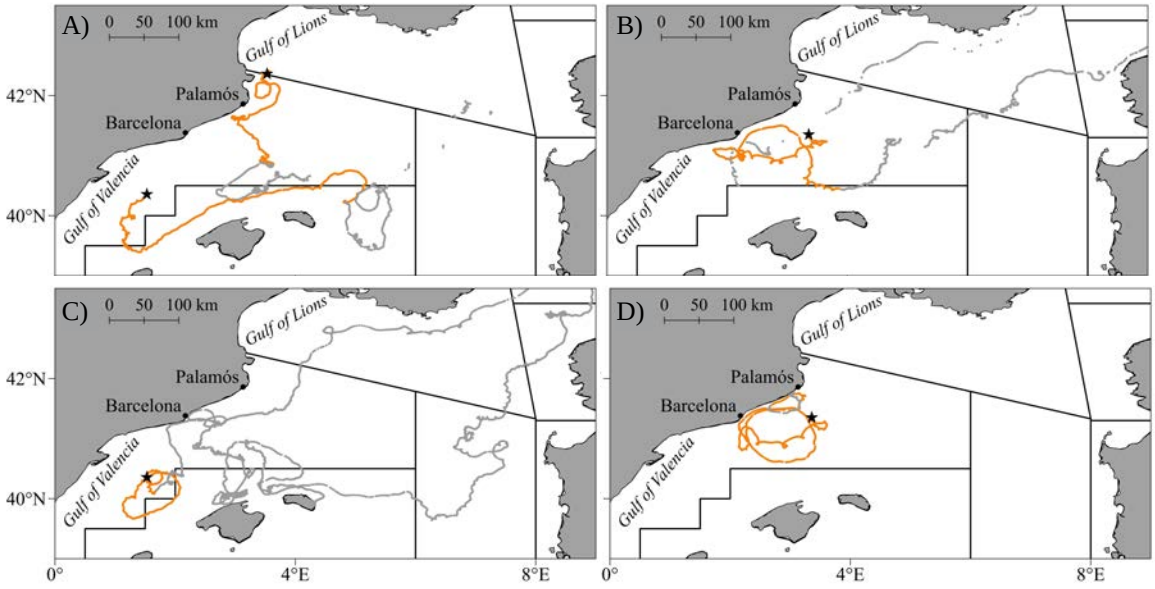

Figure 53. Trajectories of the SVP and CODE drifters from CONECTA survey. Trajectories occurring on summer and fall are in orange and grey, respectively. In panel (A), trajectories of CODE started at the coordinates (3.50º E; 42.34ºN) on August 27 and (1.58º E; 40.35º N) on August 12. In panel (B), the CODE drifter was released at the coordinates (3.37º E; 41.29º N) on August 18. In panels (C) and (D), trajectories from SVP drifters started at the coordinates (1.58º E; 40.35º N, on August 12) and (3.37º E; 41.29º N, on August 18), respectively. The drifter position was recorded every 30 minutes. Processed trajectory data were kindly provided by J. Isern and E. García Ladona (ICM-CSIC).

The precision of larval trajectories deeply relied on the modeled hydrodynamics of the northwestern Mediterranean Sea. Modeling results need sensitivity tests to identify the possible source of errors transmitted in the transport simulations and acknowledge the variability inter-model. In this thesis, a part of Chapter 1 was dedicated to localize and minimize the source of divergence from hydrodynamic models that run in the same area (larval trajectory response to two hydrodynamic models). Even though the hydrodynamic models had similar circulation patterns, the larval transport spotted one of the two for being more adequate to the study context. In this thesis, the climatologic model was developed into an interannual hydrodynamic model (see Chapter 4) and we assumed that the larval transport simulations in both versions of the hydrodynamic model remained suitable. With the climatologic model, we could see the general trend of the connectivity path over several years averaged. Those paths in the interannual implementation were hidden by the noise from the variability of the hydrodynamics from one year to another, giving us a side-thought for developing a long-term management plan instead of five years management plan (BOE 2013, 2018).

3.2. Oceanic circulation and larval traits of *A. antennatus*

Even though the lacking and sporadic information were constraining factors for the larval transport simylation, the objectives addressed to model the main paths of larval transport and to identify potential larval traits that significantly influenced the larval dispersal were achieved.

Some uncertainties in the larval transport relied on the indirect adjustment of the embryonic and larval vertical position (i.e., buoyancy), which intrinsically echoes on the pelagic larval duration and the connectivity path. Buoyancy is part of the ontogenetic migration that changed significantly the vertical position of the individuals over a few days of simulation. Then, in the layer from the surface to a few meters below reached by the eggs and larvae, strong gradients of temperature and current velocity limit the duration of the larval development and dispersal, respectively. In general, egg buoyancy is not a very well described behavior for prawn species and swimming over the whole water column (from ~ 600 m to 0 m) is a hypothesis barely evocated in the realm of the Penaeoid suborder. Therefore, we assumed that the buoyancy was the main behavior heading the embryonic and larval stages to the surface (hereby thesis; Dall et al., 1990). For including a buoyant behavior with greater exactitude (i.e., closer to the real buoyancy), future modeling studies should consider the individual development during the buoyant phases. Egg diameters and densities evolve with time such as the egg volume rises and the egg density drops (Herrings, 1974; Ronquillo et al., 2006). Yet, only a few larval transport studies have already experimented a numerical module that includes those embryonic changes (Myksvoll et al., 2014; Ospina-Álvarez et al., 2012a; Parada et al., 2012). These studies estimated that a small vertical adjustment of the incubating eggs occurred within the superficial water layer (i.e., from surface to the thermocline depth). However, their models were based on pelagic fish species (i.e., anchovy, cod), for which the knowledge about the embryonic development is well known. No larval transport simulations have assessed the same effect for eggs of decapod crustaceans because except for the majority of Dendrobranchiata specimens, they are gravid species (i.e., eggs carried by the females).

By drifting in the uppest water layer, the larvae had 1) a shorter pelagic larval duration, 2) a dispersal influenced by the main jet and 3) a restrained dispersal close to the spawning areas if eddies advected them, or if a front deviated the main flow. Over the temporal dimension, as the surface water masses and circulation can be daily, monthly and yearly modified by multiple forcings (e.g., wind, heatwaves; Millot and Taupier-Letage, 2005), the larval transport could widely vary among the different parameterization of the IBM (see Chapter 2 and Chapter 4). Over the horizontal dimension, front, and eddy diameter and its residence time were likely to improve the retention of larvae in the region of submarine canyons and to prevent the crossing of the insular channels (Eivissa, Majorca). Those oceanographic influences on the larval dispersal variability have already been identified for other species in the northwestern Mediterranean Sea. For example, we pointed out that the interface between the old hot and cold recent Modified Atlantic Water nearby the area of submarine canyons (see Figure 7) was a boundary for estimating shorter and longer Pelagic Propagule durations. This and the influence of the front on the larval dispersal can be foreseen in the Balearic Archipelagos water where a trawling fleet also harvests *A. antennatus* (Guijarro et al., 2008). Actually, similar oceanographic perturbations have already been described (i.e., two types of MAW; Jordi et al., 2009) and correlated to the larval dispersion of various species (Alvaréz et al., 2015; Galarza et al., 2009; Mariani et al., 2010).

The combination of different mesoscale influences (i.e., eddies and a front) was approached in Chapter 4. In addition, it would be interesting in further studies to consider the combination of similar mesoscale circulations (i.e., eddies). Indeed, with the presence of several eddies in the semi-enclosed basin, the phenomenon of divergence or convergence of water masses (Figure 54) implied the pooling or dispersal of larvae, respectively (Bradbury and Snelgrove, 2001; Condie and Condie, 2016). This is of great importance for connectivity because areas at the eddies confluence can have a connection with spatially opposite populations.

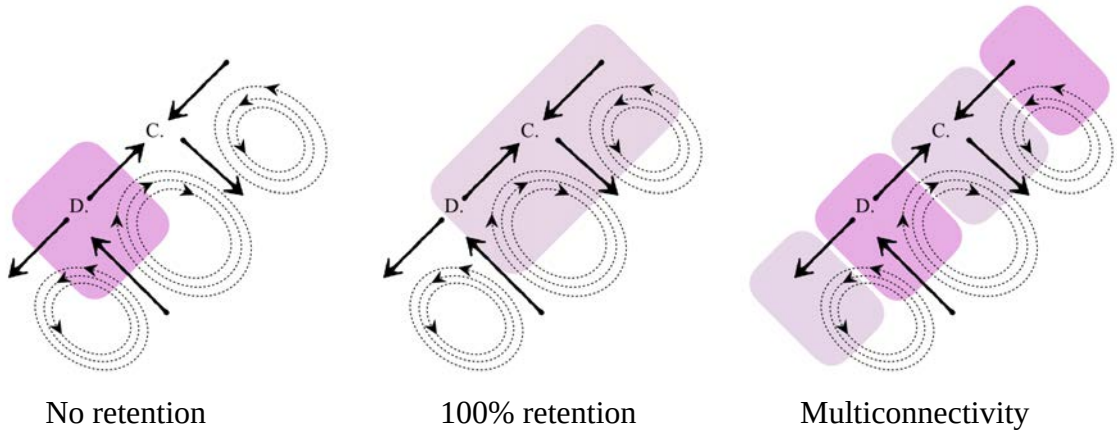

Figure 54. Diagram of Convergent (C.) and Divergent (D.) waters with the combination of counter- and clockwise eddies (dotted circles). According to the habitat size and population span (colored polygons), eddies inferred no retention (left panel), a total retention (middle panel) or multiconnectivity (right panel). Adapted from Bradbury and Snelgrove (2001).

The last gate for variability in larval transport was introduced by water turbulence (Chapter 2 and Chapter 5). In our dispersal simulation, the higher effect from vertical mixing takes place in the northern Mediterranean Sea (Chapter 5), where the surface is sheared by the northwesterly (i.e., Tramuntana). It can cause the spread of pooled larvae, but it unlikely modifies the main path of larval transport in the northwestern Mediterranean Sea. Overall, water turbulence is very powerful on larval drift when the mixing modifies the vertical position of the larvae (North et al., 2004). Yet, with some active larval behavior (i.e., swimming) to maintain their vertical position, the effect of vertical mixing can be neglected.

Occasionally, our theoretical approach estimated that larvae drifting in the subsurface layers can escape the influence of eddies and follow different dispersal paths (Chapter 2). In fact, many larvae have a phototaxis migration (Criales and McGowan, 1994; Ponce and Gracia, 2008) or a tidal migration (Kunze et al., 2013) in the water column. Therefore, larvae can interact several times during their pelagic cycle with the surface mesoscale circulation. Additional precisions in the larval dispersal simulations can be added with a module simulating the diel vertical migration (DVM), which is an ability to swim a few meters up and down as a function of the day/night period or ebb/flood tide. In particular, the phototaxis migration allows reducing the exposure to predators and accessing to feeding places. Besides, most of the time, the DVM behavior modifies the distance of drifts (see Criales et al., 2015) instead of significantly affecting the

connectivity path. With further fieldworks dedicated to *A. antennatus*, observed depth of planktotrophic larval stages (protozoea and mysis) by day period should provide new elements to be included in a larval transport model. For Penaeid larvae, the depth reached with DVM is dependent on the species, its stages and the hydrography of the water column (Ponce and Gracia, 2008). Even though there are too many incertitudes for generalizing the behavior in our larval transport model, the Chapter 2 indirectly gives an illustration of what would be the connectivity path for larvae drifting at various positions within the upper water layer.

Larval dispersal modeling is a useful tool for setting up and testing further new hypotheses about the unknown larval traits. This kind of model application can also be applied to the early juveniles (i.e., pelagic stage after the mysis), that is the last piece for closing the life cycle of *A. antennatus*.

3.3. Closing the cycle: pelagic, settlement, recruitment

Up to date, the intermediate stage between the surfaced larvae and the recruited juveniles of *A. antennatus* has not been found. However, this period is determinant for settlement and recruitment of the shrimp on the sea-bottom (Carbonell et al., 2010; Sardà et al., 2004).

Like for the case of eggs and larvae, analyses on Penaeid early juveniles (n.b., the postlarvae in many works) can be assigned to fill the current knowledge gap. Including this intermediate phase in the future transport models will need to assess the vertical locomotion and postlarval growth. Like for the embryonic and larval stages, important variabilities exist in those traits among Penaeid species and its adult habitats (i.e., estuary/mangrove, shore; see Dall et al., 1990). No clear evidence is given about the postlarval duration but laboratory experiments easily last over a month (Castille et al., 1993; Niu et al., 2003), and field works caught postlarvae on a time frame between two and eight months after the spawning period (Meager et al., 2003). The duration is not recognized as an important option in the literature about Penaeid species, which preferred optimizing the postlarval growth. Indeed, growth is not related to time (Castille et al., 1993), but is limited by the temperature (Kumlu and Eroldogan, 2000). Examining the

juvenile growth through Individual-Based Models can be used for comparison of their simulated size on the settlement areas with the size of the *A. antennatus* juveniles caught during scientific surveys. Before the CONECTA project, several studies found small juveniles (<10 mm CL) in early and late fall, below 1000 m depth (see Table 7). These findings suggested that the duration between early juveniles and recruitment sets in one to three months.

Table 7. Smallest juveniles reported in 5 peer-reviewed articles, with sea-bottom depth and period of sampling. CL; Carapace Length; n/a: unavailable information.

Smaller size (mm CL)	Depth range (m)	Month	Reference
6 – 7	1300 – 1500	October	Cartes et al., 2017
10 – 14	1000 – 1200	April	D'Onghia et al., 2009
12	1007 – 1212	n/a	Follesa et al., 2009
<15	1000 – 1800	n/a	Cartes and Demestre, 2003
6	1248 – 1256	December	Sardà and Cartes, 1997

The transport between the mysis (i.e., last larval stage) at the surface and the juvenile at the seafloor can be explained by strong swimming abilities with orientation within the flows towards recruitment zones. This orientation capacity relied on different kinds of cues for Penaeid juveniles. For species inhabiting the estuaries and inshore water (types 1 and 2, see Dall et al., 1990), cues are hydrostatic pressures, chemistry and hydrography assisting the juveniles to select a tidal stream transport (ebb- or flood-tide; Vance and Pendrey, 2008; Criales et al., 2011). Behavior or swimming capacity of juveniles from open oceans (types 3 and 4, see Dall, 1900) are less known due to the hardship to sample the wide offshore and the deep oceans. Nonetheless, individuals swimming down within the submarine canyons can be boosted by the internal vertical current within them (see Chapter 1). For other Crustacean Decapoda species, the light intensity, gravity, and hydrostatic pressures are among the stimulus explaining the downwards movements of megalopae (i.e., postlarval stage of crabs) and there is even the possibility of passively sinking (Sulkin, 1984). Except for light intensity, which is non-existent deeper 1000 m depth, these cues can be applied for the early juveniles of *A. antennatus*.

Including the early juvenile period in the dispersal model may lead to interesting results in continuity with the larval transport. Several simulations can be run with different

scenarios from the former position of the mysis (i.e., last larval stage) like:

1) Postlarvae passively sink.
2) Postlarvae actively swim downwards.
3) Postlarvae actively swim downwards in the first 100 – 200 meters below the surface to escape quickly the high dynamics due to the main jet. Then, it sinks passively.

Those three scenarios need to consider potential sinking or swimming velocities and consider that the early juveniles have to feed. If their diet is similar to the small juveniles of *A. antennatus* collected near the seafloor (i.e., suprabenthic peracarid crustaceans; Sardà and Cartes, 1997), we can consider the second scenario as the most probable.

3.4. Drivers of connectivity in *A. antennatus* larval cycle

To our knowledge, this work represents the most complete approached larval cycle of *A. antennatus*. In Figure 55, the life cycle of *A. antennatus* has been schemed with details on the pelagic stages and the environmental/species influencing the dispersal. The figure shows that during embryonic and larval development, many larval traits (e.g., growth, and duration) are regulated by numerous hydrographic drivers (e.g., salinity and temperature). Then, these traits regulate the position of larvae in different hydrodynamic patterns (e.g., jet and eddies) and control the duration of dispersal, which result in enhancing or limiting the larval transport.

Within the limits of knowledge, the different studies carried out in the thesis focused on identifying drivers which modify the transport and the connectivity link between zones. Significant hydrodynamic and hydrographic changes related to time and location and biological/behavioral drivers related to egg density and drift duration have influenced *A. antennatus* larval dispersal. Progressively, the analyses (Sections 2.1 to 2.5) showed and consolidated that potential connectivity between *A. antennatus* populations depended on:

1) dispersal pattern that likely prevail every year,
2) dispersal variability due to hydrodynamics,
3) dispersal variability due to intrinsic larval characteristics.

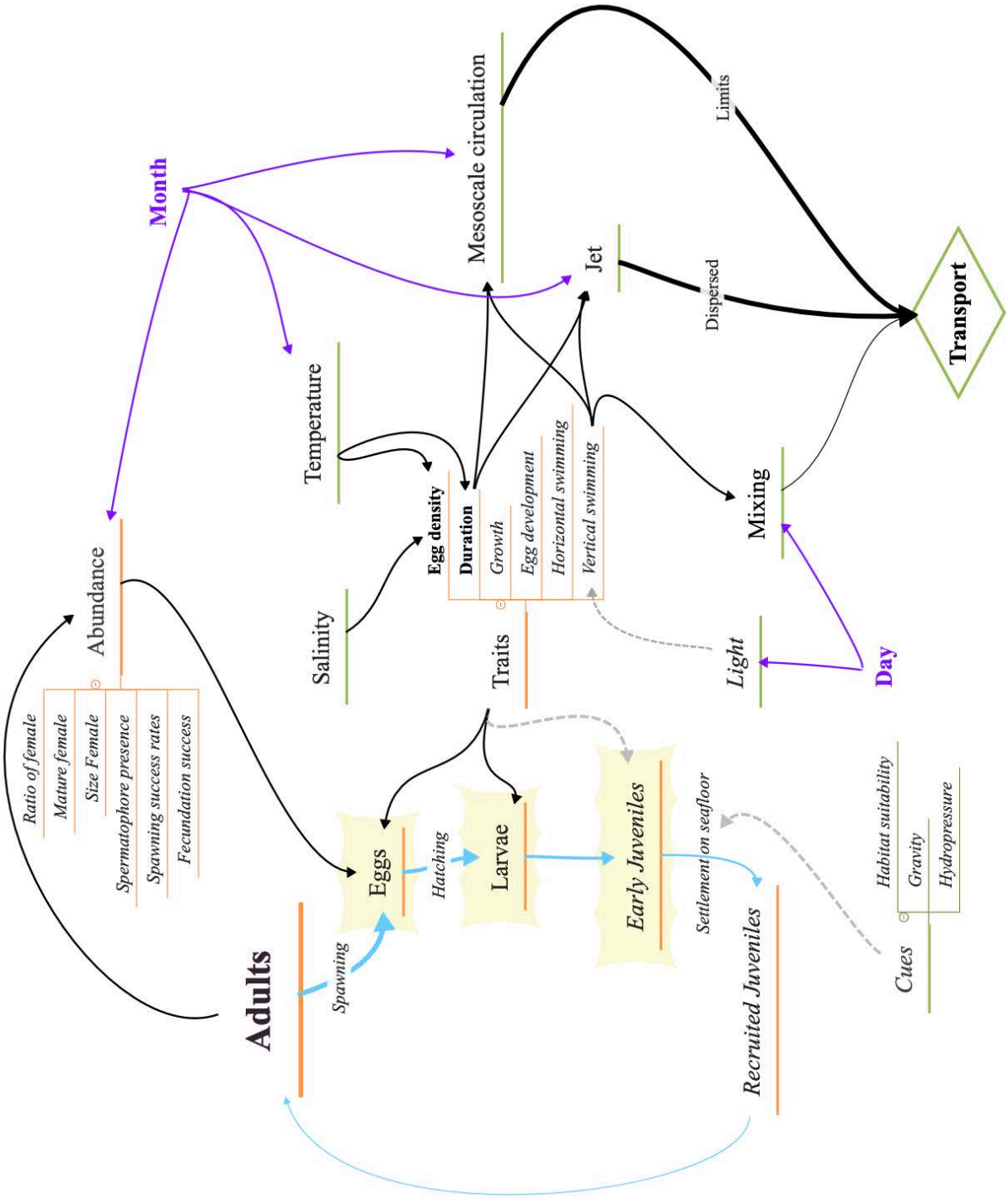

Figure 55. Connectivity diagram of *A. antennatus* life cycle and the larval transport. Phase in yellow polygons are the pelagic young stages of *A. antennatus*. Elements related to the species characteristics are underlined in orange. Elements related to the environmental influence are underlined in green. *Italic* are elements not considered in the present thesis. Elements related to the temporal dimension are in violet. Dashed arrows are relationships between environment and larvae that were not available in the literature. Blue arrows with decreasing thickness symbolized the stage development with natural mortality. The thickness of the blue arrows is not proportional to any mortality rates but represent the loss of individuals during the life cycle.

As defined by Cowen and Sponaugle (2009) and Pineda et al. (2007), connectivity between *A. antennatus* populations depend on a fourth driver, which is the number of settled juveniles related to the number of spawned eggs. This connectivity accounts for the dispersal rates of individuals and the quantitative loss of individuals from spawning to recruitment. To assess this connectivity, a first step consists in estimating the most realistic number of spawned eggs which depends on the ready-to-spawn female conditions (e.g., carapace length and spermatophore presence) and abundance (see Figure 55). For *A. antennatus* shrimp case, the size of the female was related to the number of oocytes (e.g., a female of 30 mm CL spawns ~102 000 eggs; Kapiris and Thessalou-Legaki, 2006). Then, a second step is carried out during the pelagic phases when losses of eggs and larvae are inflected by natural mortality. Natural mortality is hardly known for most of the marine larvae and depends on numerous environmental and biological factors (i.e., predation, hydrography, larval conditions). Ultimately, a last step should estimate the loss of juveniles due to their settlement competency and the habitat suitability on which juveniles recruits (Table 56).

Then, in order to improve the estimates of *A. antennatus* connectivity, future dispersal simulations should be provided with accurate or/and additional larval traits. Nonetheless, it is needed to understand the behaviors of *A. antennatus* eggs and larvae (e.g., swimming), to approach the factors controlling the larval abundance and conditions, and to have knowledge of the processes influencing the settlement of juveniles.

3.5. Suggestions for management of the shrimp fishery

The larval transport simulation provided paths of potential connectivity and new elements for the stakeholders involved in the *A. antennatus* fishery.

Currently, the management of the shrimp fishery is only adopted at Palamós fishing grounds, where one of the most important Spanish landings comes from. Fishing activities are restricted in seven places distributed over the closest submarine canyon walls and neighbored open slope. As evoked in the Introduction and reminded in Hinrichsen et al. (2011), larval transport modeling could be helpful to localize and estimate the size of areas to be managed. In this context, our results indicate that the

population close to Palamós canyon is a type of step-stone habitat that combines the three cases schemed in Figure 3. Indeed, virgin stocks of Palamós (i.e., the seafloor below 1000 m depth) received many individuals from northern fishing grounds (i.e., Roses, Llançá, Port de la Selva) and from the spawners aggregated on the fishable continental margin of Palamós. Yet, part of the offsprings is transported towards southern places (i.e., around submarine Blanes Canyon). These paths showed that grounds near the fishing zone of Palamós canyon could favor the mixing between autorecruited juveniles and those from other populations.

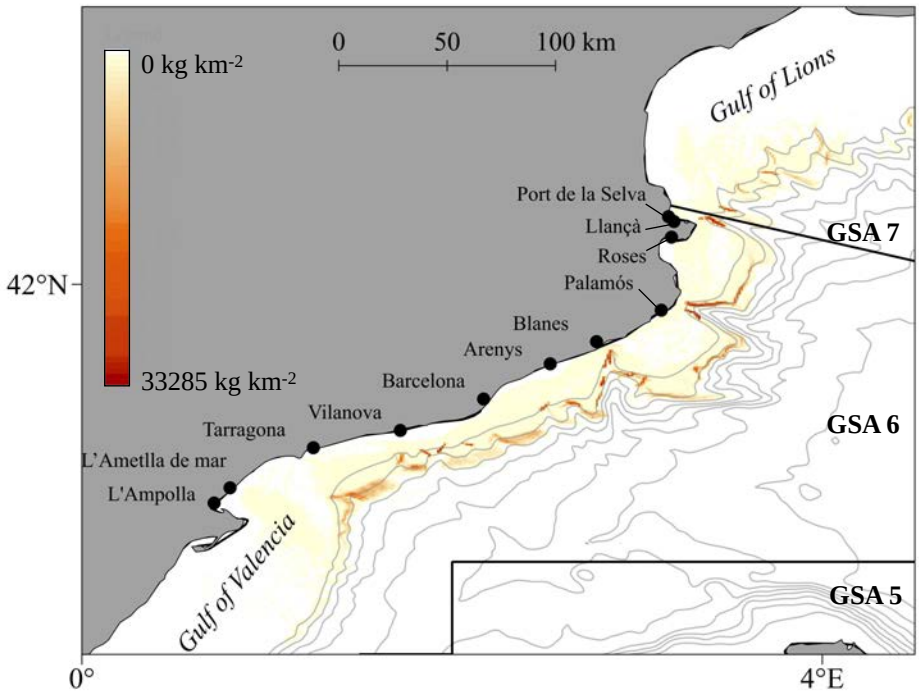

Figure 56. Total *A. antennatus* landings (kg km^{-2}) from 2005 to 2016 along the Catalan continental margin (from Port de la Selva to L'Ampolla in the NW Mediterranean Sea). Isobaths from 200 m to 1600 m with 200 m steps. Credits: JA Garcia.

In Gorelli's thesis (2017), the idea to expand the local management plan to a regional one was recommended because of the numerous similarities among the fishing fleets, fishing habits, and socio-economic conditions. In the present thesis, we noticed that larval transport simulation identified three regions along a latitudinal range where the settlement of recruits depended on different hydrodynamic regimes. The northern region is a place that is under a high fishing pressure because of the canyon influences (see Chapter 3 and Figure 56) while the fisheries in southern regions of the GSA 6 yield less. The northern region is as well a hydrodynamic unity (Rossi et al., 2014), where synchronous events (like the DSWC) affect the whole area. Accounting for the two regional populations that recruited in a relatively independent way from each other, two

units of managements would be rather equilibrated for tackling the economy of the harbors and the sustainability of the shrimp stocks (Figure 57).

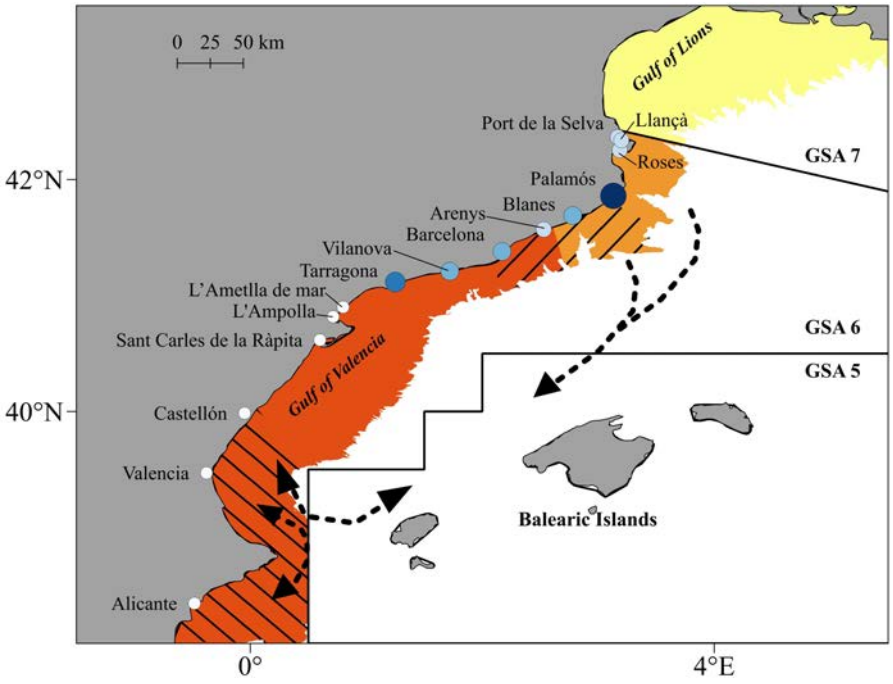

Figure 57. Regions of two potential management units (red and orange polygons) in GSA 6 with "buffered" regions (diagonal lines) depending on the mesoscale circulation. Sea-bottom below 1000 m (white) is already protected by the ban from the GFCM. Yellow polygon is on continuity with the orange polygon but dependent on French governance. The potential flow of individuals between GSAs 5 and 6 are materialized by dotted arrows. Color dots and size represents the landings of the *A. antennatus* shrimps in 2018 from different harbors of the studied area: white: 0 – 10 mT, light blue: 10 – 40 mT, blue: 40 – 60 mT, dark blue: 60 – 80mT, deep blue: 80 – 100 mT. See Table 8 for the annual landings values by fishing harbors.

Table 8. Landings (in tonnages) of *A. antennatus* in 2018 from the fishing harbors related to the GSA 6. Fishing harbors are ordered by their latitudinal gradient from north to south.

Fishing harbor	Coordinates	Landings	Reference
Llançà	(3.14 º E; 42.36 ºN)	12 537	Generalitat de Catalunya
Port de la Selva	(3.1833 º E; 42.33 ºN)	30 669	
Roses	(3.20 º E; 42.26 ºN)	35 724	
Palamós	(3.13 º E; 41.86 ºN)	99 205	
Blanes	(2.78 º E; 41.69 ºN)	57 800	
Arenys	(2.53 º E; 41.57 ºN)	38 269	
Vilanova	(1.72 º E; 41.21 ºN)	54 084	
Barcelona	(2.17 º E; 41.38 ºN)	42 514	
Tarragona	(1.25 º E; 41.17 ºN)	61 333	
L'Ametlla de mar	(0.8 º E; 40.9 ºN)	9 840	
L'Ampolla	(0.708 º E; 40.81 ºN)	1 646	
Sant Carles de la Ràpita	(0.6 º E; 40.62 ºN)	214	
Castellón	(-0.05 º E; 39.99 ºN)	2.45	Generalitat Valenciana
Valencia	(-0.38 º E; 39.47 ºN)	14.09	
Alicante	(-0.48 º E; 38.35 ºN)	202	

Considering the high temporal variability in the mesoscale circulation, the area between the two units is likely to receive individuals from the north or the south from year to year. Those temporal variabilities are unpredictable ahead of time. That is why, fishery restrictions in that area should be flexible based on a yearly follow-up of the summer hydrodynamics and fishermen evaluation of the catches during that period. A yearly supervision will account for 1) the decline of spawning period (i.e., less mature spawners), 2) the casual adult disappearance due to external perturbations in summer (case in Balearic Argipelagos, see post from Pere, 2016), and 3) the arrival of juveniles in the catches. Late or perturbed spawning events can lead to different connectivity patterns in the area where the mesoscales structures have high temporal variability (see Chapter 2). Because 1 to 1.5 years period is required before the recruitment of juveniles on the fishing grounds (D'Onghia et al., 2005; Sardà and Company, 2012; Sardà and Demestre, 1987), the connectivity in a specific year has repercussion in the following years. In conclusion, the yearly fishery supervision can detect when exceptional measures should be necessary.

Our study was related to the GSA6, yet, high connectivity rates and the absence of strong physical barrier between the humanly-set management unit implied that the management in GSAs 6 and 5 (both being Spanish fishing grounds) should be combined together. The present thesis revealed that depending on the location and strength of North Balearic Front, the area of submarine canyons could connect with the northern continental margin of the Balearic Islands. Besides, on the bottleneck ground of the Eivissa channel, special attention requires the persistence of an eddy hindering the supply of stock at one of the channel sides. There, GSAs 5 and 6 can discontinuously exchange individuals regulated by the eddy presence.

Last but not least, in the area of submarine canyons, the steady flows driven by the Northern Current could continuously connect the GSA 7 to the GSA 6 and involve a dependence of the population in the canyons to the upstream French fishery management. This issue implies the regionalization of the shared stock management between French and Spanish governments.

CHAPTER 4

General conclusions

Larval transport models are useful and reliable methods for approaching the unknown larval cycle of *A. antennatus*, and for estimating the connectivity path between different subpopulations of the shrimps along the northwestern Mediterranean Sea margin. The principal conclusions derived from the previous chapters are summarized below,

1 - Simulation results of deep-sea transport depend on the near-bottom parameterization of hydrodynamic models. The awareness of those settings is fundamental for selecting the most adequate circulation model and for expecting accuracy in the transport model.

2 - In a month-lasting transport of deep-sea particles, the connectivity between the main submarine canyons of the NW Mediterranean Sea margin was established from Cap de Creus Canyon to Palamós Canyon. Given the conditions applied on passive particles, simulated drifts from Palamós to Blanes canyons were not assessed if the hydrodynamic model was implemented with a good representation of the bottom topography.

3 - The vertical circulation within submarine canyons could not explain the ascent of particles towards the surface layers. However, it averagely supported the transport of particles down to the continental margin, with particles released in Palamós canyon having the deepest displacement. It potentially favors the migration of late larval stages to settle on the bottom as juveniles.

4 - At the very beginning of *A. Antennatus*'s life cycle (egg and nauplius stages), a ascent of individuals from the spawning ground to the surface could use the buoyancy force, which controls the vertical velocity of individuals.

5 - Pelagic propagule durations, or pelagic larval duration that includes the embryonic period, were based on the water temperature and were estimated between 20 and 40 days depending on the depth at which the larvae drifted.

6 - Surfacing rate was higher when we considered two lecithotrophic stages of *A. antennatus (*eggs and nauplii). It implied the surfacing of larvae after eight days, but connectivity paths were almost equivalent with the ones defined when only eggs surfaced after two days of transport simulations.

7 - Depth position of larvae influenced the direction of the dispersal and connectivity between regions of the NW Mediterranean Sea. Model implementation estimated that the

average path of dispersal could connect one spawning sites to two distinct regions of the Mediterranean Sea if the individuals were drifted above or below 5 m depth.

8 - High retention rates in spawning ground areas were associated with the presence of mesoscale structures such as eddies. Those structures have various impact on the connectivity path as a function of their locations and the depths where larvae drifted. It was particularly noticeable in the bottleneck area where an eddy limited the larvae to cross the Eivissa Channel.

9 - Further adjustments in the IBM considered the initial distribution of the spawning biomass set by a species distribution model. Locations with high shrimp biomass emphasized the release of eggs from a narrower bathymetric range in the main submarine canyons over the release on the open slope.

10 - The species distribution model was dependent on environmental and bathymetric predictors that allowed estimating the potential impact from the global warming on the shrimp catches in the canyon grounds.

11 - The area of the three main submarine canyons (Cap de Creus, Palamós and Blanes canyons) is located at the convergence of flows around a surface density. Larvae concentrated in that area were transported by the Northern Current from the upstream spawning grounds or by a clockwise eddy located at the south of the last important canyon (Blanes Canyon).

12 - Due to the interannual variability in the hydrodynamics, the position and impact of the surface density front have consequences on the retention of larvae near Palamós Canyon and the connectivity from Palamós to Blanes canyons.

13 - Simulation of time-reversed transports estimated that larvae found in a meroplankton survey were from the different fishing ground and mixed while drifting at the surface.

14 - Backtracking simulations showed that connectivity between spawning site of the NW Mediterranean Sea would have a higher source of uncertainty mainly because of the larval drift duration, and to a lesser extent by the impact of the vertical turbulences and other hydrodynamics features.

15 - The shrimp fishery management is suggested to take into account two regions that should have distinct regulations based on the distribution of the resource, the efforts in the exploitation of the stocks, and the hydrodynamic regimes dominating the basin and transporting larvae.

References

Adams DK, McGillicuddy Jr. DJ, Zamudio L, Thurnherr AM, Liang X, Rouxel O, German CR, Mullineaux LS. Surface-generated mesoscale eddies transport deep-sea products from hydrothermal vents. *Science*. 2011; 332: 580–583.

Adani M, Dobricic S, Pinardi, N. Quality assessment of a 1985-2007 Mediterranean Sea reanalysis. *Journal of Atmospheric and Oceanic Technology.* 2011; 28(8): 569–589.

Ahumada-Sempoal MA, Flexas MM, Bernardello R, Bahamon N, Cruzado A. Northern Current variability and its impact on the Blanes Canyon circulation: A numerical study. *Progress in Oceanography.* 2013; 118: 61–70.

Ahumada Sempoal MA, Ahumada-Sempoal MA, Flexas MM, Bernardello R, Bahamon N, Cruzado A, Reyes Hernaández C. Shelf-slope exchanges and particle dispersion in Blanes submarine canyon (NW Mediterranean Sea): A numerical study. *Continental Shelf Research.* 2015; 109: 35–45.

Aktas M, Eroldogan OT, Kumluo M. Combined effect of temperature and salinity on egg hatching rate and incubation time of *Penaeus semisulcatus* (Decapoda: Penaeidae). *The Israeli Journal of Aquaculture-Bamigeh.* 2004; 56(2): 124–128.

Aktas M, Çavdar N. The combined effects of salinity and temperature on the egg hatching rate, incubation time, and survival until protozoal stages of *Metapenaeus monoceros* (Fabricius) (Decapoda: Penaeidae). *Turkish Journal of Zoology.* 2012; 36(12): 249–253.

Albérola C, Millot C, Font J. On the seasonal and mesoscale variabilities of the Northern Current during the PRIMO-0 experiment in the western Mediterranean sea. *Oceanologica Acta.* 1995; 18(2): 163–192.

Álvarez I, Rodríguez JM, Catalán IA, Hidalgo M, Álvarez-Berastegui D, Balbín R, Aparicio-González A, Alemany F. Larval fish assemblage structure in the surface layer of the northwestern Mediterranean under contrasting oceanographic scenarios. *Journal of Plankton Research.* 2015; 37(4): 834–850.

Amores A, Rueda L, Monserrat S, Guijarro B, Pasqual C, Massutí E. Influence of the hydrodynamic conditions on the accessibility of *Aristeus antennatus* and other demersal species to the deep water trawl fishery off the Balearic Islands (western Mediterranean). *Journal of Marine Systems.* 2014; 138: 203–210.

Anderson W, King J, Lindner M. Early stages in the life history of the common marine shrimp, *Penaeus setiferus* (Linnaeus). *Biological Bulletin*. 1949; 96(2): 168–172.

Andrade-Vizcaino K. Descripción del desarrollo larval del camarón blanco *Litopenaeus stylirostris* (Boone, 1931), y evaluación del indice de desarrollo en función del regimen de alimentación. (B.S.), Universidad Autonoma de Baja California Sur, La Paz B.C.S. 2010.

Andrello M, Mouillot D, Beuvier J, Albouy C, Thuiyse W, Manel S. Low connectivity between Mediterranean Marine Protected Areas: a biophysical modeling approach for the dusky grouper *Epinephelus marginatus*. *PLoS ONE.* 2013; 8(7): e68564.

Apollonio S. Breeding and fecundity of the glass shrimp, *Pasiphae multidentata* (Decapoda, Caridea) in the Gulf of Maine. *Journal of the Fisheries Research Board of Canada.* 1969; 26: 1969–1983.

Arellano SM, Van Gaest AL, Johnson SB, Vrijenhoek RC, Young CM. Larvae from deep-sea methane seeps disperse in surface waters. *Proceedings of the Royal Society B: Biological Sciences.* 2014; 281: 20133276.

Bahamon N, Aguzzi J, Bernardello R, Ahumada-Sempoal M-A, Puigdefabregas J, Cateura J, Munoz E, Velasquez Z, Cruzado A. The new pelagic Operational Observatory of the Catalan Sea (OOCS) for the multisensor coordinated measurement of atmospheric and oceanographic conditions. *Sensors.* 2011; 11: 11251–11272.

Bakun A. Fronts and eddies as key structures in the habitat of marine fish larvae: opportunity, adaptive response and competitive advantage. *Scientia Marina*. 2006; 70(S2): 105–122.

Balbar AC, Metaxas A. The current application of ecological connectivity in the design of marine protected areas. *Global Ecology and Conservation.* 2019; 17: e00569.

Basterretxea G, Jordi A, Catalán IA, Sabatés A. Model-based assessment of local-scale fish larval connectivity in a network of marine protected areas. *Fisheries Oceanography*. 2012; 21(4): 291–306.

Bauer RK, Graewe U, Stepputtis D, Zimmermann C, Hammer C. Identifying the location and importance of spawning sites of Western Baltic herring using a particle backtracking model. *ICES Journal Of Marine Science*. 2014; 71(3): 499–509.

Beard TW, Wickins JF, Arnstein DR. The breeding and growth of *Penaeus merguiensis* de Man in laboratory recirculation systems. *Aquaculture*. 1977; 10(3): 275–289.

Beaulieu SE, Sayre−McCord RT, Mills SW, Pradillon F, Watanabe H. Swimming speeds of polychaete larvae collected near deep−sea hydrothermal vents. *Marine Ecology.* 2015; 36: 133–143.

Bendtsen J, Hansen JLS. A model of life cycle, connectivity and population stability of benthic macro-invertebrates in the North Sea/Baltic Sea transition zone. *Ecological Modelling.* 2013; 267: 54–65.

Bethoux JP, Gentili B, Raunet J, Taillez D. Warming trend in the western Mediterranean deep water *Nature*. 1990; 347: 660–662.

Bode M, Leis JM, Mason LB, Williamson DH, Harrison HB, Choukroun S, Jones GP. Successful validation of a larval dispersal model using genetic parentage data. *PLOS Biology.* 2019; 17(7): e3000380.

Boff MH, Marchiori MA. The effect of temperature on larval development of the pink shrimp *Penaeus paulensis*. *Atlantica.* 1984; 7: 7–13.

Boletín Oficial del Estado. Orden AAA/923/2013 de 16 de Mayo, nº 126, Sec. III; 2013; 40016–40022.

Boletín Oficial del Estado. Orden APM/532/2018 de 26 de Mayo, nº 128, Sec. III; 2018: 55045–55051.

Borghini M, Bryden H, Schroeder K, Sparnocchia S, Vetrano A. The Mediterranean is becoming saltier. *Ocean Science* 2014; 10(4): 693–700.

Boschi EE, Scelzo MA. Rearing the Penaeid shrimp *Artemesia longinaris* from egg to juvenile in the laboratory. *Proceedings of the annual meeting - World Mariculture Society.* 1974 5(1–4): 443–444.

Boschi EE, Scelzo MA. Desarrollo larval y cultivo del camarón comercial de Argentina *Artemesia longinaris* Bate (Crustacea, Decapoda, Penaeidae). *FAO, Informe de Pesca.* 1977; 159(1): 287–327.

Bracken-Grissom HD, Felder DL, Vollmer NL, Martin JW, Crandall KA. Phylogenetics links monster larva to deep-sea shrimp. *Ecology and Evolution.* 2012; 2(10): 2367–2373.

Bradbury I, Snelgrove P. Contrasting larval transport in demersal fish and benthic invertebrates: The roles of behaviour and advective processes in determining spatial pattern. *Canadian Journal of Fisheries and Aquatic Sciences.* 2011; 58: 811–823.

Branicki M, Mancho AM, Wiggins S. A Lagrangian description of transport associated with a Front-Eddy interaction: application to data from the North-Western Mediterranean Sea. *Physica D: Nonlinear Phenomena.* 2008*;* 240 (3): 282–304.

Bray L, Reizopoulou S, Voukouvalas E, Soukissian T, Alomar C, Vázquez-Luis M, Deudero S, Attrill M, Hall-Spencer JM. Expected effects of offshore wind farms on Mediterranean marine life. *Journal of Marine Science and Application.* 2016; 4(1): 18 pp.

Brown JL, Yoder AD. Shifting ranges and conservation challenges for lemurs in the face of climate change. *Ecology and Evolution.* 2015; 5(6): 1131–1142.

Canals M, Puig P, Xavier Durrieu De M, Heussner S, Palanques A, Fabres J. Flushing submarine canyons. *Nature*. 2006; 444(7117): 354–357.

Canals M, Danovaro R, Heussner S, Lykousis V, Puig P, Trincardi F, Calafat AM, Durrieu de Madron X, Palanques A, Sanchez-Vidal A. Cascades in Mediterranean submarine grand canyons. *Oceanography.* 2009; 22: 26–43.

Cannas R, Sacco F, Follesa MC, Sabatini A, Arculeo M, Lo Brutto S, Maggio T, Deiana AM, Cau A. Genetic variability of the blue and red shrimp *Aristeus antennatus* in the Western Mediterranean Sea inferred by DNA microsatellite loci. *Marine Ecology.* 2012; 33: 350–363.

Carbonell A, Carbonell M, Demestre M, Grau A, Monserrat S. The red shrimp *Aristeus antennatus* (Risso, 1816) fishery and biology in the Balearic Islands, Western Mediterranean. *Fisheries Research.* 1999; 44(1): 1–13.

Carbonell A, Dos Santos A, Alemany F, Vélez-Belchi P. Larvae of the red shrimp *Aristeus antennatus* (Decapoda: Dendrobranchiata: Aristeidae) in the Balearic Sea: new occurrences fifty years later. *Marine Biodiversity Records.* 2010; 3: 4 pp.

Carbonell A, Llompart PJ, Gaza M, Mir A, Aparicio-González A, Álvarez-Berastegui D, Balbín R, Cartes JE. Long-term climatic influences on the physiological condition of the red shrimp *Aristeus antennatus* in the Western Mediterranean Sea. *Climate Research.* 2017; 72(2): 111–127.

Cardona Y, Ruiz-Ramos DV, Baums IB, Bracco A. Potential connectivity of coldwater black coral communities in the Northern Gulf of Mexico. *PLoS ONE*. 2016; 11(5): e0156257.

Calvo EM, Coma R, Gili JM, Pascual J, Pelejero C, Ribes M, Sabatès A, Simó R. Effects of climate change on Mediterranean marine ecosystems: the case of the Catalan Sea. *Climate Research.* 2011; 50: 1–29.

Cariton JT, Geller JB. Ecological Roulette: The global transport of nonindigenous marine organisms. *Science*. 1993; 261(5117): 78–82.

Carlton JT, Keith I, Ruiz GM. Assessing marine bioinvasions in the Galápagos Islands: implications for conservation biology and marine protected areas. *Aquatic Invasions*. 2019; 14(1): 1–20.

Carr MH, Robinson SP, Wahle C, Davis G, Kroll S, Murray S, Schumacker EJ, Williams M. The central importance of ecological spatial connectivity to effective coastal marine protected areas and to meeting the challenges of climate change in the marine environment. *Aquatic Conservation: Marine and Freshwater Ecosystem*. 2017; 27(S1): 6–29.

Carretón M. Spatial and temporal fleet dynamics of the deep-sea red shrimp *Aristeus antennatus* fishery in the submarine canyons off Blanes and Palamós (NW Mediterranean). Master thesis. University of Barcelona, Spain. 2014

Carretón M, Company JB, Planella L, Heras S, García-Marín J-L, Agulló M, Clavel-Henry M, Rotllant G, dos Santos A, Roldán MI. Morphological identification and molecular confirmation of the deep-sea blue and red shrimp *Aristeus antennatus l*arvae. *PeerJ*. 2019; 7: e6063.

Cartes J, Demestre M. Estimating secondary production in the deep-water shrimp, *Aristeus antennatus* (Risso, 1816) in the Catalano-Balearic basin (Western Mediterranean). *Journal of Northwest Atlantic Fishery Science*. 2003; 31: 355–361.

Cartes JE, López-Pérez C, Carbonell A. Condition and recruitment of *Aristeus antennatus* at great depths (to 2,300 m) in the Mediterranean: Relationship with environmental factors. *Fisheries Oceanography.* 2018; 27(2): 114–126.

Castellón A, Font J, Garcıa E. The Liguro–Provençal–Catalan current. *Scientia Marina.* 1990; 54: 269–276.

Castille FL, Samocha TM, Lawrence AL, He H, Frelier P, Jaenike F. Variability in growth and survival of early postlarval shrimp (*Penaeus vannamei* Boone 1931). *Aquaculture*. 1993; 113(1): 65–81.

Catalán I, Tejedor A, Alemany F, Reglero P. Trophic ecology of Atlantic bluefin tuna *Thunnus thynnus* larvae. *Journal of Fish Biology*. 2011; 78: 1545–1560.

Cau A, Carbonell A, Follesa MC, Mannini A, Orsi Relini L, Politou CY, Ragonese S, Rinelli P. MEDITS-based information on the deep-water red shrimps *Aristaeomorpha foliacea* and *Aristeus antennatus* (Crustacea: Decapoda: Aristeidae). *Scientia Marina*. 2002; 66(S2): 103–124.

Cerrano C, Cardini U, Bianchelli S, Corinaldesi C, Pusceddu A, Danovaro R. Red coral extinction risk enhanced by ocean acidification. *Scientific Reports.* 2013; 3: 1457.

Chace FA. Plankton of the Bermuda Oceanographic expeditions, IX: The Bathypelagic Caridean Crustacea. *Zoologica.* 1940; 25(11): 117–209.

Chan TY, Cleva R, Chu KH. On the genus Trachysalambria Burkenroad, 1934 (Crustacea, Decapoda, Penaeidae), with descriptions f three new species. *Zootaxa*. 2016; 4150(3): 201–254.

Chen C, Liu H, Beardsley RC. An unstructured grid, finite-volume, three-dimensional, primitive equations ocean model: Application to coastal ocean and estuaries. *Journal of Atmospheric and Oceanic Technology*. 2003; 20(1): 159–186.

Choi, Jh, Hong SH. Larval development of the kishi velvet shrimp, *Metapenaeopsis dalei* (Rathbun) (Decapoda: Penaeidae), reared in the laboratory. *Fishery Bulletin.* 2001; 99(2); 275–291

Chong VC, Sasekumar A. Larval development of the fiddler shrimp, *Metapenaeopsis stridulans* (Alcock, 1905) (Decapoda: Penaeidae) reared in the laboratory. *Journal of Natural History.* 1994; 28(6): 1265–1285.

Choy SC. Larval development of *Penaeus* (*Melicertus*) *canaliculatus* (Oliver, 1811) reared in the laboratory (Decapoda, Natantia). *Crustaceana*. 1984; 46: 1–22.

Chu K. Larval rearing of the shrimps *Metapenaeus ensis* (de Haan) and *Penaeus chinensis* (Osbeck) on artificial feed. *Aquaculture Research*. 1991; 22: 473–479.

Chu K, Ovsianico-Koulikowsky N. Ontogenetic changes in metabolic activity and biochemical composition in the shrimp, *Metapenaeus ensis*. *Journal of Experimental Marine Biology and Ecology*. 1994; 183(1): 11–26.

Chu KH, Sze CC, Wong CK. Swimming behaviour during the larval development of the shrimp *Metapenaeus ensis* (De Haan, 1844) (Decapoda, Penaeidae). *Crustaceana.* 1996; 69(3): 368–378.

Clark MR, Althaus F, Schlacher TA, Williams A, Bowden DA, Rowden AA. The impacts of deep-sea fisheries on benthic communities: a review. *ICES Journal of Marine Science.* 2016; 73(S1): 51–69.

Clavel-Henry M, Solé J, Bahamon N, Briton F, Rotllant G, Company JB. Influence of the summer deep-sea circulations on passive drifts among the submarine canyons in the Northwestern Mediterranean Sea. *Ocean Science*. 2019*;* 15(6): 1745-1759.

Clavel-Henry M, Solé J, Kristiansen T, Bahamon N, Rotllant G, Company JB. Modelled buoyancy of eggs and larvae of the deep-sea shrimp *Aristeus antennatus* (Crustacean, Decapoda) in the northwestern Mediterranean Sea. *PLoS ONE*. 2020; 15(1): e0223396.

Cockcroft AC, Emmerson WD. The effect of temperature on the growth, development and survival of *Macropetasma africanus* (Balss) (Penaeoidea:Penaeidae) larvae reared in the laboratory. *Journal of Experimental Marine Biology and Ecology*. 1994; 84(3): 203–210.

Cockcroft AC. The larval development of *Macropetasma africanum* (Balss, 1913) (Decapoda, Penaeoidea) reared in the laboratory. *Crustaceana.* 1985; 49(1): 52–74.

Coll M, Steenbeek J, Solé J, Palomera I, Christensen W. Modelling the cumulative spatial–temporal effects of environmental drivers and fishing in a NW Mediterranean marine ecosystem. *Ecological Modelling*. 2016; 331: 100–114.

Company JB, Sardà F, Puig P, Cartes JE, Palanques A. Duration and timing of reproduction in decapod crustaceans of the NW Mediterranean continental margin: is there a general pattern? *Marine Ecology Progress Series.* 2003; 261: 201-216.

Company JB, Maiorano P, Tselepides A, Politou C-Y, Plaity W, Rotllant G, Sardà F. Deep-sea decapod crustaceans in the western and central Mediterranean Sea: preliminary aspects of species distribution, biomass and population structure. *Scientia Marina.* 2004; 68(3): 73–86.

Company JB, Puig P, Sardà F, Palanques A, Latasa M, Scharek R. Climate influence on deep sea populations. *PLoS ONE*. 2008; 3(1): e1431.

Condie S, Condie R. Retention of plankton within ocean eddies. *Global Ecology and Biogeography.* 2016; 25: 1264–1277.

Cook HL, Murphy MA. The culture of larval Penaeid shrimp. *Transactions of the American Fisheries Society*. 1969; 98(4): 751–754.

Coombs S, Boyra G, Rueda L, Uriarte A., Santos M, Conway D, Halliday N. Buoyancy measurements and vertical distribution of eggs of sardine (*Sardina pilchardus*) and anchovy (*Engraulis encrasicolus)*. *Marine Biology.* 2004; 145(5): 959–970.

Cooper AB, Weir K. A guide to fisheries stock assessment: from data to recommendations. University of New Hampshire, Sea Grant College Program; 2006.

Corell H, Moksnes P, Engqvist A, Döös K, Jonsson PR. Depth distribution of larvae critically affects their dispersal and the efficiency of marine protected areas. *Marine Ecology Progress Series.* 2012; 467: 29–46.

Courties C. Description des premiers stades larvaires de trois crevettes pénéides pêchées a Madagascar: *Penaeus indicus* H. Milne Edwards; P*enaeus semisulcatus* De Haan; *Metapenaeus monoceros* (Fabricius). *Cahiers Orstom Oceanographie.* 1976; 14: 49–70.

Cowen RK, Paris CB, Srinivasan A. Scaling of connectivity in marine populations. *Science.* 2006; 311(5760): 522–527.

Cowen RK, Lwiza KMM, Sponaugle S, Paris, CB, Olson DB. Connectivity of marine populations: open or closed? *Science.* 2008; 287(5454): 857–859.

Cowen RK, Sponaugle S. Larval dispersal and marine population connectivity. *Annual Review of Marine Science.* 2009; 1: 443–466.

Criales MM, McGowan MF. Horizontal and vertical distribution of Penaeidean and Caridean larvae and micronektonic shrimps in the Florida Keys. *Bulletin of Marine Science.* 1994; 54(3): 843–856.

Criales MM, Wang J, Browder J, Robblee MB. Tidal and seasonal effects on transport of pink shrimp postlarvae. *Marine Ecology Progress Series*. 2005; 286: 231–238.

Criales MM, Robblee MB, Browder JA. Cardenas H, Jackson TL. Field observations on selective tidal-stream transport for postlarval and juvenile pink shrimp in Florida Bay. *Journal of Crustacean Biology*. 2011; 31(1): 26–33.

Criales MM, Cherubin LM, Browder JA. Modeling larval transport and settlement of pink shrimp in South Florida: dynamics of behavior and tides. *Marine and Coastal Fisheries.* 2015; 7(1): 148–176.

Cripe G. Spawning and larval survival of the pink shrimp, *Penaeus duorarum*, in a small culture facility. *Journal of Applied Aquaculture.* 1997; 7(1): 29–41.

Crisp JA, Tweedley JR, D'souza FML, Partridge GJ, Moheimani NR. Larval development of the western school prawn *Metapenaeus dalli* Racek, 1957 (Crustacea: Decapoda: Penaeidae) reared in the laboratory. *Journal of Natural History.* 2016; 1–26.

Cromey CJ, Black KD. Modelling the impacts of finfish aquaculture. In: Hargrave B.T. (eds) Environmental Effects of Marine Finfish Aquaculture. Handbook of Environmental Chemistry. Springer, Berlin, Heidelberg. 2005; 5: p. 129–155.

Crosnier A, Forest J. Les crevettes profondes de l'Atlantique oriental tropical. Faune tropicale XIX. *ORSTOM*, Paris; 1973. 409 pp.

D'Onghia G, Capezzuto F, Mytilineou C, Maiorano P, Kapiris K, Carlucci R, Sion L, Tursi A. Comparison of the population structure and dynamics of *Aristeus antennatus* (Risso, 1816) between exploited and unexploited areas in the Mediterranean Sea. *Fisheries Research*. 2005; 76(1): 22–38.

D'Onghia G, Maiorano P, Capezzuto F, Carlucci R, Battista D, Giove A, Sion L, Tursi A. Further evidences of deep-sea recruitment of *Aristeus antennatus* (Crustacea: Decapoda) and its role in the population renewal on the exploited bottoms of the Mediterranean. *Fisheries Research*. 2009; 95(2–3): 236–245.

D'Ortenzio F, Iudicone D, de Boyer Montegut C, Testor P, Antoine P, Marullo S, Santoleri R, Madec G. Seasonal variability of the mixed layer depth in the Mediterranean Sea as derived from in situ profiles. *Geophysical Research Letter.* 2005; 32(12): 4 pp.

Dagestad K-F, Röhrs J. OpenDrift v1.0: a generic framework for trajectory modelling. *Geoscientific Model Development.* 2018; 11: 1405–1420.

Dallavalle JM. Micromeritics. The technology of fine particles. 2nd Ed. Pitman Publishing Corporation (Eds). Pitman, New York. 1948: 11–30.

Dall W, Hill BJ, Rothlisberg PC, Staples DJ. The Biology of the Penaeidae. *Advances in Marine Biology.* 1990; 27: 489 pp.

Dall W. Australian species of Aristeidae and Benthesicymidae (Penaeoidea: Decapoda). Memoirs of the Queensland Museum. 2001; 46(2): 409–441.

Danovaro R, Company JB, Corinaldesi C, D'Onghia G, Galil B, Gambi C, Gooday AJ, Lampadariou N, Luna GM, Morigi C, Olu K, Polymenakou P, Ramirez-Llodra E, Sabbatini A, Sardà F, Sibuet M, Tselepides A. Deep-Sea biodiversity in the Mediterranean Sea: the known, the unknown, and the unknowable. *PLoS ONE.* 2010; 5(8): e11832.

Debreu L, Marchesiello P, Penven P, Cambon G. Two-way nesting in split-explicit ocean models: algorithms, implementation and validation. *Ocean Modelling*. 2012; 49–50: 1–21.

Dee DP, Uppala SM, Simmons AJ, Berrisford P, Poli P, Kobayashi S, et al. The ERA-Interim reanalysis: configuration and performance of the data assimilation system. *Quaterly Journal of Royal Meteorological Society.* 2011; 137: 553–597.

Demestre M, Fortuño JM. Reproduction of the deep-water shrimp *Aristeus antennatus* (Decapoda: Dendrobranchiata). *Marine Ecology Progress Series.* 1992; 84(1): 41–51.

Demestre M, Lleonart J. Population dynamics of *Aristeus antennatus* (Decapoda: Dendrobranchiata) in the northwestern Mediterranean. *Scientia Marina.* 1993; 57: 183–189.

Devarajan K, Nayagam JS, Selvaraj V, Pillai NN. Larval development-IV. *Penaeus semisulcatus* de Haan. Larval development of Indian *Penaeus prawns*. *CMFRI Bulletin.* 1978; 28(4): 22–30.

Dibacco C, Levin L, Sala E. Connectivity in marine ecosystems: The importance of larval and spore dispersal. In K. Crooks & M. Sanjayan (Eds.), Connectivity Conservation (Conservation Biology, pp. 184–212). Cambridge: Cambridge University Press. 2006.

Ditty JG, Salas JA. Misidentification of mysis stages of *Xiphopenaeus kroyeri* (Heller, 1862) and *Rimapenaeus* Pérez-Fargante and Kensley, 1997 (Decapoda: Penaeidae) in the Western Atlantic. *Journal of Crustacean Biology*. 2012; 32(6): 931–939.

Dobkin S. Larvae of the pink shrimp (*Penaeus duorarum*). Presented at Proceedings of the Gulf and Caribbean Fisheries Institute 12, Miami (United States). 1960.

Dormann CF, McPherson JM, Araújo MB, Bivand R, Bolliger J, Carl G,Davies RG, Hirzel A, Jetz W, Kissling WD, Kühn I, Ohlemüller R, Peres-Neto PR, Reineking B, Schröder B, Schurr FM, Robert W. Methods to account for spatial autocorrelation in the analysis of species distributional data: a review. *Ecography.* 2007; 30: 609–628.

Dos Santos A. On the occurrence of larvae of *Parapenaeus longirostris* (Crustacea: Decapoda: Penaeoidea) off the Portuguese coast. *Journal of Natural History*. 1998; 32: 1519–1523.

Durrieu de Madron X, Radakovitch O, Heussner S, Loye-Pilot MD, Monaco A. Role of the climatological and current variability on shelf-slope exchanges of particulate matter: Evidence from the Rhône continental margin (NW Mediterranean). *Deep Sea Research Part I: Oceanographic Research Papers*. 1999; 46(9): 1513–1538.

Echevin V, Crépon M, Mortier L. Simulation and analysis of the mesoscale circulation in the northwestern Mediterranean Sea. *Annales Geophysicae, European Geosciences Union.* 2003; 21(1): 281–297.

Escudier R, Renault L, Pascual A, Brasseur P, Chelton D, Beuvier J. Eddy properties in the Western Mediterranean Sea from satellite altimetry and a numerical simulation. *Journal of Geophysical Research: Oceans.* 2016; 121(6): 3990–4006.

Espinosa DI, GarcÌa-Mederos A, Gonzalez JA, Santana JI, Tuset VM. Egg development and fecundity estimation in deep-sea red crab, *Chaceon affinis* (Geryonidae), off the Canary Islands (NE Atlantic). *Fisheries Research.* 2011; 109(2–3): 373–378.

Estévez A, Papandroulakis N, Wille M, Sorgeloos P. Early life stages and weaning. In: Lembo G., Mente E. (eds) Organic Aquaculture. Springer, Cham. 2019; p. 79–102.

Etter RJ, Bower AS. Dispersal and population connectivity in the deep North Atlantic estimated from physical transport processes. *Deep Sea Research Part I: Oceanographic Research Papers.* 2015; 104: 159–172.

Everett JD, Sebille E, Taylor MD, Suthers IM, Setio C, Cetina-Heredia P, Smith JA. Dispersal of eastern king prawn larvae in a western boundary current: new insights from particle tracking. *Fisheries Oceanography*. 2017; 26: 513– 525.

Ewald JJ. The laboratory rearing of pink shrimp, *Penaeus duorarum* Burkenroad. *Bulletin of Marine Science.* 1965; 15(2): 436–449.

Fairall CW, Bradley EF, Rogers DO, Edson JB, Young GS. Bulk parameterization of air-sea fluxes for tropical ocean-global atmosphere coupled-ocean atmosphere response experiment. *Journal of Geophysical Research.* 1996; 101: 3747–3764.

FAO 2010-2019. Fisheries and Aquaculture Department. About us - Fisheries and Aquaculture Department. In: FAO Fisheries and Aquaculture Department [online]. Rome. Updated 17 March 2017. [Cited 24 September 2019]. http://www.fao.org/fishery/

Fernández MV, Heras S, Maltagliati F, Turco A, Roldán MI. Genetic structure in the blue and red shrimp *Aristeus antennatus* and the role played by hydrographical and oceanographical barriers. *Marine Ecology Progress Series.* 2011; 421: 163–171.

Fernández MV, Heras SE, Viñas JP, Maltagliati F, Roldán MI. Multilocus comparative phylogeography of two Aristeid shrimps of high commercial interest (*Aristeus antennatus* and *Aristaeomorpha foliacea*) reveals different responses to past environmental changes. *PLoS ONE*. 2013; e59033.

Fernandez-Arcaya U, Ramirez-Llodra E, Aguzzi J, Allcock AL, Davies JS, Dissanayake A, Harris P, Howell K, Huvenne VAI, Macmillan-Lawler M, Martín J, Menot L, Nizinski M, Puig P, Rowden AA, Sanchez F, Van den Beld IMJ. Ecological role of submarine canyons and need for canyon conservation: a review. *Frontiers in Marine Science.* 2017; 4(5): 26 pp.

Fielder D, Greenwood, J, Ryall J. Larval development of the tiger prawn, *Penaeus esculentus* Haswell, 1879 (Decapoda, Penaeidae), reared in the laboratory. *Marine and Freshwater Research.* 1975; 26(2): 155–175.

Fiedler PC. Comparison of objective descriptions of the thermocline. *Limnology and Oceanography: Methods.* 2010; 8(6): 313–325.

Fiksen Ø, Jørgensen C, Kristiansen T, Vikebø F, Huse G. Linking behavioural ecology and oceanography: larval behaviour determines growth, mortality and dispersal. *Marine Ecology Progress Series*. 2007; 347: 195–206.

Flexas MM, Boyer DL, Espino M, Puigdefábregas J, Rubio A, Company JB. Circulation over a submarine canyon in the NW Mediterranean. *Journal of Geophysical Research.* 2008; 113: 12 pp.

Fogarty M, Botsford L. Population connectivity and spatial management of marine fisheries. *Oceanography.* 2007; 20(3): 112–123.

Follesa MC, Porcu C, Gastoni A, Mulas A, Sabatini A, Cau A. Community structure of bathyal decapod crustaceans off South-Eastern Sardinian deep-waters (Central-Western Mediterranean). *Marine Ecology*. 2009; 30(s1): 188–199.

Font J, Salat J, Tintoré J. Permanent features of the circulation in the Catalan Sea. *Oceanologica Acta.* 1988; 9: 51–57.

Forbes AT, Benfield MC. Tidal behaviour of post-larval penaeid prawns (Crustacea: Decapoda: Penaeidae) in a southeast African estuary. *Journal of Experimental Marine Biology and Ecology*. 1986; 102(1): 23–34.

Galarza JA, Carreras-Carbonell J, Macpherson E, Pascual M, Roques S, Turner GF, Rico C. The influence of oceanographic fronts and early-life-history traits on connectivity among littoral fish species. *Proceedings of the National Academy of Sciences*. 2009; 106(5): 1473–1478.

Gallardo B, Clavero M, Sánchez MI, Vilà M. Global ecological impacts of invasive species in aquatic ecosystems. *Global Change Biology*. 2016; 22: 151–163.

Gannier A, Praca E. SST fronts and the summer sperm whale distribution in the northwest Mediterranean Sea. *Journal of Marine Biological Association of the United Kingdom*. 2007; 87: 187–193.

García del Arco J, Company JB, Aguzzi J, Gorelli G. Integrating data from vessel monitoring system and fish landings in Mediterranean small fleets, using a PostgreSQL database with PostGIS extension. 7th International Workshop on Marine Technology : MARTECH 2016; Vilanova i la Geltrú 2016.

García-Ladona E, Castellón A, Font J, Tintore J. The Balearic current and volume transports in the Balearic basin. *Oceanologica Acta*. 1996; 19(5): 489–497.

Generalitat de Catalunya. Departament d'Agricultura, Ramaderia, Pesca i Alimentació. Estadístiques de pesca. Dades per llotges, Any 2018; Informació relacionada: Captures d'espècies per llotja. http://agricultura.gencat.cat/ca/ambits/pesca/ dar_estadistiques_pesca_subhastada/dar_captures_llotges/. Last view on October 24, 2019.

Generalitat Valenciana. Conselleria de Agricultura, Desarollo Rural, Emergencia Climática y transición Ecoloógica. Estadísticas agrarias y pesqueras. Principales especies desembarcadas 2018. http://www.agroambient.gva.es/es/estadisticas1. Last view on October 24, 2019.

Gopalakrishnan K. Larval rearing of red shrimp *Penaeus marginatus* (Crustacea). *Aquaculture*. 1976; 9: 145–154.

Gorelli G, Company JB, Sardà F. Management strategies for the fishery of the red shrimp *Aristeus antennatus* in Catalonia (NE Spain). *Marine Stewardship Council Science Series*. 2014; 2: 116–127.

Gorelli G, Blanco M, Sardà F, Carretón M, Company JB. Spatio-temporal variability of discards in the fishery of the deep-sea red shrimp *Aristeus antennatus* in the northwestern Mediterranean Sea: implications for management. *Scientia Marina*. 2016; 80(1): 79–88.

Gorelli G, Company JB, Bahamón N, Sardà F. Improving codend selectivity in the fishery of the deep-sea red shrimp *Aristeus antennatus* in the northwestern Mediterranean Sea. *Scientia Marina*. 2017; 81: 381–386.

Gorelli G. Developing a management strategy for the red shrimp *Aristeus antennatus* fishery in the northwestern Mediterranean Sea. Doctoral thesis, University of Barcelona, Spain. 2017.

Granata TC, Vidondo B, Duarte CM, Satta MP, Garcia M. Hydrodynamics and particle transport associated with a submarine canyon off Blanes (Spain), NW Mediterranean Sea. *Continental Shelf Research*. 1999; 19(10): 1249–1263.

Granata TC, Estrada M, Zika U, Merry C. Evidence for enhanced primary production resulting from relative vorticity induced upwelling. *Scientia marina*. 2004; 68(1): 113–119.

Gray CA, Kingsford MJ. Variability in thermocline depth and strength, and the relationships with vertical distributions of fish larvae and mesozooplankton in dynamic coastal waters. *Marine Ecology Progress Series*. 2003; 247: 221–224.

Grifoll M, Aretxabaleta A, Pelegrí J, Infantes M, C. Warner J, Sánchez−Arcilla A. Seasonal circulation over the Catalan inner−shelf (northwest Mediterranean Sea). *Journal of Geophysical Research: Oceans*. 2013; 118: 5844–5857.

Guijarro B, Massutí E, Moranta J, Díaz P. Population dynamics of the red shrimp *Aristeus antennatus* in the Balearic Islands (western Mediterranean): short spatio-temporal differences and influence of environmental factors. *Journal of Marine Systems*. 2008; 71(3): 385–402.

Gula J, Molemaker MJ, McWilliams JC. Topographic vorticity generation, submesoscale instability and vortex street formation in the Gulf Stream. *Geophysical Research Letters*. 2015; 42: 4054–4062.

Gula J, Molemaker MJ, McWilliams JC. Topographic generation of sub-mesoscale centrifugal instability and energy dissipation. *Nature Communication*. 2016; 7: 7 pp.

Gurney R. Larvae of decapod Crustacea. London: The Ray Society. 1942

Hassan H. Early developmental stages of *Metapenaeus affinis* (Decapoda, Penaeidae) reared in a laboratory. *ICES Journal of Marine Science*. 1980; 39(1): 30–43.

Hassan H. The larval development of *Penaeus semisulcatus* de Haan, 1850 (Decapoda, Penaeidae) reared in the laboratory. *Journal of Plankton Research.* 1982; 4(1): 1–17.

Hassan H. Larval development of *Parapenaeopsis stylifera* (H. Milne-Edwards) (Decapoda, Penaeidae), reared in a laboratory. *ICES Journal of Marine Science*. 1984; 41(3): 293–303.

Heldt JH. La Reproduction chez les crustacés décapodes de la famille des Pénéides. *Annales de l'Institut. Océanographique de Paris.* 1938; 28: 1–206.

Heldt JH. Contribution à l'étude de la biologie des crevettes pénéides *Aristeomorpha foliacea* (Risso) et *Aristeus antennatus* (Risso) (formes larvaires) *Bulletins de la Société des Sciences Naturelles de Tunisie*. 1955; VIII(1–2): 1–29.

Heng L, Rui-yu L. Comparative studies on the larval development of the penaeid shrimps, *Penaeus chinensis*, *P. merguiensis* and *P. penicillatus*. *Chinese Journal of Oceanology and Limnology*. 1994; 12(4): 295–307.

Herbaut C, Martel F, Crépon M. A sensitivity study of the general circulation of the western Mediterranean Sea. Part II: The response to atmospheric forcing. *Journal of Physical Oceanography.* 1997; 27: 2126–2145.

Herring PJ. Observations on the embryonic development of some deep-living decapod crustaceans, with particular reference to species of *Acanthephyra*. *Marine Biology*. 1974; 25(1): 25–33.

Hilário A, Metaxas A, Gaudron SM, Howell KL, Mercier A, Mestre NC, Ross RE, Thurnherr AM, Vraig Y. Estimating dispersal distance in the deep sea: challenges and applications to marine reserves. *Frontiers in Marine Science*. 2015; 2(6): 14 pp.

Hill AE, Brown J, Fernand L. The western Irish Sea gyre: a retention system for Norway lobster (*Nephrops norvegicus*)? *Oceanologica Acta.* 1996; 19(2–3): 357–368.

Hillman JR, Lundquist CJ, Thrush SF. The challenges associated with connectivity in ecosystem processes. *Frontiers in Marine Science.* 2018; 5(364): 9 pp.

Hinrichsen H-H, Dickey-Collas M, Huret M, Peck MA, Vikebø FB. Evaluating the suitability of coupled biophysical models for fishery management. *ICES Journal of Marine Science*. 2011; 68(7): 1478–1487.

Hixon M, Green S, Albins M, Akins J, Morris J. Lionfish: A major marine invasion. *Marine Ecology Progress Series*. 2016; 558; 161–165.

Holliday D, Beckley LE, Millar N, Olivar MP, Slawinski D, Feng M, Thompson PA. Larval fish assemblages and particle back-tracking define latitudinal and cross-shelf variability in an eastern Indian Ocean boundary current. *Marine Ecology Progress Series.* 2012; 460: 127–144.

Houpert L, Testor P, Durrieu de Madron X, Somot S, D'Ortenzio F, Estournel C, Lavigne H. Seasonal cycle of the mixed layer, the seasonal thermocline and the upper-ocean heat storage rate in the Mediterranean Sea derived from observations. *Progress in Oceanography*. 2015; 132: 333–352.

Hu ZY, Petrenko AA, Doglioli AM, Dekeyser I. Numerical study of eddy generation in the western part of the Gulf of Lion. *Journal of Geophysical Research: Oceans*. 2011; 116(C12): 727–745.

Hudinaga M. On the nauplius stage of *Penaeopsis monoceros* and *Penaeopsis affinis*. *Tokyo Scientific Fishery Association Proceedings.* 1941; 10(2): 282–287.

Hudinaga M. Reproduction, development and rearing of *Penaeus japonicus* Bate. *Japanese Journal of Zoology*. 1942; 10: 305–393.

Hudinaga M, Miyamura M. Breeding of the 'Kuruma' prawn (*Penaeus japonicus* Bate). *Journal of the Oceanographic Society of Japan.* 1962; 20: 694–706.

Hunter JR, Craig PD, Phillips HE. On the use of random walk models with spatially variable diffusivity. *Journal of Computational Physics*. 1993; 106(2): 366–376.

Iorio MI, Scelzo MA, Boschi EE. Desarrollo larval y postlarval del langostino *Pleoticus muelleri* Bate, mediante cultivos de laboratorio y muestras de planctón (Crust.Decap.Solonoceridae). *Scientia Marina.* 1990; 45(4): 329–342.

Johannesson K, Smolarz K, Grahn M, André C. The future of Baltic Sea populations: local extinction or evolutionary rescue? *Ambio.* 2011; 40(2): 179–190.

Jones GP, Planes S, Thorrold SR. Coral reef fish larvae settle close to home. *Current Biology.* 2005; 15(14): 1314–1318.

Jones MC, Cheung WWL. Multi-model ensemble projections of climate change effects on global marine biodiversity. *ICES Journal of Marine Science*. 2015; 72(3): 741–752.

Jones CE, Dagestad K-F, Breivik Ø, Holt B, Röhrs J, Christensen KH, Skrunes S. Measurement and modeling of oil slick transport. *Journal of Geophysical Research: Oceans*. 2016; 121(10): 7759–7775.

Jones DOB, Kaiser S, Sweetman AK, Smith CR, Menot L, Vink A, Trueblood D, Greinert J, Billett DSM, Martinez Arbizu P, Radziejewska T, Singh R, Ingole B, Stratmann T, Simon-Lledó E, Durden JM, Clark MR. Biological responses to disturbance from simulated deep-sea polymetallic nodule mining. *PLoS ONE*. 2017; 12(2): e0171750.

Jorda G, Flexas MM, Espino M, Calafat A. Deep flow variability in a deeply incised Mediterranean submarine valley (Blanes canyon). *Progress in Oceanography.* 2013; 118: 47–60.

Jordi A, Basterretxea G, Orfila A, Tintoré J. Analysis of the circulation and shelf-slope exchanges in the continental margin of the northwestern Mediterranean. *Ocean Science*. 2006; 2(2): 173–181.

Karimova S. Observation of the surface circulation of the Mediterranean Sea from space. Paper presented at the ESA Living Planet Symposium, Netherlands. 2016

Khafage AR, Abdel Razek FA, Gobashy AFA, Taha SM. Early larval development of Egyptian metapenaeid shrimp, *Metapenaeus Monoceros* (Fabricius) reared under laboratory conditions. *Egyptian Journal of Aquatic Research.* 2009; 35(3): 371–383.

Kitani H. Larval development of the pink shrimp *Penaeus duorarum* BURKENROAD reared in the laboratory and the comparison with earlier descriptions. *Nippon Suisan Gakkaishi.* 1985; 51(8): 1239–1248.

Kitani H. Larval development of naupliar stage of the northern brown shrimp *Penaeus aztecus* Ives and comparison with its earlier description. *Bulletin of the Japanese Society of Scientific. Fisheries.* 1986a; 52: 1285–1288.

Kitani H. Larval development of the blue shrimp *Penaeus stylirostris* STIMPSON reared in the laboratory. *Nippon Suisan Gakkaishi.* 1986b; 52(7): 1121–1130.

Kitani H. Larval development of the white shrimp *Penaeus vannamei* BOONE reared in the laboratory and the statistical observation of its naupliar stages. *Nippon Suisan Gakkaishi.* 1986c; 52(7): 1131–1139.

Kitani H. Larval Development of the western white shrimp *Penaeus occidentalis* reared in the laboratory. *Fisheries Science.* 1996; 62(6): 883–891.

Kitani H. Larval Development of the crystal shrimp *Penaeus* (*Farfantepenaeus*) *brevirostris* under laboratory conditions. *Fisheries Science.* 1997; 63(2): 218–227.

Kitani H, Alvarado N. The larval development of the Pacific brown shrimp *Peneaus californiensis* HOLMES reared in the laboratory. *Nippon Suisan Gakkaishi.* 1982; 48(3): 375–389.

Klaoudatos S. Breeding of *Penaeus kerathurus* larvae in the laboratory as a proposition to culture them on a commercial scale. *Thalassografika.* 1978; 2(1): 99–113.

Komai T, Amaoka K. Records of some rare deep-sea Decapod Crustaceans from the Okhotsk coast of Hokkaido (Caridea and Anomura). *Bulletin of the Faculty of Fisheries, Hokkaido University*. 1989; 40(4): 278–291.

Koamai T. Deep-sea shrimps of the family Aristeidae (Decapoda: Dendrobranchiata) from northern Japan, with the description of a new species of the genus *Aristeus*. *Crustacean Research.* 1993; 22: 21–34.

Kool JT, Huang Z, Nichol SL. Simulated larval connectivity among Australian southwest submarine canyons. *Marine Ecology Progress Series.* 2015; 539: 77–91.

Korres G, Pinardi N, Lascaratos A. The ocean response to low-frequency interannual atmospheric variability in the Mediterranean Sea. Part I: Sensitivity experiments and energy analysis. *Journal of Climate*. 2000; 13: 705–731.

Kough AS, Paris CB, Butler IV MJ. Larval connectivity and the international management of fisheries. *PLoS ONE*. 2013; 8(6):e64970.

Kough AS, Paris CB, Behringer DC, Butler MJ. Modelling the spread and connectivity of waterborne marine pathogens: the case of PaV1 in the Caribbean, *ICES Journal of Marine Science*. 2015; 72(S1): 139–146.

Krantz GE, Norris JP. Culture of pink shrimp, *Penaeus duorarum* Ives at the Turkey Point Experimental mariculture laboratory. *Sea Grant Technical Bulletin*. 1976; 36: 41 pp.

Kristiansen T, Jørgensen C, Lough R, Vikebø F, Fiksen Ø. Modeling rule-based behavior: habitat selection and the growth-survival trade-off in larval cod. *Behavioral Ecology.* 2009; 20(3): 490–500.

Krüger L, Ramos JA, Xavier JC, Grémillet D, González-Solís J, Kolbeinsson Y, Militão T, Navarro J, Petry MV, Phillips RA, Ramírez I, Reyes-González JM, Ryan PG, Sigurðsson IA, Van Sebille E, Wanless RM, Paiva VH. Identification of candidate pelagic marine protected areas through a seabird seasonal-, multispecific- and extinction risk-based approach. *Animal Conservation*. 2017; 20(5): 409–424.

Kumlu M, Eroldogan OT. Effects of temperature and substrate on growth and survival of *Penaeus semisulcatus* (Decapoda: Penaeidae) postlarvae. *Turkish Journal of Zoology*. 2000; 24: 337–341.

Kumlu M, Eroldogan OT, Aktas M, Sagˇlamtimur B. Larval growth, survival and development of *Metapenaeus monoceros* (Fabricius) cultured in different salinities. *Aquaculture Research*. 2001; 32(2): 81–86.

Kungvankij P, Ruangpanit N, Dangsakul S, Chirastit C. An experiment on artificial propagation of *Penaeus semisulcatus* de Haan. *Contribution No 2, Phuket Marine Fisheries Station.* 1972; 23: 36 pp..

Kunze HB, Morgan S, Lwiza KM. Field test of the behavioral regulation of larval transport. *Marine Ecology Progress Series.* 2013; 487: 71–87.

Kurata H, Vanitchkul P. Larvae and early postlarvae of a shrimp, *Metapenaeus burkenroadi*, reared in the laboratory. *Bulletin of the Nansei Fisheries Research Laboratory.* 1974; 7: 69–84.

Lafuente J, Jurado J, Lucaya N, Yanez M, Garcia J. Circulation of water masses through the Ibiza Channel. *Oceanologica acta.* 1995; 18(2): 245–254.

Landeira JM, Lozano-Soldevilla F, Hernaández-León S, Barton ED. Horizontal distribution of invertebrate larvae around the oceanic island of Gran Canaria: the effect of mesoscale variability. *Scientia Marina*. 2009; 73(4): 761–771.

Landeira JM, Brochier T, Mason E, Lozano-Soldevilla F, Hernández-León S, Barton ED. Transport pathways of decapod larvae under intense mesoscale activity in the Canary-African coastal transition zone: implications for population connectivity. *Scientia Marina*. 2017; 81(3): 17 pp.

Lapouyade A, Durrieu de Madron X. Seasonal variability of the advective transport of suspended particulate matter and organic carbon in the Gulf of Lions (NW Mediterranean). *Oceanologica Acta.* 2001;24(3): 295–312.

Large W, McWilliams J, Doney S. Oceanic vertical mixing: a review and a model with a nonlocal boundary layer parameterization. *Reviews of Geophysics.* 1994; 32: 363–403.

La Violette PE. Overview of the major forcings and water masses of the western Mediterranean Sea. In Seasonal and interannual variability of the Western Mediterranean Sea, La Violette PE (Ed.). 1995: 1–11.

Lebreton LCM, Greer SD, Borrero JC. Numerical modelling of floating debris in the world's oceans. *Marine Pollution Bulletin*. 2012; 64(3): 653–661.

Lee BD, Lee TY. Studies on the larval development of *Metapenaeus joyneri* (Miers). *Publication of the Marine Laboratory pf the Pusan Fisheries College.* 1969; 2: 19–25.

Leis J, Lockett M. Localization of reef sounds by settlement-stage larvae of coral-reef fishes (Pomacentridae). *Bulletin of Marine Science.* 2005; 76: 715–724.

Leis JM. Ontogeny of behaviour in larvae of marine demersal fishes. *Ichthyological Research.* 2010; 57(4): 325–342.

Lemos D, Phan NV. Ontogenetic variation in metabolism, biochemical composition and energy content during the early life stages of *Farfantepenaeus paulensis* (Crustacea: Decapoda: Penaeidae). *Marine Biology.* 2001; 138(5): 985–997.

Leo FCD, Smith CR, Rowden AA, Bowden DA, Clark MR. Submarine canyons: hotspots of benthic biomass and productivity in the deep sea. *Proceedings of the Royal Society B: Biological Sciences.* 2010; 277(1695): 2783–2792.

Leong PKK, Chu KH, Wong CK. Larval development of *Metapenaeus ensis* (de Haan) (Crustacea: Decapoda: Penaeidae) reared in the laboratory. *Journal of Natural History.* 1992; 26(6): 1283–1304.

Lett C, Verley P, Mullon C, Parada C, Brochier T, Penven P, Blanke BA. Lagrangian tool for modelling ichthyoplankton dynamics. *Environmental Modelling and Software.* 2008; 23(9): 1210–1214.

Levin LA, Bridges TS. Pattern and diversity in reproduction and development. McEdward L, editor. Boca Raton, FL: CRC Press, 1995.

Levin LA. Recent progress in understanding larval dispersal: new directions and digressions. *Integrative and Comparative Biology*. 2006; 46(3): 282–297.

Lindley JA. Eggs and their incubation as factors in the ecology of planktonic crustacea. *Journal of Crustacean Biology*. 1997;17(4):569–576.

Lindner MJ, Cook HL. Synopsis of biological data on the white shrimp *Penaeus setiferus* (Linnaeus) 1767. *FAO Fisheries Report.* 1970; 4(57), 1439–1468.

Lloyd ÑJ, Metaxas A, deYoung B. Patterns in vertical distribution and their potential effects on transport of larval benthic invertebrates in a shallow embayment. *Marine Ecology Progress Series*. 2012; 469: 37–52.

Lodge M, Johnson D, Le Gurun G, Wengler M, Weaver P, Gunn V. Seabed mining: international seabed authority environmental management plan for the Clarion–Clipperton Zone. A partnership approach. *Marine Policy.* 2014; 49: 66–72.

López-García MJ, Millot C, Font J, García-Ladona E. Surface circulation variability in the Balearic Basin. *Journal of Geophysical Research: Oceans.* 1994; 99(C2): 3285–3296.

Lopez-Fernandez P, Calafat A, Sanchez-Vidal A, Canals M, Flexas MM, Cateura J, Company JB. Multiple drivers of particle fluxes in the Blanes submarine canyon and southern open slope: Results of a year round experiment. *Progress in Oceanography. 2013;* 118: 95–107.

Lowe WH, Allendorf FW. What can genetics tell us about population connectivity. *Molecular Ecology.* 2010; 19: 3038–3051.

Lumare G, Gozzo S. *O*sservazioni sulla morfogenesi del nauplio di *Penaeus kerathurus* nelle sue relazioni con *Penaeus japonicus*. Paper presented at the Atti della Societa Peloritana di Scienze Fisiche Matematiche e Naturali., 165/175, 3/4, CNR-Roma. 1973.

Ma KY, Chan T, Chu KH. Phylogeny of penaeoid shrimps (Decapoda: Penaeoidea) inferred from nuclear protein-coding genes. *Molecular phylogenetics and evolution*. 2009; 53(1): 45–55.

Macías D, Catalán IA, Solé J, Morales-Nin B, Ruiz J. Atmospheric-induced variability of hydrological and biogeochemical signatures in the NW Alboran Sea. Consequences for the spawning and nursery habitats of European anchovy. *Deep Sea Research Part I: Oceanographic Research Papers*. 2011; 58(12): 1175–1188.

Macías D, Stips A, Garcia-Gorriz E. The relevance of deep chlorophyll maximum in the open Mediterranean Sea evaluated through 3D hydrodynamic-biogeochemical coupled simulations. *Ecological Modelling.* 2014; 281: 26–37.

Mamouridis V, Maynou F, G: AP. Analysis and standardization of landings per unit effort of red shrimp *Aristeus antennatus* from the trawl fleet of Barcelona (NW Mediterranean). *Scientia Marina*. 2014; 78(1): 7–16.

Manca B, Burca M, Giorgetti A, Coatanoan C, Garcia MJ, Iona A. Physical and biochemical averaged vertical profiles in the Mediterranean regions: An important tool to trace the climatology of water masses and to validate incoming data from operational oceanography. *Journal of Marine Systems.* 2004; 48(1–4): 83–116.

Mancho AM, Hernández-García E, Small D, Wiggins S, Fernández V. Lagrangian transport through an ocean front in the Northwestern Mediterranean Sea. *Journal of Physical Oceanography.* 2008; 38: 1222–1237.

Manush SM, Pal AK, Das T, Mukherjee SC. The influence of temperatures ranging from 25 to 36°C on developmental rates, morphometrics and survival of freshwater prawn (*Macrobrachium rosenbergii)* embryos. *Aquaculture.* 2006; 256(1): 529–536.

Mariani P, MacKenzie BR, Iudicone D, Bozec A. Modelling retention and dispersion mechanisms of bluefin tuna eggs and larvae in the northwest Mediterranean Sea. *Progress in Oceanography*. 2010; 86(1–2): 45–58.

Maris RC. Larvae of *Xiphopenaeus kroyeri* (Heller, 1862) (Crustacea, Decapoda, Penaeidae) from offshore waters of Virginia, USA. *Proceedings of the Biological Society of Washington*. 1986; 99: 600–603.

Marra A, Mona S, Sà RM, D'Onghia G, Maiorano P. Population genetic history of *Aristeus antennatus* (Crustacea: Decapoda) in the western and central Mediterranean Sea. *PLoS ONE*. 2015; 10(3): e0117272.

Martin JW, Criales MM, Dos Santos A. Dendrobranchiata. In: Martin JW, Høeg JT, Olesen J, editors. Atlas of Crustacean Larvae. Baltimore, MD: Johns Hopkins University Press; 2014. 235 pp.

Martín P, Muntadas A, de Juan S, Sánchez P, Demestre M. Performance of a northwestern Mediterranean bottom trawl fleet: How the integration of landings and VMS data can contribute to the implementation of ecosystem-based fisheries management. *Marine Policy*. 2014; 43: 112–121.

Matsuno S, Abe Y. Larval recruitment and distribution of three small penaeid shrimp species in the Iyo-Nada region off Yamaguchi prefecture. *Bulletin of Yamaguchi Prefectural Fisheries Research Center.* 2006; 4: 87–102.

Maynou F. Environmental causes of the fluctuations of red shrimp (*Aristeus antennatus*) landings in the Catalan Sea. *Journal of Marine Systems*. 2008; 71: 294–302.

McManus MA, Woodson CB. Plankton distribution and ocean dispersal. *The Journal of Experimental Biology*. 2012; 215(6): 1008–1016.

McVeigh DM, Eggleston DB, Todd AC, Young CM, He R. The influence of larval migration and dispersal depth on potential larval trajectories of a deep-sea bivalve. *Deep-Sea Research Part I: Oceanographic Research Papers*. 2017; 127: 57–64.

Meager JJ, Vance DJ, Loneragan NR, Williamson I. Seasonal variation and environmental influences on juvenile banana prawn (*Penaeus merguiensis*) abundance in a subtropical estuary (Logan River) of eastern Australia. *Estuarine, Coastal and Shelf Science*. 2003; 57(4): 569–576.

Medina A, Aranda G, Gherardi S, Santos A, Mèlich B, Lara M. Assessment of spawning of Atlantic bluefin tuna farmed in the western Mediterranean Sea. *Aquaculture Environment Interactions.* 2016; 8: 89–98.

Megrey BA, Hinckley S. Effect of turbulence on feeding of larval fishes: a sensitivity analysis using an individual-based model. *ICES Journal of Marine Science.* 2001; 58: 1015–10129.

Metaxas A. Behaviour in flow: Perspectives on the distribution and dispersion of meroplanktonic larvae in the water column. *Canadian Journal of Fisheries and Aquatic Sciences.* 2001; 58: 86–98.

Metaxas A, Lacharité M, de Mendonça S. Hydrodynamic connectivity of habitats of deep-water corals in Corsair Canyon, Northwest Atlantic: A case for cross-boundary conservation. *Frontiers in Marine Science.* 2019; 6: 19 pp.

Mileikovsky SA. Types of larval development in marine bottom invertebrates, their distribution and ecological significance: a re-evaluation. *Marine Biology*. 1971; 10(3): 193–213.

Millot C. Circulation in the Western Mediterranean Sea. *Journal of Marine Systems.* 1999; 20(1–4): 423–442.

Millot C, Taupier-Letage I. Circulation in the Mediterranean Sea. In: Saliot A, editor. The Mediterranean Sea. Berlin, Heidelberg: Springer Berlin Heidelberg; 2005: 29–66.

Mohamed KH, Vedavyasa Rao P, George MJ. Postlarvae of penaeid prawns of southwest coast of India with a key to their identification. Paper presented at the FAO World scientific conference on the biology and culture of shrimps and prawns, Mexico. 1967.

Molcard A, Pinardi N, Iskandarani M, Haidvogel DB. Wind driven general circulation of the Mediterranean Sea simulated with a spectral element ocean model. *Dynamics of Atmospheres and Oceans*. 2002; 35(2): 97–130.

Molen (van der) J, García-García LM, Whomersley P, Callaway A, Posen PE, Hyder K. Connectivity of larval stages of sedentary marine communities between hard substrates and offshore structures in the North Sea. *Scientific Reports*. 2018; 8(1): 14 pp.

Monismith SG, Fong DA. A note on the potential transport of scalars and organisms by surface waves. *Limnology and Oceanography.* 2004; 49(4): 1214–1217.

Montefalcone M, Parravicini V, Vacchi M, Albertelli G, Ferrari M, Morri C, Bianchi CN. Human influence on seagrass habitat fragmentation in NW Mediterranean Sea. *Estuarine, Coastal and Shelf Science*. 2010; 86(2): 292–298.

Montero JT, Chesney TA, Bauer JR, Froeschke JT, Graham J. Brown shrimp (*Farfantepenaeus aztecus*) density distribution in the Northern Gulf of Mexico: an approach using boosted regression trees. *Fisheries Oceanography*. 2016; 25(3): 337–348.

Morel-Journel T, Piponiot C, Vercken E, Mailleret L. Evidence for an optimal level of connectivity for establishment and colonization. *Biology Letters*. 2016; 12(11): 4 pp.

Mori M, Corney SP, Melbourne-Thomas J, Welsford DC, Klocker A, Ziegler PE. Using satellite altimetry to inform hypotheses of transport of early life stage of Patagonian toothfish on the Kerguelen Plateau. *Ecological Modelling.* 2016; 340: 45–56.

Motoh H. Larvae of Decapod Crustacea of the Philippines - III. Larval development of the giant tiger prawn *Penaeus monodon* reared in the laboratory. *Bulletin of Japanese Society of Scientific Fisheries.* 1979; 45(10): 1201–1216.

Motoh H, Buri P. Larvae of decapod crustacea of the Philippines. 4. Larval development of the banana prawn, *Penaeus merguiensis* reared in the laboratory. *Bulletin of Japanese Society of Scientific Fisheries*. 1979; 45: 1217–1235.

Moum JN, Smyth WD. Upper ocean mixing processes. In: Steele JH, editor. Encyclopedia of ocean sciences (Second Edition). Oxford: Academic Press; 2001. p. 185–191.

Munk P, Larsson PO, Danielssen DS, Moksness E. Variability in frontal zone formation and distribution of gadoid fish larvae at the shelf break in the northeastern North Sea. *Marine Ecology Progress Series.* 1999; 177: 221–233.

Museu de la Pesca. Distribució de les larves de gamba vermella desde el Golf de València fins al Golf de Lleó. Pesca i Ciencia 2019. M. Carretón. Youtube. 2019a.

Museu de la Pesca. CONECTA-GEN. Demografía genética de *Aristeus antennatus* en Palamós: resultados preliminares. Pesca i Ciencia 2019. M. Roldán. Youtube. 2019b.

Muthu MS, Pillai NN, George KV. On the spawning and the rearing of *Penaeus indicus* in the laboratory with a note on the eggs and larvae. *Indian Journal of Fisheries.* 1974; 21(2): 571–574

Muthu MS, Pillai NN, George KV.(1979a). Larval development -*Metapenaeus affinis* (H. Milne Edwards). *CMFRI Bulletin.* 1979a; 28: 40–49.

Muthu MS, Pillai NN, George KV. Larval development - *Metapenaeus dobsoni* (Miers). *CMFRI Bulletin.* 1979b; 28: 30–39.

Muthu MS, Pillai NN, George KV. Larval development - *Parapenaeopsis stylifera* (H. Milne Edwards). *CMFRI Bulletin.* 1979c; 28: 65–74.

Myksvoll MS, Jung K-M, Albretsen J, Sundby S. Modelling dispersal of eggs and quantifying connectivity among Norwegian coastal cod subpopulations. *ICES Journal of Marine Science*. 2013; 71(4): 957–969.

Nandakumar G, Pillai NN, Telang KY, Balachandran K. Larval development of *Metapenaeus moyebi* (Kishinouye) reared in the laboratory. *Journal of the Marine Biological Association of India.* 1989; 31: 86–102.

Nandakumar G. Reproductive biology of the speckled shrimp *Metapenaeus monoceros* (Fabricius). *Indian Journal of Fisheries.* 2001; 48(1): 1–8

Nencioli F, Dong C, Dickey T, Washburn L, McWilliams JC. A vector geometry–based eddy detection algorithm and its application to a high-rResolution numerical model product and high-frequency radar surface velocities in the Southern California Bight. *Journal of Atmospheric and Oceanic Technology.* 2010; 27(3): 564–579.

Nichols C, Herman J, Gaggiotti OE, Dobney KM, Parsons K, Hoelzel AR. Genetic isolation of a now extinct population of bottlenose dolphins (*Tursiops truncatus*). *Proceedings of the Royal Society: Biological Sciences.* 2007; 274(1618): 1611–1616.

Nicolle A, Moitié R, Ogor J, Dumas F, Foveau A, Foucher E, Thiébaut E. Modelling larval dispersal of *Pecten maximus* in the English Channel: a tool for the spatial management of the stocks. *ICES Journal of Marine Science.* 2017; 74(6): 1812–1825.

Niu C, Lee D, Goshima S, Nakao S. Effects of temperature on food consumption, growth and oxygen consumption of freshwater prawn *Macrobrachium rosenbergii* (de Man 1879) postlarvae. *Aquaculture Research.* 2003; 34(6): 501–506.

North EW, Hood RR, Zhong L, Li M, Gross TF. The influence of mixing processes and behavior on larval transport and mortality estimates in a stratified ind- and tidally-forced system. ICES CM. 2004; /J:10/ P:24:13.

North E, Schlag Z, Hood R, Zhong L, Li M, Gross T. Modeling dispersal of *Crassostrea ariakensis* oyster larvae in Chesapeake Bay. Final report to Maryland Department of Natural Resources. 2006: 77 pp.

North EW. Vertical swimming behavior influences the dispersal of simulated oyster larvae in a coupled particle-tracking and hydrodynamic model of Chesapeake Bay. *Marine Ecology Progress Series*, 2008; 359: 99 pp.

North EW, Gallego A, Petitgas P, Ådlandsvik B, Bartsch J, Brickman D, et al. Manual of recommended practices for modelling physical-biological interactions during fish early life. *ICES Cooperative Research Report*. 2009.

O'Connor MI, Bruno JF, Gaines SD, Halpern BS, Lester SE, Kinlan BP, Weiss JM. Temperature control of larval dispersal and the implications for marine ecology, evolution, and conservation. *Proceedings of the National Academy of Sciences.* 2007; 104(4): 1266–1271.

Ogburn MB, Criales MM, Thompson RT, Browder JA. Endogenous swimming activity rhythms of postlarvae and juveniles of the penaeid shrimp *Farfantepenaeus aztecus*, *Farfantepenaeus duorarum,* and *Litopenaeus setiferus*. *Journal of Experimental Marine Biology and Ecology.* 2013; 440: 149-155.

Oka M. Studies on *Penaeus orientalis*, Kishinouye V. Fertilization and development. *Bulletin of the Faculty of Fisheries, Nagasaki University.* 1967; 23: 71–87.

Okubo A. Oceanic diffusion diagrams. *Deep Sea Research and Oceanographic Abstracts*. 1971;18(8):789–802.

Olivar MP, Emelianov M, Villate F, Uriarte I, Maynou F, Álvarez I, Morote E. The role of oceanographic conditions and plankton availability in larval fish assemblages off the Catalan coast (NW Mediterranean). *Fisheries Oceanography*, 2010; 19: 209–229.

Orsi Relini L, Relini G. Long term observations of *Aristeus antennatus*: Size-structures of the fished stock and growth parameters, with some remarks about the 'recruitment'. In: Lleonart J, editor. Dynamique des populations marines. Cahiers Options Méditerranéennes. 35: Zaragoza : CIHEAM; 1998: 311–322.

Orsi Relini L, Mannini A, Relini G. Updating knowledge on growth, population dynamics, and ecology of the blue and red shrimp, *Aristeus antennatus* (Risso, 1816), on the basis of the study of its instars. *Marine Ecology.* 2013; 34(1): 90–102.

Ospina-Álvarez A, Palomera I, Parada C. Changes in egg buoyancy during development and its effects on the vertical distribution of anchovy eggs. *Fisheries Research.* 2012a; 117–118: 86–95.

Ospina-Álvarez A, Parada CE, Palomera I. Vertical migration effects on the dispersion and recruitment of European anchovy larvae: From spawning to nursery areas. *Ecological Modelling*. 2012b; 231: 65–79.

Ospina-Álvarez A, Bernal M, Catalán IA, Roos D, Bigo J-L, Palomera I. Modeling fish egg production and spatial distribution from acoustic data: A step forward into the analysis of recruitment. *PLoS ONE*. 2013; 8(9): e73687.

Ospina-Álvarez A, Catalán IA, Bernal M, Roos D, Palomera I. From egg production to recruits: Connectivity and inter-annual variability in the recruitment patterns of European anchovy in the northwestern Mediterranean. *Progress in Oceanography*. 2015; 138(PartB): 431–447.

Palacios E, Perez-Rostro CI, Ramirez JL, Ibarra AM, Racotta IS. Reproductive exhaustion in shrimp (*Penaeus vannamei*) reflected in larval biochemical composition, survival and growth. *Aquaculture.* 1999; 171(3–4): 309–321.

Palanques A, García-Ladona E, Gomis D, Martín J, Marcos M, Pascual A, Puig P, Gili J-M, Emelianov M, Monserrat S, Guillén J, Tintoré J, Segura M, Jordi A, Basterretxea G, Font J, Blasco D, Pagès F. General patterns of circulation, sediment fluxes and ecology of the Palamós (La Fonera) submarine canyon, northwestern Mediterranean. *Progress in Oceanography*. 2005; 66(2–4): 89–119.

Palmas F, Olita A, Addis P, Sorgente R, Sabatini A. Modelling giant red shrimp larval dispersal in the Sardinian seas: Density and connectivity scenarios. *Fisheries Oceanography*. 2017; 26; 364–378.

Pan CH, Yu HP. Larval development of the red tailed prawn, *Penaeus penicillatus* reared in the laboratory. *Journal of the Fisheries Society of Taiwan.* 1990; 17(4): 247–265.

Pandian TJ. Reproduction and development in Crustacea. In: CRC Press Taylor and Francis group, editors. Reproduction and development in aquatic invertebrates; 2016: 27–69.

Parada C, van der Lingen C, Mullon C, Penven P. Modelling the effect of buoyancy on the transport of anchovy (*Engraulis capensis*) eggs from spawning to nursery grounds in the southern Benguela: An IBM approach. *Fisheries Oceanography.* 2003; 12(3): 170–184.

Parada C, Colas F, Soto-Mendoza S, Castro L. Effects of seasonal variability in across- and alongshore transport of anchoveta (*Engraulis ringens*) larvae on model-based pre-recruitment indices off central Chile. *Progress in Oceanography.* 2012; 92–95: 192–205.

Paradinas Aranjuelo I. Species distribution modelling in fisheries science. PhD thesis, Universitat de València, 2017.

Paris CB, Helgers J, van Sebille E, Srinivasan A. Connectivity Modeling System: A probabilistic modeling tool for the multi-scale tracking of biotic and abiotic variability in the ocean. *Environmental Modelling and Software.* 2013; 42: 47–54.

Pascual A, Buongiorno Nardelli B, Larnicol G, Emelianov M, Gomis D. A case of an intense anticyclonic eddy in the Balearic Sea (western Mediterranean). *Journal of Geophysical Research.* 2002; 107(C11): 3183.

Paulinose VT. Larval and postlarval stages of Sicyonia H. M. Edwards (Decapoda, Penaeidea: Sicyoniidae). *Mahasagar-Bulletin of the National Institute of Oceanography*. 1982a; 15(4): 231–235.

Paulinose VT. Key to the identification of larvae and postlarvae of the penaeid prawns (Decapoda, Penaeidea) of the Indian Ocean. *Mahasagar-Bulletin of the National Institute of Oceanography*. 1982b; 15: 223–229.

Peck MA, Kühn W, Hinrichsen H-H, Pohlmann T. Inter-annual and inter-specific differences in the drift of fish eggs and yolksac larvae in the North Sea: A biophysical modeling approach. *Scientia Marina.* 2009; 73(S1): 23–36.

Peixoto S, Wasielesky W, Martino RC, Milach Â, Soares R, Cavalli RO. Comparison of reproductive output, offspring quality, ovarian histology and fatty acid composition between similarly-sized wild and domesticated. *Aquaculture.* 2008; 285(1–4): 201–206.

Peñuelas J, Ciais P, Canadell JG, Janssen, IA, Fernández-Martínez M, Carnicer J, Obersteiner M, Piao S, Vautard R, Sardans J. Shifting from a fertilization-dominated to a warming-dominated period. *Nature Ecology and Evolution.* 2017;1: 1438–1445.

Penven P, Marchesiello P, Debreu L, Lefèvre J. Software tools for pre- and post-processing of oceanic regional simulations. *Environmental Modelling and Software*. 2008; 23(5): 660–662.

Pepin P. Effect of temperature and size on development, mortality, and survival rates of the pelagic early life history stages of marine fish. *Canadian Journal of Fisheries and Aquatic Sciences.* 1991; 48(3): 503–518.

Pere O. ¿Qué pudo ocurrir para que en julio de 2016 desapareciera la gamba en los caladeros del norte de Mallorca?. El mar, la pesca y la investigación marina. 2016; 46. http://pereoliver.com.

Pérez-Morales A, Band-Schmidt CJ, Martínez-Díaz SF. Mortality on zoea stage of the Pacific white shrimp *Litopenaeus vannamei* caused by *Cochlodinium polykrikoides* (Dinophyceae) and *Chattonella* spp. (Raphidophyceae). *Marine Biology*. 2017;164(3): 10 pp.

Perry RI, Harding GC, Loder JW, Tremblay MJ, Sinclair MM, Drinkwater KF. Zooplankton distributions at the Georges Bank frontal system: retention or dispersion? *Continental Shelf Research.* 1993; 13(4): 357–383.

Pickett T, David AA. Global connectivity patterns of the notoriously invasive mussel, *Mytilus galloprovincialis* Lmk using archived CO1 sequence data. *BMC Research Notes.* 2018; 11(231): 7 pp.

Pineda J, Hare JA, Sponaugle S. Larval dispersal and transport in the coastal ocean and consequences for population connectivity. *Oceanography.* 2007; 20: 22–39.

Pinot JM, López-Jurado JL, Riera M. The CANALES experiment (1996–1998). Interannual, seasonal and mesoscale variability of the circulation in the Balearic Channels. *Progress in Oceanography.* 2002; 55: 335–370.

Pinto LG, Ewald JJ. Desarollo larval del camarón blanco, *Penaeus schmitti* Burkenroad, 1936. *Boletín del Centro de Investigaciones Biologicas de la Universidad del Zulia.* 1974; 12: 61 pp.

Ponce MAG, Gracia A. Vertical distribution of shrimp larvae of the superfamily Penaeoidea during a diurnal cycle in the southern Gulf of Mexico. *Crustaceana*. 2008; 81(2): 143–153.

Pongtippatee-Taweepreda P, Chavadej J, Plodpai P, Pratoomchart B, Sobhon P, Weerachatyanukul W, Withyachumnarnkul B. Egg activation in the black tiger shrimp *Penaeus monodon*. *Aquaculture.* 2004; 234(1–4): 183–198.

Pradillon F, Le Bris N, Shillito B, Young C, Gaill F. Influence of environmental conditions on early development of the hydrothermal vent polychaete *Alvinella pompejana. Journal of Experimental Biology.* 2005; 208: 1551–1561.

Prahl Hv, Gardeazábal M. Descripción de las larvas del camarón azul *Penaeus stylirostris* Stimpson. *Anales del Instituto de Investigaciones marinas de Punta Betín.* 1977; 9: 157–172.

Preston NP. The combined effects of temperature and salinity on hatching success and the survival, growth, and development of the larval stages of *Metapenaeus bennettae* (Racek & Dall). *Journal of Experimental Marine Biology and Ecology.* 1985; 85(1): 57–74.

Preston NP. Some factors affecting the survival of the larvae of the Penaeid prawns *Penaeus plebejus (Hess), Metapenaeus macleayi (Haswell)* and *Metapenaeus bennettae (Racek & Dall)*: University of Sydney. 1985.

Price ARG. Distribution of Penaeid shrimp larvae along the Arabian Gulf coast of Saudi Arabia. *Journal of Natural History.* 1982; 16(5): 745–757.

Puig P, Ogsto AS, Mullenbach BL, Nittrouer CA, Sternberg RW. Shelf-to-canyon sediment transport processes on the eel continental margin (Nothern California). *Marine Geology.* 2003; 193: 129–149.

Puig P, Palanques A, Orange DL, Lastras G, Canals M. Dense shelf water cascades and sedimentary furrow formation in the Cap de Creus Canyon, northwestern Mediterranean Sea. *Continental Shelf Research.* 2008; 28(15): 2017–2030.

Qiu ZF, Doglioli AM, He YJ, Carlotti F. Lagrangian model of zooplankton dispersion : numerical schemes comparisons and parameter sensitivity tests. *Chinese Journal of Oceanology and Limnology*. 2011; 29(2): 438–445.

Queiroga H, Blanton J. Interactions Between Behaviour and Physical Forcing in the Control of Horizontal Transport of Decapod Crustacean Larvae. *Advances in Marine Biology*. 2004; 47: 107–214.

Rao GS. Larval development - *Metapenaeus brevicornis* (H. Milne Edwards). *CMFRI Bulletin.* 1979; 28: 60–64.

Reyes EP. Effect of temperature and salinity on the hatching of eggs and larval development of sugpo, *Penaeus monodon*. Paper presented at the Proceedings of the first international conference on the culture of penaeid prawns/shrimps, Iloilo City, Philippines. 1985.

Rinelli P, Bianchini M, Casciaro L, Giove A, Mannini A, Profeta A, Politou YC, Ragonese S, Sabatini A. Occurrence and abundance of the deep-water red shrimps *Aristeus antennatus* (Risso, 1816) and *Aristaeomorpha foliacea* (Risso, 1827) in the central eastern Mediterranean Sea. *Cahiers de Biologie Marine.* 2013; 54(4): 335–347.

Roberts SD, Dixon CD; Andreacchio L. Temperature dependent larval duration and survival of the western king prawn, *Penaeus* (*Melicertus*) *latisulcatus* Kishinouye, from Spencer Gulf, South Australia. *Journal of Experimental Marine Biology and Ecology.* 2012; 411: 14–22.

Robins PE, Neill SP, Gimenez L, Jenkins SR, Malham SK. Physical and biological controls on larval dispersal and connectivity in a highly energetic shelf sea. *Limnology and Oceanography*. 2013; 58(2): 505–524.

Rodgers GG, Roberts SD, Dixon CD. The effects of temperature on larval size in the western king prawn, *Penaeus* (*Melicertus*) l*atisulcatus* Kishinouye, from Spencer Gulf, South Australia: implications for fishery management. *Marine and Freshwater Research*. 2013; 64(10): 976–985.

Rodriguez de la Cruz MC. Descripción de las larvas del camarón café *Penaeus californiensis* Holmes. *Instituto Nacional de Pesca.* 1975; INP/SC:10: 31 pp.

Rojas P, García MA, Sospedra J, Figa J, De Fàbregas J, López O, Espino M, Ortiz V, Sanchezarcilla A, Manriquez M, Shirasago B. On the structure of the mean flow in the Blanes Canyon Area (NW Mediterranean) during summer. *Oceanologica Acta.* 1995; 18(4): 443–454.

Rojas E, Alfaro J. In vitro manipulation of egg activation in the open thelycum shrimp *Litopenaeus*. *Aquaculture.* 2007; 264(1): 469–474.

Rojas PM, Landaeta MF. Fish larvae retention linked to abrupt bathymetry at Mejillones Bay (northern Chile) during coastal upwelling events. *Latin American Journal of Aquatic Research*. 2014; 42(5): 989–1008.

Ronquillo JD, Saisho T. Early developmental stages of greasyback shrimp, *Metapenaeus ensis* (de Haan, 1844) (Crustacea, Decapoda, Penaeidae). *Journal of Plankton Research.* 1993; 15(10): 1177–1206.

Ronquillo JD, Saisho T. Developmental stages of *Trachypenaeus curvirostris* (Stimpson, 1860) (Decapoda, Penaeidae) reared in the laboratory. *Crustaceana.* 1995; 68(7): 833–863.

Ronquillo JD, Saisho T, McKinley RS. Early developmental stages of the green tiger prawn, *Penaeus semisulcatus* de Haan (Crustacea, Decapoda, Penaeidae). *Hydrobiologia*. 2006; 560(1): 175–196.

Rosa R, Calado R, Narciso L, Nunes ML. Embryogenesis of decapod crustaceans with different life history traits, feeding ecologies and habitats: a fatty acid approach. *Marine Biology*. 2006; 151(3): 935–947.

Ross RE, Nimmo-Smith WAM, Howell KL. Increasing the depth of current understanding: sensitivity testing of deep-sea larval dispersal models for ecologists. *PLoS ONE*. 2016; 11(8): e0161220.

Rossi V, Ser-Giacomi E, López C, Hernández-García E. Hydrodynamic provinces and oceanic connectivity from a transport net-work help designing marine reserves. *Geophysical Research Letters.* 2014; 41: 2883–2891.

Rothlisberg PC, Church JA. Processes controlling the larval dispersal and postlarval recruitment of penaeid prawns. In: Sammerco PW, Heron ML, editors. The bio-physics of marine larval dispersal. Washington DC: American Geophysical Union; 2013: 235–252.

Rubio A, Arnau PA, Espino M, Flexas MM, Jordà G, Salat J, Puigdefàbregas J, Sanchez-Arcilla A. A field study of the behaviour of an anticyclonic eddy on the Catalan continental shelf (NW Mediterranean). *Progress in Oceanography*. 2005; 66(2): 142–156.

Rubio A, Barnier B, Jordà G, Espino M, Marsaleix P. Origin and dynamics of mesoscale eddies in the Catalan Sea (NW Mediterranean): Insight from a numerical model study. J*ournal of Geophysical Research: Oceans.* 2009;114(C6): 17 pp.

Sabatés A, Olivar M. Variation of larval fish distributions associated with variability in the location of a shelf-slope front. *Marine Ecology Progress Series.* 1996; 135(1–3); 11–20.

Sabatés A, Salat J, Raya V, Emelianov M. Role of mesoscale eddies in shaping the spatial distribution of the coexisting *Engraulis encrasicolus* and *Sardinella aurita* larvae in the northwestern Mediterranean. *Journal of Marine Systems*. 2013; 111–112; 108–119.

Sabatini A, Follesa MC, Locci I, Pendugiu AA, Pesci P, Cau A. Assemblages in a submarine canyon: influence of depth and time. *Hydrobiologia*. 2007; 580(1): 265–271.

Sacci F, Marcias S, Deiana AM, Cannas R. Population genetics of the red and blue shrimp *A. antennatu*s in the western mediterranean Sea. *Biologia Marina Mediterranea.* 2011; 18(1): 364–365.

Salat J, Cruzado A. Masses d'eau dans la Méditerranée Occidentale. Mer Catalane et eaux adjacentes. *Rapport Commission Internationale Mer Méditerranée.* 1981; 27: 201–209.

Salat J. The interaction between the Catalan and Balearic currents in the southern Catalan Sea. *Oceanologica Acta.* 1995; 18(2): 227–234.

Salat J. Review of Hydrographic environmental factors that may influence anchovy habitats in northwestern Mediterranean. *Scientia Marina.* 1996; 60(2): 21–32.

Sardà F, Demestre M. Estudio biológico de la gamba *Aristeus antennatus* (Risso, 1816) en el mar Catalan (NE de España). *Investigaciones Pesqueras*. 1987; 51(1): 213–232.

Sardà F, Cartes JE, Norbis W. Spatio-temporal structure of the deep-water shrimp *Aristeus antennatus* (Decapoda: Aristeidae) population in the western Mediterranean. *Fishery Bulletin.* 1994; 92(3): 599–607.

Sardà F, Maynou F, Tallo L. Seasonal and spatial mobility patterns of rose shrimp *Aristeus antennatus* in the western Mediterranean: results of a long-term study. *Marine Ecology Progress Series*. 1997; 159: 133–141.

Sardà F, Cartes JE. Morphological features and ecological aspects of early juvenile specimens of the aristeid shrimp *Aristeus antennatus* (Risso, 1816). *Marine and Freshwater Research.* 1997;48(1): 73–77.

Sardà F, Company JB, Maynou F. Deep-sea Aristeus antennatus Risso 1816 in the Catalan Sea: a review and perspective. Scientific council Meeting, Deep-sea Fisheries symposium - Oral. 2001; 4483.

Sardà F, Company JB, Castellón A. Intraspecific aggregation structure of a shoal of a western Mediterranean (Catalan Coast) deep-sea shrimp, *Aristeus antennatus* (Risso, 1816), during the reproductive period. *Journal of Shellfish Research*. 2003a; 22(2): 569–579.

Sardà F, Company JB, Maynou F. Deep-sea Shrimp *Aristeus antennatus* Risso 1816 in the Catalan Sea, a review and Perspectives. *Journal of Northwestern Atlantic Fishery Sc*ience. 2003b; 31: 10 pp.

Sardà F, D'Onghia G, Politou CY, Company JB, Maiorano P, Kapiris K. Deep-sea distribution, biological and ecological aspects of *Aristeus antennatus* (Risso, 1816) in the Western and Central Mediterranean Sea. *Scientia Marina*. 2004; 68(3): 117–127.

Sardà F, Company JB, Bahamón N, Rotllant G, Flexas MM, Sánchez JD, Zúñiga D, Coenjaerts J, Orellana D, Jordà G, Puigdefábregas J, Sánchez-Vidal A, Calafat A, Martín D, Espino M. Relationship between environment and the occurrence of the deep-water rose shrimp *Aristeus antennatus* (Risso, 1816) in the Blanes submarine canyon (NW Mediterranean). *Progress in Oceanography.* 2009; 82(4): 227–238.

Sardà F, Roldán MI, Heras S, Maltagliati F. Influence of the genetic structure on the red and blue shrimp, *Aristeus antennatus* (Risso, 1816), on the sustainability of a deep-sea population along a depth gradient in the western Mediterranean. *Scientia Marina.* 2010; 74(3): 569–575.

Sardà F, Company JB. The deep-sea recruitment of *Aristeus antennatus* (Risso, 1816) (Crustacea: Decapoda) in the Mediterranean Sea. *Journal of Marine Systems*. 2012; 105–108: 145–151.

Sardà F, Roldán Borassi MI, Heras Mena S, Maltagliati F. Influence of the genetic structure of the red and blue shrimp, *Aristeus antennatus* (Risso, 1816), on the sustainability of a deep-sea population along a depth gradient in the western Mediterranean. *Scientia Marina.* 2017; 74(3): 569–575.

Sayol J−M, Orfila A, Simarro G, López C, Renault L, Galán A, Conti D. Sea surface transport in the Western Mediterranean Sea: A Lagrangian perspective. *Journal of Geophysical Research: Oceans.* 2013; 118(12): 6371–6384.

Schram F, von Vaupel Klein C, Charmantier-Daures M, Forest J. Treatise on Zoology - Anatomy, Taxonomy, Biology. The Crustacea, Volume 9 Part A: Eucarida: Euphausiacea, Amphionidacea, and Decapoda (partim): Brill, 2010.

Schroeder K, Chiggiato J, Bryden HL, Borghini M, Ben Ismail S. Abrupt climate shift in the Western Mediterranean Sea. *Scientific Report.* 2016; 6: 23009.

Seridji R. Contribution à l'étude des larves crustacés décapods en Baie d'Alger. *Pelagos*. 1971; 3(II):1–105.

Serra T, Granatasupbsu T, Colomer J, Stips A, Møhlenberg F, Casamitjana X. The role of advection and turbulent mixing in the vertical distribution of phytoplankton. *Estuarine Coastal and Shelf Science*. 2003: 56: 53–62.

Sgrò CM, Lowe AJ, Hoffmann AA. Building evolutionary resilience for conserving biodiversity under climate change. *Evolutionary Applications*. 2011; 4: 326–337.

Shan S, Sheng J, Greenan BJW. Physical processes affecting circulation and hydrography in the Sable Gully of Nova Scotia. *Deep Sea Research Part II: Topical Studies in Oceanography.* 2014; 104: 35–50.

Shchepetkin AA. Method for computing horizontal pressure-gradient force in an oceanic model with a nonaligned vertical coordinate. *Journal of Geophysical Research.* 2003; 108(C3): 3090.

Shchepetkin AF, McWilliams JC. The regional oceanic modeling system (ROMS): a split-explicit, free-surface, topography-following-coordinate oceanic model. *Ocean Modelling*. 2005; 9(4): 347–404.

Shokita S. A note on the development of eggs and larvae of *Penaeus latisulcatus* Kishinouye, reared in an aquarium. *Biology Monograph of Okinawa.*1970; 6: 34–36.

Siegel DA, Kinlan BP, Gaylord B, Gaines SD. Lagrangian descriptions of marine larval dispersion. *Marine Ecology Progress Series*. 2003; 260: 83–96.

Siegel DA, Mitarai S, Costello CJ, Gaines SD, Kendall BE, Warner RR, Winters KB. The stochastic nature of larval connectivity among nearshore marine populations. *Proceedings of the National Academy of Sciences.* 2008; 105(26): 8974–8979.

Sigman DM, Hain MP. The Biological Productivity of the Ocean. N*ature Education Knowledge*. 2012; 3(10): 21pp.

Silas EG, Muthu MS, Pillai NN, George KV. Larval development - *Penaeus monodon* Fabricus. *CMFRI Bulletin.* 1979; 28: 2–11.

Simons RD, Siegel DA, Brown KS. Model sensitivity and robustness in the estimation of larval transport: A study of particle tracking parameters. *Journal of Marine Systems*. 2013; 119–120: 19–29.

Smolarkiewicz PK, Margolin LG. MPDATA: A finite-difference solver for geophysical flows. *Journal of Computation Physics.* 1998; 140: 459–480.

Smith WHF, Sandell DT. Global seafloor topography from satellite altimetry and ship depth soundings. *Science*. 1997; 277: 1957–1962.

Snauffer EL, Masson D, Allen SE. Modelling the dispersal of herring and hake larvae in the Strait of Georgia for the period 2007–2009. *Fisheries Oceanography*. 2014; 23: 375–388.

Solé J, Ballabrera-Poy J, Macías D, Catalán IA. The role of ocean velocities in chlorophyll variability. A modeling study in the Alboran Sea. *Scientia Marina.* 2016; 80(S): 249–256.

Solé J, Emelianov M, García-Ladona E, Ostrovskii A, Puig P. Fine-scale water mass variability inside a narrow submarine canyon (the Besòs Canyon) in the NW Mediterranean Sea. *Scientia Marina.* 2016; 80(1): 195–204.

Subrahmanyam CB. On the unusual occurrence of penaeid eggs in the inshore waters of madras. *Journal of the Marine Biological Association of India.* 1965; 7(1): 83–88.

Sudnik SA, Falhenhaug T. Maturation, fecundity and embryos development in three deep-water shrimps (Decapoda: Caridea: Pasiphaeidae, Oplophoridae) along the mid-Atlantic Ridge from Iceland to the Azores. *Arthropoda Selecta.* 2015; 24(4): 401–416.

Sudnik SA. Biology of the shrimp *Oplophorus spinosus* (Brullé, 1839) (Decapoda, Oplophoridae) in the continental slope waters of the coast of northwest Africa. *Crustacean.* 2017; 90(7–10): 1235–1249.

Sulkin SD. Behavioral basis of depth regulation in the larvae of brachyuran crabs. *Marine Ecology Progress Series.* 1984; 15: 181–205.

Sundby S. A one-dimensional model for the vertical distribution of pelagic fish eggs in the mixed layer. Deep Sea Research Part A. *Oceanographic Research Papers.* 1983; 30(6): 645–1661.

Sundby S, Kristiansen T. The principles of buoyancy in marine fish eggs and their vertical distributions across the world oceans. *PLoS ONE.* 2015; 10(10): e0138821.

Suresh Babu C, Shailander M. Effect of salinity and temperature on larval growth and survival of black shrimp *Penaeus Monodon* (Fabricius) in laboratory conditions. *International Journal of Biopharma Research*. 2013; 2(1): 72–177.

Sweetman AK, Thurber AR, Smith CR, Levin LA, Mora C, Wei C-L, Gooday AJ, Jones DOB, Rex M, Yasuhara M, Ingels J, Ruhl HA, Frieder CA, Danovaro R, Würzberg L, Baco A, Grupe BM, Pasulka A, Meyer KS, Dunlop KM, Henry L-A, Roberts JM. Major impacts of climate change on deep-sea benthic ecosystems. *Elementa: Science of Anthropocene*. 2017;5: 4.

Taylor KE Summarizing multiple aspects of model performance in a single diagram. *Journal of Geophysical Research: Atmospheres.* 2001; 06(D7): 7183–7192.

Temple RF, Fischer CC. Seasonal distribution and relative abundance of planktonic- stage shrimp (*Penaeus* spp.) in the northwestern Gulf of Mexico, 1961. *Fisheries Bulletin.* 1967; 66: 323–334.

Teng SK. Observations on certain aspects of the biology of *Metapenaeus brevicornis (H. Milne-Edwards)* and *Penaeus merguiensis (de Man)* in the Brunei Estuarine system. (Master), University of Singapore, Singapore. 1971.

Thatje S, Bacardit R, Arntz W. Larvae of the deep-sea Nematocarcinidae (Crustacea: Decapoda: Caridea) from the Southern Ocean. *Polar Biology.* 2005, 28(4), 290–302.

Thomas MM, Kathirvel M, Pillai NN. Spawning and rearing of the penaeid prawn, *Metapenaeus affinis* (H.Milne Edwards) in the laboratory. *Indian Journal of Fisheries.* 1974; 21(2): 543–556.

Thomas CD, Cameron A, Green RE, Bakkenes M, Beaumont LJ, Collingham YC, et al. Extinction risk from climate change. *Nature.* 2004; 427: 145–148.

Thorpe SA. An introduction to ocean turbulence. 1st ed. Cambridge University Press; 2007

Thorrold S, Jones GE, Hellberg M, Burton R, Swearer S, Neigel J, Morgan S, Warner R. Quantifying larval retention and connectivity in marine populations with artificial and natural markers. *Bulletin of Marine Science.* 2002; 70: 291–308.

Tiessen MCH, Fernard L, Gerkema T, van der Molen J, Ruardij P, van der Veer HW. Numerical modelling of physical processes governing larval transport in the sourthern North Sea. *Ocean Science.* 2014; 10: 357–376.

Tirmizi N, Hasan M-U, Kazmi QB. The larval development and spawning of *Metapenaeus affinis* (H. Milne Edwards) under laboratory conditions. *Pakistan Journal of Zoology.* 1981; 13: 141–155.

Torres AP, Santos A, Alemany F, Massutí E. Larval stages of crustacean species of interest for conservation and fishing exploitation in the Western Mediterranean. *Scientia Marina.* 2013; 77: 149–160.

Torres AP, Dos Santos A, Balbín R, Alemany F, Massutí E, Reglero P. Decapod crustacean larval communities in the Balearic Sea (western Mediterranean): Seasonal composition, horizontal and vertical distribution patterns. *Journal of Marine Systems.* 2014; 138: 112–126.

Torres A. Decapod crustacean larvae inhabiting oggshore Balearic Sea waters (western Mediterranean): taxonomy and ecology. PhD thesis, Universitat de les Illes Baleards, Departament de Biologia. 2015: 226 pp.

Thorson G. Reproductive and larval ecology of marine bottom invertebrates. *Biological reviews of the Cambridge Philosophical Society.* 1950; 25: 1–45.

Triay-Portella R, González JA, Santana JI, García-Martín V, Romero M, Jiménez-Martín S, Hernández-Castro D, Pajuelo JG. Reproductive pattern and egg development of the deep-sea crab *Paromola cuvieri* (Brachyura, Homolidae) around the Canary Islands (NE Atlantic). *Deep Sea Research Part I: Oceanographic Research Papers.* 2013; 85: 1–14.

Treml EA, Ford JR, Black KP, Swearer SE. Identifying the key biophysical drivers, connectivity outcomes, and metapopulation consequences of larval dispersal in the sea. *Movement Ecology.* 2015; 3(1): 17pp.

Tudela S, Sardà F, Maynou F, Demestre M. Influence of submarine canyons on the distribution of the deep-water shrimp, *Aristeus antennatus* (Risso, 1816) in the NW Mediterranean. *Crustaceana.* 2003; 76(2): 217–225.

Tudela S. Ecosystem effects of fishing in the Mediterranean: an analysis of the major threats of fishing gear and practices to biodiversity and marine habitats. Studies and Reviews. *General Fisheries Commission for the Mediterranean. 2004;* 74. Rome, FAO. 44 pp.

Türkmen G. Larval Development of the Grooved Shrimp (*Penaeus kerathurus* Forskal, 1775) Under Laboratory Conditions. *Turkish Journal of Fisheries and Aquatic Sciences.* 2003; 3(2): 97–103.

Uglem I, Dempster T, Bjørn PA, Sanchez-Jerez P, Økland F. High connectivity of salmon farms revealed by aggregation, residence and repeated movements of wild fish among farms. *Marine Ecology Progress Series.* 2009; 384: 251−260.

Uppala SM, Kållberg, PW, Simmons AJ, Andrae U, Da Costa Bechtold V, Fiorino M, et al. The ERA-40 re-analysis. *Quaterly Journal of the Royal Meteorological Society.* 2005; 131: 2961–3012.

Vance DC. Pendrey R. Vertical migration of postlarval penaeid prawns in two Australian estuaries: The effect of tide and day/night. *Marine and Freshwater Research*. 2008; 59(8): 671–683.

Velazquez MP, Gracia A. Fecundity of *Litopenaeus setiferus*, *Farfantepenaeus aztecu*s and *F. duorarum*, in the Southwestern Gulf of Mexico. *Gulf and Caribbean Research*. 2000; 12(1): 1–19.

Vélez-Belchó, Tintoré J. Vertical velocities at an ocean front. *Scientia Marina.* 2001; 65(1): 291–300.

Vic C, Gula J, Roullet G, Pradillon F. Dispersion of deep-sea hydrothermal vent effluents and larvae by submesoscale and tidal currents. *Deep Sea Research Part I: Oceanographic Research Papers.* 2018; 133: 1–18.

Villaluz DK, Villaluz A, Ladrera B, Sheik M, Gonzaga A. Reproduction, larval development and cultivation of sugpo (*Penaeus monodon* Fabricius). *The Philippine Journal of Science*. 1969*;* 98*:* 3–14(205–233).

Villate F, Uriarte I, Olivar MP, Maynou F, Emelianov M, Ameztoy I. Mesoscale structure of microplankton and mesoplankton assemblages under contrasting oceanographic conditions in the Catalan Sea (NW Mediterranean). *Journal of Marine Systems*. 2014; 139: 9–26.

Villareal H, Hernandez-Llamas A. Influence of temperature on larval development of Pacific brown shrimp *Farfantepenaus californiensis. Aquaculture*. 2005; 249(1–14): 257–263.

Visser A. Using random walk models to simulate the vertical distribution of particles in a turbulent water column. *Marine Ecology Progress Series.* 1997; 158: 275–281.

Warner JC, Sherwood HG, Arango HG, Signell RP. Performance of four turbulence closure methods implemented using a generic length scale method. *Ocean Modelling*. 2005; 8: 81–113.

Watson JR, Mitarai S, Siegel DA, Caselle JE, Dong C, McWilliams JC. Realized and potential larval connectivity in the Southern California Bight. *Marine Ecology Progress Series.* 2010; 401: 31–48.

Williamson DI. Larval morphology and diversity. Abele LG, editor. New York [etc.]: New York etc., 1982; 489 pp.

Wilson MFJ, O'Connell B, Brown C, Guinan JC, Grehan AJ. Multiscale terrain analysis of multibeam bathymetry data for habitat mapping on the continental slope. *Marine Geodesy.* 2007; 30(1–12): 3–135.

Wood S. R Package 'mgcv' (Version 1.8-23). 2018.

Woodson CB, McManus MA, Tyburczy JA, Barth JA, Washburn L, Caselle JE, Carr MH, MAlone DP, Raimondi PT, Menge BA, Palumbi SR. Coastal fronts set recruitment and connectivity patterns across multiple taxa. *Limnology and Oceanography.* 2012; 57(2): 582–596.

Yasuhara M, Danovaro R. Temperature impacts on deep-sea biodiversity. *Biological Reviews.* 2016; 91(2): 275–287.

Yearsley JM, Sigwart JD. Larval transport modeling of deep-sea invertebrates can aid the search for undiscovered populations. *PLoS ONE*. 2011; 6(8): e23063.

Young CM, He R, Emlet RB, Li Y, Qian H, Arellano SM, Van Gaest A, Bennett KC, Wolf M, Smart TI, Rice ME. Dispersal of deep-sea larvae from the intra-American seas: Simulations of trajectories using ocean models. *Integrative and Comparative Biology.* 2012; 52(4): 483–496.

Yúfera M, Rodriguez A, Lubián LM. Zooplankton ingestion and feeding behavior of *Penaeus kerathurus* larvae reared in the laboratory. *Aquaculture.* 1984; 42(3): 217–224.

Zhang X, Haidvogel D, Munroe D, Powell EN, Klinck J, Mann R, Castruccio, FS. Modeling larval connectivity of the Atlantic surfclams within the Middle Atlantic Bight: model development, larval dispersal and metapopulation connectivity. *Estuarine, Coastal and Shelf Science.* 2015; 153: 38–53.

Zacharia S, Kakati VS. Optimal salinity and temperature for early developmental stages of *Penaeus merguiensis* De man. *Aquaculture.* 2004; 232(1–4): 373–382.

ANNEXES

Annex 1

Ocean Sci., 15, 1–15, 2019
https://doi.org/10.5194/os-15-1-2019

Ocean Science Open Access EGU

Influence of the summer deep-sea circulations on passive drifts among the submarine canyons in the northwestern Mediterranean Sea

Morane Clavel-Henry[1], Jordi Solé[1], Miguel-Ángel Ahumada-Sempoal[2], Nixon Bahamon[1,3], Florence Briton[4], Guiomar Rotllant[1], and Joan B. Company[1]

[1]Institut de Cienciès del Mar, Consejo Superior de Investigaciones Científicas, Barcelona, Spain
[2]Universidad del Mar, Puerto Angel, 70902, Oaxaca, Mexico
[3]Centre d'estudis avançats de Blanes, Consejo Superior de Investigaciones Científicas, Blanes, Spain
[4]Ecole Nationale Supérieure de Techniques Avancées, Paris Tech. Palaiseau, France

Correspondence: Morane Clavel-Henry (morane@icm.csic.es)

Received: 4 June 2019 – Discussion started: 4 July 2019
Revised: 30 October 2019 – Accepted: 12 November 2019 – Published:

Abstract. Marine biophysical models can be used to explore the displacement of individuals in and between submarine canyons. Mostly, the studies focus on the shallow hydrodynamics in or around a single canyon. In the northwestern Mediterranean Sea, knowledge of the deep-sea circulation and its spatial variability in three contiguous submarine canyons is limited. We used a Lagrangian framework with three-dimensional velocity fields from two versions of the Regional Ocean Modeling System (ROMS) to study the deep-bottom connectivity between submarine canyons and to compare their influence on the particle transport. From a biological point of view, the particles represented eggs and larvae spawned by the deep-sea commercial shrimp *Aristeus antennatus* along the continental slope in summer. The passive particles mainly followed a southwest drift along the continental slope and drifted less than 200 km considering a pelagic larval duration (PLD) of 31 d. Two of the submarine canyons were connected by more than 27 % of particles if they were released at sea bottom depths above 600 m. The vertical advection of particles depended on the depth where particles were released and the circulation influenced by the morphology of each submarine canyon. Therefore, the impact of contiguous submarine canyons on particle transport should be studied on a case-by-case basis and not be generalized. Because the flows were strongly influenced by the bottom topography, the hydrodynamic model with finer bathymetric resolution data, a less smoothed bottom topography, and finer sigma-layer resolution near the bottom should give more accurate simulations of near-bottom passive drift. Those results propose that the physical model parameterization and discretization have to be considered for improving connectivity studies of deep-sea species.

1 Introduction

Lagrangian particles coupled with three-dimensional hydrodynamic models are useful to assess the impact of ocean circulation on the drift of small elements or individuals. It allows for the exploration of various scenarios of dispersal and increases knowledge in several fields of marine systems, such as predicting the direction of oil spills (Jones et al., 2016); understanding the circulation of microplastics (Lebreton et al., 2012); estimating the impact of aquaculture (Cromey and Black, 2005); and describing the spatial dispersion of crustaceans, fish, and other marine larvae (Ahumada-Sempoal et al., 2015; North, 2008; Ospina-Aìlvarez et al., 2013). Particles in the open ocean are susceptible to advection between locations, influenced by regional currents and mesoscale features such as eddies and meanders (Ahumada-Sempoal et al., 2013). The particles without implemented behavior are called passive and are efficiently used to study the inactive transport of elements. They also provide a useful approximation of larval drifts when the ecological knowledge on the early life cycle is scarce. The individual-based models

Published by Copernicus Publications on behalf of the European Geosciences Union.

(IBM) configure each Lagrangian particle with characteristics parameterized by the modeler. In marine ecological studies, IBMs provide a representation of the potential connectivity between geographically separated subpopulations, with implications for fishery management and conservation plans (Andrello et al., 2013; Basterretxea et al., 2012; Kough et al., 2013; Siegel et al., 2003).

Simulation of marine passive drifts provides a picture of the highly dynamic circulation in the vicinity of the submarine canyons. Influence of canyons on the transport of particles and living organisms has begun to raise interest, but only a few studies are dealing with the Lagrangian transport of particles specifically in those small-scale topographic structures (Ahumada-Sempoal et al., 2015; Kool et al., 2015; Shan et al., 2014). In the northwestern (NW) Mediterranean Sea, several submarine canyons, whose heads are incising the continental shelf (i.e., Cap de Creus, Palamós, and Blanes canyons), generate mesoscale features from the main circulation pattern (Millot, 1999) called the Northern Current (NC). When the NC crosses a canyon, it causes a downwelling on the upstream wall and an upwelling on the downstream wall in the 100–200 m layer depth (Ahumada-Sempoal et al., 2015; Jordi et al., 2006), or it causes the opposite at lower depths (Flexas et al., 2008). Within the canyons, near-bottom currents produce a closed circulation (Palanques et al., 2005; Solé et al., 2016), which loses strength with the depth (Flexas et al., 2008; Granata et al., 1999). The canyon shape enhances the downwelling of water and its components (sediment and organic carbon; Puig et al., 2003, biogenic or inorganic particles; Granata et al., 1999), and it provides favorable and diverse habitats for benthic species (Fernandez-Arcaya et al., 2017). Those exchanges proceed at different velocity rates following the condition of the waters. For example, cascading of winter water masses drives suspended substances along the funnel structure of the canyons (Canals et al., 2009). In summer, the stratification of the water column is well-established in the NW Mediterranean Sea decoupling the mixed layer from the rest of the water column (Rojas et al., 1995) and slowing the downward sink of biogenic particles (Granata et al., 1999). During that season, the circulation of the NC is shallower (250 m deep), wider (50 km wide) and less intense than in winter (Millot, 1999).

To date, the impact of the circulation on the dispersal of particles was estimated with hydrophysical data (Ahumada-Sempoal et al., 2015; Granata et al., 1999; Rojas et al., 1995) and with sediment traps (Durrieu de Madron et al., 1999; Lopez-Fernandez et al., 2013) in shallow waters above the NW Mediterranean submarine canyons. None of the previous studies simulated the particle transport at a deeper layer or showed the particle exchanges among different water layers of submarine canyons. Information on the roles of the upper part of the canyon on both horizontal and vertical transport of particles is not clear (e.g., 0–300 m; Granata et al., 1999), and for deeper parts this information is rarely provided. In accordance with those facts, we questioned if the deep-sea circulation mechanism in each submarine canyons of the NW Mediterranean Sea can be generalized.

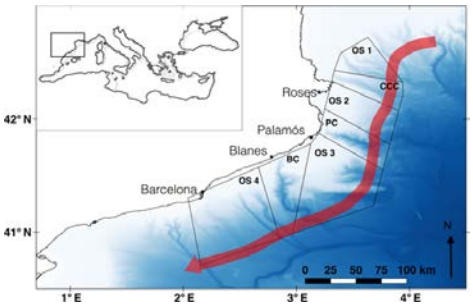

Figure 1. Map of the study area. Release zones are represented along the northwestern Mediterranean Sea: open slope (OS) 1, Cap de Creus canyon (CCC), OS 2, Palamós canyon (PC), OS 3, Blanes canyon (BC), and OS 4. The red arrow indicates the direction of the Northern Current. Bathymetry was extracted from EMODnet (http://www.emodnet-bathymetry.eu TSI).

In this study, deep passive drifts along the NW Mediterranean continental slope are simulated to determine the influence of the summer circulation modulated by the presence of the submarine canyons. We partly focused on the drift sensitivity to deep circulation using the outputs of two hydrodynamic numerical models to approach the transport uncertainties. With this study, we are expecting to provide a first insight into the deep connectivity between submarine canyons to improve the management of their grounds, namely of the deep-sea shrimp *Aristeus antennatus*.

2 Material and methods

The influence of deep circulation on passive drifts among the submarine canyons of the NW Mediterranean Sea was analyzed through the dispersal of Lagrangian particles.

2.1 Hydrodynamic models

The sensitivity of dispersal to the circulation was generated with the use of two available hydrodynamic models, which covered the area of the submarine canyons in the northwestern Mediterranean Sea (see Fig. 1). Because of the parameterization related to the topography (i.e., bathymetric data sets and smoothing) and the vertical layer discretization in the two hydrodynamic models, small differences in morphology of the submarine canyons were expected to impact the flow circulation.

The two hydrodynamic models were climatological simulations using the Regional Ocean Model System (ROMS; Shchepetkin and McWilliams, 2005), a free-surface terrain-

following primitive equations ocean model. ROMS includes accurate and efficient physical and numerical algorithms (Shchepetkin, 2003). The two models were referred to by their implementation versions, ROMS-Rutgers and ROMS-Agrif (Debreu et al., 2012), for the sake of clarity. In the present paper, the ROMS-Rutgers configuration and its validations are presented, while ROMS-Agrif has already been used and validated in Ahumada-Sempoal et al. (2013, 2015).

The ROMS-Rutgers model was forced by a climatological atmospheric forcing. The air temperature, shortwave radiation, longwave radiation, precipitation, cloud cover, and freshwater flux used to force the model came from the ERA-40 reanalysis (Uppala et al., 2005). Surface pressure came from the ERA-Interim reanalysis (Dee et al., 2011). All these variables had a spatial resolution of 1° and a time resolution of 6 h. QuikSCAT blend data were used for wind forcing (both zonal and meridional). The wind had a spatial resolution of 0.25° and a time resolution of 6 h. The boundary conditions were obtained from NEMO (available from https://www.nemo-ocean.eu/, last access: March 2012; these simulations were reported in Adani et al., 2011) and interpolated to the ROMS grid to define a sponge layer of 10 horizontal grid points with a nudging relaxation time of 30 d. This methodology for the implementation of the model in the area followed the same procedure as the one already tested in the Alboran Sea (Solé et al., 2016). This model implementation was already used in previous publications as a hydrodynamic model coupled with a fisheries model (Coll et al., 2016).

The simulation domain ranges from 0.65° W to 6.08° E and from 38 to 43.69° N. The grid resolution is 2 km (with 256×384 grid points horizontally) and the vertical domain is discretized using 40 vertical levels with a finer resolution near the surface (S coordinate surface and bottom parameter are $\theta_s = 5$ and $\theta_b = 0.4$). Thus, the thickness of the near-bottom layer on the continental slopes delimited by the 500 and 800 m isobaths is 24 m (± 3.2 m). The advection scheme used in our simulations was MPDATA (recursive flux-corrected 3-D advection of particles; Smolarkiewicz and Margolin, 1998) and Large–McWilliams–Doney (LMD) mixing as a subgrid-scale turbulent mixing closure scheme (Large et al., 1994), also known as the K-Profile Parameterization (KPP) scheme. The air–sea interaction used for the boundary layer in ROMS was based on the bulk parameterization (Fairall et al., 1996). Bathymetry grid with a horizontal resolution of 100 m was provided by the Geoscience department of the Institute of Marine Sciences (ICM-CSIC, Barcelona) and fitted to the grid of the model. We ran the ROMS-Rutgers model version 3.6 using climatological atmospheric forcing and boundary conditions. The initial conditions to start the simulations were obtained using the same interpolated fields as the ones used for the boundary conditions for all variables. After an 8-year spin-up period with a baroclinic time step of 120 s, we used the ninth year as the study period.

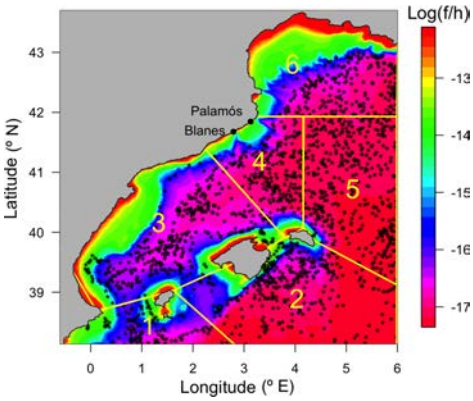

Figure 2. Map of the ROMS-Rutgers model domain and position of ARGO buoys. The color bar represents the Coriolis parameter (f) divided by the depth (h) (f/h in a zebra color palette). The six subareas selected to validate the model using ARGO float observations are shown by yellow polygons. The black dots in the domain represent all the ARGO profiles considered.

The regional ROMS-Rutgers implementation has been daily saved and validated. First, we compared the simulations with the coarser model used for the initial and boundary conditions (NEMO). Second, the model was compared to the ARGO float vertical data profiles of temperature and salinity to test the correct structure of the simulated water column within the year. For the ARGO tests, we selected 1900 casts in the area from October 2003 to December 2012. The data collected cover depths from the surface down to a maximum of 720 m. The ARGO vertical profile resolution was 5 m from the surface to 200 and 25 m from 200 to 720 m. We grouped the ARGO casts by months and by six subareas dividing the domain according to the Coriolis force divided by the bottom depth (Fig. 2). Then, we selected the subareas that have more than 30 ARGO profiles for each month, we calculated a monthly averaged profile of ARGO, and we compared them with the modeled climatologic profile (monthly average).

The main general behavior of the ROMS-Rutgers model simulation was coherent with the lower-resolution model (NEMO) and with the reported hydrography of the northwestern Mediterranean Sea. The model also successfully reproduced the main seasonal behavior of the different water masses. A Taylor diagram (Taylor, 2001) was used to display the correlation, root mean square error (RMSE), and standard deviation (SD) between the monthly averages of the ROMS-Rutgers model profiles and ARGO profiles by subareas (Fig. 3). The comparison showed reasonably good correlations of statistical significance. For temperature, the correlation between model and ARGO was higher than 0.7 during

10 of the 12 months, while for salinity it was higher than 0.95 for all the months. As it is shown in Fig. 3, during the month of September, the correlations in the Taylor diagram for temperature and salinity were higher than 0.9 in both variables. The month of September was selected because the thermocline in our domain disappears and the mixing process at that period of the year is likely to vary the most. Consequently, it shows that the circulation over different depths has been well reproduced in the model.

The second set of velocity and thermodynamic fields was provided by ROMS-Agrif, built and validated in Ahumada-Sempoal et al. (2013). The simulation domain ranges from 40.21 to 43.93° N and 0.03° W to 6° E. It has a finer horizontal resolution (∼ 1.2 km), with 32 sigma levels of a finer resolution near the surface and coarser resolution near the bottom (S coordinate surface and bottom parameters are $\theta s = 7$ and $\theta b = 0$) than ROMS-Rutgers. The average thickness of the near-bottom layer is 54 m and is approximately 2 times thicker than the near-bottom layer from ROMS-Rutgers. The model was one-way nested from a coarse regional resolution model of 4 km. Bathymetry was derived from the ETOPO2-arcminute model (with horizontal grid resolution of 3 km) from Smith and Sandell (1997). Surface forcing and initial and boundary conditions were built with the ROMSTOOLS package (Penven et al., 2008), running a 10-year simulation of the model.

In the ROMS-Rutgers configuration, the bottom circulation followed a southward direction along the bottom slope, except in the area south of Blanes canyon (Fig. 4). Over the bottom floor of the continental slope, the highest velocities reached 8.5 cm s^{-1} on the southern mouth of Palamós canyon. The fastest vertical velocities were at sea bottom deeper than 400 m and are mostly located among the submarine canyons. The minimum and maximum velocity values (−1.4 and 1.7 mm s^{-1}, respectively) were located in Palamós canyon. In ROMS-Agrif, the hydrodynamic model had higher near-bottom currents in the areas at the north and south of Palamós canyon. The maximum velocity reached 11.6 cm s^{-1} off the continental slope between Palamós and Blanes canyons. Higher intensities of vertical near-bottom current were also in those areas (see Fig. 4) even though the most extreme values of vertical velocity were −1.23 and 1.11 mm s^{-1} on the bottom off the continental rise.

2.2 Practical study

In this study, we considered some characteristics of the deep-sea shrimp *Aristeus antennatus* for the initial configuration of the simulated passive drifters. *A. antennatus* is a benthic commercial species distributed over the area of study (Demestre and Lleonart, 1993; Sardà et al., 1997), and it is an important source of income for the fishing harbors of the NW Mediterranean Sea (Gorelli et al., 2014).

The spawning peak of *A. antennatus* – and release of particles – occurred in summer (July to September; Demestre and Fortuño, 1992) in the sea bottom delimited by the isobaths of 500 and 800 m, i.e., on average 650 m (Sardà et al., 1997; Tudela et al., 2003) at midnight (Schram et al., 2010). The ecology of the early pelagic stages (eggs and larvae) is hardly known due to the difficulty to catch the larvae in the open sea and to keep the adults in captivity alive.

For setting the duration of simulated drift, we used the pelagic larval duration (PLD) of the shrimp, i.e., the time a larva spends in the water column from spawning to the first post-larval stage. As individuals of the superfamily Penaeidae (which contains the species *A. antennatus*) release eggs in the environment before hatching (Dall, 1990), the PLD definition was extended to account for the duration of the embryonic stage. To overcome the situation of an unknown PLD for *A. antennatus*, we fitted a linear model to the relation between the duration of eggs developing into the post-larvae stage from 43 penaeid species by reviewing research articles (see Table S1 in the Supplement) and the temperature of the water in which the larvae were reared. The linear model, whose initial assumptions were verified (see Fig. S1) and had a coefficient of determination $R^2 = 56\,\%$, was the following:

$$\mathrm{PLD} = 64.71 \cdot \exp(-0.06 \cdot T), \quad (1)$$

where T is water temperature in degrees Celsius. Then, the effect of water temperature on the duration of the larval stage had the shape of an exponential law (O'Connor et al., 2007; Pepin, 1991). When particles were at the deep-sea bottom, we could estimate their PLD to be 31 d because the seawater temperature was approximately 13.2 °C. The duration appeared to be shorter than the PLD for other deep-sea species (Arellano et al., 2014: Etter and Bower, 2015; Young et al., 2012) but was in agreement with PLD for temperate invertebrates (Levin and Bridges, 1995; Thatje et al., 2005; Williamson, 1982) and PLDs of penaeid species predicted in Dall (1990).

Using the passive drift simulations, we started to explore the simplest hypothesis around the larval ecology, which corresponds to the absence of larval behavior (such as egg buoyancy or swimming abilities). The drift of particles is used as a first step to approach the unknown larval cycle. The good management of the fishery has raised the interest of science to have a better knowledge of the species ecology. Last, the particles are used to estimate potential connections among the fishing grounds of *A. antennatus*. It contributes to complement the research made in parental genetic studies (Sardà and Company, 2012), which have shown the high dispersive capacity of *A. antennatus* without revealing its connectivity paths.

2.3 Biophysical model

Particle dispersal was simulated with the open-source IBM code Ichthyop (Lett et al., 2008) version 3.3, which is a free user-friendly toolset used in numerous individual disper-

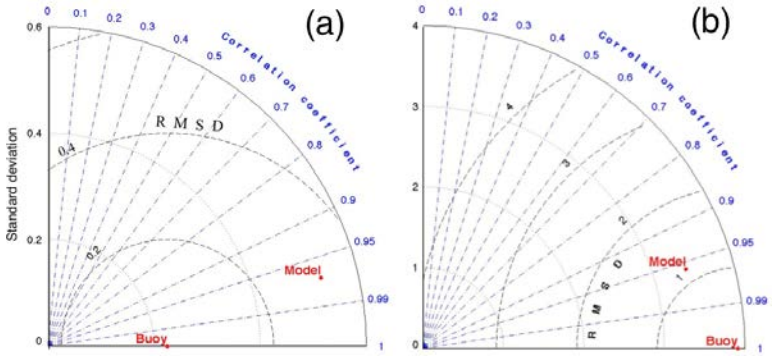

Figure 3. Taylor diagrams for validation of ROMS-Rutgers. Example of comparison between buoys (ARGO floats) and ROMS-Rutgers model simulations during September. **(a)** The temperature of float versus model and **(b)** the salinity of float versus model. Radial from the origin (0, 0) are the correlation coefficients, internal circles centered on the origin are standard deviations, and internal circles centered at the buoy position are root mean square differences (RMSDs).

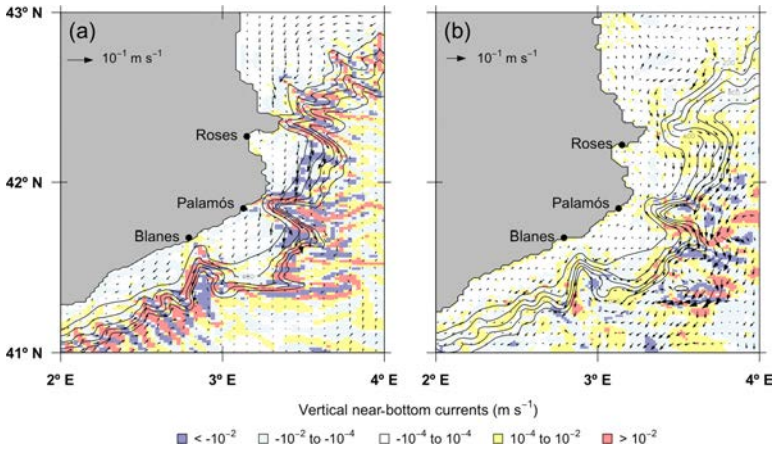

Figure 4. Vertical velocity and horizontal velocity vectors at bottom in the northwestern Mediterranean Sea in the **(a)** ROMS-Rutgers and **(b)** ROMS-Agrif models. Colors from blue to red according to the downward or upward (negative or positive) vertical velocity. Continuous black lines are the isobaths adapted from the bathymetry of the hydrodynamic models.

sal studies in the western Mediterranean Sea (e.g., Ospina-Alvarez et al., 2013; Palmas et al., 2017). Displacements of virtual particles are computed by integrating the differential equation using a Runge–Kutta 4th order (RK4) advection scheme:

$$\mathrm{d}\boldsymbol{X} = \boldsymbol{U} \cdot \mathrm{d}t, \quad (2)$$

where $\mathrm{d}\boldsymbol{X}$ is the three-dimensional displacement vector of the particles during a time step $\mathrm{d}t$ of 30 min under the velocity vector $\boldsymbol{U}$ from the hydrodynamic models. RK4 is a stable and reliable multistep method for numerical integration (North et al., 2009; Qiu et al., 2011) and is commonly used in Lagrangian dispersal models (North et al., 2009; Chen et al., 2003; Paris et al., 2013). The Ichthyop algorithm used trilinear and linear interpolations in space and time from the daily average ROMS velocity field output to each particle position at all time steps. Attributes (geographical coordinates

and depth) of each particle were saved in an output file at a daily time step.

To reach the optimal number of released particles, we carried out an analysis following a slightly modified protocol proposed in Hilário et al. (2015) and Simons et al. (2013). The drifts of 200 000 advective-only particles were carried out over 31 d (PLD computed in the above section), released at midnight for each day of July and August at the bottom. A subset of N particles ($N = 1000, 2000, 5000, 10\,000, 25\,000, 50\,000, 75\,000, 100\,000$, and $150\,000$) was randomly chosen among the 200 000 originally released. Then, relative to the N particles released, the density of particles in each cell of a two-dimensional (2-D) horizontal grid with a 2 km resolution (i.e., density matrix) was computed.

This operation was replicated 100 times, leading to a sample of one hundred 2-D horizontal density matrices for a given N. The difference between the 100 replicates of that sample was evaluated by calculating the two-by-two fraction of unexplained variance (FUV):

$$\mathrm{FUV} = 1 - r^2, \quad (3)$$

where r^2 is the squared Pearson linear correlation coefficient within the density matrices. Based on the results, the number of particles showing a FUV lower than 5 % rounded at 20 000 units. This number was set as the reference number of particles to be released per event.

2.4 Dispersal analysis

Seven zones were defined along the NW Mediterranean Sea continental slope including the Cap de Creus, Palamós, and Blanes submarine canyons (CCC, PC, and BC, respectively) and the open slopes (OS) between them (see Fig. 1). Those zones were also drawn to incorporate the continental shelf, slope, and rise as large polygons. Resulting from the prior knowledge of adult *A. antennatus* and the previous analysis, we released 20 000 particles in those areas on 1 and 15 July, 1 and 15 August, and 1 September.

The contribution of hydrodynamics to particle dispersions was explored through their horizontal and vertical displacements. The horizontal displacements drifted by particles (called drift distances) were the sum of the traveled distances between the daily recorded positions of particles. A Student two-sample test was computed to assess if the difference between those values according to a given factor (e.g., release zone, canyons, and hydrodynamics models) was significant.

In this study, the last position of the particles was attributed to the zone beneath the particle. The proportion of particles released from a release zone reaching a settlement zone was displayed in a connectivity matrix. Each cell represents the proportion of particles $P_{i,j}$ from a zone i that has settled into a zone j:

$$P_{i,j} = N_{i,j}/N_i, \quad (4)$$

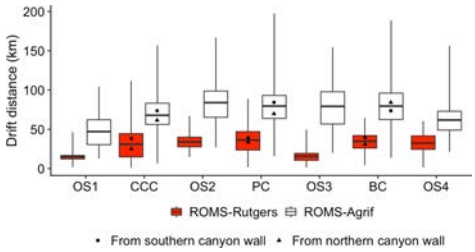

Figure 5. Horizontal transport of passive particles (km) from the release zones in the ROMS-Rutgers (red bars) and ROMS-Agrif (white bars) simulations. Boxplots represent the minimum, 25 % quantile, mean, 75 % quantile, and maximum. Release zone codes are as indicated in Fig. 1.

where (i, j) is in the interval $[1 : 10]$, $N_{i,j}$ represents the number of particles settled in the zone j which has been released in zone i, and N_i is the number of particles released in zone i. Retention proportions are assumed to be the ratio of particles that remained in the zone where they were released ($P_{i,i}$ with $j = i$) and appear on the diagonal of the matrix.

3 Results

Dispersal of particles in both configurations of ROMS had common general patterns and mostly diverged on the transport magnitude.

3.1 Lagrangian dispersal within the ROMS-Rutgers outputs

Releases in canyons generally made the drift distance larger and variable (Fig. 5). Lagrangian simulations carried out with the ROMS-Rutgers model transported particles over 27 km on average and up to 111 km for the longest trajectory. First, from the canyons, passive particles drifted 33 km, 6 km more than the average distance, while from open slopes, particles drifted 25 km, which was 3 km less than the average distance. Besides, the highest average drift distance was 36.3 km (±15.1 km) from the releases in the PC. Second, when released on the northern walls of the canyons, the particles drifted 29 km, which was 10 km less than the particles released on the southern walls. Last, the open slope 1 (OS 1) and OS 3 were the release zones with the shortest transports from which particles drifted 15.2 km (±5.5 km) and 15.7 km (±6.8 km), respectively.

Particle retentions in the release zones were high and particles from canyons generally seeded the nearby zones (see Fig. 6). The overall retention rate was averaged at 60 % (±33 %), because 42 % to 100 % of the particles stay in their release zones, except for the particles from the OS 2 (99 % of

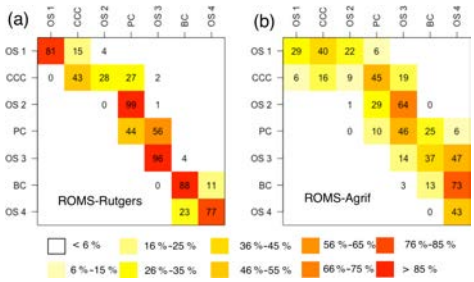

Figure 6. Dispersal rate (%) of passive particles between the zones of release (*y* axis) and settlement (*x* axis). The retention rates are on the diagonal. Release zone codes are as indicated in Fig. 1.

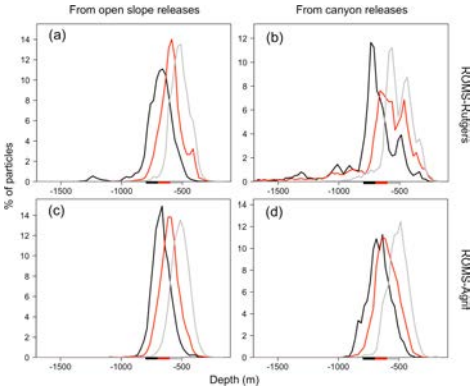

Figure 7. Depth range (m) of particles after 31 d of drift. Particles were released between the following three depth ranges: 500–600 m (gray), 600–700 m (red), and 700–800 m (black) denoted by colored bars on the *x* axis.

particles drifted into the PC). Particles released in the CCC can drift up to 28 % and 27 % in the southern zones of OS 2 and PC, respectively. The connectivity of CCC with PC is possible for particles having drifted approximately 50 km (±7 km) from 624 m (±92 m) depth. The zone OS 3 has received 56 % of particles from the PC and has retained 96 % of particles released inside. Last, we observe a drift direction opposite to the general southwestward direction of the main current in the south of our study area. Twenty-three percent of particles from the OS 4 drifted northward to the BC.

The vertical displacement of particles at the end of the 31 d simulation was relatively independent of the bottom depth at the release event (Fig. 7). Generally, more than 26 % of particles rise above the isobath of 500 m, around 30 % of particles drifted without having vertically displaced, and 5 % of particles go deeper than 800 m (see Fig. 7). More specifically, 12.8 % of particles released above the bottom between the isobaths of 700 and 800 m (hence, 700/800 m) arrived below 800 m. There are only 0.7 % and 4.8 % of bottom-released particles between the isobaths of 500 and 600 m and the isobaths of 600 and 700 m (hence, 500/600 and 600/700 m), respectively, which also reach such a depth. Moreover, the downward displacement is greater for particles released in canyons than on open slopes. From the three depth layers, 500/600, 600/700, and 700/800 m, as previously defined, 0.2 %, 1 %, and 11.1 % of particles on open slopes and 2 %, 13.5 %, and 19.7 % of particles on canyon slopes, respectively, go deeper than 800 m. Besides, the particles released in the middle layer (600/700 m) of the canyons were likely to be more dispersed vertically than from similar release conditions on the open slope (retention on the depth 27.3 % and 36.8 %, respectively).

In submarine canyons, the particles had a broader vertical displacement than over open slopes. Intensity and amplitudes in the vertical displacement of particles were dependent on the canyons and their walls, especially when they were released above both walls of the Blanes canyon (Fig. 8). On average, the particle vertical displacements in canyons or above the open slope are ascents of 28 and 24 m, respectively. Furthermore, the variability of the vertical displacement of particles in canyons (±154 m) is 2 times higher than on open slopes (±67.5 m). The drifts in PC have on average the highest ascent of 133 m. The PC is also the canyon with the widest vertical displacements where the maxima upward and downward displacements are 490 and 1163 m, respectively. From its southern wall, particles averagely rise 145 m, while on the northern wall there is an ascent of 58 m. Particles from the CCC averagely rose 44 m as did particles from the PC, but the vertical displacements were limited to a small range of 86 m in the CCC compared to 170 m in the PC. The drifts from BC have on average the furthest descent (127 m down). The drifts within BC went downward by 62 m when particles were above the northern wall and went upward by 36 m when particles drift above the southern wall. Contrary to the different days of release in the other canyons, the northern and southern walls of BC are where the temporal variability of the vertical displacements is the highest with a standard deviation of 53 and 34 m, respectively.

The influence of submarine canyons on the transport paths resulted in a common drift direction with small divergences in the trajectories (see Fig. 9). Indeed, particles southwardly followed the continental slope and spread differently according to the canyon in which they were released. To begin with, transport paths starting in the CCC and at one depth layer (500/600, 600/700, or 700/800 m) did not overlap with the ones starting at another depth layer, and they kept a linear direction when particles left the CCC. Second, the simulated drifts that began from the PC were affected by internal circulation within the canyon (i.e., recirculation of the particles

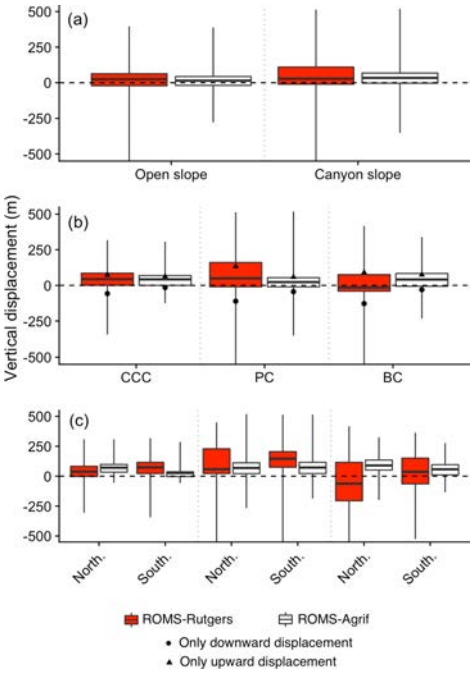

Figure 8. Particles vertical displacement. Vertical displacement according to particles drifting on the open slope or the canyon slope **(a)**, drifting within the canyons **(b)**, and released on the northern wall (North.) or southern wall (South.) of the canyons **(c)** in the ROMS-Rutgers and the ROMS-Agrif simulations. Release zone codes are as indicated in Fig. 1.

between the walls), and transport paths intersected. Last, the transport paths initialized from the BC barely left the canyon area and overlapped with the trajectories set up in a different depth layer. The overlap or intersection of the transport paths may be a consequence from the vertical displacement of the particles (see Figs. 7 and 8) that were constrained by the horizontal and vertical circulation variability (see Figs. 5 and 8).

3.2 Lagrangian dispersal within ROMS-Agrif outputs

The particles were transported further in the ROMS-Agrif configuration than in the ROMS-Rutgers configuration (Fig. 5), and particles from the canyon zones had traveled slightly further than particles from the open slopes. The general drift distances of particles are approximately 70.8 km (±26.3 km) and 44 km longer than drift in ROMS-Rutgers. Particles could drift up to the maximum distance of 197 km, detected for particles from the PC (see Fig. 5). Among the canyons, particles from CCC were transported the least distance: 47.1 km (±21 km). Oppositely, the released particles on PC averagely travel the furthest with drifts of 84.2 km (±24.9 km). Particles from canyon slope zones or open slope zones were transported 73.7 and 68.8 km, respectively, and even though the difference of drift distances is low (5 km), it is significantly different ($p < 0.05$). Within the canyons, the particles from the northern walls of the CCC and PC drift 66 km, which was 13 km less than the particles from the southern walls. In the BC, the tendency was for particles released on the northern wall to travel 84 km, or 10 km more than particles from the southern wall.

Southern transport of particles was on a broader scope than in ROMS-Rutgers (see Fig. 6). After a simulation period of 31 d, the retention rate by the release zones is 1 % to 43 % of particles (Fig. 6), making an average of 18 % (±14 %) of particles. Like in ROMS-Rutgers, the open slope OS 2 retains the least of particles (1 %). Consequently, a small proportion of 29 % of particles ends up in the PC, while the majority (64 %) connects with open slope OS 3. The particles from the CCC also have drifted in more zones than any other release places. They were transported in four different zones, which were OS 1 at 6 %, OS 2 at 9 %, PC at 45 %, and OS 3 at 19 %. Particularly, 45 % of particles connect to the PC and those particles are characterized by a drift of 70.5 km (±9 km) from 575 m (±77 m). A lower rate of dispersal is detected, as well, from PC to BC. On average, 25 % of particles drift approximately 86.6 km (±14.9 km) from 600 m (±82 m) to reach BC.

The pattern of vertical particle displacements in ROMS-Agrif was similar among the different release depths and topographic structures of the NW Mediterranean Sea (see Fig. 7). Overall, 37.3 % of particles reaches the layer above 500 m depth, while only 0.8 % of particles go deeper than 800 m. Particles released over the upper bottom depths (500/600 and 600/700 m) presented comparable but still significantly different ($p < 0.05$) vertical displacements even if they were released in canyons or on open slopes. Around 41 % and 43 % of particles drifted within the same depth layer as their releases and 44 % to 48 % ascended in upper depths. On the contrary and overall, from releases between isobaths 700/800 m, a majority of the particles (65 %) went upward, a high proportion of particles (6.1 %) went down below 800 m, and fewer particles were transported in the depth layer of their release (retention in the deeper layer of 29 %).

The average vertical displacement of particles was a small ascent in the water column (see Fig. 8), with canyons being the places of higher ascents. On average, particles rose 15 m (±53 m) when released on open slopes, and twice that, 34 m (±65 m), when released in canyons. Among the different canyons, particles released in the PC were vertically displaced the least (23 m on average, or half the rise of particles from the CCC and BC), but the widest vertical displacements of 352 m downwards and 519 m upwards were from PC. We

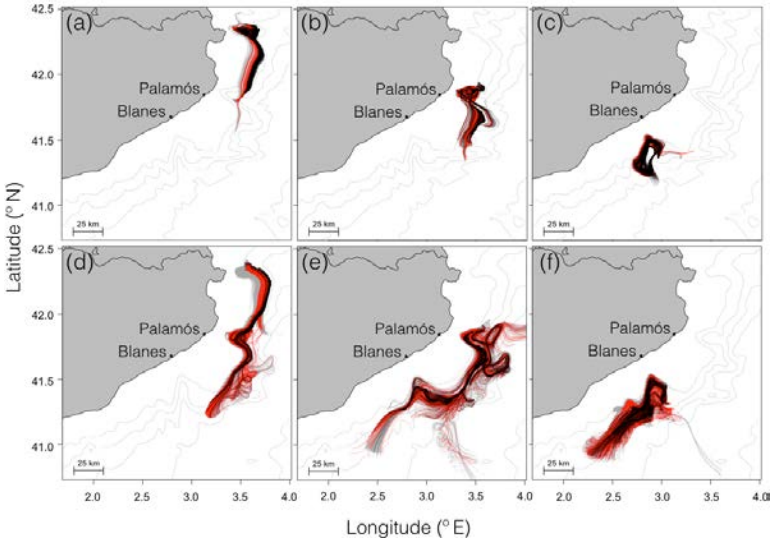

Figure 9. Estimated transport paths of passive particles during 31 d. Passive particles were released in the Cap de Creus canyon **(a, d)**, Palamós canyon **(b, e)**, Blanes canyon **(c, f)**, and advected by the modeled hydrodynamics from ROMS-Rutgers **(a–c)** and ROMS-Agrif **(d–f)**. Colors of the transport paths are associated with the depth ranges 500–600 m (gray), 600–700 m (red), and 700–800 m (black) on which particles were released.

furthermore notice that the average ascent and descent of particles were the highest in BC (74 m) and in PC (44 m), respectively, which are reversed directions of movement compared to the results in ROMS-Rutgers. Lastly, particles drifting above the northern wall of all the canyons significantly ($p < 0.05$) rise higher than for particles above the southern wall. In CCC, the rise of particles was 2.7 times higher on the northern wall (71 m) than on the southern wall, which represents the highest change in displacement between the walls. In contrast, in PC, the rise of particles reaches 68 m on the northern wall, which was 4 m less than for particles on the other wall. Over the different release dates, the southern wall of PC is where the vertical movement of particles temporally varies the most (standard deviation of 39 m).

With the simulation of passive drifts in ROMS-Agrif, patterns of particle trajectory were similar to the ones in ROMS-Rutgers, especially the southward drift direction and the spread of particles from the submarine canyons (see Fig. 9). Nonetheless, the length of the transport paths, as demonstrated by the drift distance values (see Fig. 5), was longer than in ROMS-Rutgers, and the spread of trajectories was wider. The spread was particularly amplified when particles drifted in the Palamós and Blanes canyons. For example, transport paths from the PC disclosed the advection of particles taken in two circular flows near this canyon, and the span of the transport paths from the BC widened once the particles left the canyon. Like for the simulations in ROMS-Rutgers, the variability in the transport path originated in the depth position of the particles (see Figs. 7 and 8). However, the spread of the trajectory was intensified as a consequence of the current intensity estimated in the ROMS-Agrif (see Fig. 4).

4 Discussions

Two hydrodynamic models with different implementations allowed for testing the sensitivity of particle dispersals to the Mediterranean Sea thermohaline circulation. The dispersal rates were low and similar to observations or simulations of deep larvae from other marine ecosystems like in the Baltic Sea and in another basin of the Mediterranean Sea (Corell et al., 2012; Palmas et al., 2017).

4.1 Deep-sea connectivity between submarine canyons

For the first time in the NW Mediterranean Sea, the connectivity between submarine canyons has been demonstrated through the Lagrangian transport of deep particles. The southwestward circulation having important amplitude in upper layers also predominated in the bottom drift simula-

tion and explained the particle trajectories from the northern canyons to the southern canyons. On a local scale (i.e., canyon area), submarine canyon areas received drifters from upstream release and seeded the nearest downstream open slopes. In fact, this result is related to the flows of the NW Mediterranean Sea following the right-hand side canyon walls (Flexas et al., 2008; Palanques et al., 2005; Granata et al., 1999; Jorda et al., 2013). With this, our drift simulations supported one of the submarine canyon functions, which consisted of seeding particles in neighboring zones.

Nonetheless, each submarine canyon has a singular topography and a different angle of exposure to the main circulation, resulting in different patterns of particle dispersals. In the horizontal dimension and inside each submarine canyon, particle drifts were different because they did not begin from the same depth, the same day, or with the same exposure to the current (i.e., releases on upstream or downstream canyon walls) even though the general canyon influence led to common north–south drift patterns. Those differences also appeared in analyses of sediment flux in the Mediterranean Sea (Durrieu de Madron et al., 1999; Lopez-Fernandez et al., 2013) and in simulations of passive particle drifts in different water layers (Ross et al., 2016). In the vertical dimension, our results reflected the uncorrelated currents occurring inside a canyon (Jorda et al., 2013) that could be one of the origins of the drift differences between canyons. For example, the amplitude of vertical drifts in Palamós canyon was greater than vertical drifts in the other canyons. The uncorrelated currents could also explain the general upward displacement of particles that were released on the upstream canyon walls. On the contrary, in shallow waters, previous flow studies on those canyon sides estimated a downward flux (Ahumada-Sempoal et al., 2015; Flexas et al., 2008; Granata et al., 1999).

Even though the main trajectory patterns persisted, canyon influence on dispersals changed over the summer releases. In Kool et al. (2015), the main deep circulation pattern over 3 years was consistent enough to not strongly impact the dispersals. This finding also applied for our results when the range of releases was over 2 months. Temporal variability around the main patterns was likely caused by the dynamic of the internal circulation over time inside the canyons (Ahumada-Sempoal et al., 2013; Palanques et al., 2005; Jorda et al., 2013). Nonetheless, further simulations of drifts need to be done to identify the minimum frequency of release to observe significant changes in the drift variability.

4.2 Sensitivity of the passive transport to deep-sea circulations

In our study, the large amplitude of dispersals in ROMS-Agrif was the main origin of differences between the drifts. Particle retention was 3.3 times higher with the simulation carried out with ROMS-Rutgers than with ROMS-Agrif. Whether the particles were released on canyon slopes or on open slopes did not change the fact that distance drifts were 2 times longer in simulations from ROMS-Agrif. The largest difference in amplitude of drifts (an average difference of 64.2 km) was simulated from the open slope between Palamós and Blanes canyons. There, in the ROMS-Rutgers bathymetric grid, the presence of a submarine valley in the slope ($\sim 41.5°$ N, $\sim 3.25°$ E) lowered the dispersal rates, and acted as a wall that generated distinct dispersal lengths depending on the side on which particles were released. In contrast, on the open slope between the Cap de Creus and Palamós canyons, the continental slope did not have specific topographic structure, and in both models the zone retention was low.

Thus, small topographic differences (e.g., the submarine valley) indirectly influenced the particle transport by conditioning the flow circulation when the hydrodynamic models were run. The main cause of topographic differences was related to the resolution of the bathymetric data sets chosen by the modelers. Indeed, an adequate bathymetric data set would approximate better the mesoscale structures of the water circulation (Gula et al., 2015). Then, it made the simulated drifts from the ROMS-Rutgers more appropriate for the deep passive drifts because the bathymetric data set was more precise (i.e., horizontal resolution of 100 m instead of 3 km) even though it has a lower horizontal resolution than the ROMS-Agrif. Another major difference within the drifts in the two hydrodynamic models was the northward drifts from Blanes canyon and from the open slope at its southern end (OS4) in ROMS-Rutgers. The northward particle drift is a consequence of an anticyclonic flow generated at the mouth of Blanes canyon that also affects the local deep water circulation (Ahumada-Sempoal et al., 2013; Jorda et al., 2013). The southwestward flow in ROMS-Agrif may be the consequence of the bathymetric data set used before the run of the hydrodynamic model and the hydrodynamic model parameterization of the water profile discretization. In ROMS models, the water is discretized by terrain-following sigma layers that generally have high resolution near the surface and relax the circulation variability near the bottom.

The generated drift uncertainties gave arguments for choosing one hydrodynamic model over another, above all when drifts are in deep water. In the absence of more hydrodynamic models, we encourage the deep-sea Lagrangian modeler to cross-validate the Lagrangian drifts with the existing literature. Our work evidences the importance of two major sources of uncertainty in the particle drifts from the hydrodynamic models: bathymetry and model discretization (i.e., choice of S-coordinate parameters). These two factors are shown to be particularly important in the zones near the canyons (all the water column) and open-slope areas. This is an important outcome for modeling studies. In this sense, this study shows the areas where uncertainty grows and so helps to evaluate when and where the choice of the hydrodynamic models will have a large impact on the drift results.

4.3 Relation between deep-sea circulation and larval cycle of *A. antennatus*

The association of eggs and larvae of *Aristeus antennatus* with passive particles comprised the first approach to their drift. Our study revealed interesting dispersal features which could be related to the ecology of *A. antennatus*. First, few particles in canyons were transported near 1000 m depth, where peaks of juvenile abundances have been reported at the end of fall (Sardà et al., 1997; D'Onghia et al., 2009; Sardà and Cartes, 1997). It would imply that the late larvae are helped or constrained by the vertical circulation to settle in the deep zones. Second, the low dispersal rates from the canyons highlighted that inactive larvae may be retained by those topographic structures. In fact, the morphology of the canyons facilitates the retention of pelagic particles for a few days (Ahumada-Sempoal et al., 2015; Rojas et al., 2014). In that case, it would mean that subpopulations of *A. antennatus* strongly depend on their own. Then, the surface of management plans should be structured to local shrimp fishing grounds, like the one in Palamós canyon (Boletín Oficial del Estado, 2013, 2018). Furthermore, because the submarine valley is localized between two areas of high fishing effort (Palamós and Blanes), there is an interest in its potential role for marine populations. Literature categorizes submarine valley effects as canyon influences, but, due to the exposure of the submarine valley to the current, an evaluation of whether the valley deviates or recirculates the flow is needed.

In this study, the duration of simulation corresponded to the first PLD approximation of *Aristeus antennatus* larvae generalized from penaeid larvae. Nonetheless, further studies need to explore the variability of the estimated dispersal features with longer PLDs. In the framework of the *A. antennatus* case study, the PLD length can be expanded in accordance with a plausible time range of 6 months, i.e., time between the beginning of the spawning peak in July and the period of sampled early juveniles (Sardà et al., 1997; D'Onghia et al., 2009; Sardà and Cartes, 1997). The effect of PLD length can also be estimated with water temperature changes during the larval drift, as they are likely to affect the PLD when *A. antennatus* larvae reach the warm surface waters (O'Connor et al., 2007). The larval behavior needs to be taken into account, because it can significantly affect the vertical position of decapod larvae in the water column and may influence the larval dispersal (Cowen and Sponaugle, 2009; Levin, 2006; Queiroga and Blanton, 2004). Few studies on *A. antennatus* larvae sampled in open ocean have revealed their presence in the surface water layer (Carbonell et al., 2010; Carretón et al., 2019; Heldt, 1955; Seridji, 1971; Torres et al., 2013). Sardà et al. (2004) and Palmas et al. (2017) assumed that positive buoyancy of eggs partly underlined the presence of individuals in the shallowest water layer. The buoyancy mechanism needs to be analyzed through sensitivity tests in order to compensate for the lack of accurate knowledge about it (Hilário et al., 2015; Ross et al., 2016).

5 Conclusions

Passive drifts of particles simulated by a Lagrangian transport model coupled with two hydrodynamic models (ROMS-Rutgers and ROMS-Agrif) were compared. The particle releases used characteristics of deep-sea red shrimp, *A. antennatus*, spawners and scarce knowledge of their free-living period (i.e., eggs and larvae). Then, drift simulations began in a highly disturbed circulation induced by the submarine canyons of the NW Mediterranean Sea. In general, horizontal dispersion of deep-sea passive particles was relatively short during the 31 d simulation, but their transports could establish links between the submarine canyons. Like numerous other studies, our work concludes that marine topographic features (i.e., the deep submarine canyons and submarine valleys) favored particle reception and retention. It also supports that the amplitude and variability of vertical displacement (upward and downward in the water column) are higher inside submarine canyons than on other parts of the continental slope. Besides, the variability in the particle vertical displacement was dependent on the three-dimensional distribution of particle releases in a submarine canyon. Variability in particle dispersions was also a consequence of differences between canyon topography and their exposure to the currents. This sensitivity to the topography highlighted the importance of the modeler choice before running hydrodynamic models. Having a finer bathymetry data input and a finer vertical resolution near the bottom (i.e., like in ROMS-Rutgers) is important for estimating the circulation and the passive dispersions with more accuracy, even though the hydrodynamic model has a coarse horizontal resolution (i.e., 2 km vs. 1.2 km). Therefore, the ROMS-Rutgers model was approved by better modeling the bottom drifts, and it will be used for future studies on the benthic deep-sea species *A. antennatus*. Numerical simulations of the larval drift are one of the best approaches that allowed for approximating the unknown dispersal paths of *A. antennatus* in the NW Mediterranean Sea. This study is the first step of a work conducted with the final focus to improve fishery management of a deep-sea species. However, observation of the pelagic larval traits, validation of the dispersals, and simulation including biological behaviors (vertical migration, buoyancy, and swimming abilities) are required before involving the results in the management strategies.

Code and data availability. The outputs (ROMS, script for Lagrangian model parameterization, and scripts for analysis) presented in this article are available from the first author upon request.

Supplement. The supplement related to this article is available online at: https://doi.org/10.5194/os-15-1-2019-supplement.

Author contributions. MCH carried out most of the research from the Lagrangian drift simulations to the analysis of the outputs. JS developed and validated the ROMS-Rutgers model. MAAS used his ROMS-Agrif model output to simulate Lagrangian drifts. FB provided codes for analyzing the Lagrangian drift sensitivity. GR and JBC guided the first author with the biology of the red shrimp. JBC is the principal researcher of CONECTA's project and provided the scholarship to MCH to realize this study. MCH prepared the article with contributions from all co-authors.

Competing interests. The authors declare that they have no conflict of interest.

Acknowledgements. The authors greatly thank for their time and support: Marta Carretón, the computer technicians from the Centre d'Estudis Avançats de Blanes (CEAB), and the personal from the Institut de Cienciès del Mar(ICM) at Barcelona. The authors also appreciated the numerous comments which helped to structure the article.

Financial support. Funding was provided through the CONECTA project supported by the Ministerio de Economia, Industria y Competividad from the Spanish Government. Morane Clavel-Henry is funded under an FPI PhD program of the Spanish Government (grant no. BES-2015-074126).

Review statement. This paper was edited by John M. Huthnance and reviewed by Xavier Durrieu de Madron and one anonymous referee.

References

Adani, M., Dobricic S, and Pinardi, N.: Quality assessment of a 1985–2007 Mediterranean Sea reanalysis, J. Atmos. Ocean. Tech., 28, 569–589, https://doi.org/10.1175/2010JTECHO798.1, 2011.

Ahumada-Sempoal, M. A., Flexas, M. M., Bernardello, R., Bahamon, N., and Cruzado, A.: Northern Current variability and its impact on the Blanes Canyon circulation: A numerical study, Prog. Oceanogr., 118, 61–70, https://doi.org/10.1016/j.pocean.2013.07.030, 2013.

Ahumada-Sempoal, M. A., Flexas, M. M., Bernardello, R., Bahamon, N., Cruzado, A., and Reyes Hernández, C.: Shelf-slope exchanges and particle dispersion in Blanes submarine canyon (NW Mediterranean Sea): A numerical study, Cont. Shelf Res., 109, 35–45, 2015.

Andrello, M., Mouillot, D., Beuvier, J., Albouy, C., Thuiyse, W., and Manel, S.: Low Connectivity between Mediterranean Marine Protected Areas: A Biophysical Modeling Approach for the Dusky Grouper *Epinephelus marginatus*, PLOS ONE, 8, e68564, https://doi.org/10.1371/journal.pone.0068564, 2013.

Arellano, S. M., Van Gaest, A. L., Johnson, S. B., Vrijenhoek, R. C., and Young, C. M.: Larvae from deep-sea methane seeps disperse in surface waters, P. Roy. Soc. B-Biol. Sci., 281, 20133276, https://doi.org/10.1098/rspb.2013.3276, 2014.

Basterretxea, G., Jordi, A., Catalán, I. A., and Sabatés, A.: Model-based assessment of local-scale fish larval connectivity in a network of marine protected areas, Fish. Oceanogr., 21, 291–306, https://doi.org/10.1111/j.1365-2419.2012.00625.x, 2012.

Boletín Oficial del Estado: Orden AAA/923/2013 de 16 de Mayo, no 126, Sec. III, 2013.

Boletín Oficial del Estado, Orden APM/532/2018 de 26 de Mayo, no 128, Sec. III, 2018.

Canals, M., Danovaro, R., Heussner, S., Lykousis, V., Puig, P., Trincardi, F., and Sanchez-Vidal, A.: Cascades in Mediterranean submarine grand canyons, Oceanography, 22, 26–43, 2009.

Carbonell, A., Dos Santos, A., Alemany, F., and Vélez-Belchi, P.: Larvae of the red shrimp *Aristeus antennatus* (Decapoda: Dendrobranchiata: Aristeidae) in the Balearic Sea: new occurrences fifty years later, Mar. Biodivers. Rec., 3, E103, https://doi.org/10.1017/s1755267210000758, 2010.

Carretón, M., Company, J. B., Planella, L., Heras, S., García-Marín, J. L., Agulló, M., Clavel-Henry, M., Rotllant, G., dos Santos, A., and Roldán, M. I.: Morphological identification and molecular confirmation of the deep-sea blue and red shrimp *Aristeus antennatus* larvae, Peer J., 7, e6063, https://doi.org/10.7717/peerj.6063, 2019.

Chen, C., Liu, H., and Beardsley, R. C.: An Unstructured Grid, Finite-Volume, Three-Dimensional, Primitive Equations Ocean Model: Application to Coastal Ocean and Estuaries, J. Atmos. Ocean. Tech., 20, 159–186, https://doi.org/10.1175/1520-0426(2003)020<0159:AUGFVT>2.0.CO;2, 2003.

Coll, M., Steenbeek, J., Solé, J., Palomera, I., and Christensen, W.: Modelling the cumulative spatial–temporal effects of environmental drivers and fishing in a NW Mediterranean marine ecosystem, Ecol. Modell., 331, 100–114, https://doi.org/10.1016/j.ecolmodel.2016.03.020, 2016.

Corell, H., Moksnes, P. O., Engqvist, A., Döös, K., and Jonsson, P. R.: Depth distribution of larvae critically affects their dispersal and the efficiency of marine protected areas, Mar. Ecol. Prog. Ser., 467, 29–46, 2012.

Cowen, R. K. and Sponaugle, S.: Larval dispersal and marine population connectivity, Annu. Rev. Mar. Sci., 1, 443–466, https://doi.org/10.1146/annurev.marine.010908.163757, 2009.

Cromey, C. J. and Black, K. D.: Modelling the Impacts of Finfish Aquaculture, in: Environmental Effects of Marine Finfish Aquaculture, edited by: Hargrave B. T., Handbook of Environmental Chemistry, vol 5M, Springer, Berlin, Heidelberg, 129–155, 2005.

Dall, W.: The biology of the Penaeidae, Adv. Mar. Biol., 27, 489 pp., 1990.

Debreu, L., Marchesiello, P., Penven, P., and Cambon, G.: Two-way nesting in split-explicit ocean models: algorithms, implementation and validation, Ocean Modell., 49–50, 1–21, https://doi.org/10.1016/j.ocemod.2012.03.003, 2012.

Dee, D. P., Uppala, S. M., Simmons, A. J., Berrisford, P., Poli, P., Kobayashi, S., Andrae, U., Balmaseda, M. A., Balsamo, G., Bauer, P., Bechtold, P., Beljaars, A. C. M., van de Berg, L. Bidlot, J., Bormann, N., Delsol, C., Dragani, R., Fuentes, M., Geer, A. J., Haimberger, L., Healy, S. B., Hersbach, H., Hólm, E. V., Isaksen, L., Kållberg, P., Köhler, M., Matricardi, M., McNally, A. P., Monge-Sanz, B. M., Morcrette, J.-J., Park, B.-K.,Peubey, C.,de Rosnay, P., Tavolato, C., Thépaut, J.-N., and Vitart, F.: The

ERA-Interim reanalysis: configuration and performance of the data assimilation system, Q. J. Roy. Meteorol. Soc., 137, 553–597, https://doi.org/10.1002/qj.828, 2011.

Demestre, M. and Fortuno, J. M.: Reproduction of the deep-water shrimp *Aristeus antennatus* (Decapoda: Dendrobranchiata), Mar. Ecol. Prog. Ser., 84, 41–51, 1992.

Demestre, M. and Lleonart, J.: Population dynamics of *Aristeus antennatus* (Decapoda: Dendrobranchiata) in the northwestern Mediterranean, Sci. Mar., 57, 183–189, 1993.

D'Onghia, G., Maiorano, P., Capezzuto, F., Carlucci, R., Battista, D., Giove, A., and Tursi, A.: Further evidences of deep-sea recruitment of *Aristeus antennatus* (Crustacea: Decapoda) and its role in the population renewal on the exploited bottoms of the Mediterranean, Fish. Res., 95, 236–245, https://doi.org/10.1016/j.fishres.2008.09.025, 2009.

Durrieu de Madron, X., Radakovitch, O., Heussner, S., Loye-Pilot, M. D., and Monaco, A.: Role of the climatological and current variability on shelf-slope exchanges of particulate matter: Evidence from the Rhône continental margin (NW Mediterranean), Deep-Sea Res. Pt. I, 46, 1513–1538, https://doi.org/10.1016/S0967-0637(99)00015-1, 1999.

Etter, R. J. and Bower, A. S.: Dispersal and population connectivity in the deep North Atlantic estimated from physical transport processes, Deep-Sea Res. Pt. I, 104, 159–172, https://doi.org/10.1016/j.dsr.2015.06.009, 2015.

Fairall, C. W., Bradley, E. F., Rogers, D. P., Edson, J. B., and Young, G. S.: Bulk parameterization of air-sea fluxes for tropical ocean-global atmosphere coupled-ocean atmosphere response experiment, J. Geophys. Res., 101, 3747–3764, https://doi.org/10.1029/95JC03205, 1996.

Fernandez-Arcaya, U., Ramirez-Llodra, E., Aguzzi, J., Allcock, A. L., Davies, J. S., Dissanayake, A., and Van den Beld, I. M. J.: Ecological Role of Submarine Canyons and Need for Canyon Conservation: A Review, Front. Mar. Sci., 4, 26, https://doi.org/10.3389/fmars.2017.00005, 2017.

Flexas, M. M., Boyer, D. L., Espino, M., Puigdefábregas, J., Rubio, A., and Company, J. B.: Circulation over a submarine canyon in the NW Mediterranean, J. Geophys. Res., 113, C12002, https://doi.org/10.1029/2006JC003998, 2008.

Gorelli, G., Company, J. B., and Sardà, F.: Management strategies for the fishery of the red shrimp *Aristeus antennatus* in Catalonia (NE Spain), Marine Stewardship Council Science Series, 2, 116–127, 2014.

Granata, T. C., Vidondo, B., Duarte, C. M., Satta, M. P., and Garcia, M.: Hydrodynamics and particle transport associated with a submarine canyon off Blanes (Spain), NW Mediterranean Sea, Cont. Shelf Res., 19, 1249–1263, https://doi.org/10.1016/S0278-4343(98)00118-6, 1999.

Gula, J., Molemaker, M. J., and McWilliams, J. C.: Topographic vorticity generation, submesoscale instability and vortex street formation in the Gulf Stream, Geophys. Res. Lett., 42, 4054–4062, 2015.

Heldt, J. H.: Contribution à l'étude de la biologie des crevettes pénéides: *Aristaeomorpha foliacea* (Risso) et *Aristeus antennatus* (Risso), formes larvaires, Bulletin de la Société des Sciences Naturelles de Tunisie, VIII(1–2), 1–29, 1955.

Hilário, A., Metaxas, A., Gaudron, S., Howell, K., Mercier, A., Mestre, N., and Young, C.: Estimating dispersal distance in the deep sea: challenges and applications to marine reserves, Front. Mar. Sci., 2, 14, https://doi.org/10.3389/fmars.2015.00006, 2015.

Jones, C. E., Dagestad, K.-F., Breivik, Ø., Holt, B., Röhrs, J., Christensen, K. H., and Skrunes, S.: Measurement and modeling of oil slick transport, J. Geophys. Res.-Oceans, 121, 7759–7775, https://doi.org/10.1002/2016JC012113, 2016.

Jorda, G., Flexas, M. M., Espino, M., and Calafat, A.: Deep flow variability in a deeply incised Mediterranean submarine valley (Blanes canyon), Prog. Oceanogr., 118, 47–60, https://doi.org/10.1016/j.pocean.2013.07.024, 2013.

Jordi, A., Basterretxea, G., Orfila, A., and Tintoré, J.: Analysis of the circulation and shelf-slope exchanges in the continental margin of the northwestern Mediterranean, Ocean Sci., 2, 173–181, https://doi.org/10.5194/os-2-173-2006, 2006.

Kool, J. T., Huang, Z., and Nichol, S. L.: Simulated larval connectivity among Australian southwest submarine canyons, Mar. Ecol. Prog. Ser., 539, 77–91, 2015.

Kough, A. S., Paris, C. B., and Butler IV, M. J.: Larval connectivity and the International Management of fisheries, PLOS ONE, 8, e64970, https://doi.org/10.1371/journal.pone.0064970, 2013.

Large, W., McWilliams, J., and Doney, S.: Oceanic vertical mixing: a review and a model with a nonlocal boundary layer parameterization, Rev. Geophys., 32, 363–403, 1994.

Lebreton, L. C. M., Greer, S. D., and Borrero, J. C.: Numerical modelling of floating debris in the world's oceans, Mar. Pollut. Bull., 64, 653–661, 2012.

Lett, C., Verley, P., Mullon, C., Parada, C., Brochier, T., Penven, P., and Blanke, B. A.: Lagrangian tool for modelling ichthyoplankton dynamics, Environ. Modell. Soft., 23, 1210–1214, https://doi.org/10.1016/j.envsoft.2008.02.005, 2008.

Levin, L. A. and Bridges, T. S.: Pattern and diversity in reproduction and development, edited by: McEdward, L., CRC Press, Boca Raton, 1995.

Levin, L. A.: Recent progress in understanding larval dispersal: new directions and digressions, Integr. Comparat. Biol., 46, 282–297, https://doi.org/10.1093/icb/icj024, 2006.

Lopez-Fernandez, P., Calafat, A., Sanchez-Vidal, A., Canals, M., Mar Flexas, M., Cateura, J., and Company, J. B.: Multiple drivers of particle fluxes in the Blanes submarine canyon and southern open slope: Results of a year round experiment, Prog. Oceanogr., 118, 95–107, https://doi.org/10.1016/j.pocean.2013.07.029, 2013.

Millot, C.: Circulation in the Western Mediterranean Sea, J. Mar. Syst., 20, 423–442, 1999.

North, E. W.: Vertical swimming behavior influences the dispersal of simulated oyster larvae in a coupled particle-tracking and hydrodynamic model of Chesapeake Bay, Mar. Ecol. Prog. Ser., 359, 99–115, https://doi.org/10.3354/meps07317, 2008.

North, E. W., Gallego, A., and Petitgas, P.: Manual of recommended practices for modelling physical-biological interactions during fish early life, ICES Cooperative Research Report, 295, 111 pp., 2009.

O'Connor, M. I., Bruno, J. F., Gaines, S. D., Halpern, B. S., Lester, S. E., Kinlan, B. P., and Weiss, J. M.: Temperature control of larval dispersal and the implications for marine ecology, evolution, and conservation, P. Natl. Acad. Sci. USA, 104, 1266–1271, https://doi.org/10.1073/pnas.0603422104, 2007.

Ospina-Álvarez, A., Bernal, M., Catalán, I. A., Roos, D., Bigot, J.-L., and Palomera, I.: Modeling Fish Egg Production and

Spatial Distribution from Acoustic Data: A Step Forward into the Analysis of Recruitment, PLOS ONE, 8, e73687, https://doi.org/10.1371/journal.pone.0073687, 2013.

Palanques, A., García-Ladona, E., Gomis, D., Martín, J., Marcos, M., Pascual, A., and Pagès, F.: General patterns of circulation, sediment fluxes and ecology of the Palamós (La Fonera) submarine canyon, northwestern Mediterranean, Prog. Oceanogr., 66, 89–119, https://doi.org/10.1016/j.pocean.2004.07.016, 2005.

Palmas, F., Olita, A., Addis, P., Sorgente, R., and Sabatini, A.: Modelling giant red shrimp larval dispersal in the Sardinian seas: density and connectivity scenarios, Fish. Oceanogr., 26, 364–378, https://doi.org/10.1111/fog.12199, 2017.

Paris, C. B., Helgers, J., van Sebille, E., and Srinivasan, A.: Connectivity Modeling System: A probabilistic modeling tool for the multi-scale tracking of biotic and abiotic variability in the ocean, Environ. Modell. Soft., 42, 47–54, https://doi.org/10.1016/j.envsoft.2012.12.006, 2013.

Penven, P., Marchesiello, P., Debreu, L., and Lefèvre, J.: Software tools for pre- and post-processing of oceanic regional simulations, Environ. Modell. Soft., 23, 660–662, https://doi.org/10.1016/j.envsoft.2007.07.004, 2008.

Pepin, P.: Effect of Temperature and Size on Development, Mortality, and Survival Rates of the Pelagic Early Life History Stages of Marine Fish, Can. J. Fish. Aquat. Sci., 48, 503–518, https://doi.org/10.1139/f91-065, 1991.

Puig, P., Ogsto, A. S., Mullenbach, B. L., Nittrouer, C. A., and Sternberg, R. W.: Shelf-to-canyon sediment transport processes on the Eel Continental Margin (Nothern California), Mar. Geol., 193, 129–149, 2003.

Qiu, Z. F., Doglioli, A. M., He, Y. J., and Carlotti, F.: Lagrangian model of zooplankton dispersion: numerical schemes comparisons and parameter sensitivity tests, Chin. J. Oceanol. Limn., 29, 438–445, https://doi.org/10.1007/s00343-011-0015-9, 2011.

Queiroga, H. and Blanton, J.: Interactions Between Behaviour and Physical Forcing in the Control of Horizontal Transport of Decapod Crustacean Larvae, Adv. Mar. Biol., 47, 107–214, 2004.

Rojas, P., Garcia, M.A., Sospedra, J., Figa, J., De Fàbregas, J., López, O., Espino, M., Ortiz, V., Sanchez-Arcilla, A., Manriquez, M., and Shirasago, B.: On the structure of the mean flow in the Blanes Canyon Area (NW Mediterranean) during summer, Oceanologica Acta, 18, 443–454, 1995.

Rojas, P. M. and Landaeta, M. F.: Fish larvae retention linked to abrupt bathymetry at Mejillones Bay (northern Chile) during coastal upwelling events, Lat. Am. J. Aquat. Res., 42, 989–1008, 2014.

Ross, R. E., Nimmo-Smith, W. A. M, and Howell, K. L.: Increasing the Depth of Current Understanding: Sensitivity Testing of Deep-Sea Larval Dispersal Models for Ecologists, PLOS ONE, 11, e0161220, https://doi.org/10.1371/journal.pone.0161220, 2016.

Sardà, F. and Cartes, J. E.: Morphological features and ecological aspects of early juvenile specimens of the aristeid shrimp *Aristeus antennatus* (Risso, 1816), Mar. Freshwater Res., 48, 73–77, https://doi.org/10.1071/MF95043, 1997.

Sardà, F. and Company, J. B.: The deep-sea recruitment of *Aristeus antennatus* (Risso, 1816) (Crustacea: Decapoda) in the Mediterranean Sea, J. Mar. Syst., 105–108, 145–151, https://doi.org/10.1016/j.jmarsys.2012.07.006, 2012.

Sardà, F., Maynou, F., and Tallo, L.: Seasonal and spatial mobility patterns of rose shrimp *Aristeus antennatus* in the western Mediterranean: results of a long-term study, Mar. Ecol.-Prog. Ser., 159, 133–141, 1997.

Sardà, F., D'Onghia, G., Politou, C. Y., Company, J. B., Maiorano, P., and Kapiris, K.: Deep-sea distribution, biological and ecological aspects of *Aristeus antennatus* (Risso, 1816) in the Western and Central Mediterranean Sea, Sci. Mar., 68, 117–127, 2004.

Schram, F., von Vaupel Klein, C., Charmantier-Daures, M., and Forest, J.: Treatise on Zoology – Anatomy, Taxonomy, Biology, The Crustacea, Volume 9 Part A: Eucarida: Euphausiacea, Amphionidacea, and Decapoda (partim), Brill, Leiden, the Netherlands, 2010.

Seridji, R.: Contribution à l'étude des larves crustacés décapods en Baie d'Alger, Pelagos, 3, 1–105, 1971.

Shan S., Sheng J., and Greenan B. J. W.: Physical processes affecting circulation and hydrography in the Sable Gully of Nova Scotia, Deep-Sea Res. Pt. II, 104, 35–50, 2014.

Shchepetkin, A. A.: Method for computing horizontal pressure-gradient force in an oceanic model with a nonaligned vertical coordinate, J. Geophys. Res., 108, 3090, https://doi.org/10.1029/2001JC001047, 2003.

Shchepetkin, A. F. and McWilliams, J. C.: The regional oceanic modeling system (ROMS): a split-explicit, free-surface, topography-following-coordinate oceanic model, Ocean Modell., 9, 347–404, https://doi.org/10.1016/j.ocemod.2004.08.002, 2005.

Siegel, D. A., Kinlan, B. P., Gaylord, B., and Gaines, S. D.: Lagrangian descriptions of marine larval dispersion, Mar. Ecol. Prog. Ser., 260, 83–96, 2003.

Simons, R. D., Siegel, D. A., and Brown, K. S.: Model sensitivity and robustness in the estimation of larval transport: A study of particle tracking parameters, J. Mar. Syst., 119–120, 19–29, https://doi.org/10.1016/j.jmarsys.2013.03.004, 2013.

Smith, W. H. F. and Sandell, D. T.: Global seafloor topography from satellite altimetry and ship depth soundings, Science, 277, 1957–1962, 1997.

Smolarkiewicz, P. K. and Margolin L. G.: MPDATA: A finite-difference solver for geophysical flows, J. Comput. Phys., 140, 459–480, https://doi.org/10.1006/jcph.1998.5901, 1998.

Solé, J., Ballabrera-Poy, J., Macías, D., and Catalán, I. A.: The role of ocean velocities in chlorophyll variability. A modeling study in the Alboran Sea, Sci. Mar., 80, 249–256, https://doi.org/10.3989/scimar.04290.04A, 2016.

Solé, J., Emelianov, M., García-Ladona, E., Ostrovskii, A., and Puig, P.: Fine-scale water mass variability inside a narrow submarine canyon (the Besòs Canyon) in the NW Mediterranean Sea, Sci. Mar., 80, 195–204, https://doi.org/10.3989/scimar.04322.05A, 2016.

Taylor, K. E.: Summarizing multiple aspects of model performance in a single diagram, J. Geophys. Res.-Atmos., 106, 7183–7192, 2001.

Thatje, S., Bacardit, R., and Arntz, W.: Larvae of the deep-sea Nematocarcinidae (Crustacea: Decapoda: Caridea) from the Southern Ocean, Polar Biol., 28, 290–302, https://doi.org/10.1007/s00300-004-0687-0, 2005.

Torres, A. P., Santos, A., Alemany, F., and Massutí, E.: Larval stages of crustacean species of interest for conservation and fishing exploitation in the Western Mediterranean, Sci. Mar., 77, 149–160, https://doi.org/10.3989/scimar.03749.26D, 2013.

Tudela, S., Sardà, F., Maynou, F., and Demestre, M.: Influence of Submarine Canyons on the Distribution of the Deep-Water Shrimp, *Aristeus antennatus* (Risso, 1816) in the NW Mediterranean, Crustaceana, 76, 217–225, 2003.

Uppala, S. M., KÅllberg, P. W., Simmons, A. J., Andrae, U., Bechtold, V. D. C., Fiorino, M., Gibson, J. K., Haseler, J., Hernandez, A., Kelly, G. A., Li, X., Onogi, K., Saarinen, S., Sokka, N., Allan, R. P., Andersson, E., Arpe, K., Balmaseda, M. A., Beljaars, A. C. M., Berg, L. V. D., Bidlot, J., Bormann, N., Caires, S., Chevallier, F., Dethof, A., Dragosavac, M., Fisher, M., Fuentes, M., Hagemann, S., Hólm, E., Hoskins, B. J., Isaksen, L., Janssen, P. A. E. M., Jenne, R., Mcnally, A. P., Mahfouf, J.-F., Morcrette, J.-J., Rayner, N. A., Saunders, R. W., Simon, P., Sterl, A., Trenberth, K. E., Untch, A., Vasiljevic, D., Viterbo, P., and Woollen, J.: The ERA-40 re-analysis, Q. J. Roy. Meteorol. Soc., 131, 2961–3012, https://doi.org/10.1256/qj.04.176, 2005.

Williamson, D. I.: Larval morphology and diversity, in: The Biology of Crustacea, edited by: Abele, L. G., Vol. 2, Embryology, Morphology, and Genetics, Academic Press, New York, 489 pp., 1982.

Young, C. M., He, R., Emlet, R. B., Li, Y., Qian, H., Arellano, S. M., and Rice, M. E.: Dispersal of Deep-Sea Larvae from the Intra-American Seas: Simulations of Trajectories using Ocean Models, Integr. Comparat. Biol., 52, 483–496, https://doi.org/10.1093/icb/ics090, 2012.

Annex 2

PLOS ONE

RESEARCH ARTICLE

Modeled buoyancy of eggs and larvae of the deep-sea shrimp *Aristeus antennatus* (Crustacea: Decapoda) in the northwestern Mediterranean Sea

Morane Clavel-Henry[1☯]*, Jordi Solé[2☯], Trond Kristiansen[3☯], Nixon Bahamon[1,4☯], Guiomar Rotllant[1☯], Joan B. Company[1☯]

1 Department of Renewable Marine Resources, Institut de Ciències del Mar—Consejo Superior de Investigaciones Científicas, Barcelona, Spain, **2** Department of Physical and Technological Oceanography, Institut de Ciències del Mar—Consejo Superior de Investigaciones Científicas, Barcelona, Spain, **3** Department of Marine Biogeochemistry and Oceanography, Norwegian Institute for Water Research, Oslo, Norway, **4** Centro de Estudios Avanzados de Blanes—Consejo Superior de Investigaciones Científicas, Blanes, Spain

☯ These authors contributed equally to this work.
* morane@icm.csic.es

OPEN ACCESS

Citation: Clavel-Henry M, Solé J, Kristiansen T, Bahamon N, Rotllant G, Company JB (2020) Modeled buoyancy of eggs and larvae of the deep-sea shrimp *Aristeus antennatus* (Crustacea: Decapoda) in the northwestern Mediterranean Sea. PLoS ONE 15(1): e0223396. https://doi.org/10.1371/journal.pone.0223396

Editor: Atsushi Fujimura, University of Guam, GUAM

Received: September 18, 2019

Accepted: December 11, 2019

Published: January 29, 2020

Peer Review History: PLOS recognizes the benefits of transparency in the peer review process; therefore, we enable the publication of all of the content of peer review and author responses alongside final, published articles. The editorial history of this article is available here: https://doi.org/10.1371/journal.pone.0223396

Data Availability Statement: All relevant data are within the paper and its Supporting Information files.

Abstract

Information on the buoyancy of eggs and larvae from deep-sea species is rare but necessary for explaining the position of non-swimming larvae in the water column. Due to embryonic morphology and ecology diversities, egg buoyancy has important variations within one species and among other ones. Nevertheless, it has hardly been explored if this buoyancy variability can be a strategy for deep-sea larvae to optimize their transport beyond their spawning areas. In the northwestern Mediterranean Sea, protozoea and mysis larvae of the commercial deep-sea shrimp *Aristeus antennatus* were recently found in upper layers, but to present, earlier stages like eggs and nauplii have not been collected. Using a Lagrangian transport model and larval characteristics, we evaluate the buoyancy and hydrodynamic effects on the transport of *A*. *antennatus'* larvae in the northwestern Mediterranean Sea. The transport models suggested that 75% of buoyant eggs released between 500 and 800 m depth (i.e., known spawning area), reached the upper water layers (0–75 m depth). Then, according to the modeled larval drifts, three spawning regions were defined in the studied area: 1) the northern part, along a continental margin crossed by large submarine canyons; 2) the central part, with two circular circulation structures (i.e., eddies); and 3) the southern part, with currents flowing through a channel. The number of larvae in the most upper layer (0–5 m depth) was higher if the larval transport model accounted for the ascent of eggs and nauplii (81%) instead of eggs reaching the surface before hatching (50%). The larvae reaching the most water upper layer (0–5 m depth) had higher rates of dispersal than the ones transported below the surface layer (deeper than 5 m depth). The results of larval dispersal simulations have implications for the understanding of *A*. *antennatus* larval ecology and for management decisions related to the shrimp fisheries in the northwestern Mediterranean Sea.

Funding: This work was supported by the Ministerio de Economía, Industria y Competitividad, Gobierno de España (BES-2015-074126) to support her PhD within the CONECTA project (CTM2014-54648-C2-1-R) to MC-H. The funder had no role in study design, data collection and analysis, decision to publish, or preparation of the manuscript.

Competing interests: The authors have declared that no competing interests exist.

Introduction

Numerous species have a pelagic larval cycle which links the spawning places to the recruitment areas. Larval cycle is a relatively short time lapse compared to the life cycle of marine animal, but it is the phase when large dispersions occur [1]. For benthic species, the distribution of the species mostly relies on the transported larvae. Larvae have several mechanisms for positioning themselves in productive and favorable waters that optimize their growth and displacement [2]. According to those mechanisms, the larvae can be retained on the spawning places or connect to other areas that are of high interest for species with high commercial value. For that reason, many studies specifically addressed larval drifts in order to determine the efficiency of the fisheries management [3, 4].

Aristeus antennatus is a deep-sea shrimp with a high commercial value in the northwestern Mediterranean Sea. Since 1980, the reproductive cycle, biology, and the temporal and spatial dynamics of *A*. *antennatus* have been intensively studied based on data from commercial and scientific surveys [5–8]. The acquired knowledge has contributed to shape a local management plan which restricts fishing activity on *A*. *antennatus* since 2012 for the harbor with the highest landings (Palamós) [9, 10]. The current local management plan was implemented, partly assuming that the protected population of *A*. *antennatus* would increase the following years on the trawling grounds, and partly based on the idea that recruited juveniles are related to the spawners living on the trawling restricted area.

Nonetheless, like many deep-sea species, knowledge about the early-life stages of *A*. *antennatus* and their behaviors is scarce. In the case of *A*. *antennatus*, knowledge can be gathered from various larvae of Dendrobranchiata species, which is the taxonomic family of *A*. *antennatus*, *e.g*., larvae molt after the hatching of eggs with the following order: nauplii, protozoea, and mysis. Lecithotrophic stages (eggs and nauplii) of *A*. *antennatus* have not been observed yet, but its first planktotrophic stage (protozoea) is largely found in the surface layer [11]. Because ripe females spawn on the sea bottom, the embryonic and nauplius stages are assumed to have abilities (buoyancy, swimming ability) that take them to the surface. In [12], an Individual-Based Model (IBM) study showed that the near-bottom circulation has minor effect on passive individual dispersal (encompassing neutral eggs and inactive larvae of *A*. *antennatus*). The study indicated that near-bottom vertical currents do not advect individuals up to shallower layers, and suggested that the vertical distribution of eggs or larvae can only be explained by their capacity of moving across the water column. To our knowledge, the youngest stage of *A*. *antennatus*' larvae found in superficial waters is the first substage of protozoea [11, 13]. This finding supports the hypothesis of positive buoyancy in the previous stages of *A*. *antennatus*' larvae.

Buoyancy adjusts the vertical egg position in the water column by the difference between egg and water densities [14–16]. To date, because either some deep-sea species are gravid (i.e., eggs carried by the spawners) or egg information is unavailable, larval dispersal of deep-sea species rarely accounted for the simulation of the stages that interact with the water density. Within the Dendrobranchiata family or within other deep-sea Decapod species, diverse egg sizes and densities [17] were observed but were not comparable with the assumed characteristics of *A*. *antennatus*' eggs. In advanced stages of Decapod larvae from various ecosystems (coastal, estuarine, and deep-sea), several patterns of vertical distribution and displacements have also been described [17]. For example, Penaeid nauplii can be found in superficial layers [18, 19] or near the bottom [20]. This biodiversity translates how challenging and delicate is the generalization of the larval behavior to each unknown larval stage of the deep-sea red shrimp.

Although little is known about the *A*. *antennatus*' larvae, and as for other deep-sea species, it is likely that the vertical position of larvae is determinant for dispersal because the surface

water has stronger velocity and higher temperature than deeper water layers [21, 22]. A number of hydrodynamic processes in the upper waters of the northwestern Mediterranean Sea can disperse or retain the larvae. The main circulation is driven by the Northern Current that flows southwestward between the surface and 250 m depth with maximum velocities around 0.30 m/s [23]. Several eddies circulate in a clockwise or anticlockwise direction and drive the distribution of larvae in the surface layer [24]. Those structures are unstably present during a few weeks and have different sizes and locations [25]. In summer, the Mediterranean Sea is also well-stratified by a thermocline around 15 m deep [26]. This thermocline forms a physical barrier for some small-scale ocean processes such as water mixing [27], and therefore can limit vertical displacement of Decapod larval stages [28, 29].

In this paper, we analyze the impact of buoyancy variability and three-dimensional water mass circulation on the drifts of eggs and larvae between spawning and recruitment areas for the benthic deep-sea shrimp *A. antennatus* species in the northwestern Mediterranean Sea. This work was an opportunity to test for the first time a protocol to define buoyancy values for undescribed larval stages of a deep-sea species and to provide new elements for the management plan makers.

Material and methods

An Individual-Based Model (IBM) for embryonic and larval stages of the deep-sea red shrimp (*A. antennatus*) was implemented with a Lagrangian particle-tracking framework. It simulated the early life-cycle behavior and dispersal patterns of shrimp larvae using 3D hydrodynamic model outputs of the northwestern (NW) Mediterranean Sea.

The hydrodynamic model

A climatological simulation of the NW Mediterranean Sea hydrodynamics was run using the Regional Ocean Modeling System (ROMS; [30]), a free-surface, terrain-following, primitive equation ocean model. A Mellor-Yamada 2.5 turbulence closure scheme is used for subgrid-scale mixing in the simulation [31]. Different models (IBM in [12], and a spatiotemporal food web model (Ecopath with Ecosim) in [32]) have successfully used the daily outputs of the ROMS model in the NW Mediterranean Sea and on the Valencian Gulf. The simulation domain ranged from 38˚ N to 43.69˚ N and from 0.65˚ W to 6.08˚ E (Fig 1), with a grid spacing of 2 km (with 256 x 384 grid points horizontally). The vertical domain is discretized using 40 vertical levels with a finer resolution near the surface (surface layer thickness between 0.49 m and 5.91 m). ROMS is built forced by a high resolution and accurate bathymetry of the western Mediterranean basin, which is fundamental for the drift study of *A. antennatus*' eggs and larvae because adults are benthic and females spawn around 800 m depth [33].

The ROMS outputs are validated in [12] and provided realistic products of the hydrodynamic and hydrographic characteristics (current velocities, salinity, and temperature) of the NW Mediterranean Sea. The upper water layers were characterized by the main southward current (i.e., the Northern Current) following the eastern coast of Spain and by several mesoscale circulations, like eddies. We estimated eddy size and center over monthly-averaged ROMS current velocities field with an algorithm described in [34]. Seawater density is a derived product of the salinity and temperature (equation 13 in [35]). On the horizontal dimension, average estimated temperature, salinity, and seawater density in summer (i.e., July to September) are 27.6˚C, 37.5 PSU, and 1026.3 kg/m^3 at the surface and 13.1˚C, 38.2 PSU and 1035.35 kg/m^3, at bottom, respectively. Those values are in the range of seawater measurements carried out in the NW Mediterranean Sea [23, 36].

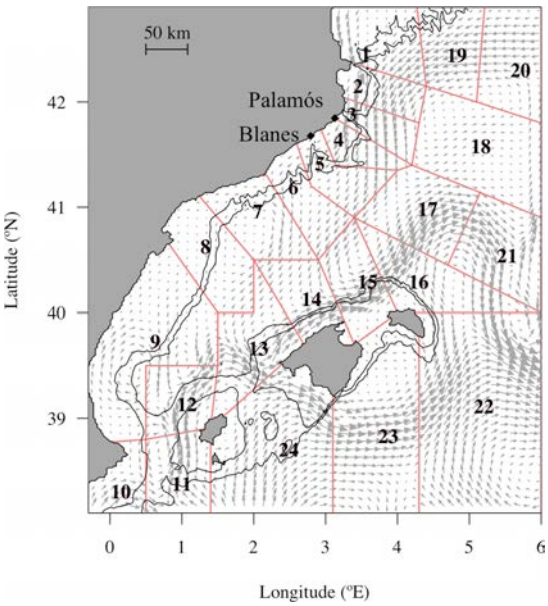

Fig 1. Release and settlement zones defined in the northwestern Mediterranean Sea for this study. The domain is divided by release zones (polygons from 1 to 12) and settlement zones (polygons from 1 to 24) along the continental margins of the management unit called Geographical Sub Area 6 (GSA 6) from the Food and Agriculture Organization. Eggs were spawned in the release zones at the seafloor between the 500 m and 800 m isobaths (black lines) where the mature female shrimp aggregates. All the zones (polygons from 1 to 24) are considered potential settlement zones of the deep-sea red shrimp. Arrows represent the average surface current (m/s) over July from the hydrodynamic model used in the study.

https://doi.org/10.1371/journal.pone.0223396.g001

The Individual-Based Model

The Lagrangian drift of individuals was calculated using the Python framework OpenDrift ([37]; available on https://github.com/OpenDrift). The equation for the advection of individuals in the three dimensions is resolved by a fourth-order Runge-Kutta scheme. Particles were defined as 'stranded' when they came into contact with the coastline. The modules for turbulence and buoyancy were activated by the modeler. The number of particles, the release coordinates and the duration of the drift setting the initial conditions of the Individual-Based Model are also described in the following sections.

Horizontal and vertical components. The trajectories of individuals, representing virtual embryonic or larval stages, were based on the following equation:

$$\frac{dX}{dt} = U(X,t) + B(X,t) + D_h(X,t) + D_v(X,t) \quad (1)$$

where dX/dt is the 3D displacement of the individuals from their geographical and vertical position X on a time step dt; U is the advection component composed by the meridional, zonal

and vertical velocities from ROMS; B is the biological component, and D_h and D_v are the small-scaled turbulent velocities in the horizontal and vertical dimensions, respectively.

The vertical velocity of individuals due to turbulent diffusivity (D_v) is adjusted by the random displacement scheme [38] with an internal time step of 20 s and a 1 m vertical resolution. Values of K_v were provided from the coefficient of salinity vertical diffusion from ROMS outputs. In our simulation, the vertical mixing was activated until individuals crossed the oceanic surface boundary layer (around 15 m deep [26]). Because the Mediterranean Sea is well-stratified in summer, above the oceanic surface boundary layer, the turbulence was accounted by simulating the horizontal mixing.

The horizontal velocity due to turbulent diffusivity was computed by a random walk scheme:

$$D_h = rand \cdot \sqrt{2 \cdot K_h} \cdot dt \quad (2)$$

with *rand* representing a random value sampled in a Gaussian distribution G(0,1), *dt* the time step, and K_h the horizontal diffusivity coefficient. For K_h, we used the yearly constant and average value of 10 m^2/s estimated by [39] in the Western Mediterranean Sea from a hydrodynamic model with similar horizontal resolution than ours.

The biological component *B(X, t)* represented the vertical terminal velocity due to the buoyancy force adjusted to the seawater density by the equilibrium of the Archimedes, gravitational, and friction forces under laminar flow (Reynolds number < 0.5) on a spherical object characterized by diameter and density. For the present study, this object size was randomly sampled in a Gaussian distribution with the average *A. antennatus*' egg diameter of $3.3^{*}10^{-4}$ m and its standard deviation at $0.45^{*}10^{-4}$ m [6]. The density of the sphere was selected after the analysis described in the sections below. The terminal velocity is computed by the equation provided in [40], or by Dallavalle equations [41] if the flow is transient (Reynolds number > 0.5).

Adaptation of the IBM to the shrimp larval cycle. Following the temporal and spatial spawners distribution, virtual eggs [6, 12, 33] were set to be released in summer at midnight [42] on the bottom of the NW Mediterranean continental slope between 500 m and 800 m isobaths.

The IBM included activation and deactivation of the buoyancy force according to the individual stage during the drifts. The buoyancy module was initially activated at the release of the eggs. The eggs were positively buoyant by assuming that on the one hand, young larvae of *A. antennatus* are found in the surface layer [11, 13] and on the other hand, if the buoyancy is neutral or negative, the swimming abilities of the nauplius could not explain an average vertical rise on 600 m. When individuals reached a non-buoyant stage, the module was deactivated. For simplification, and due to lack of knowledge, we neglected the temporal change of egg size and density.

The drift duration was the sum of the pelagic egg and larval stage durations approximated by the temperature-dependent Pelagic Propagule Duration [43, 44]. Due to missing information regarding the embryonic and larval stages of *A. antennatus*, we assumed that its early-life development duration was similar to the near taxonomic Penaeid species. We reviewed 72 research articles (see S2 File) in which the larval stage duration of 42 Penaeid species was associated with the rearing water temperature. Then, we fitted a multiple linear model on those data to estimate *A. antennatus* larval stage durations (D, in day) according to the seawater temperature, such as:

$$\log(D) = T + Stage + \varepsilon, \quad (3)$$

where T is the rearing water temperature; *Stage*, a categorical variables characterizing the Penaeid larval stage and ε a random error. This model, whose initial assumptions were verified with a coefficient of determination R^2 = 96%, had the following shape:

$$D_{stage} = \exp(-0.072 * T + \begin{cases} 1.51, & if\ stage = eggs \\ 2.66, & if\ stage = nauplius \\ 3.68, & if\ stage = protozoea \\ 3.64, & if\ stage = mysis \end{cases}). \quad (4)$$

We estimated egg stage duration before the beginning of the drift simulations and larval stage duration was estimated each time an individual molted into the next stage (e.g., from nauplius to protozoea). The water temperature involved in Eq 4 was extracted at embryonic or larval position from ROMS model. Molting was allowed only if the simulation time was bigger than the cumulated duration of the previous and current stages.

Number of particles. The methodology of [45] adjusted in [12] was used to determine the lowest number of individuals to be released and to guarantee that 95% of the dispersal variability is considered in our results. It is based on the average of the Fraction of Unexplained Variance [45], which is got by extracting randomly 100 subsamples of N drifts from 350,000 simulated trajectories and by computing the cross-correlation between the 100 subsamples. The subsample size N ranged between 1,000 and 300,000. The drifts of 350,000 individuals directly started at the surface with underneath sea bottom estimated between 500 and 800 m. Assuming to catch the full range of dispersal possibilities for larvae, the 350,000 drifts lasted the maximum PPD (38.8 days). The PPD was predicted from the relationship as described in the previous section, considering the coldest water near the bottom of the studied area (12.6˚C) where eggs are spawned. Turbulent diffusivity was as well included for the drifts of 350,000 individuals. To avoid the underestimation of needed individual number, the 350,000 drifts also included a horizontal turbulent random walk with the maximum value of the coefficient K_h estimated at 100 m^2/s in [39] instead of its average at 10 m^2/s. Finally, the Fraction of Unexplained Variance was lower than 5% if 50,000 individuals are used (S1 Fig) to simulate the larval dispersal.

Larval dispersions

Modeled dispersion started with buoyant stages having predicted densities (in kg/m^3) to rise toward upper water layers. When the stages were no more buoyant, the individuals were neutrally advected by the currents of the reached water mass layer.

Preliminary IBMs. Beforehand, considering the few biological data available on taxonomically close species to *A. antennatus* and the important differences in larval ecology of deep-sea species (see S1 File), the density for the eggs reaching the surface needed to be estimated. This estimation was carried out relying on physical explanation (e.g., forces applied on the particles) to model the egg rise instead of unknown biological values.

To obtain the estimation (hence called optimal buoyancy), the depth reached by the individuals was analyzed when the buoyant stages ended. In the early summer (July 1), 50,000 particles were released and tracked up to the end of the nauplius stage (~ 7.5 days). The Lagrangian drift simulations of eggs were repeated for every 10 kg/m^3 increment, between 800 and 1030 kg/m^3. Then, for each particle reaching the surface (0–5 m depth layer), their densest value was kept. It represented the threshold where a denser value would not make the individual reach the surface and a lighter value would likely lead the individual to the surface. The average and standard deviation of the highest density values were kept to implement the drift simulation of the particles.

Other averages and standard deviations of the egg density were estimated by modifying one parameter in the configuration of the previous preliminary IBM. Independently, we computed those parameters i) for individuals reaching the upper boundary of the seasonal thermocline (about 15 m under the surface; [26]) instead of the surface layer, ii) when the buoyancy was applied during egg and nauplius stages, instead of egg stage only, iii) when the turbulence was activated, and iv) when the drift began at late summer (September 1). In case i), the method used to find the seasonal thermocline depth, we used the maximum slope of difference in the temperature profile during summer days [46]. In case ii), the particles were tracked up to the end of the nauplius stage (~7.5 days). In total, the preliminary experiment consisted of the analysis of simulations made with 24 values of egg density for six configurations of IBM (S1 Table).

Runs and sensitivity scenarios of IBMs. We used six scenarios with different configurations of IBM. Sensitivity tests were performed introducing small or high variability due to the buoyant larvae or the hydrodynamics changes (Table 1). The scenario of reference IBM_0 started in early summer at the beginning of the peak period of spawning and with buoyant eggs. We modified the average egg density to lead the individuals to different depths (surface or mixed layer depth), to use different buoyant stages (eggs or eggs + nauplii), to include the vertical and horizontal turbulent components, and to begin the drift simulation in either early or late summer (1st July or 1st September). In the last scenario IBM_{Hot}, the temperature in the upper 200 meters was incremented by 0.4˚C, corresponding to the thermal increase expected in the upper layer of the western Mediterranean Sea over a decade [47].

Those scenarios were operated to consider the factors associated with larval ecology (IBM_0, IBM_{PZ}, and IBM_{MLD}) and to the hydrodynamics (IBM_{LS}, IBM_{Turb}, IBM_{Hot}). Through IBM_{MLD}, we explored the fact that the thermocline created a physical barrier for the larvae [28, 29]. In $IBM_{PZ,}$ we explored the possibility that buoyancy was still taken into account in the vertical movements of nauplius after hatching. The swimming abilities of the spheroid nauplius of Penaeid can hardly lead them to the surface [48, 49]. Yet, the nauplius stages of some coastal shrimps were found in the superficial layer [50], which means that an underlying process helps them to rise in the water column. Finally, the last scenarios allowed making a sensitivity analysis on the turbulent mesoscale impact on the main advection with the turbulent component (IBM_{Turb}), and on the temporal changes in the physical environment (late summer hydrodynamic circulation) on the drifts (IBM_{LS}). IBM_{hot} was used to estimate the impact of a scenario of climate change on the larval drifts, through the rising of water temperature above average, which is expected to have a major impact on the larval duration and in seawater density.

Table 1. Configurations of IBM scenarios for egg and larval drifts.

IBM Scenario	Buoyant larval stages	Displacement schemes	Depth reached by buoyant stages	Release event	Density (kg/m^3)
IBM_0	Eggs	U(X, t) + B(X, t)	Surface	July 1	884 ± 36
IBM_{PZ}	*Eggs + Nauplii*	U(X, t) + B(X, t)	Surface	July 1	979± 14
IBM_{Turb}	Eggs	U(X, t) + B(X, t) + *Dh(X, t) + Dv(X, t)*	Surface	July 1	885 ± 36
IBM_{MLD}	Eggs	U(X, t) + B(X, t)	*15 m*	July 1	887 ± 36
IBM_{LS}	Eggs	U(X, t) + B(X, t)	Surface	*September 1*	882 ± 36
IBM_{Hot}	Eggs	U(X, t) + B(X, t)	*Surface**	July 1	884 ± 36

U, advective component by the meridional, zonal and vertical velocities; *B*, velocity due to the buoyancy force; D_v and D_h, the velocity due to the vertical and horizontal diffusivity; *PZ*, Protozoea; *Turb*, Turbulence; *MLD*, Mixed Layer Depth; *LS*, Late Summer. Changes in parameterization with respect to the base scenario IBM_0 are in italics.

* Temperature in the 0–200 m layer has been increased by 0.4˚C.

https://doi.org/10.1371/journal.pone.0223396.t001

For each scenario, the density (kg/m^3) of the individuals was randomly sampled from a Gaussian distribution (Fig 2), using the average and standard deviation density values from the preliminary analysis. The simulation duration lasted the time that an egg developed into early juvenile according to the water temperature when larvae molted. The time step to advect individuals was one hour. The characteristics of the individuals (density, egg size, stages, duration of the stage) and their spatial position (latitude, longitude, and depth) were saved on a daily basis for further analyses.

Analysis of the drift simulations

The water characteristics during the drifts, the drift duration, the vertical rise of the individuals from spawning depths and the traveled distance were used to analyze the simulated drifts from the six scenarios. Distance *d* between two geographical positions given by the coordinates (X, Y) was computed by the haversine formula of great-circle distances;

$$d = arcos[\sin(Y_1) \cdot \sin(Y_2) + \cos(Y_1) \cdot \cos(Y_2) \cdot \cos(X_1 - X_2)] \cdot R, \quad (5)$$

with *R* as the radius of Earth. The drift distances corresponded to the aggregated distance during the simulation. The straight distance corresponded to the distance between the beginning and the end of the drifts.

In our study, we also analyzed the individual dispersals within and among areas with the connectivity matrices. Therefore, the NW Mediterranean Sea domain was divided into 24 zones (Fig 1) shaped by the main structures of topography like the Eivissa channel, the submarine canyons (Cap de Creus, Palamós, Blanes), and the gulfs (Valencian Gulf or Lion Gulf). In creating the zones we took account of the zoning criteria provided by the General Fisheries Commission for the Mediterranean (Geographical Sub-Areas 5, 6 and 7). Then, the connectivity rates between one release zone *i* and one settlement zone *j* were computed from the ratio of individuals in the settlement zone to the initial individuals from their release zone N_{jli}/N_i. The release zones were the zones 1 to 12 while the settlement zones included all the 24 zones

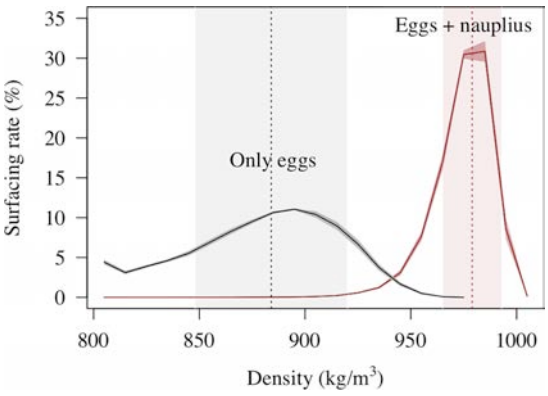

Fig 2. Modeled surfacing rates for eggs and nauplii of *A. antennatus*. Surfacing rate of buoyant eggs (black line) or buoyant eggs and nauplii (brown line) related to different tested densities (kg/m^3). The average (vertical dashed lines) and standard deviation (colored ranges along the X-axis) of the water densities were used in different scenarios of Individual-Based Model (IBM). See details in Table 1.

https://doi.org/10.1371/journal.pone.0223396.g002

(Fig 1). In order to focus on the most relevant results, statistical tests and principal component analyses were implemented with averaged and scaled data with the basic packages of R.

Results

The simulated larval drifts significantly varied with the spawning places, the number of buoyant stages, the spawning period and the depth layer reached by buoyant phase.

Larval drifts in three spawning regions

The temporal hydrodynamic and individual buoyancy variations allowed setting relevant scenarios to use for connectivity analysis. Using the characteristics of the larval drifts ant the environmental influences (PPD, drift distances, water current, and water temperature) by scenarios, a Principal Component Analysis (PCA) differentiated three clusters of scenarios (Fig 3). One gathered all the IBM parameterized by small changes with respect to IBM_0 (i.e., IBM_{Turb}, IBM_{hot}, and IBM_{MLD}). The non-parametric Kruskal-Wallis test revealed that their PPD and drift distances were significantly different (p-values > 0.05). Nevertheless, their larval drifts expanded over a longer period (25.6 days) and over longer distances (118 km) even though larvae drifted at the thermocline depth (IBM_{MLD}), or within small-turbulent water (IBM_{Turb}), or in warmer water (IBM_{hot}). The two other clusters were defined by the scenario IBM_{LS}, in which larval drifts traveled the smallest distances (93 km), and by the scenario

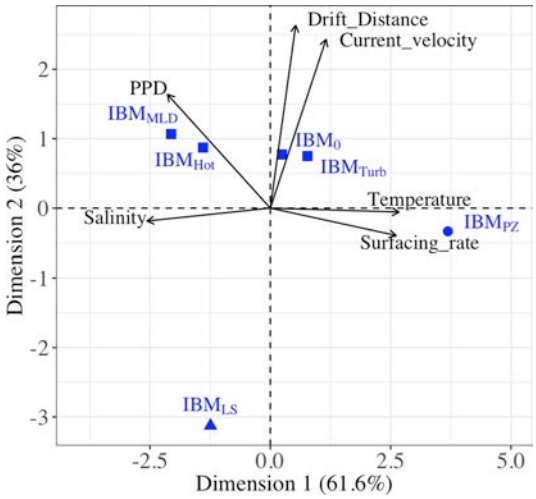

Fig 3. Scenarios of Individuals-Based Models related to the larval drift characteristics and the environmental influences. The different scenarios of Individuals-Based Models used in this study are represented by blue symbols (circle, triangle or square) and visualized with the characteristics of larval drift and environmental influences (arrow). In the Principal Component Analysis (PCA), the correlation among the characteristics is indicated by the angle between arrows (i.e., an angle of 90˚ indicates no correlation and an angle of 180˚ indicates a negative correlation). Scenarios were correlated to the larval drift characteristics and environmental influences by the closeness of their Cartesian coordinates. The PCA grouped IBM_0, IBM_{MLD}, IBM_{Hot}, and IBM_{Turb} (square), and separated IBM_{PZ} (circle) and IBM_{LS} (triangle). IBM scenarios are described in Table 1.

https://doi.org/10.1371/journal.pone.0223396.g003

IBM_{PZ}, in which the surfacing of larvae had higher rates (80%) and PPDs were the shortest (23.2 days). The present analysis focused on the drifts simulated in the scenarios IBM_0, IBM_{PZ} and IBM_{LS} that were separated into distinct clusters and had important differences in their drift characteristics (S3 Fig).

Generally, the larval drifts had similar trends for individuals released in specific latitudinal ranges of the NW Mediterranean Sea. For each scenario previously selected, a PCA (Fig 4) was carried out on the larval drift characteristics and environmental influences by release zones, gathering them into three regions. Besides, those three regions were driven by the same variables in each scenario. The region 1 gathered larvae released from zones 1 to 4 (approximately 41.39˚N– 42.74˚N) with the longest PPD and the straightest transports. The region 2 gathered individuals released between zones 5 and 10 (approximately 38.86˚N– 41.39˚N), which were abundant in the surface water but drifted the shortest distances. The region 3 gathered the individuals from the zones 11 and 12, and overlapped each side of the Eivissa Channel. Those individuals drifted the furthest and had low surfacing rates.

In each three regions, the individual drifts followed different circulation patterns. In region 1, Fig 5 shows an expanded and linear distribution of the individuals towards the Southwest. The dispersal of individuals from the region 2 shaped different eddies, which are almost-circular structures of the hydrodynamics. In all scenarios, those eddy-like structures were localized where the Gulf of Valencia widens (0.5˚ E; 39.5˚ N, and 2˚ E; 40.5˚ N). These eddies had only differences in their average radius and the position of their center changed between the early and late summer releases (IBM_0 and IBM_{LS}). For instance, these eddies get 6 to 8 km larger in IBM_{LS} (S2 Table) and their center displaced 9.5 km to 14.7 km further (S2 Table) than eddies in IBM_0. Last, individuals from region 3 were affected by the presence of an eddy with a center averagely positioning in the Eivissa channel (0.72˚ E; 38.70˚N, S2 Table) in early summer (IBM_0).

Advantage of two buoyant stages in the larval drifts

The highest surfacing rate regardless of the regions was when the ascent of larvae occurred with two buoyant stages. With an average density of 979 kg/m^3 in IBM_{PZ}, 93 kg/m^3 denser than in IBM_0, 81% of the eggs and nauplii rose to the shallower water layers, while in IBM_0, 52% of the eggs reached the surface layer (Fig 6). Overall, the average time for the ascent of two buoyant stages (IBM_{PZ}) lasted 7.5 days (i.e., 5.5 days longer than in IBM_0). Nevertheless, at the end of the simulations in IBM_{PZ} and for individuals at the surface, the drift durations increased by approximately two days and the drift distances were hardly 3.6 and 4.5 km longer (regions 1 and 2) or 12.6 km shorter (region 3) than in IBM_0 (Table 2).

The time lag between early and late arrival of individuals at the surface was small enough for not implying important divergences in the drift characteristics. Indeed, in the two scenarios IBM_0 and IBM_{PZ}, the surfaced larvae were not spatially exposed to different currents. When nauplii reached the upper 5 m layers in IBM_{PZ}, they were 20.5 km away from the location where the eggs have surfaced in IBM_0. However, this distance was mostly kept to the nearest kilometer between the individuals of IBM_0 with the same age (7.5 days) than the surfaced individuals of IBM_{PZ}. It illustrated that while the buoyant nauplii in IBM_{PZ} were still rising in the water column, the surface current in which the individuals from IBM_0 were advected, had not important amplitude or direction changes.

The overall consequences from tardive and abundant individuals at the surface were that the connectivity and retention strengthened between and within zones of the NW Mediterranean Sea. In both IBM_0 and IBM_{PZ}, the same settlement zones were connected but with different amplitudes (Fig 6). First, the dispersal rate between the release zones from the region 1 (zones 1 to 5) and from Blanes canyon and its neighboring zones (zones 5 to 7) rose from

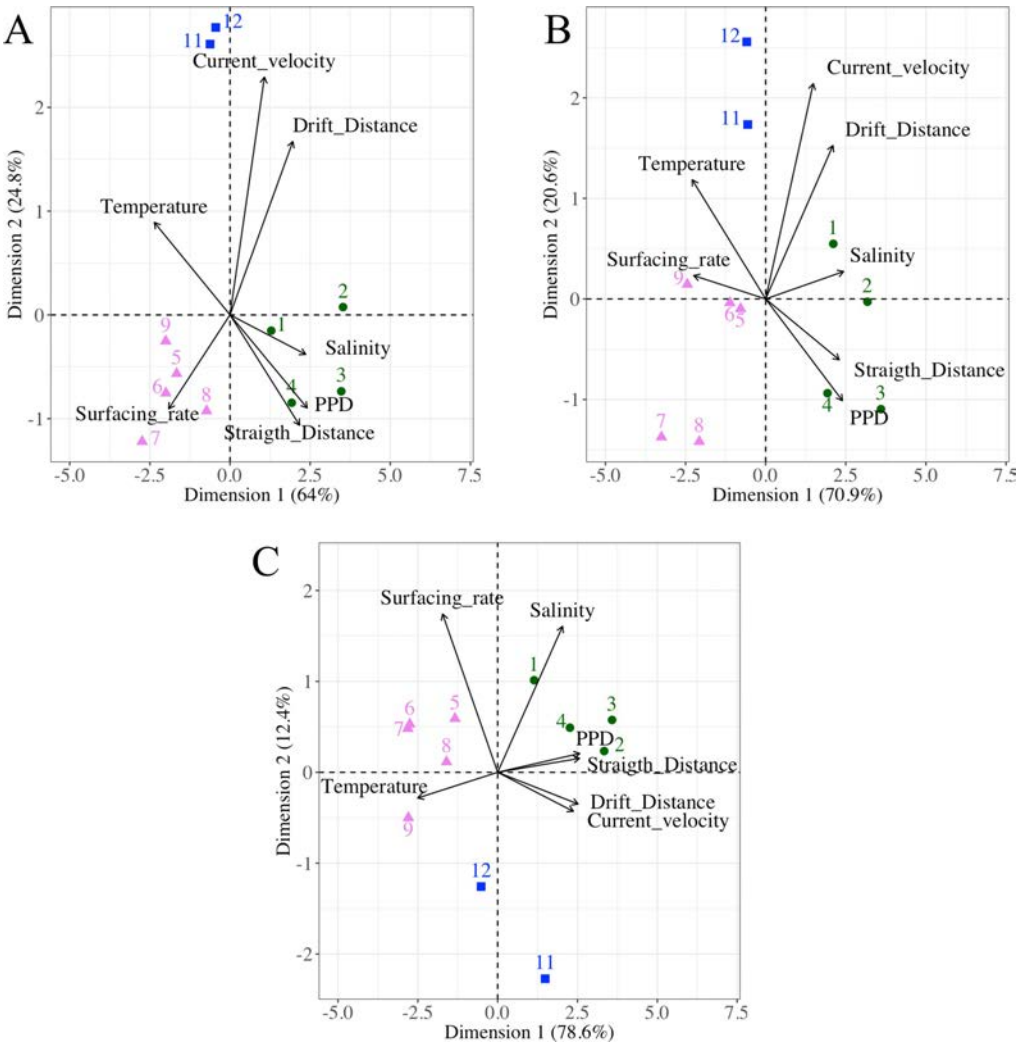

Fig 4. Larval drift characteristics and the environmental influences of the three most distinct IBM scenarios. Release zones (colored symbols and numbers) linked to characteristics of the larval drift (arrows) in a Principal Component Analysis for A) the base scenario IBM_0, B) the scenario with the buoyant stages up to Protozoea IBM_{PZ}, and C) the scenario initialized at late summer IBM_{LS}. The correlation among the characteristics of the larval drift is indicated by the angle between arrows (i.e., an angle of 90˚ indicates no correlation and an angle of 180˚ indicates a negative correlation). Release zones were correlated to the larval drift characteristics and environmental influences by the closeness of their Cartesian coordinates. The PCA grouped three regions: the release zones 1–4 (full green circle), the release zones 5–9 (full pink triangle) and the release zones 11 and 12 (full blue square). IBM scenarios are described in Table 1.

https://doi.org/10.1371/journal.pone.0223396.g004

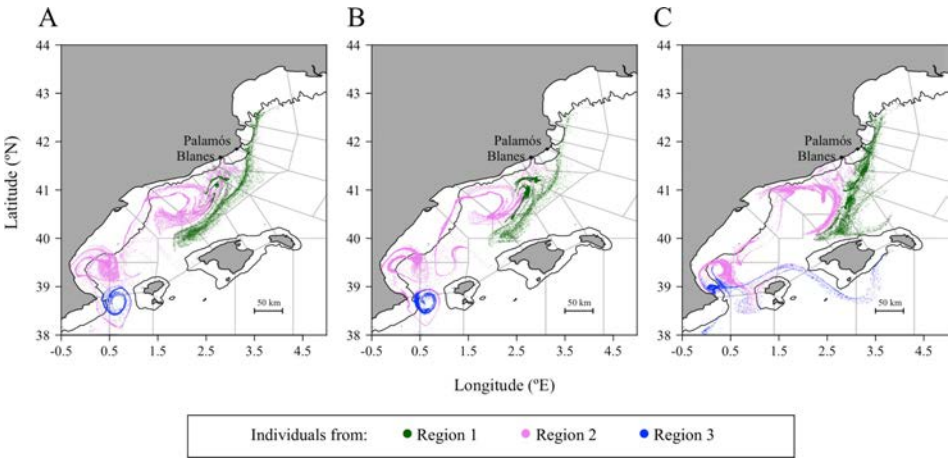

Fig 5. Settlement position of early juveniles at the end of the simulated drifts by regions and by the three selected IBM scenarios. The early juveniles are positioned after the simulation with A) the base scenario IBM_0, B) the scenario with the buoyant stages up to Protozoea IBM_{PZ}, and C) the scenario initialized at late summer IBM_{LS}. The regions are defined according to the results of a Principal Component Analysis (Fig 4). The black line represents the shelf break at 200 m. IBM scenarios are described in Table 1.

https://doi.org/10.1371/journal.pone.0223396.g005

42.6% in IBM_0 to 56.7% in IBM_{PZ}. Second, in the Gulf of Valencia's zones (zones 7 to 9), corresponding to the south of region 2, the retention rates were from 33.4% to 43.6% higher in IBM_{PZ} than IBM_0. Last, each side of the Eivissa Channel (zone 11 and 12 in the region 3) connected with the other side if the surfacing was earlier like in IBM_0. Indeed, in this scenario, the

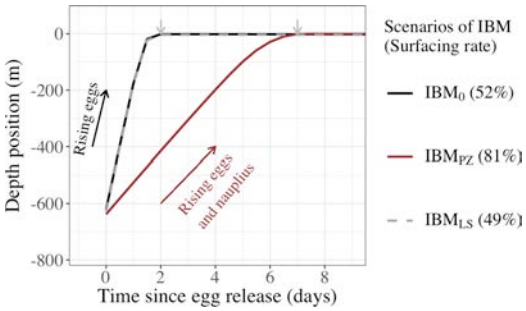

Fig 6. Depth position of eggs (IBM_0 and IBM_{LS}), and eggs and nauplius (IBM_{PZ}) after spawning. The depth position is recorded from the release day (Time = 0) to the end of the buoyant stages (grey arrow) in three Individual-Based Models. In IBM_0 (black line) and IBM_{LS} (grey dashed line), eggs were spawn at early and late summer, respectively, and buoyant eggs rose during 2 days. In IBM_{PZ} (brown line), eggs and nauplii were buoyant and rose in the water column during 7.5 days.

https://doi.org/10.1371/journal.pone.0223396.g006

Table 2. Characteristics of the larval drifts by the three selected IBM scenarios, by regions of the NW Mediterranean Sea and by depth of drifts.

				Drift in the 0–5 m depth water layer			Drift in the water layer below 0–5 m depth		
IBM Scenario	Region	Release zones	Surfacing rate	T	PPD	Drift	T	PPD	Drift
IBM_0	1	1–4	48.0	24.5	20.3	153.5	15.7	32.6	162
	2	5–9	55.6	25.9	17.6	80.1	16.5	31.2	105
	3	11–12	43.8	27	16.3	174.5	17.9	28.9	170.6
IBM_{PZ}	1	1–4	70.9	23.7	22.4	158	16.3	31.9	173.1
	2	5–9	85.8	24.9	20.1	83.7	17.2	30.3	102
	3	11–12	77.4	25.8	19.0	161.9	17.9	29.5	168.9
IBM_{LS}	1	1–4	45.4	22.4	20.1	147.9	16.5	30.8	145.1
	2	5–9	55.3	24.2	17.2	54	17.7	28.6	79.8
	3	11–12	26.0	25.2	15.7	57.7	18.4	27.6	113

PPD, Pelagic Propagule Duration (in days); T, the average seawater temperature (in˚C); Drift, the drift distance (in km); Surfacing rate, the percentage of individuals reaching the surface (0–5 m layer); PZ, Protozoea; LS; Late Summer. The regions 1–3 are defined in Fig 4.

https://doi.org/10.1371/journal.pone.0223396.t002

exchange of surfaced individuals between the two sides was bidirectional, with a tendency for individuals to cross northwardly the channel. A rate of 21.3% individuals from zone 11 connected to the northern zones of the Eivissa Channel (zone 9 and zone 12) and 11.5% individuals from the zone 12 crossed the channel and arrived on the southern zones of the Eivissa Channel (zones 10 and 11). While in IBM_{PZ}, the exchange of late surfaced individuals across the channel was unidirectional and it was done by the northern zones of the channel. Under the influence of an eddy (Fig 4), the southern zones (zone 11 and 10) of the Eivissa Channel received 63.2% individuals from zone 12 and zone 11 kept 61.4% individuals (or 55.6% individuals more than in IBM_0).

Larval drifts after early and late summer spawning

The present results distinguished the circulation in the water from the northernmost region (region 1) from the southern and warmer regions (regions 2 and 3). The drifts at the surface were exposed to higher temporal variability in the circulation fields if they started in the warmer regions of the NW Mediterranean Sea. In IBM_{LS}, 49% of individuals (i.e., 3% fewer than in scenario IBM_0) rose to the surface, and drifted 24.1 days (i.e., around one day less than in scenario IBM_0). Yet, as shown in Fig 3, individuals from IBM_{LS} traveled less. The temporal current changes were measured with the differences in drifted distance per day in scenario IBM_{LS}. In region 2, surfaced larvae traveled 26 km less than in IBM_0 (i.e., 3.1 km/day instead of 4.6 km/day) and in region 3, surfaced individuals traveled 96.4 km less (i.e., 3.7 km/day instead of 10.7 km/day). In contrast, the individuals in the colder region 1 had similar drifting velocity in IBM_{LS} (i.e., 7.4 km/day) and in IBM_0 (i.e., 7.6 km/day).

Besides the temporal changes in the intensity of the circulation fields, two circular structures in the NW Mediterranean Sea boosted the dispersal rates of the surface individuals. First, the diameter of an eddy-like structure between the latitudes 41˚N and 42˚N had modified the surface connectivity of individuals toward the Balearic Islands. In IBM_{LS}, the north side of the Majorca Island (biggest island; zone 13 and 14) received 40.9% and 37.9% individuals from the Blanes canyon (zone 4) and its southern zone (zone 5 in Fig 7), while in IBM_0, the reception rate of the individuals was lower than 3.5%. This new connection leaned on the changes in the current direction at the end of the summer and the size of the eddy-like structure. Individuals

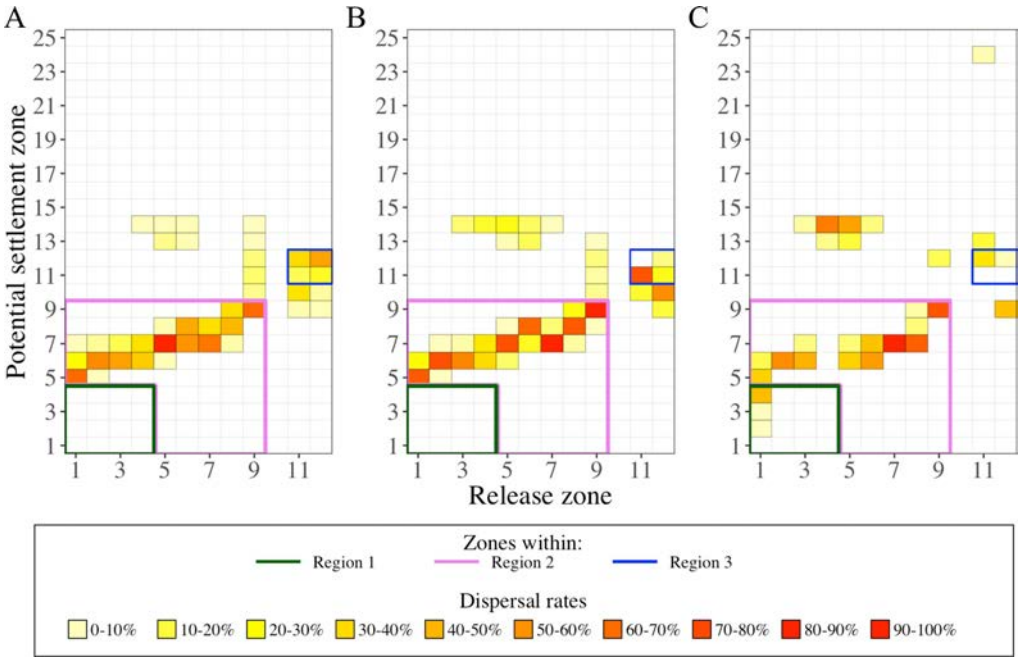

Fig 7. Dispersal rate in the upper water layers (0–5 m) by the three selected IBM scenarios. Dispersal rates were calculated from release zones (X-axis) to potential settlement zones (Y-axis) from simulated larval drifts in A) the base scenario IBM_0, B) the scenario with the buoyant stages up to Protozoea IBM_{PZ}, and C) the scenario initialized at late summer IBM_{LS}. For clarity purposes, we contoured the dispersal rates in regions 1 (green lines), 2 (pink lines) and 3 (blue lines). Identification of zones and regions as defined in Figs 1 and 4, respectively. Code color is related to the dispersal rate (%). The sum of the dispersal rates over a column gives the percentage of individuals in the surface layer.

https://doi.org/10.1371/journal.pone.0223396.g007

from the region 1 traveled a similar distance per day in IBM_0 and IBM_{LS} (7.5 km/day and 7.1 km/dayrespectively), but the circulation pattern had an angle closer to the south direction, which advected the individuals more southwardly in IBM_{LS} (26˚ clockwise from geographical South) than in IBM_0 (36˚ clockwise from geographical South). Fig 5 suggests that the eddy-like circulation over the north of the region 2 qualitatively had a bigger diameter. Second, the transport of surfaced individuals across the Eivissa Channel was limited without eddy structure. Indeed, the absence of an eddy in the Eivissa Channel (Fig 5C) paired with the fact that all surfaced individuals from zone 11 were transported unidirectionally across the Eivissa Channel. Additionally, most of the surfaced individuals from zone 12 mostly (25.2%) were advected in the eddy-like structure located at the south of the region 2.

Larval drifts in different depths of water layer

A part of the individuals did not reach the surface because of the variability in egg characteristics. For example, the decrease in the rate of surfaced larvae from region 3 between IBM_0 and IBM_{LS} was related to smaller egg diameters. Nonetheless, deeper drifts brought valuable knowledge on several features that are developed below.

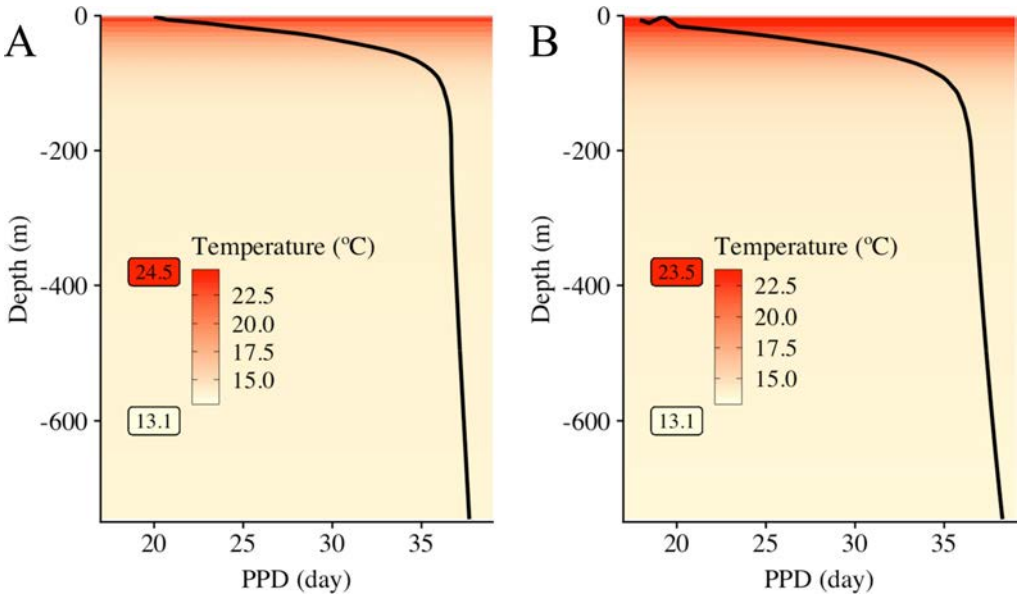

Fig 8. Pelagic Propagule Duration (PPD) according to water temperature estimated at different depths. The average duration of propagules (from eggs to early juveniles) of *Aristeus antennatus* is in relation with the decreasing temperature (color gradient,˚C) with increasing depths (Y-axis, m). In (A), PPD and water temperature from the IBM scenarios in early summer (IBM_0 and IBM_{PZ}) were averaged, and water temperature ranged between 13.1˚C and 24.5˚C. In (B), PPD and water temperature are from the IBM scenario in late summer (IBM_{LS}), where water temperature ranged between 13.1˚C and 23.5˚C. IBM scenarios are described in Table 1.

https://doi.org/10.1371/journal.pone.0223396.g008

First, the water temperature gradient in different depth layers was advantageous for longer transports. Due to the variability in egg size and egg density, the buoyant stages stabilized at different vertical positions from zero to 75 m for more than 75% of individuals. The drifts were 20 km longer because they lasted 11 supplementary days in the deeper layers regardless of the scenario involved. The highest gradient in the drift duration occurred in the upper 100 m layer where the drift lasted 12 supplementary days at 100 m than at the surface (Fig 8). Beyond 100 m, the drift duration was stabilized at 36–38 days. Nonetheless, the scale of the deeper drifts by region showed that the circulation was still stronger and weaker in the region 1 and 2, respectively, where the drifts were the longest (167.5 km) and the shortest (102.5 km), respectively and regardless the scenario. In a concrete case, the simulated drifts from region 3 in IBM_{LS} indicated that the upper and deeper layer were decoupled because individuals drifted two times longer than the individuals in the upper layer (Table 2).

Second, longer drifts and decoupled currents underneath the five meters depth favored the connectivity with the Balearic Islands (Fig 9). In other words, the velocity fields under the surface had slightly different directions. This was particularly seen by the drifts from the region 1 that, in two cases, provided higher arrival rates of individuals on the northwestern part of the Balearic Island grounds. One case is illustrated by the drifts in IBM_0 showing 33.1% to 40% individuals from the zones 2 to 4 in the 5–330 m layer depth were transported toward the islands. The second case is showed in the IBM_{LS}, with surfaced and deeper individuals

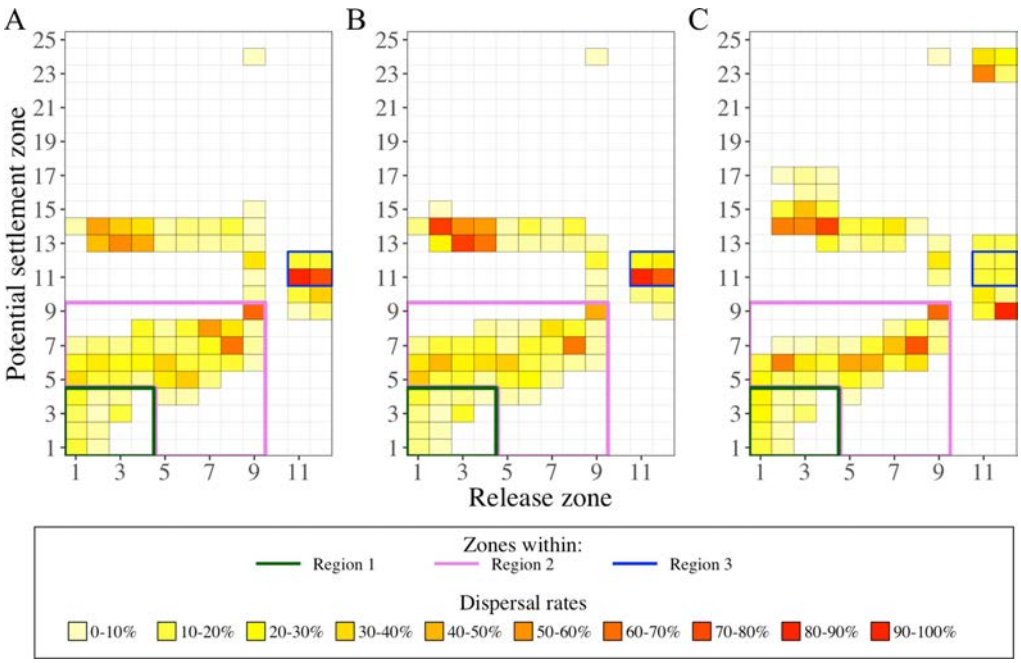

Fig 9. Dispersal rate in the lower water layers (below 5 m) by the three selected IBM scenarios. Dispersal rates were calculated from release zones (X-axis) to potential settlement zones (Y-axis) from simulated larval drifts in A) the base scenario IBM_0, B) the scenario with the buoyant stages up to Protozoea IBM_{PZ}, and C) the scenario initialized at late summer IBM_{LS}. For clarity purposes, we contoured the dispersal rates in regions 1 (green lines), 2 (pink lines) and 3 (blue lines). Identification of zones and regions as defined in Figs 1 and 4, respectively. Code color is related to the dispersal rate (%). The sum of the dispersal rate over a column gives the percentage of individuals below the surface layer.

https://doi.org/10.1371/journal.pone.0223396.g009

reaching the zones 13 and 14, though the connection with zone 15 was established if only individuals were in the deeper layer (8 to 381 m depth). The same concept prevailed in the region of the Eivissa Channel. Within the first 100 m layer, longer drifts (160 to 400 km) from the Eivissa Channel connected to the south ground of the biggest Balearic Island (Majorca Island) by 39.5% individuals from zone 11 and 13.4% individuals from zone 12.

Finally yet importantly, the deeper and variable drifts of the individuals allowed broader connectivity. One release area could be connected up to eight other areas (Fig 9). Those connections were allowed by small numbers of individuals, which remained near the release areas, like for the case of individuals from region 1, which had a northwestward dispersal and thus, an opposite direction of dispersal than particles at the surface.

Discussion

Model results emphasized the importance of the buoyant phases and their variability in the larval cycle of deep-sea species. In the upper water layer of the northwestern Mediterranean Sea,

the larval transport of *A*. *antennatus* relied on different circulation patterns and their spatio-temporal variability.

Importance of buoyant phases

The simulations of different buoyant phases in the larval drift of the red shrimp *A*. *antennatus* emphasized the importance of the lecithotrophic stage in the drifts. In the recommendation guide for IBMs by [51], buoyancy is a key parameter for explaining the changes in the larval drifts. However, prior to our study in the Mediterranean Sea, only [15] studied the impact of egg buoyancy on simulated drifts for the deep-sea shrimp *Aristaeomorpha foliacea* (taxonomically close to *A*. *antennatus)*, using Atlantic anchovy egg density [52].

In our study, over half of the released individuals reached the layer where a high quantity of *A*. *antennatus'* larvae is found (i.e., the surface layer [11]). We estimated an average egg density of 884 kg/m^3, which was around 100 kg/m^3 lighter than the ones described for other deep-sea shrimp eggs (1025–1082 kg/m^3; [17]) and the seawater densities of the northwestern Mediterranean Sea (from 1025.3 kg/m^3 in Cap de Creus to 1024.1 kg/m^3 in the Eivissa channel; [23]). Nonetheless, egg density is partly species-dependent and therefore, egg density of deep-sea Decapod egg with bigger sizes than *A*. *antennatus'* oocyte [17] may not be appropriate to use in our Lagrangian model. However, the displacement of *A*. *antennatus'* eggs to the surface was comparable with some Penaeid eggs that were observed at the surface in laboratory water tanks and sea planktonic samples [50, 53], but this fact could not be quantitatively verified due to lack of Penaeid egg density data. To improve the next larval drift simulations with buoyant eggs of *A*. *antennatus*, the relationship between egg density and diameter (e.g., [17]) during the egg incubation should be considered. Indeed, when the eggs develop, several chemical reactions (i.e., the production of a perivitelline space by cortical activation of the eggs [54], the egg hydration [55], and embryonic development) likely modify the lipid rate, egg size, and egg density [53, 56]. Nevertheless, information about egg growth of deep-sea species and Penaeid eggs needs to be provided.

Extended to the nauplius stage, the rise of individuals illustrated the important role of the nauplius for increasing the probability to reach the surface layer. However, due to lack of knowledge, two parameters were not considered in the density values of IBM_{PZ}: the loss of weight at hatching and the change of shape at hatching [57]. In the Penaeid family, the elliptical and hairy morphology of the nauplius leads to a change in the buoyancy effect [58], which may speed up or slow down the ascent of the larvae after hatching. Furthermore, at this stage, previous studies provided the implication of the swimming behavior in the control of the larval vertical migration. Indeed, although erratically [20], [59] and [60] observed a rise of the Penaeid nauplii followed by a resting time in which the nauplii slowly sank. The velocity of *Penaeus* larvae is poorly informed although [20] suggested that larvae rise quickly after hatching, guided by phototaxis. Nevertheless, all authors emitted doubts about the ability of nauplii to swim up to the surface. We underline the necessity to carry out studies on the locomotion of decapod shrimp larvae in the open ocean to define the potential balance between the buoyancy of the nauplii and their swimming ability.

Dispersal modulated by current variations

We noted that the main linear circulation along with eddy-like structures supported distinct dispersals of the red shrimp larvae according to their drift depths. Turbulence (in scenario IBM_{Turb}) or individuals at the thermocline depth (in scenario IBM_{MLD}) introduced small variations during the drift simulation that hardly modified the final dispersals of individuals. Dominant circulation patterns particularly controlled the larval dispersal rates according to

three regions in our study (instead of two in [61]). In region 1, the spatial distribution of larvae near the surface was strongly influenced by the Northern Current and winds, as reported in other drift analyses of marine larval species with egg buoyancy on our study area [62, 63]. In regions 2 and 3, the larval drift was limited by local mesoscale eddies, which have high importance in retaining larvae [64]. Near Blanes Canyon, the beginning of Ebro shelf, and the Eivissa Channel, previous studies identified eddies potentially trapping larvae of various species such as *Engraulis encrasicolus* and *Sardinella aurita* close to the North side of the Ebro shelf [65–69]. Decapod larvae have never been reported trapped in eddies in our study area, but [13] and [70] showed that decapod larvae were also aggregated by eddies south of the Balearic Islands and on the Norway lobster (*Nephrops norvegicus*) in the Irish Sea.

New connection or reinforcement of connection between zones by larval transport and resulted from the temporal changes of the eddy characteristics (i.e., if present, the diameter and the spatial position). During summer, the displacement and intensity changes in eddies along the Iberian Coast [65, 68] modified the simulated drifts, and therefore, the connectivity between areas. The drifts were influenced by a cyclonic eddy in the western part of the Eivissa Channel, as described previously by [71]. Its presence changed the larval dispersal by preventing the larvae from crossing the channel. However, during our late summer simulation, the fishing ground of *A. antennatus* near the Cabrera Harbor of Majorca Island [72], was supplied by individuals from the Eivissa Channel. The present study modeled and described for the first time how the Palamós canyon or the southern Eivissa Channel fishing grounds could connect to the fishing grounds of Majorca Island. Nonetheless, exploring the temporal evolution of eddies and their influence on the larval drift is needed to consider the possibility of persistent connectivity.

Dispersals related to the location and position of larvae

Larval duration of surface *A. antennatus'* individuals depended to the Modified Atlantic Water mass dynamics. In our study, the PPD of larvae drifting at the surface varied along with a latitudinal gradient of near-surface temperatures of the NW Mediterranean Sea, which were colder in the vicinity of Cap de Creus and warmer at the Eivissa Channel [73]. This gradient has already been outlined by the interface of the old and cold Modified Atlantic water with the hot and recent Modified Atlantic water [74]. Additionally, it conveyed that larvae spawn from one of those regions will have distinct drifts from the other and partially explained the delimitation of the three zones in our study. The late summer dispersal enlightened a change of seawater temperature, which, besides the change in atmospheric conditions, can be related to the position of those two water masses. Indeed, the old Modified Atlantic water goes southward driven by wind and the southern entrance of the recent Modified Atlantic water is modulated by the water circulation in the channels of the Balearic Sea [74].

The larval drift in deeper layers can be a positive strategy induced by the buoyant stages. First, it implied that when the hatching occurred in deeper water layers, the PPD was longer. Second, the larvae drifted in the core of the North Current, which is maximal between 10 and 100 m [75, 76]. Third, the underneath surface is advantageous to larval dispersal because it may provide a good growth environment with nutrients located near the deep chlorophyll maximum [77] and protection from predators [28]. Fourth, the dispersal rate was wider and revolved round close settlement zones as well as far away zones. Consequently, for the first time, our study presents a potential connectivity between the two distant fishing grounds of Palamós and Soller (in Majorca Island from the Balearic Islands) areas and the expected drift conditions to link those places, where catches of *A. antennatus* are relatively important [72, 77].

Conclusions

Our study analyzed the larval drift of *A*. *antennatus* under the hypothesis that either the nauplius stage or the protozoea stage is in the upper water masses. We considered concurrently the effects of two main factors on the connectivity that both contribute to the dispersal strategy of this benthic deep-sea species: buoyancy and water mass circulation. The buoyancy linked the eggs spawned at sea bottom to the larvae in the upper layers of the ocean. A consequence of the buoyancy was the split of the Lagrangian drifts into three latitudinal spawning areas in accordance with similar larval dispersal. Simultaneously, we found that connectivity patterns and retention rates were influenced by the presence of mesoscale structures such as meanders above the head of Blanes Canyon and eddies along the Valencian Gulf and in the Eivissa Channel. The drift of larvae in early and late summer followed the persistent main circulation pattern of the NW Mediterranean Sea, with temporally variable mesoscale structures adjusting the connectivity between the different zones. The application of buoyancy on different larval stages also highlighted that positions of the larvae in the water column influenced the dispersal direction and the intensity of connectivity between zones of the NW Mediterranean Sea. This study contributes to increasing the knowledge of *A*. *antennatus*' egg and larval ecology, and illustrates the potential dispersal paths of the individuals during their pelagic life. The spatio-temporal influence of mesoscale circulations in the larval dispersal should be tackled in further studies to better understand the red shrimp population connectivity, and to upgrade advice towards fishing practices and fisheries management.

Supporting information

S1 Fig. Decreasing Pelagic Propagule Duration (PPD) with increasing water temperature. Continuous lines are the fitted exponential curves on reviewed data (cross) for each stage: eggs (orange), nauplius (red), protozoa (brown), and mysis (black). Reviewed data of PPD and temperatures were extracted from published articles and referenced in S2 File.
(TIF)

S2 Fig. Number of particles needed to decrease the Fraction of Unexplained Variance (FUV) below the statistical threshold of 0.05. The FUV expressed the bias created by a low number of particles (FUV $>$ 0.05) after dispersal simulation. Whiskers show the minimum and maximum of the 100 FUV calculated for each number of particles tested (1000, 2000, 5000, 10000, 50000, 100000, 200000, 300000). Horizontal dashed line is the statistical threshold of 0.05.
(TIF)

S3 Fig. Kernel density estimates from 50000 simulated individuals in different scenarios. The simulated transport characteristics were A) the drift distances, B) the Pelagic Propagule Duration, and C) the water temperature during the drifts. Black lines indicate the scenarios grouped together by the PCA (Fig 3) with IBM_0, IBM_{MLD}, IBM_{Diff} and IBM_{Hot} in four different line types. Blue line indicates the scenario IBM_{PZ}, and grey line indicates the scenario IBM_{LS}. See Table 1 for a description of the IBM scenarios.
(TIF)

S1 File. Information on eggs from deep-sea species and Penaeid species. Deep-sea crustaceans (Decapoda) species and taxonomically close species to *Aristeus antennatus* with the depth ranges of adult distribution, egg diameter and egg density. Depth range extracted from Sealife Base (https://www.sealifebase.ca) or EOL (https://eol.org). * Studied species; *n/a*, non available data; in grey cells, species taxonomically close to *Aristeus antennatus*.
(DOCX)

S2 File. Database on Penaeid embryonic and larval duration by stages. T, water temperature (˚C).
(DOCX)

S1 Table. Frequence of surfacing individuals (in percentage) in the preliminary experiments. Percentage of buoyant stages reaching the surface or the Mixed Layer Depth (MLD) for a given density (kg/m^3) in Individual-Based Model modified by the release period (early summer and late summer) and by the activation of random turbulences.
(DOCX)

S2 Table. Characteristics of eddies involved in the larval dispersals. Three eddies were shaped by the larval dispersal simulation (see Fig 5). Coordinates of the eddy center were estimated with an algorithm from [34]. The edge of eddies was got from the streamlines. Computation of the eddy radius is based on the circle surface (Area = pi*Radius^2 and approximated the estimated eddy size.
(DOCX)

Acknowledgments

The main author thanks all the Norwegian researchers from NIVA (Oslo, NO) who contributed to this paper: Johannes Röhrs, Knut-Frode Dagestad, Trine Bekkby and her family. The main author also thanks the editing from Hanna Morrissette and the advice from Elizabeth North from HPL-UMCES in Maryland (US). This study was possible thanks to the Spanish project CONECTA (CTM2014-54648-C2-1-R) lead from the ICM-CSIC in Barcelona (ES).

Author Contributions

Conceptualization: Morane Clavel-Henry, Jordi Solé, Nixon Bahamon, Guiomar Rotllant, Joan B. Company.

Data curation: Morane Clavel-Henry.

Formal analysis: Morane Clavel-Henry.

Funding acquisition: Joan B. Company.

Investigation: Morane Clavel-Henry, Jordi Solé, Trond Kristiansen, Nixon Bahamon.

Methodology: Morane Clavel-Henry, Jordi Solé, Trond Kristiansen.

Resources: Jordi Solé.

Supervision: Jordi Solé, Nixon Bahamon, Guiomar Rotllant, Joan B. Company.

Visualization: Morane Clavel-Henry, Jordi Solé.

Writing – original draft: Morane Clavel-Henry.

Writing – review & editing: Morane Clavel-Henry, Jordi Solé, Trond Kristiansen, Nixon Bahamon, Guiomar Rotllant, Joan B. Company.

References

1. Cowen RK, Paris CB, Srinivasan A. Scaling of connectivity in marine populations. *Science* (New York, NY). 2006; 311(5760):522–27.
2. Rothlisberg PC, Church JA. Processes Controlling the Larval Dispersal and Postlarval Recruitment of Penaeid Prawns. In: Sammerco PW, Heron ML, editors. The Bio-Physics of Marine Larval Dispersal. Washington DC: American Geophysical Union. 2013:235–52. https://doi.org/10.1029/CE045p0235

3. Criales MM, Cherubin LM, Browder JA. Modeling Larval Transport and Settlement of Pink Shrimp in South Florida: Dynamics of Behavior and Tides. Marine and Coastal Fisheries. 2015; 7(1):148–76. https://doi.org/10.1080/19425120.2014.1001541
4. Siegel DA, Mitarai S, Costello CJ, Gaines SD, Kendall BE, Warner RR, et al. The stochastic nature of larval connectivity among nearshore marine populations. *Proceedings of the National Academy of Sciences*. 2008; 105(26):8974–79. https://doi.org/10.1073/pnas.0802544105 PMID: 18577590
5. Company JB, Puig P, Sardà F, Palanques A, Latasa M, Scharek R. Climate Influence on Deep Sea Populations (Climate Influence on Deep Sea). PLoS ONE. 2008; 3(1):e1431. https://doi.org/10.1371/journal.pone.0001431 PMID: 18197243
6. Demestre M, Fortuno JM. Reproduction of the deep-water shrimp *Aristeus antennatus* (Decapoda: Dendrobranchiata). *Marine ecology progress series*. Oldendorf, 1992; 84(1):41–51.
7. Maynou F. Environmental causes of the fluctuations of red shrimp (*Aristeus antennatus*) landings in the Catalan Sea. *Journal of Marine Systems*. 2008; 71:294–302
8. Sardà F, Company JB, Bahamón N, Rotllant G, Flexas MM, Sánchez JD, et al. Relationship between environment and the occurrence of the deep-water rose shrimp *Aristeus antennatus* (Risso, 1816) in the Blanes submarine canyon (NW Mediterranean). Progress in Oceanography. 2009; 82(4):227–38. https://doi.org/10.1016/j.pocean.2009.07.001
9. Boletín Oficial del Estado (2013) Orden AAA/923/2013 de 16 de Mayo, nº 126, Sec. III, pp. 40016. http://www.boe.es/boe/dias/2013/05/27/pdfs/BOE-A-2013-5555.pdf.
10. Boletín Oficial del Estado (2018) Orden APM/532/2018 de 26 de Mayo, nº 128, Sec. III, pp. 55045–51. https://www.boe.es/boe/dias/2018/05/26/pdfs/BOE-A-2018-7015.pdf
11. Carretón M, Company JB, Planella L, Heras S, García-Marín J-L, Agulló M, et al. Morphological identification and molecular confirmation of the deep-sea blue and red shrimp *Aristeus antennatus* larvae. *PeerJ*. 2010; 7:e6063.
12. Clavel-Henry M, Solé J, Bahamon N, Briton F, Rotllant G, Company JB. Influence of the summer deep-sea circulations on passive drifts among the submarine canyons in the Northwestern Mediterranean Sea. Ocean Sci. 2019; 15:1745–59. https://doi.org/10.5194/os-2019-61
13. Torres AP, Dos Santos A, Balbín R, Alemany F, Massutí E, Reglero P. Decapod crustacean larval communities in the Balearic Sea (western Mediterranean): Seasonal composition, horizontal and vertical distribution patterns. Journal of Marine Systems. 2014; 138:112–26.
14. Lindley JA. Eggs and their incubation as factors in the ecology of planktonic crustacea. *Journal of Crustacean Biology*. 1997; 17(4):569–76.
15. Palmas F, Olita A, Addis P, Sorgente R, Sabatini A. Modelling giant red shrimp larval dispersal in the Sardinian seas: Density and connectivity scenarios. Fisheries Oceanography. 2017; 26(3):364–78. https://doi.org/10.1111/fog.12199
16. Sundby S, Kristiansen T. The Principles of Buoyancy in Marine Fish Eggs and Their Vertical Distributions across the World Oceans. PLOS ONE. 2015; 10(10):e0138821. https://doi.org/10.1371/journal.pone.0138821 PMID: 26465149
17. Herring PJ. Observations on the embryonic development of some deep-living decapod crustaceans, with particular reference to species of *Acanthephyra*. *Marine Biology*. 1974; 25(1):25–33. https://doi.org/10.1007/bf00395105
18. Subrahmanyam CB. On the unusual occurrence of penaeid eggs in the inshore waters of madras. J. Mar. Biol Ass. India. 1965; 7(1):83–8.
19. Temple RF, Fischer CC. Seasonal distribution and relative abundance of planktonic-stage shrimp (Penaeus spp.) in the northwestern Gulf of Mexico, 1961. Fisheries Bulletin. 1967; 66:323–34.
20. Gurney R. Larvae of decapod Crustacea. London: The Ray Society. 1942
21. Fiksen Ø, Jørgensen C, Kristiansen T, Vikebø F, Huse G. Linking behavioural ecology and oceanography: larval behaviour determines growth, mortality and dispersal. *Marine Ecology Progress Series*. 2007; 347:195–206.
22. Kristiansen T, Jørgensen C, Lough R, Vikebø F, Fiksen Ø. Modeling rule-based behavior: habitat selection and the growth-survival trade-off in larval cod. *Behavioral Ecology*. 2009; 20(3):490–500.
23. Salat J. The interaction between the Catalan and Balearic currents in the southern Catalan Sea. *Oceanologica Acta*. 1995; 18(2):227–34.
24. Bakun A. Fronts and eddies as key structures in the habitat of marine fish larvae: opportunity, adaptive response and competitive advantage. *Scientia Marina*. 2006; 70(S2):105–22.
25. Rubio A, Barnier B, Jordà G, Espino M, Marsaleix P. Origin and dynamics of mesoscale eddies in the Catalan Sea (NW Mediterranean): Insight from a numerical model study. *Journal of Geophysical Research*: *Oceans*. 2009; 114:C06009. https://doi.org/10.1029/2007JC004245

26. Houpert L, Testor P, Durrieu de Madron X, Somot S, D'Ortenzio F, Estournel C, et al. Seasonal cycle of the mixed layer, the seasonal thermocline and the upper-ocean heat storage rate in the Mediterranean Sea derived from observations. *Progress in Oceanography*. 2015; 132:333–52. https://doi.org/10.1016/j.pocean.2014.11.004

27. Thorpe SA. *An introduction to ocean turbulence*. 1st ed. Cambridge University Press. 2007

28. Lloyd ÑJ, Metaxas A, deYoung B. Patterns in vertical distribution and their potential effects on transport of larval benthic invertebrates in a shallow embayment. *Marine Ecology Progress Series*. 2012; 469:37–52.

29. Queiroga H, Blanton J. Interactions Between Behaviour and Physical Forcing in the Control of Horizontal Transport of Decapod Crustacean Larvae *Advances in Marine Biology*. 2004; 47:107–214

30. Shchepetkin AF, McWilliams JC. The regional oceanic modeling system (ROMS): a split-explicit, free-surface, topography-following-coordinate oceanic model. *Ocean Modelling*. 2005; 9(4):347–404. https://doi.org/10.1016/j.ocemod.2004.08.002

31. Warner JC, Sherwood HG, Arango HG, Signell RP. Performance of four turbulence closure methods implemented using a generic length scale method. *Ocean Modelling*. 2005; 8:81–113.

32. Coll M, Steenbeek J, Sole J, Palomera I, Christensen V. Modelling the cumulative spatial–temporal effects of environmental drivers and fishing in a NW Mediterranean marine ecosystem. *Ecological Modelling*. 2016; 331:100–14. https://doi.org/10.1016/j.ecolmodel.2016.03.020

33. Sardà F, Company JB, Castellón A. Intraspecific aggregation structure of a shoal of a western Mediterranean (Catalan Coast) deep-sea shrimp, Aristeus antennatus (Risso, 1816), during the reproductive period. *Journal of Shellfish Research*. 2003; 22(2):569–79.

34. Nencioli F, Dong C, Dickey., Washburn L, McWilliams JC. A Vector Geometry–Based Eddy Detection Algorithm and Its Application to a High-Resolution Numerical Model Product and High-Frequency Radar Surface Velocities in the Southern California Bight. *Journal of Atmospheric and Oceanic Technology*. 2010; 27(3):564–79. https://doi.org/10.1175/2009jtecho725.1

35. Fofonof NP, Millard RC Jr. Algorithms for the computation of fundamental properties of seawater. UNESCO Technical Papers in Marine Sciences. 1983; 44:53 pp.

36. Manca B, Burca M, Giorgetti A, Coatanoan C, Garcia MJ, Iona A. Physical and biochemical averaged vertical profiles in the Mediterranean regions: An important tool to trace the climatology of water masses and to validate incoming data from operational oceanography. *Journal of Marine Systems*. 2004; 48(1–4):83–116. https://doi.org/10.1016/j.jmarsys.2003.11.025

37. Dagestad K-F, Röhrs J. OpenDrift v1.0: a generic framework for trajectory modelling. *Geosci. Model Dev*. 2018; 11:1405–20. https://doi.org/10.5194/gmd-11-1405-2018

38. Visser A. Using random walk models to simulate the vertical distribution of particles in a turbulent water column. *Marine Ecology Progress Series*. 1997; 158:275–81. https://doi.org/10.3354/meps158275

39. Sayol J-M, Orfila A, Simarro G, López C, Renault L, Galán A, et al. Sea surface transport in the Western Mediterranean Sea: A Lagrangian perspective. Journal of Geophysical Research: Oceans. 2013; 118 (12):6371–84. https://doi.org/10.1002/2013JC009243

40. Sundby S. A one-dimensional model for the vertical distribution of pelagic fish eggs in the mixed layer. *Deep Sea Research Part A. Oceanographic Research Papers*. 1983; 30(6):645–61.

41. Dallavalle JM. Micromeritics. The technology of fine particles. Pitman, New York. 1948:11–30.

42. Tavares C, Martin JW. Suborder Dendrobranchiata Bate, 1988. In: Schram F, von Vaupel Klein C, editors, *Treatise on Zoology—Anatomy*, *Taxonomy*, *Biology*. *The Crustacea*, *Volume* 9 *Part A*. Leiden: Brill. 2010:99–164. https://doi.org/10.1163/ej.9789004164413.i-562

43. Hilário A, Metaxas A, Gaudron SM, Howell KL, Mercier A, Mestre NC, et al. Estimating dispersal distance in the deep sea: challenges and applications to marine reserves. *Frontiers in Marine Science*. 2015; 2(6). https://doi.org/10.3389/fmars.2015.00006

44. O'Connor MI, Bruno JF, Gaines SD, Halpern BS, Lester SE, Kinlan BP, et al. Temperature control of larval dispersal and the implications for marine ecology, evolution, and conservation. *Proceedings of the National Academy of Sciences*. 2007; 104(4):1266–71. https://doi.org/10.1073/pnas.0603422104 PMID: 17213327

45. Simons RD, Siegel DA, Brown KS. Model sensitivity and robustness in the estimation of larval transport: A study of particle tracking parameters. *Journal of Marine Systems*. 2013; 119–20:19–29. https://doi.org/10.1016/j.jmarsys.2013.03.004

46. Fiedler PC. Comparison of objective descriptions of the thermocline. *Limnology and Oceanography: Methods*. 2010; 8(6):313–25. https://doi.org/10.4319/lom.2010.8.313

47. Calvo EM, Coma R, Gili JM, Pascual J, Pelejero C, Ribes M, et al. Effects of climate change on Mediterranean marine ecosystems: the case of the Catalan Sea. Climate Research. 2011; 50:1–29.

48. Chu KH, Sze CC, Wong CK. Swimming Behaviour during the Larval Development of the Shrimp Metapenaeus ensis (De Haan, 1844) (Decapoda, Penaeidae). Crustaceana. 1996; 69(3):368–78.

49. Martin JW, Criales MM, Dos Santos A. Dendrobranchiata. In: Martin JW, Høeg JT, Olesen J, editors. *Atlas of Crustacean Larvae*. Baltimore, MD: Johns Hopkins University Press. 2014

50. Price ARG. Distribution of Penaeid shrimp larvae along the Arabian Gulf coast of Saudi Arabia. *Journal of Natural History*. 1982; 16(5):745–57. https://doi.org/10.1080/00222938200770571

51. North EW, Gallego A, Petitgas P. Manual of recommended practices for modelling physical–biological interactions during fish early life. *ICES Cooperative Research Report*. 2009;295.

52. Parada C, van der Lingen C, Mullon C, Penven P. Modelling the effect of buoyancy on the transport of anchovy (*Engraulis capensis*) eggs from spawning to nursery grounds in the southern Benguela: An IBM approach. *Fisheries Oceanography*. 2003; 12(3):170–84. https://doi.org/10.1046/j.1365-2419.2003.00235.x

53. Dall W, Hill BJ, Rothlisberg PC, Staples DJ. The Biology of the Penaeidae. *Advances in Marine Biology*. 1990; 27:489 pp.

54. Pongtippatee-Taweepreda P, Chavadej J, Plodpai P, Pratoomchart B, Sobhon P, Weerachatyanukul W, et al. Egg activation in the black tiger shrimp Penaeus monodon. *Aquaculture*. 2004; 234(1–4):183–98.

55. Pandian TJ. Reproduction and Development in Crustacea. In: CRC Press Taylor and Francis group, editors. Reproduction and Development in Aquatic Invertebrates. 2016:27–69.

56. Rosa R, Calado R, Narciso L, Nunes ML. Embryogenesis of decapod crustaceans with different life history traits, feeding ecologies and habitats: a fatty acid approach. *Marine Biology*. 2006; 151(3):935–47. https://doi.org/10.1007/s00227-006-0535-6

57. Chu K, Ovsianico-Koulikowsky N. Ontogenetic changes in metabolic activity and biochemical composition in the shrimp, *Metapenaeus ensis*. *Journal of Experimental Marine Biology and Ecology*. 1994; 183(1):11–26.

58. Coombs S, Boyra G, Rueda L, Uriarte A., Santos M, Conway D, Halliday N. Buoyancy measurements and vertical distribution of eggs of sardine (*Sardina pilchardus*) and anchovy (*Engraulis encrasicolus*). *Marine Biology*. 2004; 145(5):959–70.

59. Heldt JH. La Reproduction chez les crustacés décapodes de la famille des Pénéides. Annales de l'Institut. Océanographique de Paris, 1938; 28:1–206.

60. Dobkin S. Larvae of the pink shrimp (*Penaeus duorarum*). Presented at Proceedings of the Gulf and Caribbean Fisheries Institute 12, Miami (United States). 1960

61. Rossi V, Ser-Giacomi E, López C, Hernández-García E. Hydrodynamic provinces and oceanic connectivity from a transport net- work help designing marine reserves, *Geophys. Res. Lett*. 2014; 41:2883–91. https://doi.org/10.1002/2014GL059540

62. Mariani P, MacKenzie BR, Iudicone D, Bozec A. Modelling retention and dispersion mechanisms of bluefin tuna eggs and larvae in the northwest Mediterranean Sea. *Progress in Oceanography*. 2010; 86(1–2):45–58. https://doi.org/10.1016/j.pocean.2010.04.027

63. Ospina-Álvarez A, Palomera I, Parada C. Changes in egg buoyancy during development and its effects on the vertical distribution of anchovy eggs. *Fisheries Research*. 2012; 117–118:86–95. https://doi.org/10.1016/j.fishres.2011.01.030

64. Cowen RK, Lwiza KMM, Sponaugle S, Paris CB, Olson DB. Connectivity of Marine Populations: Open or Closed? *Science*. 2008; 287(5454):857–9. https://doi.org/10.1126/science.287.5454.857 PMID: 10657300

65. Escudier R, Renault L, Pascual A, Brasseur P, Chelton D, Beuvier J. Eddy properties in the Western Mediterranean Sea from satellite altimetry and a numerical simulation. *Journal of Geophysical Research*: *Oceans*. 2016; 121(6):3990–4006. https://doi.org/10.1002/2015JC011371

66. Karimova S. *Observation of the surface circulation of the Mediterranean Sea from space*. Paper presented at the ESA Living Planet Symposium, Netherlands. 2016

67. Pinot JM, López-Jurado JL, Riera M. The CANALES experiment (1996–1998). Interannual, seasonal and mesoscale variability of the circulation in the Balearic Channels. *Progress in Oceanography*. 2002; 55(3–4):335–70. https://doi.org/10.1016/s0079-6611(02)00139-8

68. Rubio A, Arnau PA, Espino M, Flexas M, Jordà G, Salat J, et al. A field study of the behaviour of an anticyclonic eddy on the Catalan continental shelf (NW Mediterranean). *Progress in Oceanography*. 2005; 66(2):142–56. https://doi.org/10.1016/j.pocean.2004.07.012

69. Sabatés A, Salat J, Raya V, Emelianov M. Role of mesoscale eddies in shaping the spatial distribution of the coexisting *Engraulis encrasicolus* and *Sardinella aurita* larvae in the northwestern Mediterranean. *Journal of Marine Systems*. 2013; 111:108–19.

70. Hill AE, Brown J, Fernand L. The western Irish Sea gyre: a retention system for Norway lobster (*Nephrops norvegicus*)? *Oceanologica Acta*. 1996; 19(2–3):357–68.

71. Lafuente J, Jurado J, Lucaya N, Yanez M, Garcia J. Circulation of water masses through the Ibiza Channel. *Oceanologica Acta*. 1995; 18(2):245–54.

72. Carbonell A, Carbonell M, Demestre M, Grau A, Monserrat S. The red shrimp *Aristeus antennatus* (Risso, 1816) fishery and biology in the Balearic Islands, Western Mediterranean. Fisheries Research. 1999; 44(1):1–13. https://doi.org/10.1016/S0165-7836(99)00079-X

73. La Violette PE. Overview of the major forcings and water masses of the western Mediterranean Sea. In La Violette PE, editors. Seasonal and Interannual Variability of the Western Mediterranean Sea. 1995:1–11. https://doi.org/10.1029/CE046p0001

74. López García MJ, Millot C, García-Ladona E. Surface circulation variability in the Balearic Basin. Journal of Geophysical Research. 1994; 99:3285–96. https://doi.org/10.1029/93JC02114

75. García-Ladona E, Castellón A, Font J, Tintore J. The Balearic current and volume transports in the Balearic basin. Oceanologica Acta. 1996; 19(5):489–97.

76. Macías D, Stips A, Garcia-Gorriz E. The relevance of deep chlorophyll maximum in the open Mediterranean Sea evaluated through 3D hydrodynamic-biogeochemical coupled simulations. *Ecological Modelling*. 2014; 281:26–37. https://doi.org/10.1016/j.ecolmodel.2014.03.002

77. Gorelli G, B Company J, Sardà F. Management strategies for the fishery of the red shrimp *Aristeus antennatus* in Catalonia (NE Spain). *Marine Stewardship Council Science Series*. 2014; 2:116–27.